NOVEL INFRASTRUCTURE MONITORING USING MULTIFACETED UNMANNED AERIAL VEHICLE SYSTEMS - CLOSE RANGE PHOTOGRAMMETRY (UAV - CRP) DATA ANALYSIS

by

SURYA SARAT CHANDRA CONGRESS

DISSERTATION

Presented to the Faculty of the Graduate School of

The University of Texas at Arlington

in Partial Fulfillment

of the Requirements

for the Degree of

DOCTOR OF PHILOSOPHY

THE UNIVERSITY OF TEXAS AT ARLINGTON

December 2018

This thesis is heartily dedicated to my father, sister, and mother who took the lead to heaven and have been with me ever since.

ACKNOWLEDGMENTS

Foremost, I would like to express my sincere gratitude to my advisor, Dr. Anand J. Puppala, for his continuous enthusiasm, support, encouragement, and motivation throughout the dissertation. It is an honor to get a chance to work under the supervision of Dr. Puppala and learn from his immense knowledge. Besides my advisor, I would like to thank the rest of my thesis committee members: Dr. Xinbao Yu, Dr. Shih-Ho Chao, Dr. Suyun Ham, and Dr. Yan Wan for their guidance and insightful comments.

I would like to acknowledge the immense support and advice of Dr. Tejo V. Bheemasetti, Dr. Aravind Pedarla, Dr. Bhaskar Chittoori, Dr. Ujwalkumar Patil, and Mr. Cody Lundberg at different stages of this dissertation work. The valuable discussions and coordination with them helped me to conduct this research work. I thank my co-workers at UT Arlington, Mr. Kevin Weinhold, Dr. Aritra Banerjee, Dr. Santiago Caballero, Dr. Minh Hai, Dr. Nagasreenivasu Talluri, Dr. Tom Taylor, Dr. Jasaswee Das, Dr. Sayantan Chakraborty, Dr. Ali Shafikhani, Mr. Shi He, Mr. Salman Hosam, Ms. Anu George, Ms. Leila Mosadegh, Mr. Puneet Bhaskar, Ms. Rinu Samuel, Mr. Burak Boluk, Mr. Ashrafuzzaman Khan, Mr. Manikanta Saladhi, Mr. Nripojyoti Biswas, Mr. Andrew Miller and Mr. Ahmed Gaily.

I am also grateful to TxDOT project members Jay Joseph, Jonathan Martin, Arturo Perez, Jim Reid, Joe Adams, Chris Glancy, Gil Wilson, Graham Bettis, Paul Rollins, John Vasquez, Wade Blackmon, Justin Thomey, Steven Brock, Jody Wall,

Todd Copenhaver and NSF project team members led by Dr. Navid Jafari for their valuable advice and support during various stages of my dissertation work. I would also like to thank Mr. Colin Brooks and MTRI team for helping me during the data collection. Furthermore, I am thankful to Dr Shima Hamidi and CTEDD for supporting my research work.

My special and hearty thanks to my well-wishers Mr. Shiva Ram Dantuluri, Mr. Viswatej Pandu, Mr. Satishkumar Bandi, Dr. Padmaja Puppala, Ms. Aneesha Puppala, Mr. Rishik Puppala, Ms. Aasritha Sarangu, and Mr. Saaketh Sarangu for their constant support throughout my research work.

Finally, I must express my very profound gratitude to my father, Subhas Chandra Bose, my mother, Padma, and my sister, Sravani, for providing me with unfailing support and continuous encouragement throughout my years of study and through the process of researching and writing this thesis.

ABSTRACT

NOVEL INFRASTRUCTURE MONITORING USING MULTIFACETED UNMANNED AERIAL VEHICLE SYSTEMS - CLOSE RANGE PHOTOGRAMMETRY (UAV - CRP) DATA ANALYSIS

Surya Sarat Chandra Congress, Ph.D.

The University of Texas at Arlington, 2018

Supervising Professor: Dr. Anand J. Puppala,

Remote sensing is a method of collecting data without making any physical contact with the object under inspection. Modern day remote sensing kicked off with the invention of the camera and continued on to the invention of advanced satellite mounted sensors. Photogrammetry is defined as a science that measures distances using one or more images captured remotely. Remote collection of images within a range of 1000 ft is termed close-range photogrammetry (CRP).

Unmanned aerial vehicle systems (UAV or UAS) have become a popular means of remotely gathering information and assessing infrastructure conditions due to their versatile nature. Multirotor and fixed-wing are two types of UAVs that are frequently used in field operations. Close-range photogrammetry (CRP) using

UAVs can generate dense point cloud images, orthomosaics, digital elevation models (DEMs), and digital terrain models (DTMs) in a short time period.

Analyses of these models help transportation engineers and agencies to understand the infrastructure health conditions. Several studies have addressed UAV-CRP surveys for infrastructure health condition assessments primarily due to restrictions imposed by the Federal Aviation Administration (FAA) on UAV studies and their operations in the field. After the introduction of Part 107 exemption of UAV operations by FAA in August 2016, more studies have been planned and performed with UAVs, evaluating their abilities to perform infrastructure condition assessments.

In the present research, the UAV-CRP technology using a hexacopter was primarily used to conduct infrastructure monitoring and assessments. As a part of the research, a comprehensive literature review of remote sensing and photogrammetry studies, UAV-related research by different states' departments of transportation, calibration checks for different accessories, as well as research on pavement and bridge infrastructure management was conducted. Then, a comprehensive calibration study was performed by conducting total system error analysis on both the UAV as well as accessories used in the research. This unique calibration analysis provided a much-needed understanding of how environmental conditions, including field temperature conditions, lens temperatures, flight altitudes, humidity, and different overlap conditions influence the quality of images

captured as well as three-dimensional dense point cloud models generated using these images.

Later, UAV-CRP technology was used in various infrastructure inspection studies owing to its multifaceted benefits. UAV-CRP studies on pavement sections showed they could provide pavement distress data including information on longitudinal and transverse cracks, permanent deformation or rutting, as well as pavement characteristics such as longitudinal and cross-slope values, and sight distances at crossings. All the photogrammetry-based imaging analyses yielded results that are in agreement with other traditional methods. UAV-CRP studies performed on various construction material stockpiles yielded volume results matching with ground truth measurements from traditional field survey results.

Bridge sites were inspected using UAVs equipped with both top and bottom gimbals to provide a complete 360° view of the bridge including substructure and superstructure elements. UAV-CRP results can provide condition assessments on approach slab settlements, movements and cracking in abutment and wing walls, bridge foundation conditions, columns, and under-bridge decks as well as upper deck. UAV-CRP studies conducted on rail corridors also proved that the photogrammetry results could be used to evaluate encroachments at crossings, and washout site detection including an appraisal of factors that may have contributed to washouts. UAVs were also used for emergency operations immediately after a

hurricane event and proved its value in providing debris assessments in post disaster reconnaissance studies performed in Beaumont, Texas.

A preliminary cost analysis indicates that UAV-CRP technology could provide an inexpensive way of monitoring infrastructure conditions and gathering valuable data related to infrastructure-related annual and biennial rating surveys. All the procedures, analyses, and results indicate the UAV-CRP tool provides a quick, efficient, and safe method for assessing infrastructure health conditions.

Keywords: Unmanned aerial vehicles, Infrastructure, Pavements, Bridges, Rail Corridor, Safety, Monitoring

TABLE OF CONTENTS

LIST OF FIGURES

LIST OF TABLES

CHAPTER 1: INTRODUCTION

1.1 RESEARCH OVERVIEW

Research guiding the implementation of unmanned aerial vehicles (UAVs) for department of transportation (DOT) agencies' applications in managing the infrastructure assets has been conducted at University of Texas at Arlington (UTA). The objectives of the research and the workflows formulated to achieve them are covered in detail in this research. The results from previous aerial inspection surveys also showed that the photogrammetry approach using the UAV platform has demonstrated and provided very good preliminary solutions to identifying infrastructure problems including pavement, rail, and bridge distress conditions (Brooks et al. 2015; Puppala et al. 2018a).

This research demonstrated the appropriate use of sensors mounted on UAVs, which can be integrated with the close-range photogrammetry (CRP) methodology to help in infrastructure performance assessment. Performance and the current state of condition of civil infrastructure can be determined using close-range photogrammetry (CRP) techniques via high-resolution digital cameras mounted on unmanned aerial vehicles (UAVs). Initial work covered selection and acquisition of equipment and accessories required for UAV-CRP technologies as well as the development of calibration procedures for testing the compatibility of UAV and accessories as a total system. After the early and promising results obtained during those calibration studies and results, the acquired UAV and

accessories were then used in transportation infrastructure investigations related to construction materials, pavements, bridges and railway tracks' assessments. This research evaluated UAV-CRP technology's ability to perform field studies with an increased safety and to obtain more data with less work at reduced expenditures. Most of all, the UAV-CRP technology has the ability to assess the transportation infrastructure condition with reasonable accuracy. The following sections introduce the key knowledge areas that are important in conducting aerial inspection studies using cameras.

1.2 PHOTOGRAMMETRY

Photogrammetry is a remote data collection technique, which can record or capture information using imaging sensors to make measurements without direct contact with the inspecting element (McGlone et al. 2004). It is also referred to as an art, science, and technology designed to obtain reliable information about physical objects and their surrounding environment through the process of recording, measuring and interpreting patterns (Ahmad and Samad 2010; Brooks et al. 2015; Udin and Ahmad 2014). Under most conditions, particularly for large areas, photogrammetric techniques have proven to be inexpensive and have even proved useful in land surveying (Ahmad 2006; Brooks et al. 2015; Mills et al. 1996; Puppala et al. 2018b; Room and Ahmad 2014; Siebert and Teizer 2014; Udin and Ahmad 2014).

UAVs can capture images at different altitudes, angles, and positions. Although UAVs are capable of flying at higher altitudes, Federal Aviation Administration (FAA) regulates the maximum UAV flying altitude in unrestricted airspace as 400 ft. However, operating at higher altitudes or within restricted airspace warrants a waiver approved by FAA. The gimbal over which the camera is mounted facilitates image capture in both nadir and oblique angles.

Some drones are also capable of mounting the camera on top whenever the need for inspecting inaccessible areas arises. Scans or images taken from a distance of less than 1000 ft (~300 m) between the sensor and the inspecting object are usually classified as close-range photogrammetry (CRP). Adoption of UAVs for photogrammetry comes under the category of close-range photogrammetry (CRP) (Brooks et al. 2015; Colomina and Molina 2014; Puppala et al. 2018b; Siebert and Teizer 2014), referred in this study as UAV-CRP.

1.3 UNMANNED AERIAL VEHICLES (UAV) AND CLOSE RANGE PHOTOGRAMMETRY (CRP)

Recent studies have revealed an active engagement of several DOTs, including California, Georgia, Michigan, Ohio, Utah and other state agencies in USA, in research related to UAV-assisted infrastructure asset management (Tony 2018). Caltrans Division of Engineering's geotechnical services have been involved in research projects using UAVs to perform geotechnical investigations pertaining to landslides, slope movements, and other steep terrain analysis (Karpowicz 2014).

Due to its versatile nature, unmanned aerial vehicles (UAVs or UASs) have become a popular means of remotely gathering information and assessing infrastructure damage in the past decade. Photogrammetry software using UAV collected data can provide a 3-dimensional dense point cloud model, an orthomosaic, a digital elevation model (DEM), and a good quality digital terrain model (DTM) in a short period (Dobson et al. 2014). The main advantages of UAVs over traditional surveying techniques are their ability to capture detailed images of the study area at low cost and with rapid deployment.

The three main components of UAV-CRP are the unmanned aerial vehicle, the ground control station, and the communication data link. This system can be controlled from the ground control station (GCS). Some previous researches also term the combination of the unmanned aerial vehicle and the base station as UAS. The availability of the global positioning system (GPS) data and gyroscope technology allows the UAV to precisely deliver the digital camera to the required location and altitude to capture the infrastructure environment and to record the location of the aerial photographs.

In photogrammetry, it is a common practice to establish the ground control points (GCP) before the aerial data collection. Size of the standard or other GCP markers used in the field should be maintained in such a way that they are distinguishable in the images during processing. Several methods such as traversing

and global positioning system (GPS) techniques can be used to establish the GCP (Cesetti et al. 2011).

The communication infrastructure is a mixture of communication mechanisms, such as radio modems and microwave links, which make sure that the continuous link between the UAV and the base station is kept open. Modern digital airborne sensors are also usually mounted with a GPS/IMU (inertial measurement unit) system. GPS technology for mapping projects can be assisted by using a series of base stations in the project area and a constellation of satellites providing positional information accessed by the GPS receiver placed on board of an aircraft. Accuracy in the combination of GPS and IMU information can be extremely beneficial for mapping areas where limited ground control information is available (e.g., rugged terrain). The different phases of CRP are detailed in Figure 1-1.

Photogrammetric output such as digital maps and orthomosaics can be successfully obtained from a compact ‘digital single lens reflex’ (DSLR) camera. Over the years, several new software tools and algorithms have been developed to analyze images or scans obtained from different remote sensing techniques. In particular, efforts have been made to develop algorithms that can identify pavement distress resulting from heaving, cracking, potholes, and surface deformation. Software has also been developed for bridge element monitoring including approach slab settlements, foundation movements, bridge deck conditions, abutment, and wing wall performance. Post analysis of the processed data obtained

from remote sensing techniques plays a crucial role in identifying the structural health condition of the civil infrastructure. After collecting the data over a period of time, the analyzed data will be utilized for timeline comparisons and assess any changes in the infrastructure over that period. Figure 1-1 presents a flow chart of the different stages of UAV-CRP implementation of aerial field survey data collection.

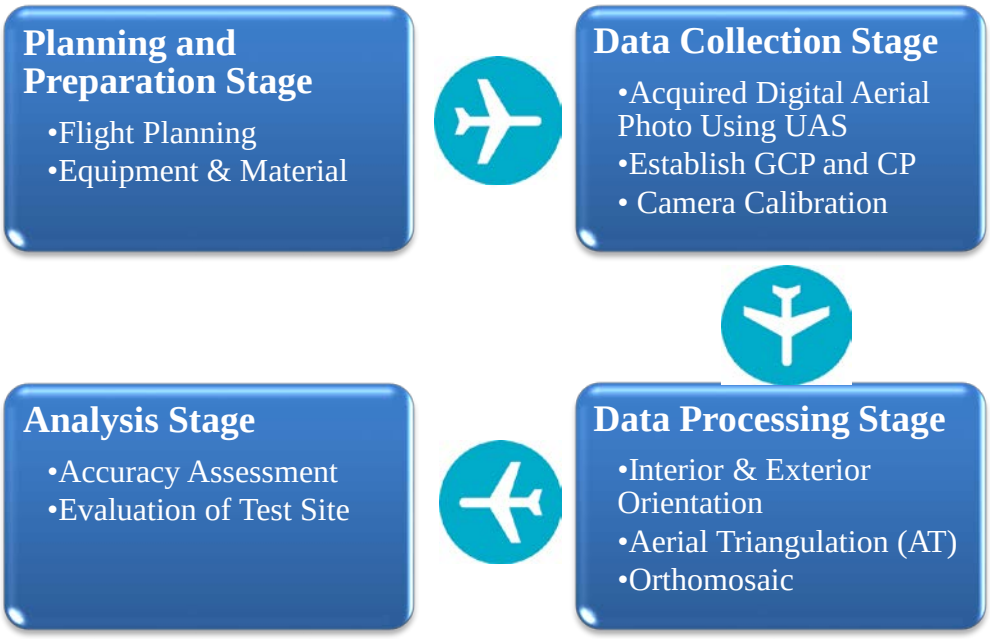

Figure 1-1. Different Stages of the Aerial Photogrammetry Process

For close range photogrammetry studies, rotary wing aircraft (Aibot X6) and fixed wing aircraft systems (SenseFly Ebee) are typically used. Figure 1-2 shows the examples of each UAV type.

(a) (b)

Figure 1-2. Types of UAVs (a) Aibot X6 Multi-rotor (b) SenseFly Ebee Fixed Wing

The Aibot X6 V2 is a versatile UAV best suited for acquiring data over relatively small areas. The hovering capability of the aircraft provides a unique data collection platform that can be applied to many areas. The Aibot X6 multi-rotor UAV can be adopted for small-scale investigations and a fixed wing UAV can be used for large-scale environments. The Aibot X6 with an on-board RTK GPS receiver allows the UAV to communicate and use real-time kinematic positioning provided by the existing TxDOT VRS network. The top gimbal of the Aibot X6 allows the UT Arlington research team to conduct a 360° bridge inspection, which includes access to the under-bridge condition data collection.

The UT Arlington team used multi-rotor systems for bridge, roadway, railway, slope, and material stockpile volumetric assessment research. Fixed wing aircraft systems are better suited for collecting data in remote areas, far from roadways, with limited access.

1.4 RESEARCH OBJECTIVE

The major objective of this research is to study and demonstrate the UAV-CRP technology for infrastructure health condition monitoring and management applications. As a part of the main objective, several subtasks were identified and executed.

The first subtask addressed a total system error analysis, which was primarily conducted to evaluate the compatibility of UAV and various sensors in providing error free imagery of the inspecting objects. The objectives of the total system error analysis are to study and address:

- Variation in accuracy due to geotagging using Global Navigation Satellite System (GNSS) and Global Positioning System (GPS) data
- Variations in the calibrated camera focal length between the ambient room conditions and the conditions encountered during field operations
- Thermal effect on the lens system, to ensure proper imagery data extraction
- Nonlinear errors induced due to distortion
- Any errors from Structure from motion (SfM) techniques
- Analysis of image resolution and resolving power of the system

This is a key subtask for the research as error analysis provides a thorough understanding of the accuracy that could be achieved in the field conditions.

Once the system error analysis was completed, the UAV-CRP surveys were performed on pavement forensics related to pavement condition surveys, determine pavement slope characteristics to approach slab pavement distress monitoring; perform railways operations including corridor inspection, rail bridge inspection, rock cut volumetric and railroad crossing mapping and others; perform bridge rating surveys and stockpile volumetric studies. This technology also resulted in reducing the inspection expenditure that is conducive for proactive monitoring that helps in preventive maintenance. All these studies and results are presented in later chapters with results and comprehensive analyses.

1.5 THESIS OUTLINE

This dissertation has eight chapters. The first Chapter describes and introduces the research objective and tasks performed. The second Chapter covers a comprehensive literature review on various topics related to UAVs and their applications in infrastructure studies. Total system error analysis procedures and results are compiled in the third Chapter.

Infrastructure studies including UAV-CRP data collection of pavement, rail, bridge, and construction material stockpile sites are provided in the fourth Chapter. UAV application for disaster management and debris assessments is covered in the fifth Chapter. Cost analysis for using UAV-CRP technologies for various inspection activities has been included in the sixth Chapter. Business

guidelines for transportation agencies have been provided in the seventh Chapter. All the key observations are summarized and concluded in the eighth Chapter.

CHAPTER 2: LITERATURE REVIEW

In this chapter, an attempt is made to provide a comprehensive literature summary on various subject topics related to autonomous unmanned aerial vehicles (UAV or UAS), remote sensing and photogrammetry topics, followed by various methods of infrastructure monitoring and disaster management. The subsequent sections provide information on the applications of unmanned aerial vehicles and traditional methods for infrastructure surveying and management studies. Disaster management that arises due to the formation of hurricanes is also discussed by examining infrastructure post Hurricane Harvey that struck the state of Texas, USA in 2018.

Most of the compiled literature focuses predominantly on the UAVs and hence only limited information on using UAVs for infrastructure monitoring is available from sources in the United States as these tools have only been recently approved for field operations. Nevertheless, the available literature information is valuable for the present dissertation research study as it provides a pathway for performing present field investigations along with an exposure to various ways of analyzing and interpreting the collected data results. Various topics including infrastructure monitoring, methods, and other related topics are also compiled in this chapter.

2.1 UNMANNED AERIAL VEHICLES (UAV OR UAS)

An unmanned aerial vehicle, also commonly referred to as a drone, is an aircraft that can fly without an actual human pilot on board, and its flight can be controlled from a ground control station (Wen and Kang 2014).

In the United States, the initial development of UAVs took place during the early nineteenth century with special interest in using them for long-term reconnaissance videos to assist with target designations and attacks in war. Since then, they have proven to be immensely helpful in eliminating pilot risks along with several other benefits (Haulman 2003). Following pioneering research and development in the military by researchers and various agencies worldwide, the last decade or so has experienced a rapid growth and demand for UAVs owing to their capabilities and potential applications in numerous missions with high social benefits (Pereira et al. 2009). However, application of UAVs in non-combat missions faced challenges due to the legal and technical constraints prevailing then with regards to the safety of flying in non-segregated spaces and flying operations related policy issues (Pereira et al. 2009).

Rotary wing and fixed wing are the two types of UAV units. A fixed wing UAV has a single rigid wing across its body that allows it to fly with high speeds and for longer flight distances, similar to manned airplanes (Tahar and Ahmad 2012). Rotary wing UAV uses lift from the continuous rotation of its blades and has the ability for vertical takeoff and landing, similar to manned helicopters. The

main advantages of these systems are that they can access remotely located areas and confined spaces, and can hover at a fixed altitude, allowing sensors (such as digital cameras) to collect precise data from hard to reach areas. Studies suggest that the difference between photogrammetric output obtained from a fixed platform and a mobile platform, such as a lightweight rotary-wing UAV, is small; hence, the unmanned aerial vehicle (UAV) can be used for large-scale mapping of aerial terrain (Tahar and Ahmad 2012).

Recent developments in remote sensing such as high-resolution images collected from satellites, radar, and UAVs fitted with high-resolution cameras in combination with newly developed and sophisticated image analyses algorithms have enabled practitioners to measure very small movements on the earth's surface and offer collections of massive spatial data of the earth, its oceans and atmosphere (Colomina and Molina 2014; Mustaffara et al. 2008; Udin and Ahmad 2014). These methods have tremendous potential towards creating alarm systems through anticipatory analysis since large amounts of information can be quickly processed. This makes remote sensing an attractive option for predictive intelligence and modeling of structures built on the earth's surface.

Recently, a growing use of UAVs has been found in many engineering applications such as aerial photography, surveillance and control of maritime traffic, construction surveillance, detection and control of coastal hazards, flood monitoring, terrain mapping, fire disasters, remote data acquisition of existing

pavement conditions, earthquake damage assessment, and post distress monitoring survey (Adu-Gyamfi et al. 2014; Pereira et al. 2009; Puppala et al. 2018b; Rathje et al. 2006; Shamsabadi et al. 2014; Suncar et al. 2013; Tahar and Ahmad 2012).

The use of UAVs for military purposes including reconnaissance, surveillance and target accusation (RSTA) had gained momentum in the past couple of decades (Murphy and Cycon 1999). They proposed using vertical take-off and landing (VTOL) UAV fitted with visual and thermal sensors for law enforcement applications.

Jacobsen (2002) dealt with the calibration aspects in direct geo-referencing the images collected by the camera mounted on UAV. He also provided information related to the use of inertial measurement system (IMU) and kinematic GPS-positioning together for direct geo-referencing (Jacobsen 2002). Kuchar (2005) stated that UAVs could be used in civil and military applications such as environmental observation, goods delivery, monitoring of construction sites, border patrol, and military surveillance. This requires UAVs to coexist in the airspace along with civilian aircrafts (Kuchar 2005).

Wu and Zhou (2006) developed a self-adaptive technique to match conjugate points in between adjacent images from UAV and automatically generate an orthomosaic from video images. They used this technique to obtain an orthoimage from the video of a forest inspected aerially for active fires (Wu and Zhou 2006). Another research work demonstrated the methodology of identifying

forest fires aerially and warning the authorities about the fire location from the orthoimage mosaics generated from the video images obtained using UAVs (Wu et al. 2007).

Carnie et al. (2006) conducted work on developing sense and obstacle avoidance capability of UAV using on-board image processing algorithms. After conducting tests in different daytime backgrounds they were successful in developing obstacle detection capability better than an alerted human observer. However, the additional computational burden required to avoid false alarms was a limitation (Carnie et al. 2006). Nisser and Westin (2006) investigated the impacts of human factors on using UAVs. Their work highlighted the importance of pilot's situational awareness, decision making, workload and performance monitoring, and the manual control ability while operating UAVs (Nisser and Westin 2006).

Wei and Zhou (2008) provided a method of real-time orthorectification of the video collected from the camera mounted on a UAV. They provided details about self-adaptive method to adjust the parallax; and also adoption of geometric and radiometric rectification for orthorectification of the video (Wei and Zhou 2008). Pereira et al. (2009) used six different fixed wing UAVs with different wingspans to conduct video surveillance and environmental monitoring operations. All the UAVs deployed had autonomous take-off and landing capabilities (Pereira et al. 2009).

Honkavaara et al. (2009) presented a review of the then prevailing research on radiometric aspects of digital photogrammetry. Typically photogrammetry consists of image blocks with 20-80% lateral and longitudinal overlap for better data quality. They provided a review of the radiometric calibration of aerial cameras in laboratory facility. Grey targets for reflectance measurement and Siemens star for resolution measurement are some of the testing methods mentioned in the literature. However, they also acknowledged that the calibration parameters determined in laboratory might differ in operational conditions (Honkavaara et al. 2009). Campoy et al. (2009) demonstrated the importance of computer vision during and after the UAV data collection for civilian purposes. They also dealt with 3D image-based visual servoing of objects using UAVs assisted with real-time image processing (Campoy et al. 2009).

Zhou (2010) developed a mathematical model considering camera's internal and external orientation parameters for geo-referencing the video data obtained from a fixed wing UAV equipped with an engine run by oil-gas mix, GPS for navigation and live video stream of the camera view. Video data was collected over a control field consisting of 21 non-traditional ground control points (GCPs) and the roll, pitch, and yaw of the UAV was tracked during the flight. A 2-D planimetric map with an accuracy of 1-2 meters was generated from the video data (Zhou 2010).

Kanistras et al. (2013) provided their survey work on UAV's role as the eye-in-the-sky for monitoring traffic. They specified that ease of maneuvering and remote communication capability provides the aerial imagery an edge over the current methods (Kanistras et al. 2013).

Nex and Remondino (2014) discussed about different UAV platforms and the then prevailing applications of UAV for Geomatics. Cost of a typical aerial platform for Geomatics applications ranges between 1,000 Euro and 50,000 Euro based on the on-board equipment, flight autonomy, and possible degree of automation. Lower the cost of the UAV, lower is the flight duration and stability, payload capacity, and data collection accuracy of the UAV. They also mentioned how safety of using UAVs is defined by the type of use in USA and by the weight of the copter in European countries (Nex and Remondino 2014). They provided typical acquisition and processing workflow of UAV data. They provided 3D model data showing the improvement in accuracy using GCPs and then asserted that using RTK georeferencing could improve the 3D model accuracy. They specified that UAVs are cost effective, quick, and reliable alternative for monitoring excavation works compared to high quality terrestrial laser scanners (Nex and Remondino 2014).

Gonçalves and Henriques (2015) provided their work on using Sensefly SwingletCam UAV equipped with a low-cost non-metric camera to monitor morphological changes induced by coastal dynamics. Period of the data collection

was planned during a low tide to map the largest area possible. Accurate 3D models were obtained using the GCPs obtained using a differential GPS. The plastic bands for the sandy areas and rigid plates for the rock surfaces were used as GCPs (Gonçalves and Henriques 2015).

Gabrlik (2015) proposed that a centimeter positional accuracy could be obtained using UAVs equipped with high-resolution camera and GNSS receiver. It can be accomplished by direct georeferencing that is accurately estimating the orientation of the camera images using the onboard GNSS and the inertial measurement unit (IMU). Hence, direct georeferencing can be used when the GCPs are not available (Gabrlik 2015).

A study demonstrated the capability of a UAV mounted with a low-cost RGB sensor to estimate the tree height for agriculture and forestry application (Zainuddin et al. 2016). Haidari et al. (2016) discussed about routine vaccine distribution and costs involved using drones. They concluded that using UAS for distribution increases the vaccine availability to public and also results in cost savings in the long run compared to the traditional ways (Haidari et al. 2016).

Jiang et al. (2016) proposed a procedure to regulate the unmanned aircraft traffic in the airspace. The unmanned aerial traffic management (UTM) includes development of a web-interface for the pilots to submit flight plans before executing them in the field. They also mentioned about the need for the training

and certification of the UTM managers handling the unmanned aerial traffic data (Jiang et al. 2016).

A study used a multi-spectral camera mounted on a fixed wing UAV for identifying the Silybum marianum (L.) Gaertn weeds that grow in patches (Tamouridou et al. 2017). Honrado et al. (2017) conducted aerial data collection using RGB and Near Infra-Red cameras to estimate seasonal production of rice and cornfields. These data were combined with ground sensor data to predict accurate crop productivity models. They also highlighted that higher number of studies used rotary wing UAVs compared to fixed wing UAVs for conducting precision agriculture (Honrado et al. 2017).

Alvear et al. (2017) proposed using UAVs equipped with a pollution detecting sensor and on-board Pollution-driven UAV Control algorithm (PdUC) that is adaptive in nature. A framework including a Raspberry Pi connected to UAV control unit and the pollution sensors was discussed. Simulation study of UAVs flying and detecting pollution levels over various regions and comparison with other models was also provided (Alvear et al. 2017).

A research study specified that drone swarms can be used as sensing grid to monitor road networks to report real-time traffic updates at the time of an accident or a natural disaster (Wu et al. 2017). These drone swarms can be utilized for sensing the pollution and noise levels along the urban road networks. Wu et al.

(2017) used a networked cyber-physical system (NCPS) for aggregation of data from all drones in the group.

Nikolakopoulos et al. (2017) compared UAV data with classical aerial photogrammetry for conducting archaeological studies. Ground truth measurements were established using tachymeter and differential GNSS system. The planimetric and vertical accuracy of models from the UAV data were found to be matching with conventional topographic survey (Nikolakopoulos et al. 2017). Daponte et al. (2017) conducted repeated experiments of aerial photogrammetry and proposed an uncertainty estimation model for determining the object height. The effects of various flight mission parameters like altitude, focal length, field of views and other factors on the height measurement had been provided (Daponte et al. 2017).

Ha et al. (2018) and Yurek and Ozmutlu (2018) worked on solving the traveling salesman problem that has emerged due to the deployment of UAVs or drones from the roof top of the delivery truck to avoid congestion, access difficult terrains, and cost effective. This is relatively a new field of application that has been explored using UAVs (Ha et al. 2018; Yurek and Ozmutlu 2018).

Blank et al. (2018) discussed about the UASs invading privacy of the public by unintended data collection about the individuals while continuously video recording the object under inspection. They also mentioned about the possibility of police-operated drones for crowd control causing noise disturbance during the

takeoff and landing to the habitants living nearby. They stressed upon the need for the UAS operators to obtain prior approval before recording the individuals, properties, and other privacy invading events. They called upon for all the UASs to have intelligent routing technology enabled by the sensors that automatically avoids flying above the location coordinates that are marked private (Blank et al. 2018). They quoted about DJI, a prominent UAV manufacturing company, having an inbuilt software in their UAVs compiled with the private area coordinates making them capable of avoiding those areas even without internet connection (Blank et al. 2018).

Blank et al. (2018) also provided the details about a website called NoFlyZones.org that had a compilation of names and addresses of property owners available for the participating UAV manufacturers. A privacy friendly UAS routing framework was developed involving the four players namely: system operators, service providers, citizens, and authentication service providers interacting with six modules. These modules include geospatial projection, data properties and storage, citizen authentication, recording property coordinates and privacy preferences, reducing the number of property coordinates, and flight path selection and calculation (Blank et al. 2018). These previous studies mark the shift from using UAVs for military operations to civilian related applications.

Federal Aviation Administration (FAA) in the United States had stipulated separate guidelines for flying different aircrafts operated manually and

autonomously. These guidelines were intended to minimize the risk and provide safety to all airborne vehicles. For now, the FAA mandates the operation of UAVs within the line of Sight (LOS) of Remote Pilot in Command (RPIC) to provide scope to see and avoid any potential aircraft flying within the path of UAV.

2.2 REMOTE SENSING AND PHOTOGRAMMETRY

Remote sensing is a non-invasive technique used to acquire information about any object. It requires sensors to remotely collect the data and can be performed via satellites, aircraft, or aerial vehicles. In recent decades, remote sensing has become a dominant tool in observing the earth's surfaces, using airborne and space borne equipment to rapidly detect any changes in infrastructure, physical features due to natural and man-made hazards, as well as performance-related changes (Hu et al. 2010; Rathje et al. 2006; Tripolitsiotis et al. 2014; Tronin 2009).

The advent of advanced technology in remote sensing has resulted in numerous new and improved techniques such as synthetic aperture radar (SAR), interferometric synthetic aperture radar (InSAR), satellite differential interferometry (DInSAR), satellite thermal imagery, light detection and ranging (LiDAR), and unmanned aerial vehicles (UAVs). The UAV is set up with a digital camera and uses non-invasive sensors to remotely collect sophisticated data on various infrastructures (Rathje et al. 2006; Suncar et al. 2013; Tripolitsiotis et al. 2014; Tronin 2009). In addition, powerful tools such as the Geographic Information Systems (GIS) can be used for organizing, analyzing, and presenting spatial image

data that is geographically referenced (Tim 1995). These high-quality images may be taken by using any of the available remote sensing techniques mentioned above.

Photogrammetry is a technique, which can measure distances from the data captured from two or more images without any direct contact with the environment. It is also referred to as the art, science, and technology of obtaining reliable information about physical objects and the surrounding environment through the process of recording, measuring and interpreting images and patterns of electromagnetic radiant energy and other phenomena (Ahmad and Samad 2010; Tahar and Ahmad 2012; Udin and Ahmad 2014). Developments in computer science and electronics have greatly influenced the progress of photogrammetry, and over time, this has led to its shift from analog to analytical and digital methods.

Oka (1998) provided the work on evaluating the feasibility of aerial photogrammetry to identify erosion. Aerial photogrammetry was used to study the formation, accumulation, and movement of eroded materials. Images were collected to characterize the materials near to the slope failure zones in steep mountainous areas. Ground control points were used to obtain reasonable accuracy in the measurements (Oka 1998). Traditionally observation piles were placed to measure the amount of erosion. Data obtained from photogrammetry results were compared with the field observations made from the observation piles. Oka (1998) concluded that the accuracy obtained from the aerial photogrammetry was sufficient to monitor active erosion zones in a region.

Mora et al. (2003) combined digital photogrammetry with global positioning systems (GPS) to measure movements of Ca' di Malta landslide, south of Bologna. GPS sensors were also placed within the actively moving landslide area and the other at a stable area to measure the relative movement between the sensors over a period of time. GPS measured points were used to orient the images collected from the aircraft. Digital photogrammetric techniques were used to develop digital elevation models (DEM) from the images collected. The combined approach was helpful in estimating the rate of landslide displacement as 10 cm/year (Mora et al. 2003).

Sturzenegger and Stead (2009) characterized the rock cuts involving terrestrial remote sensing techniques employing differential GPS, long-range reflector less total station, laser scanners and photogrammetry devices. These techniques offer a gateway to remotely inspect the inaccessible rock outcrops. Accuracy and precision of 3-dimensional models obtained from the photogrammetry devices were checked using eight points with known coordinates (Sturzenegger and Stead 2009). Accuracy of orientation measurements of eight locations in the 3-dimensional models were compared with the compass. Sturzenegger and Stead (2009) acknowledged that occlusion of a rock face area due to the shadows of the surrounding protruding features.

2.2.1 UAV-CRP Technology

Technology involving the distance measurement from image capture of an object using a sensor platform within a distance of less than 1000 ft (300 m) is classified as close-range photogrammetry (CRP). Adoption of UAVs for photogrammetry comes under the category of close-range photogrammetry (CRP) (Brooks et al. 2015; Colomina and Molina 2014; Puppala et al. 2018b; Siebert and Teizer 2014), referred in this study as UAV-CRP technology. Under most conditions, particularly for a large topographical area, photogrammetric techniques adopted using UAVs have proven to be inexpensive, and have provided solutions to land surveying methods (Ahmad 2006; Mills et al. 1996; Room and Ahmad 2014; Siebert and Teizer 2014; Udin and Ahmad 2014).

The three main components of UAV and CRP are the unmanned aerial vehicle, the ground control station (GCS) and the communication data link. This system can be controlled from the ground control station. The availability of the global positioning system (GPS) and gyroscope technology allows the UAV to precisely deliver the digital camera to the optimal location and altitude to capture the environment. In photogrammetry, it is a common practice to establish the ground control points (GCPs). There are several methods that can be used to establish GCPs and these include traversing and the GPS (Cesetti et al. 2011).

The data communication link consists of various communication mechanisms including the radio modems and microwave links and it ensures that a

continuous link stays active between the UAV and base station (Ahmad and Samad 2010). Airborne sensors can be mounted with a GPS/IMU (inertial measurement unit) system to assist in mapping the project area by using a series of base stations and a constellation of satellites providing positional information accessed by the aircraft GPS receiver (Ahmad and Samad 2010). Information obtained from GPS and IMU can be useful for mapping rugged terrains where limited ground control information is available (Ahmad and Samad 2010).

Due to its versatile nature, UAVs have become a popular tool for civilian tasks in the past couple of decades. Photogrammetry software tools can provide a digital elevation model (DEM) and a good quality digital terrain model (DTM) in a relatively short time using data collected from UAVs. The main advantages of UAV-CRP technology over traditional surveying techniques are its features of direct, rapid and detailed image capture of the study area. Adoption of UAVs for photogrammetry comes under the category of close range photogrammetry (CRP) (Colomina and Molina 2014; Siebert and Teizer 2014) and is referred in this report as UAV-CRP technology.

2.3 TRADITIONAL INFRASTRUCTURE MONITORING METHODS

This section introduces the background concepts needed for understanding the critical areas of infrastructure and the common methods that are being used for monitoring. The infrastructure assets include pavements, bridges, rail corridors, and construction materials.

2.3.1 Background

Infrastructure monitoring can be largely accomplished using various surveying equipment. Surveying is the science of defining the point's location on earth relative to the position of a known benchmark or datum. Distances and elevations with reference to the datum location are computed to estimate the horizontal and vertical position of the survey points, respectively. There are two types of surveys, geodetic survey that considers earth's curvature and plane survey that ignores earth's curvature (Skeen 2011). Normally geodetic survey cover large areas where considering earth's curvature is important for making accurate measurements and plane surveys are confined to reasonably small areas. Various surveying tasks include measuring distances, elevations, angles, topographic surveys, and recording filed works. Survey instruments for the intended purpose are selected by striking a balance between cost, required accuracy, and available time for executing the task (Skeen 2011).

Total station is an electronic instrument used for surveying the topographical features and measure lengths. GPS surveying depends upon different factors like sky visibility, cloud cover, satellite health and geometry, observation technique, and internet availability. It operates by sending and receiving radio signals to the nearest orbiting satellite constellation. Terrestrial laser scanners placed on stationary platforms collect the data by illuminating the object with light

rays and analyzing the time taken for the rays to return back. Mobile lasers also work on the same principle but with the platform in motion (Skeen 2011).

2.3.2 Pavement Forensics

Pavements form an integral part of infrastructure and its condition needs to be monitored frequently to identify distress. Pavement distress is defined as degradation of surface conditions or a decrease in the load carrying capacity of the pavement. It is divided into structural and functional distresses. Structural defects are due to insufficient bearing strength of pavements. Functional defects are mostly due to the uneven roughness of the pavement surface that causes an uncomfortable ride for the road user. These defects can be assessed and repaired by collecting pavement condition data. Pavement condition data includes the international roughness index (IRI) or present serviceability rating (PSR). McGhee (2004) pointed that all DOTs in the USA adopt automated means to collect the international roughness index (IRI) data on their road network (McGhee 2004). IRI is also obtained based on the quarter-car or golden-car math model that represents the typical behavior of most of the automobiles. It is measured by a computer algorithm that gives the response of a quarter-car model to the input longitudinal profile of the road as shown in Figure 2-1 (Sayers and Karamihas 1998).

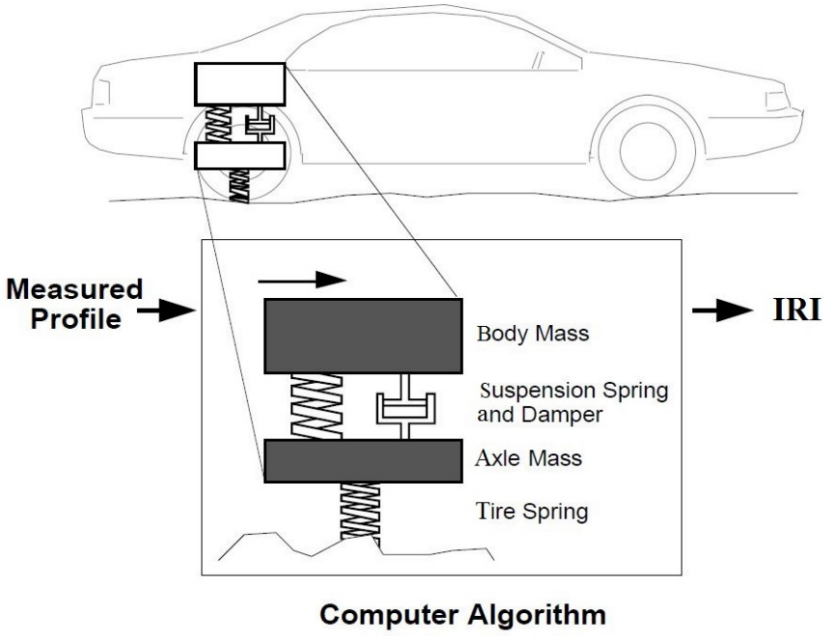

Figure 2-1. IRI Calculation (Sayers and Karamihas 1998)

PSR is determined based upon the rater's interpretation of safety and quality of ride. Considering the survey expenditure, PSR, rather than IRI, is estimated over the majority of road networks.

Carey Jr and Irick (1960) were the first to describe a detailed procedure for determining the present serviceability index (PSI) from the PSR, which was used during the American Association of State Highway Officials (AASHO) road test. It was conducted between 1958 and 1960 (Carey Jr and Irick 1960). Pavements were rated subjectively by a panel represented by all sections while the road agencies simultaneously collected road surface data. Eq. 1 presents the

mathematical formulation for calculated PSI based on roughness, cracking, and patching data obtained:

$$PSI = 5.41 - 1.80 \log (0.40R - 30) - 0.5 \sqrt{(C+P)} \quad \text{Eq. (1)}$$

Where R = Roughness Measure which varies depending on equipment used; C = % Cracking; P = % Patching

Hudson et al. (2015) asserts that the present serviceability index (PSI) is the objective form of the subjective present serviceability rate (PSR). PSI, unlike the international roughness index (IRI), represents the road user experience and can be easily perceived by the public (Hudson et al. 2015). A record of PSI over a period of time gives an idea about the pavement performance. The pavement distress features such as roughness, cracking, and patching need to be assessed to obtain the PSI value.

Cross slope can be defined as the rate of change in the height of the pavement in the transverse direction. Transverse profile data is expected to be collected according to the PP 70 standard of AASHTO (Collecting the Transverse Pavement Profile), which states that the Transverse Pavement Profile shall be collected by covering the entire section of the lane with a vertical resolution within 1 mm and data points spaced 10 mm apart across the lane. Data collected on the transverse section of the road shall have a maximum angular allowance of +/−5 degrees perpendicular to the centerline of the road (shown in Figure 2-2).

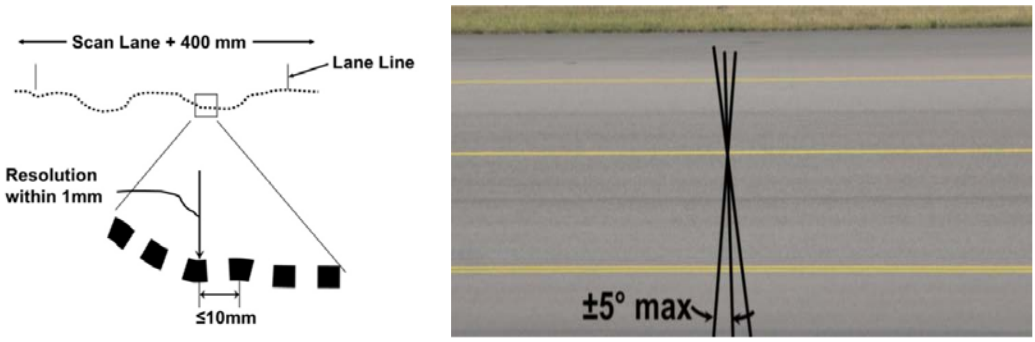

Figure 2-2. Transverse Pavement Profile Data Collection Standards (AASHTO Standard PP 70)

According to AASHTO Standard PP 69 (Determining Pavement Deformation Parameters and Cross-Slope from Collected Transverse Profiles), a cross slope can be deduced from the collected transverse profile by calculating the mean of the elevation of points on the two half-lanes. Slope of the line connecting those points is measured as cross slope.

For any road agency, accurate network-level road condition data is essential for making decisions related to repair and rehabilitation. Zhang and Murphy (2013) stated that many road agencies in the USA have developed their own pavement management systems (PMS) to preserve their road assets. TxDOT is one of the earliest agencies to adopt a PMS, dating back to 1982 (Zhang and Murphy 2013). After numerous revisions and upgrades of the PMS system, The TxDOT Pavement Management Information System (PMIS) emerged as the new PMS system in 1993. Ever since, PMIS has been evolving with continuing progress in computing and visualization fields. Zhang and Murphy (2013) have also stated that TxDOT

developed a web-based GIS system that provides color-coded details representing the condition of varied road sections.

PMIS uses the data from the ride and distress surveys in the calculation of the condition score of a given pavement. The condition score combines the distress score and ride score into a single value that corresponds to the average person's perception of pavement quality condition. The condition score ranges from 1 (very poor) to 100 (very good). Only 'Good or better condition' is defined as PMIS condition score of 70 or above. The percentage of good or better pavements is calculated by dividing the number of lane miles of pavements in good or better condition by the total number of lane miles in the system. The PMIS data set includes 100% of roadbed miles and the condition score is collected once a year. Due to cost and time limitations, road agencies rate one lane for each roadbed and considers this lane representative of all the lanes for the specific roadbed.

White et al. (2016) provided the framework required for developing a Pavement Maintenance Database System (PMDb) for the entire country. This database must be built by following nationwide consistent data inputting, reporting, and storing methods. This approach results in compiling of whole road network data and facilitates effective communication between state DOTs. They reported that most of the DOTs have detailed documentation regarding new pavement construction projects and major rehabilitation works, but lack the proper documentation of routine and preventive maintenance activities (White et al. 2016).

A good pavement condition can be maintained if preservation techniques are applied at the proper time as shown in Figure 2-3. Proposed pavement data elements that must be archived in the PMDb are as shown in Figure 2-4.

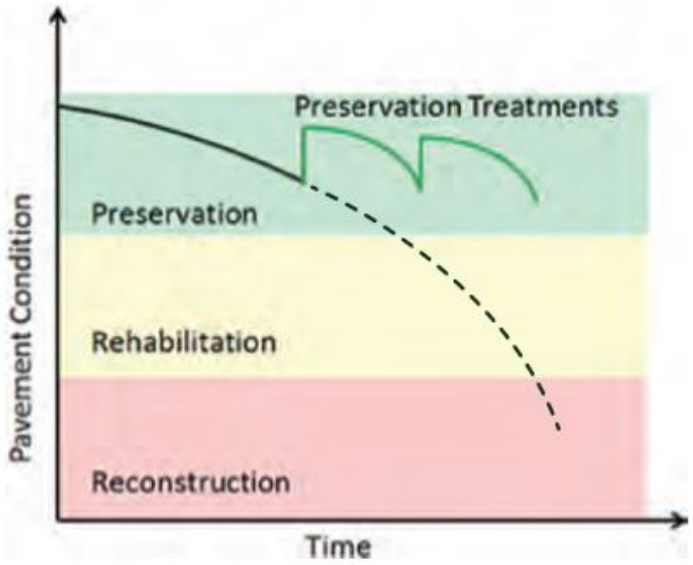

Figure 2-3. Effect of Preservation Treatments on Pavement Condition (White et al. 2016)

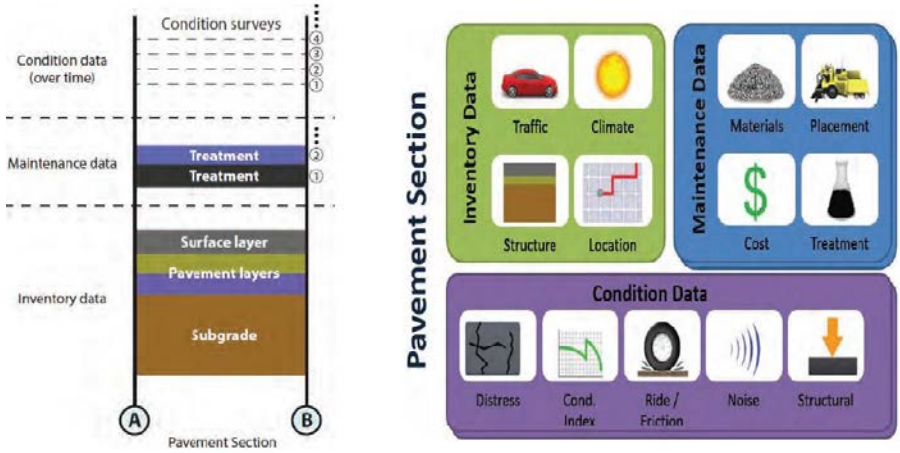

Figure 2-4. Pavement Section Data Elements (White et al. 2016)

2.3.2.1 Types of Monitoring Techniques

Pavement surface evaluation has evolved from conducting intuition-based methods to the state-of-the-art methods. They are classified into manual, semi-automated, and fully automated methods depending on the degree of human intervention involved and are summarized below.

2.3.2.1.1 Manual System

In this system, raters are employed to conduct a visual survey manually. The raters need to collect the surface data from the outermost lane in one direction if there are fewer than four lanes. Thus, the outermost lane is assessed in both directions for pavements having four or more lanes, and at times on the worst condition lane. Evaluating fewer lanes can prove to be cost effective in the short run but can also be costly considering the long-term performance of the pavement. Some minor surface distressed areas on the uninspected lanes have a tendency to accelerate the deterioration. Some of the road agencies identify pavement distress through visual inspection, except for rutting. A rut bar, as discussed below, is used to measure rut depth (Rater's Manual 2016).

A visual survey of a flexible pavement condition includes a collection of rut depths, potholes, patching areas, pavement cracking, raveling, and bleeding. Rutting information near wheel paths is collected over 0.1-mile segments with a minimum accuracy of one-tenth of an inch. Rut depth is measured by placing rut bar or a 6.0 ft. straight edge on the pavement, as shown in Figure 2-5a. Depending

upon the rut depth, rutting severity is classified as shallow (0.25-0.49 in.), deep (0.50-0.99 in.), or severe (1.00-1.99 in.). Pavement is considered a failure if the rut depth exceeds 2 in. (Rater's Manual 2016). Patched area is shown in Figure 2-5b.

(a) (b)

Figure 2-5. Pavement Condition (a) Severe Rutting (b) Patching (Rater's Manual 2016)

The presence of moisture in the pavement layers triggers potholes. According to the study conducted by the American Automobile Association in 2014, potholes contribute to one third of traffic fatalities. The patching area shown in Figure 2-5b represents the rectification of previous distress. Visual inspection identifies the degree of compaction of the replaced material and the condition of the full lane width overlay on it. Patching is measured in terms of feet for full lane width patching.

Cracking is classified into four groups: block, alligator, longitudinal, and transverse cracking, as shown in Figure 2-6. Block cracking is identified as a percentage of the lane's total surface area. Alligator cracking, a load related cracking, is expressed as a percentage of the total wheel path area on the inspected

lane. Longitudinal and transverse cracks having a minimum width of 1/8th inch and are expressed in terms of linear feet per 100 feet of the road stretch under inspection (Rater's Manual 2016).

(a)

(b)

(c)

(d)

Figure 2-6. Pavement Cracking Types (a) Block Cracking (b) Alligator Cracking (c) Longitudinal Cracking and (d) Transverse Cracking (Rater's Manual 2016)

Other distress problems include raveling and bleeding (Figure 2-7). Raveling is classified into low, medium, or high severity and is measured by expressing its area as percentage of the total lane area under inspection. Bleeding

also has the same severity rating levels as raveling but is instead measured by expressing the affected area as a percentage of the total wheel path area.

(a) (b)

Figure 2-7. Problematic Pavement Surfaces (a) Raveling (b) Flushing (Lanham 2018; Rater's Manual 2016)

A rigid pavement visual survey includes identification of spalled cracks, punch-outs, patches, faulting and other distress. The number of cracks in concrete pavement exhibiting spalling of minimum 1-in. width and 1-ft length are rated as spalled cracks. When a full depth block of continuously reinforced concrete pavement is separated, then the pavement is rated as a punch out failure. Two types of patches applied to concrete pavements are asphalt patch and concrete patch. Asphalt patches are rated as the number of 10 ft length patches whereas concrete patches are measured as the number of full-depth, full-lane width, and minimum 6 ft length patches in the concrete pavements. Concrete pavement is rated as faulted

or severely faulted when edges on either side of a crack have an elevation difference of 1/4th inch or 2 inches respectively (Rater's Manual 2016).

Ellenberg et al. (2014) also notes that some road agencies had adopted visual survey of pavements, which is often irreproducible and varies depending upon the experience of the inspector. Enhanced risk to the safety of inspectors while accessing high traffic areas contribute to the demerits of the manual inspection technique (Ellenberg et al. 2014). Many DOTs are moving towards semi-automated or automated procedures to collect pavement surface condition data.

2.3.2.1.2 Semi-automated System

A semi-automated system consists of software assisted by manual inputs. Pavement images and video data captured by automated inspection vehicles are reviewed by technicians on computer monitors to manually detect and assess pavement distress. It requires that the operator distinguishes and delineates the distress type, while the software calculates the distress areas (McGhee 2004).

Distress areas falling in the predefined wheel path areas facilitate the differentiation of load related and non-load related distress. A typical workstation (shown in Figure 2-8) used for the automated technology includes three monitors. The left monitor summarizes the distress data identified from images illustrated on the central monitor, while the right monitor simultaneously provides the forward view of the road under inspection. This workstation also features a special keyboard with keys allocated for the specific type and severity of various distresses under

consideration. The results vary depending upon the experience of raters who are subjected to challenging tasks of simultaneously observing the distresses and compiling the information into the rating software (McGhee 2004).

Figure 2-8. Typical Digital Workstation of Semi-Automated Methods (McGhee 2004)

Miller et al., (2003) described a system consisting of a digital line scan camera, a computerized controller, and an illumination system. Cracks as fine as 1 mm (0.04 in.) wide were identified at speeds up to 96 km/h (60 mph) using this system. Finer cracks were evaluated with human intervention, as the automated process is not efficient in detecting such minute features (Miller et al. 2003).

2.3.2.1.3 Automated System

Currently, many DOTs employ vendors to either collect or process the automated data needed to evaluate the performance of a pavement. Improved safety and data consistencies are some of the major benefits of the automated approach. McGhee (2004) noted a significant gap between the state-of-the-art and DOTs state-of-the-

practice automated evaluation techniques for both cracking and rutting measurements. Framework for conducting automated pavement cracking analysis is shown in the Figure 2-9. The two classes of automated data collection technologies are: 1) imaging technologies that require capturing and processing of pavement images and 2) sensing technologies that use various sensors to quantify the irregularities of the pavement surface.

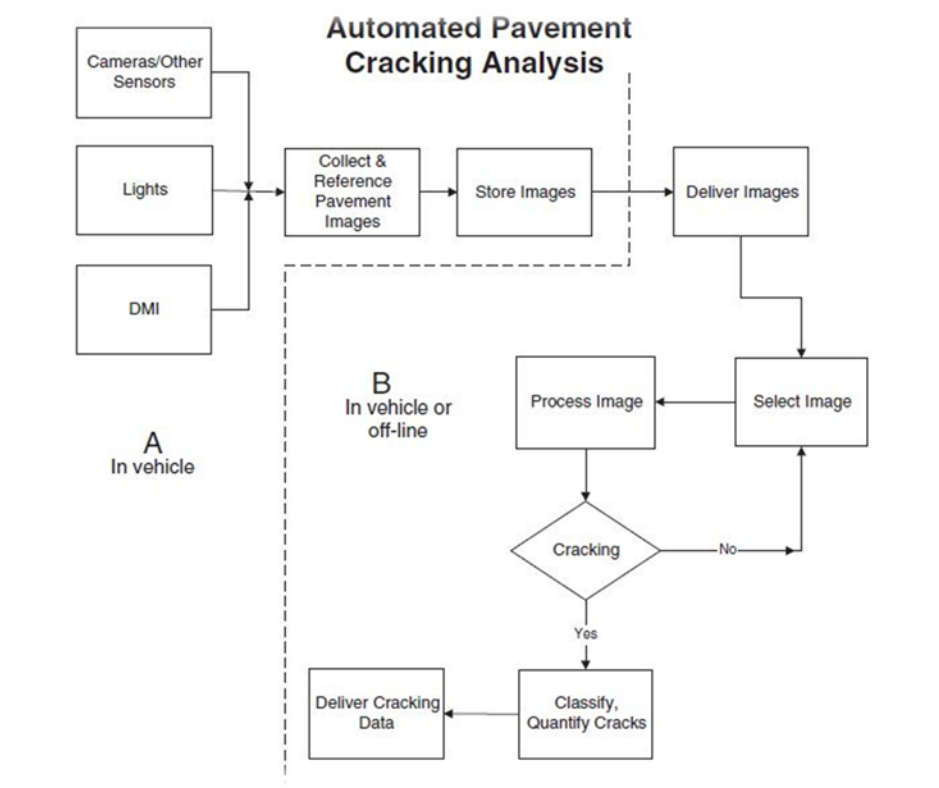

Figure 2-9. Automated Pavement Cracking Analysis (McGhee 2004)

Imaging technology requires an integrated roadway lighting system to allay shadows from the roadway features, vehicle, and equipment itself. Imaging may

result in a loss of resolution compared to the visual inspection carried out by the human eye. However, a well-equipped capturing system reduces this loss. Methods of pavement imaging include analog and digital methods. Much of the earlier pavement imaging work was carried out by an analog imaging process. It involved chemical or mechanical changes that resulted in physical imposition of images on a film. The analog method is now obsolete due to the additional time required for digitizing the analog images (McGhee 2004).

Digital imaging utilizes the electronic medium to capture and store images. High quality images that utilize automated data processing and analyzing places the digital imaging technique ahead of more cumbersome analog methods. Automated vehicles use a downward facing camera for assessing the pavement surface condition between the wheel paths, and additional cameras can be used based upon the DOT's requirement to capture right-of-way, shoulders, and other information. Shadows cast by the traffic, roadside features, and the survey vehicle conceals various features of the road surface. Hence, most of the data is collected by providing a sufficient light source during night time (McGhee 2004).

McGhee (2004) also proposed that digital imaging should facilitate random access to the database and help in discerning grayscale variations that represent the asperities on the road surface. Digital images of a pavement surface can be collected by area scan and line scan methods. The area scan method involves covering thousands of pixels, with the pre-defined pavement area usually one-half to a full-

lane wide and 10 to 16 ft long. The scanned data is used to obtain the image of pavement section. However, camera features and vehicle speed affect the image. Line scan cameras cover a single row of pixels. As the camera moves past the pavement section, a series of full pavement width transverse lines are captured and the pavement image is developed by stitching those lines together using a software program.

The sensing technology utilizes sensor signals to assess the condition of the road. The time it takes for a signal to travel from its incidence on a road surface back to the sensor helps in measuring the distance between the reference plane and pavement surface. These techniques collect the rut depth concurrently while monitoring roughness at the same intervals. Response type road roughness measuring systems (RTRRMS) were used for evaluating the roughness using meters mounted on vehicles. However, Cox meters may not be used as they measure the vehicle response to the pavement profile rather than its response to the pavement profile. Inefficiency in measuring the profile and huge investments encouraged the road agencies to opt for the cost effective profilometers, which measure the roughness of a road at high accuracy (McGhee 2004).

Buchinger and Silva (2014) stated that Google initiated a research on mapping potholes using GPS and a vertical accelerometer mounted on a vehicle. Mobile accelerometers detect vehicle shocks induced by potholes, and the GPS helps in geo-referencing the data (Buchinger and Silva 2014). Data collected is

expected to be refined and integrated with Google maps. The aim of pothole mapping is expected to assist driverless (autonomous) road vehicles. However, if successful, public road agencies will also benefit from this data while calculating ride quality.

Automated systems utilize digital recognition software capable of identifying and quantifying disparities in the grayscale image. Specific algorithms assist in relating these variations to striations or distresses on the pavement surface. Automated processing techniques employ digital recognition software capable of delimiting, quantifying and classifying distresses (Buchinger and Silva 2014).

Yu (2011) discusses various steps involved in automated image processing techniques. Fundamental steps of image processing involve image acquisition, preprocessing, segmentation, representation, description, recognition and interpretation (Yu 2011). Thresholding is a prominent segmentation technique that is being used. Several researchers have developed various thresholding algorithms to divide an image. Roadware Group developed the WiseCrax crack detection system to classify cracks. WiseCrax consists of three algorithms dedicated to crack detection, classification and rating (McGhee 2004). Initially, detection parameters for cracks were generated by comparing crack maps with the grayscale pixel variation contributed by crack contrast, brightness, and surface conditions. After assigning optimal detection parameters to the pavement, cracks can now be automatically detected by the system. Using automated pavement distress systems

enables many reliable and reproducible results to be obtained while cutting down the processing time, which in turn reduces expenditures.

2.3.3 Bridge Inspection

Bridge consists of super structure and sub structure elements that need to be monitored regularly to maintain its working condition for longer period. Super structure elements comprise of bridge deck, approach slab, railings, and joints. Sub structure elements comprise of beams, soffits, bearings, wing walls, abutment, pile and cap. Different distress parameters like spalling, rusting, joint movements, efflorescence staining, and others need to be identified during the biennial inspections. Inspecting most of the bridge elements apart from the deck requires additional equipment like a snooper truck to reach the hard-to-reach areas. These procedures often result in high expenditure along with increased traffic restrictions resulting in delay cost. There is also considerable risk involved while a worker is involved in such hazardous situations.

Bridge approach settlements has been a major concern for many DOTs over the last few decades. Several millions of dollars were spent to rehabilitate and restore the integrity of the U.S. bridge infrastructure. According to a 2016 fiscal year report on Texas bridge infrastructure, TxDOT has spent $525.1 million on system bridge maintenance, bridge replacement and rehabilitation, as well as construction of new-location bridges (TxDOT Bridge Division 2016). Of that amount, 46% of funds were spent on bridge maintenance, bridge replacement and

rehabilitation. The performance criteria of a bridge infrastructure depend on several components where bridge approach foundation settling is one of the major concerns. Approximately 25% of the 600,000 bridges in the United States have encountered the bump problem and millions of dollars were spent annually for the repair costs (Thiagarajan et al. 2010). Figure 2-10 illustrates different factors that can lead to the bump problem.

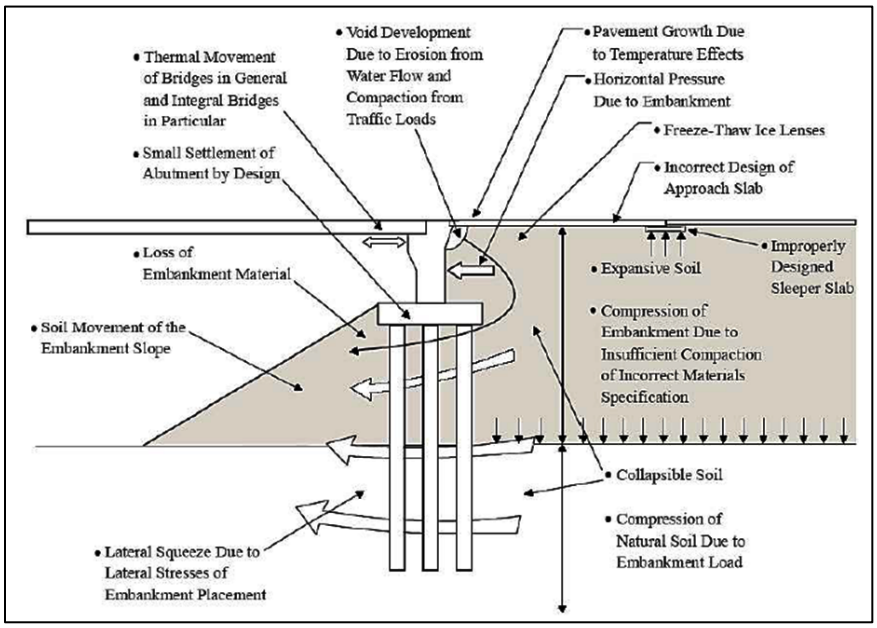

Figure 2-10. Different Factors That Lead to the Formation of Bump Problems (Briaud et al. 1997)

In the last decade, extensive studies were performed to understand the primary causes of differential settlement at the bridge approach slabs (Briaud et al. 1997; Horvath 2005; Kramer and Sajer 1991; Puppala et al. 2009). The primary factors include poor soil compaction, soil erosion, water infiltration beneath the

pavement, development of voids, and settlement of backfill material due to excessive overburden pressure.

Several techniques, such as excavation and replacement of fill material, deep soil mixing (DSM) columns, geosynthetic reinforcement, mechanically stabilized earth (MSE) wall, lightweight EPS Geofoam replacement, effective drainage and erosion control methods, were recommended and evaluated to mitigate this problem (Abu-Hejleh et al. 2006; Bartlett et al. 2000; Dupont and Allen 2002; Farnsworth et al. 2008; Horvath 2005; Hsi 2008; Jutkofsky et al. 2000; Negussey and Stuedlein 2003; Newman et al. 2009; Puppala et al. 2008; Seo 2005; Stark et al. 2004; Tadros and Benak 1989; Wahls 1990; White et al. 2007). To ensure the performance of rehabilitated bridge structures, extensive monitoring programs are required. Structural health monitoring and performance evaluation plays a pivotal role in assessing the condition of a bridge infrastructure project. Visual evidence and in-situ instrumentation are two prevalent monitoring approaches that are extensively used to evaluate an infrastructure performance.

Visual inspection is one of the most basic forms of forensic survey. This approach provides us quick visual evidence of the condition of an infrastructure. However quantifying settlement or any other pavement distress using visual surveys depends on operator perception. There are two inspections that involve examining bridge deck and underneath the bridge.

The bridge deck can be inspected using various equipment. A total station survey is the most commonly used survey that can quantify the settlements at a bridge infrastructure by determining the change in the elevation levels with respect to different time periods. Profilometer survey is another approach that can provide the profiles taken along a line perpendicular to the traffic direction to show the super elevation and crown of the road design, rutting, and other distress shown in Figure 2-11 (Sayers and Karamihas 1998).

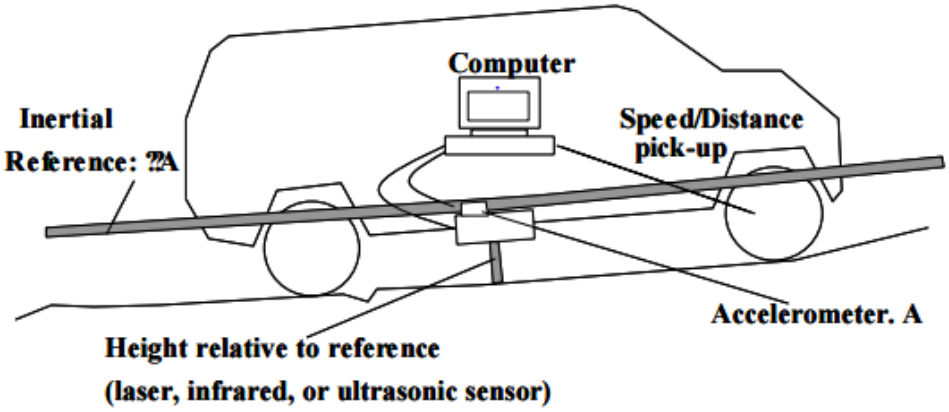

Figure 2-11. Conceptual Working Mechanism of Profilometer (Sayers and Karamihas 1998)

Ground Penetrating Radar (GPR) is a non-destructive method that can present the features of a subsurface profile (Gehrig et al. 2004). Researchers have demonstrated the usefulness of this method in determining the distress in pavement infrastructure and in attempting to detect the voids. Another effective approach is in-situ instrumentation, such as horizontal inclinometers. The general definition of

an inclinometer is a device that is used for monitoring deformations of surfaces or subsurface in a direction perpendicular to the axis of a flexible plastic casing by means of passing a probe through the casing. It can be clearly understood by the definition that the typical application of a horizontal inclinometer is to measure the settlement and/or heave under storage tanks, dams, and embankments (Archeewa 2010). The horizontal inclinometer generally consists of seven components: inclinometer casing, horizontal probe, pull-cap, pull cable, dead-end pulley, control cable, and readout. However, these methods represent the performance of the entire infrastructure based on measurements obtained at limited locations. Despite the accuracy in the measurements, the reliability of the data over the entire site is not appropriate as the failure can be triggered at any location.

Current under-bridge inspection methods include various practices to access the unreachable areas of the bridge. Aerial work platforms (AWP) such as snooper trucks, lifts, or bucket-trucks assist in inspecting the under bridge elements. However, they have the disadvantages like high mobilization costs, unsafe for the inspector, and traffic delay costs arising out of lane closures. Apart from AWPs, rope access is another common form of inspecting the under bridge elements (shown in Figure 2-12). Despite of having lower equipment and traffic delay costs, rope access is highly dangerous for the inspector and requires rigorous training (Wells et al. 2017).

Figure 2-12. Rope Access Inspection (Wells et al. 2017)

One recent advancement that have proven effective for monitoring the performance of bridge infrastructure is through remote sensing based studies. The University of Texas Arlington research team is currently using light detection and ranging (LiDAR) to monitor the performance of a rehabilitated bridge infrastructure located in Johnson County, Texas (Shafikhani et al. 2017). LiDAR is a remote sensing technique used to collect surficial information from an object or phenomena without direct physical contact (Aggarwal 2004; Campbell and Wynne 2011). Due to its ability to deal with large monitoring areas, it is considered as an effective alternative to other monitoring techniques where safe access to the inspection area is a concern (Manconi et al. 2014). The basic principle of this technique consists of projecting a laser light from the scanner onto the material

surface via a rotating mirror, thereby capturing the reflected laser beam pulses from the surface. During this process, a set of data points referred to as the “point cloud” is generated in 3D space. Based on the unabsorbed wavelengths of laser light at each point on the surface, physical features of target points such as distance, color, and reflective intensity can be recorded. For example, settlement or heave would be the vertical component of the total displacement vector of a target point.

2.3.4 Rail Corridor Inspection

Rail corridors are mostly inspected for various distress like rail buckling, improper rail and tie alignment, washout underneath the rails, debris accumulation, rusting of rails, and others. These inspections warrant hi-rail trucks equipped with costly laser scanners. They also result in substantial delays for freight and passenger trains travelling through the inspection zone. Many state-of-the-art aerial technologies that are being used for monitoring rail corridors are provided in the subsequent sections.

Washout occurs when a flood or a flash flood washes away the ballast and roadway under the track. Figure 2-13a illustrates a typical washout on the railway line. Rail tracks are made of steel and they expand as they heat up in warm climates, especially during the daytime. This expansion of rail tracks induces strong compression and may lead to buckling (Figure 2-13b). To repair track buckling, the line must be closed and this causes delays and disruption. UAVs can be deployed quickly to inspect rail buckling on tracks by collecting pertinent data remotely.

(a) (b)

Figure 2-13. Rail Track Condition (a) Typical Washout on the Rail Line (Lamb 2005) and (b) Typical Buckling of Rail Track (Kish et al. 2003)

Debris can collect on rail tracks and accumulate with time, especially in unmonitored remote areas, causing rail derailments (Figure 2-14). In areas where the rail track is laid through forests with a high density of trees, it is likely that old trees might fall on tracks and create situations that can only get worse. This is especially common in when trees are subject to the high winds associated with storms, hurricanes, and tornadoes. Although we cannot control natural hazards from occurring, there needs to be an economical way to identify debris accumulation quickly so the proper personnel can be notified in time to prevent derailment (RAIU 2010).

Figure 2-14. Train Derailment Due to Debris on Track (RAIU 2010)

Recently, Sam Inc. and TxDOT Austin District collaborated for trial studies to survey a section of a public rail line using a mobile LiDAR system (Figure 2-15). As a part of this research, they mapped asset inventory along 32 miles of rail track, including sidings and rail yards (Leslar et al. 2009).

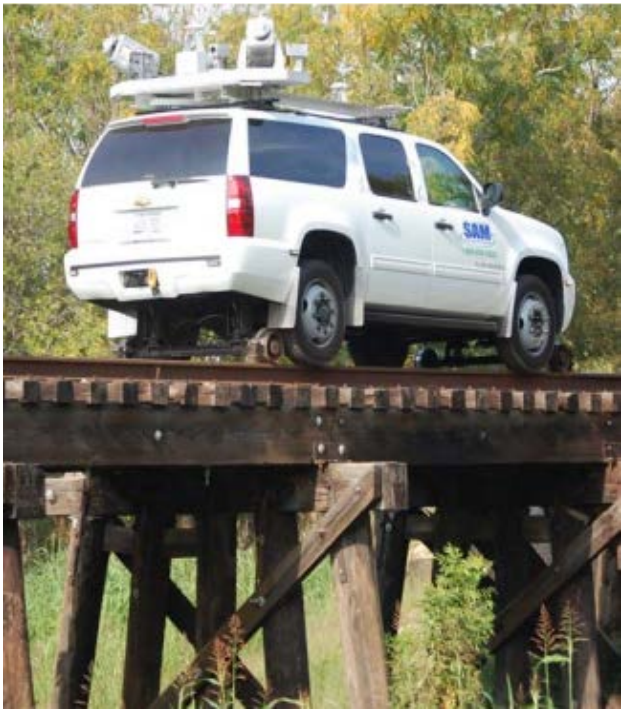

Figure 2-15. Mobile LiDAR to Survey a Railway Line for Asset Inventory (Leslar et al. 2009)

Traditional rail bridge inspection consists of a hands-on visual observation with a qualified inspector, operator, and other crew members. Safety equipment, ladders, and under-rail bridge inspection vehicles are used to inspect the inaccessible railway bridge parts. Heavy and costly under-bridge inspection units are needed, and they are mostly rented for inspection and maintenance work.

For instance, Figure 2-16a shows A-30 Hi-Rail equipment and Figure 2-16b shows A-30y bridge inspection units (N.E. Bridge Contractors 2016). During bridge inspections, inspectors must work closely above, below, or alongside the bridge with safe maneuvering. The heavy equipment needed to make traditional

bridge inspections possible are likely to obstruct road traffic and induce the need for traffic control. On the other hand, remote collection of similar information via deployment of UAVs is a safe option.

(a) (b)

Figure 2-16. Rail Bridge Inspection Using the Under-bridge Inspection Unit: (a) A-30 Hi-Rail Equipment and (b) A-30y Hi-Rail Equipment (N.E. Bridge Contractors 2016)

2.3.5 Construction Materials

Inventory of construction materials is important in planning the steps in building an infrastructure asset. Traditional surveying equipment like theodolite, total station, and differential GPS are being used to collect the 3-dimensional coordinates of points over the stockpiles and then interpolate the coordinates between the collected points to estimate the volumes. It can be clearly observed that these techniques can only obtain an approximate value of the volume measurements due to their inability to recreate the original irregular stockpile surfaces existing in the field. New technologies like terrestrial LiDAR and smartphone cameras are also

used to obtain the volumes by collecting the data around the stockpiles. These are able to capture the irregular surfaces, however, due to their inability to capture the top irregular stockpile surface deems them unfit for accurate volume computation of stockpiles that are tall and wide.

All of the above information suggest that there is a need for devising a new methodology that can complement the present methodologies with quick, efficient, and accurate data in a safe manner.

2.4 US DOT AGENCIES' EXPERIENCE WITH UAS

In March 2018, American Association of State Highway and Transportation Officials (AASHTO) conducted a survey among various state departments of transportation (DOTs) in the United States about the usage of unmanned aerial vehicle systems. The response was unprecedented as 35 out of 44 DOT respondents have approved using UAS for wide range of applications (Tony 2018). The survey reported that twenty DOTs have incorporated UAVs into various daily applications and fifteen DOTs have been researching about setting up standards and protocols to be adopted in addition to safety precautions during aerial data collection methods (Tony 2018).

UAV data collection methods complementing traditional methods is gaining popularity as more agencies are researching the drone and its innovative applications. Alaska, Arizona, Colorado, Delaware, Georgia, Iowa, Maine, Mississippi, Montana, Nebraska, Nevada, New Jersey, North Carolina, Ohio,

Oklahoma, Oregon, Pennsylvania, Tennessee, Utah and West Virginia are the twenty departments of transportation (DOT) using for their daily tasks (Tony 2018). Photography and surveying of the construction site, bridge inspection, traffic and pavement monitoring, tall light pole inspection, and emergency operations are the most common applications reported by these twenty active DOTs in UAS deployment Alabama, Connecticut, Idaho, Illinois, Indiana, Kansas, Kentucky, Louisiana, Massachusetts, Michigan, Minnesota, New Hampshire, South Carolina, Texas, and Virginia are the fifteen DOTs researching the feasibility of UAS applications as part of their daily tasks (Tony 2018). More recent developments in the research and applications of UAV by different DOTs are provided in Table 2-1.

Table 2-1. Latest Developments in UAV Studies Performed by Various Department of Transportations (DOTs) in USA

No	Department of Transportation (DOT)/ Agency	State Agencies and DOT Experience
1	North Carolina Department of Transportation (NCDOT)	In 2017, NCDOT conducted a joint study along with the North Carolina Highway Patrol to compare traditional and UAS methods in collecting the crash scene data. They realized a saving of 1.5 hours by using three drones compared to the traditional data collection methods adopted by the highway patrol Collision Reconstruction Unit. They also estimated that using a drone to collect the crash scene data on a busy highway would result in a saving of around $9,300 (Tony 2018).
2	Missouri Department of Transportation (MoDOT)	MoDOT is yet to embrace the UAS technology, Lercel et al. (2018) conducted an overview of using UAS for Missouri and reported that the bridges in the state of Missouri are typically inspected once in every two years in accordance with Federal Laws. The report stated that the 3,000 out of 24,000 bridges are structurally deficient bridges in Missouri

		might need more frequent inspections that result in high expenditure caused due to the frequent inspection costs, traffic disruptions, and safety risks (Lercel et al. 2018).
3	Iowa Department of Transportation (IDOT)	After FAA released the new Part 107 regulations, three employees in the aviation group of IDOT had obtained remote pilot certificate issued by FAA. IODT's aviation group purchased two DJI Phantom 4 drones and assisted other divisions within the DOT in capturing the assets (Lercel et al. 2018).
4	Kansas Department of Transportation (KDOT)	McGuire et al. (2016) addressed different ways in which KDOT could get benefitted by using UAS for different applications (McGuire et al. 2016). For the first time in the United States, KDOT partnered with AirMap, Inc. to ensure safer skies by integrating the unmanned aerial traffic into the national airspace through Unmanned Traffic Management (UTM). UTM implements airport notification and awareness system for UAS operators. KDOT's UAS director has founded Kansas UAS Joint Task Force (JTF) that is responsible in developing statewide protocols necessary for UAS integration (Lercel et al. 2018).
5	Minnesota Department of	Minnesota Department of Transportation (MnDOT) teamed up with external vendors to use UAS as a bridge inspection tool. They suggested using UAS for inspecting the bridge structural elements that do not need hands-on approach. MnDOT used SenseFly Albris

	Transportation (MnDOT)	drone that has a capability to fly under John A. Blatnik Bridge in Duluth, MN and inspect the elements above it. Subsequently traditional methods were used to inspect the bridge and compared with the UAS method. They estimated that UAS inspection would take 5 days compared to 8 days of traditional bridge inspection monitoring, which also contributed to more than 50 percent savings using UAS (Wells et al. 2017). MnDOT also conducted another bridge inspection in Nielsville, MN to detect the delamination using a thermal camera mounted on the drone (Wells et al. 2017).
6	North Dakota Department of Transportation (NDDOT)	NDDOT is also one of the 10 selectees of UAS-IPP program and assigned the task of evaluating the night time and beyond line of sight operation of UAS in airspaces ranging from rural to urban areas (IPP 2018).
7	Alaska Department of Transportation (AlaskaDOT)	Alaska DOT is using UAS for various daily activities like measuring elevations and stationing of culverts, in addition to monitoring massive stockpiles of road-building (Bohman 2018).

8	Arizona Department of Transportation (ADOT)	ADOT is using drones for conducting surveying works and inspecting hard-to-reach bridge areas. Although bridge inspections are conducted by the traditional methods, inaccessible data is being supplemented by UAS inspection. ADOT has already inspected a roadway damaged due to storm runoff using drones. Under a new federal grant, eight new aerial drones are added to the aviation division of ADOT. These are planned to assist the DOT personnel in monitoring highway projects thereby ensuring efficiency and safety. The DOT employees need to be undergoing training on safely using drones before inspecting state highways passing through hazardous areas (ADOT 2018).
9	Colorado Department of Transportation (CDOT)	Bly (2016) reported that CDOT had been using drones for inspection since 1990s that include assessment of rock fall sites (Bly 2016). CDOT had made an agreement with external drone operators to work on their next 5-year projects that require aerial inspection (CDOT 2017). This agreement was intended to cut down the request for proposal time for any project that requires drone inspection in the next five years. CDOT intends to use the drones for crash scene reconstruction, bridge inspection, and rockfall assessment by providing safety to the working personnel and the public. Rubino (2018) also reported that

		CDOT is embracing drones for their construction site inspection due to its cost effectiveness (Rubino 2018).
10	New Hampshire Department of Transportation (NHDOT)	NHDOT collaborated with the University of Vermont Spatial Analysis Lab to research the potential transportation sector applications of UAS technology. The applicability of the unmanned aerial technologies for various NHDOT activities including monitoring of construction sites, traffic, bridges, rock slopes, and accident scene reconstruction has been the objective of this project. Cost analysis and comparison of UAS operations with conventional methods are also planned as part of this ongoing research project (NHDOT 2018).
11	Georgia Department of Transportation (GDOT)	Based on Georgia Tech's study on possible applications of UAS for GDOT, the agency intended to use the aerial technologies for monitoring traffic on roadways. Vehicle speed and congestion monitoring, in addition to traffic signal inspection are some of the prominent uses of drones identified by the researchers at Georgia Tech. It was also reported that GDOT would outsource the drone activities to external vendors (GDOT 2014).

12	Ohio Department of Transportation (ODOT)	ODOT teamed up with commercial drone partners to inspect Sandusky River Bridge on the Ohio Turnpike. It was reported that the drone was able to provide comprehensive bridge inspection data before crashing in to the water due to a power loss (Christ 2016).
13	Maine Department of Transportation (MaineDOT)	MaineDOT contracted the aerial inspection of Max L. Wilder Memorial Bridge in Arrowsic-Woolwich, Maine to external vendors. A drone capable of mounting a top gimbal attached to a camera capable of taking pictures above it. MaineDOT also inspected the signboard truss on a road using UAS. Application of UAS for bridge inspection will not only save the reposition time but also provide safety to personnel compared to the traditional inspection methods (MaineDOT 2016).
14	Mississippi Department of Transportation (MDOT)	Chaney (2018) reported that Mississippi DOT intend to use the drones as an eye in the sky to monitor infrastructure assets. Bridge inspection and emergency response are the two main applications of UAS used by Mississippi DOT (Chaney 2018).

15	Montana Department of Transportation (Montana DOT)	Montana DOT has demonstrated the usability of drones in inspecting roads in extreme conditions. During spring 2018, Beartooth Highway, Montana located in a hilly terrain was covered with snow. Montana DOT conducted a reconnaissance study of the mountain using drones to estimate the amount of snow that they might encounter (MontanaDOT 2018).
16	Nevada Department of Transportation (NDOT)	The imagery section of Nevada DOT, composed of staff with previous work experience as military analysts, researchers, and private consultants, initiated a program involving unmanned aerial vehicle systems to support their Hydraulics, Stormwater, Design Engineering, and Construction divisions. They have a four person team, including 2 Part 107 pilots and 2 ASPRS certified mapping scientists, using a fixed and rotary wing platforms to generate point clouds, orthomosaics, and various other mapping products. Nevada DOT is also planning to collaborate with academic universities to estimate the change in sediment detection and road condition using UAS works (Stevens 2018).
17	New Jersey Department of	The introduction of drones into NJDOT has been done in a structured manner starting with appointment of a UAS coordinator within the Aeronautics division of NJDOT to lead UAS operations. NJDOT applied for three FWA grants that are directly and indirectly related to

	Transportation (NJDOT)	the usage of drones within the agency applications (Stott and Tadmori 2018). Traffic incident management and congestion assessment, infrastructure inspections, and emergency response are some of the UAS applications that NJDOT is planning to explore. Ease in deployment, low carbon footprint, and less manpower using UAS are acknowledged by the Stott and Tadmori (2018).
18	Oregon Department of Transportation (OregonDOT)	Gillins et al. (2018) stated that State transportation agencies can leverage the cutting edge unmanned aerial technology to make the inspections more efficient and cost effective in a safe manner. They focused on developing safe guidelines for Oregon DOT to adopt in conducting bridge and tower inspection using drones. A benefit- cost ratio for conducting bridge inspection using UAS was obtained as 9 with an average cost savings of $10,000 per bridge inspection (Gillins et al. 2018).
19	Pennsylvania Department of Transportation (PennDOT)	Pennsylvania Department of Transportation (PennDOT) had purchased a rotary wing UAV, Dragon Flyer X-4, and used commercial software to acquire images of rockslides and sinkholes before grounding the operations. Bureau of Aviation division in PennDOT had conducted survey of government agencies in Pennsylvania and reported that atleast six agencies anticipate using UAS in the future (Wojtowicz et al. 2017).

20	Delaware Department of Transportation (DelDOT)	All the public agencies in Delaware train their pilots to same level and use the same aerial platform. This facilitates interagency transfer of pilots and aerial platforms during different conditions. DelDOT UAS crew includes a FAA certified pilot and a visual observer. The pilot needs to perform ten basic maneuvers before being appointed as DelDOT certified pilot. DelDOT have nine FAA certified pilots and nine quadcopter UAS platforms (Day et al. 2017). DelDOT used the drones for monitoring the construction of bike bridge and road crash scene inspection. DelDOT also plans to acquire UAVs accommodating top gimbal and tethering.
21	Utah Department of Transportation (UDOT)	Barfuss et al., (2012) evaluated the applications of UAV for Utah Department of Transportation. UDOT used UAV for monitoring various stages during the construction of Southern Parkway street. The images were processed and the models developed were inputted into UDOT GIS database. UDOT also mapped the locations of culverts under roadways using UAVs (Barfuss et al. 2012).
22	Connecticut Department of	CTDOT planned to conduct inspection of 1-mile stretch Gold Star Memorial Bridge using UAVs. The inspection was intended to gauge the ability of drones in accessing the hard-to-reach areas (CTDOT 2015; Lillian 2016).

	Transportation (CTDOT)	
23	Illinois Department of Transportation (IDOT)	Linda and Bill (2017) presented the information about the role of UAS in Illinois Department of Transportation operations. Surveying, infrastructure inspection, and visual photography/videography are some of the main UAS applications identified by IDOT. They intend to inspect critical infrastructure to obtain baseline inventory information before and after any incident (Linda and Bill 2017).
24	Michigan Department of Transportation (MDOT)	Michigan technological research institute evaluated the usage of drone for various transportation infrastructure monitoring purposes including pavements, bridges, and other related applications (Brooks et al. 2015).
25	Massachusetts Department of Transportation (MassDOT)	Ni and Plotnikov (2016) conducted research to establish the prevailing practice of UASs in transportation. A survey among the DOTs was conducted to understand the practicalities of using drones for DOT purposes. Basing on the collected information, they classified asset management, disaster management, inspection of construction site, and identifying traffic

		parameters are some of the prominent applications of UAS that MassDOT could explore (Ni and Plotnikov 2016).
26	Texas Department of Transportation (TxDOT)	UT Arlington evaluated the initial applications of UAVs for monitoring infrastructure assets including pavements, bridges, rail lines, and tall structures. A flight operations manual to be adopted while conducting drone data collection has been developed by TxDOT (Puppala et al. 2018b).

In addition to the latest developments in the UAV related studies conducted by US DOTs provided in Table 2-1, there are also other notable researches that were conducted in the past decade as follows.

Kansas State University conducted a literature review, survey, and SWOT (strengths, weaknesses, opportunities, and threats or challenges) analysis for the Kansas Department of Transportation (KDOT) on potential benefits of using UAV in their operations (McGuire et al. 2016). They recommended UAV applications for bridge inspections, radio tower inspections, surveying, road mapping, high-mast light tower inspections, stockpile measurements, and aerial photography. Their studies suggest that using UAV-based techniques could result in improved safety, efficiency, and possible reductions in cost. As their studies also compared the cost of using an external agency to collect images versus using UAV imaging technology and observed a potential cost benefit using UAV technology (McGuire et al. 2016). Moreover, the Kansas DOT (2016) has started a fairly new Kansas Unmanned Aerial Systems Program to use UAVs in performing bridge and tower inspections (Hill 2016).

Michigan Department of Transportation (MDOT) worked with the Michigan Technological Research Institute (MTRI) in a research study to detect pot holes on unpaved roads, conduct bridge and pump inspection, and monitor progress of ongoing construction (Brooks et al. 2015). The University of Vermont collaborated with the Vermont Agency of Roads on a USDOT grant to conduct a

UAV study to monitor rivers to prevent flooding and damage to roadways (Asphalt Institute 2016).

In August, 2013, the State of North Carolina approved a test UAV program at North Carolina State University. Later, in March 2014, NCDOT presented a report on unmanned aircraft in response to the legislative request that included coordination with the CIO and Aviation Division. The program lists several areas that will benefit from UAVs including agriculture, surveying, wildlife monitoring, state infrastructure monitoring, migration monitoring, and emergency management (Estes 2014).

In 2013, the North Carolina state legislature have granted the authority for managing statewide drone operations to the aviation division of its state DOT. NCDOT have been reported as the pioneers of using the UAS among the DOTs. Some of the NCDOT staff have been trained on using the drones for their daily operations thereby providing a scope for the staff to come up with new application areas for drone technologies (Tony 2018).

A study by Hurwitz et al. (2018) presented their work for Oregon DOT in assessing the driver distraction due to drones. They conducted the effect of lateral offset, flight path, and land use on the driver distraction. Due to the less visual clutter in rural areas, the researchers noticed more drivers crossing into the adjacent lane in response to spotting a drone operation. They acknowledged that the farther

the drone operations are from the right of way the fewer are the unsafe glances (Hurwitz et al. 2018).

2.5 UAV APPLICATIONS IN CIVIL ENGINEERING

Federal government initiatives and research conducted by NASA in building military drones paved the way for using unmanned aerial vehicles (UAVs) for various civil engineering applications. Modern image capturing equipment provided the impetus for conducting real time mapping, surveying and monitoring of assets. The ability to remotely monitor and detect physical features in infrastructure is of great value to civil engineers. The UAV can identify features including distress in pavements, roads, rail bridges, and movement of slopes and embankments among other possibilities. Failure or delays in identifying such distress could result in injuries, risks, or loss of human lives. In addition to the DOTs related UAV work discussed in the earlier sections, there are also other agencies and researchers that conducted research on various UAV related applications that are covered below.

Rathinam et al. (2008) conducted fixed wing UAV-based monitoring of linear structures such as roads, pipelines, bridges, and canals. Linear structures were detected by visual recognition techniques controlled by a closed loop algorithm (Rathinam et al. 2008). Zongjian (2008) conducted low altitude UAV surveys using a lightweight wide-angle camera assembly comprised of four digital cameras arranged as shown in the Figure 2-17a. The arrangement facilitates a larger view of

the area at low altitudes. Overlapping of the images (shown in Figure 2-17b) helped to orient the images (Zongjian 2008).

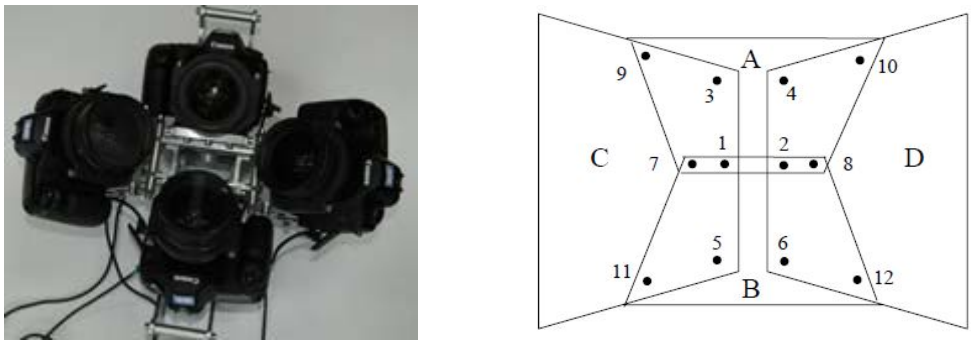

(a) (b)

Figure 2-17. Image Data Collection (a) Super-Wide-Angle Camera Assembly (b) Overlapping Images Projected from the Four Camera Data (Zongjian 2008)

Steffen and Förstner (2008) discussed the benefits of UAV mapping carried out with the help of real time surface information. The real-time feedback adjusts the flight trajectory to cover the whole area under consideration (Steffen and Förstner 2008). Fu et al. (2015) developed a method to support autonomous flight of the Asctec Pelican quadrotor UAV in the absence of GPS. It includes camera calibration, visual feature detection and tracking of consecutive images. The UAV is equipped with a stereovision pre-processing system that processes the visual information and transfers it to the on-board host computer. Based upon the real-time built environment and obstacle detection, the flight path is dynamically adjusted to collect the required data (Fu et al. 2015).

Zhang (2008) demonstrated a system using a low-cost model UAV having an onboard GPS. Flight assembly is powered by a 26 cc, single cylinder, Zenoah G260H engine capable of generating 1940 W at 12,000 rpm, giving an operating head speed of approximately 1250–1500 rpm. The UAV had a flight time of 30 minutes with full payload of 6.4 Kg. A UEye 2220c USB video camera was used for capturing data. The combination of the automatic flight control system (AFCS) hardware and mission control system (MCS) software assisted in autonomous control and navigation during flight (Zhang 2008).

Eisenbeiß (2009) demonstrated that an autonomously controlled UAV is more stable than a manually operated UAV. The elevation models developed from laser and image data were compared. He envisaged developing digital surface models by using LiDAR and image data collected simultaneously. The combination of dense point clouds generated by LiDAR data and texture mapping by image data offered detailed information about the area under inspection (Eisenbeiß 2009).

Figure 2-18a shows an aerial photograph of the University of Technology, Malaysia (UTM), main campus, acquired using a digital camera placed under the wing of an UAV. The collected series of aerial photographs with an approximate 60% longitudinal overlap and 30% lateral overlap were assembled to form a single image known as an uncontrolled mosaic (shown in Figure 2-18b).

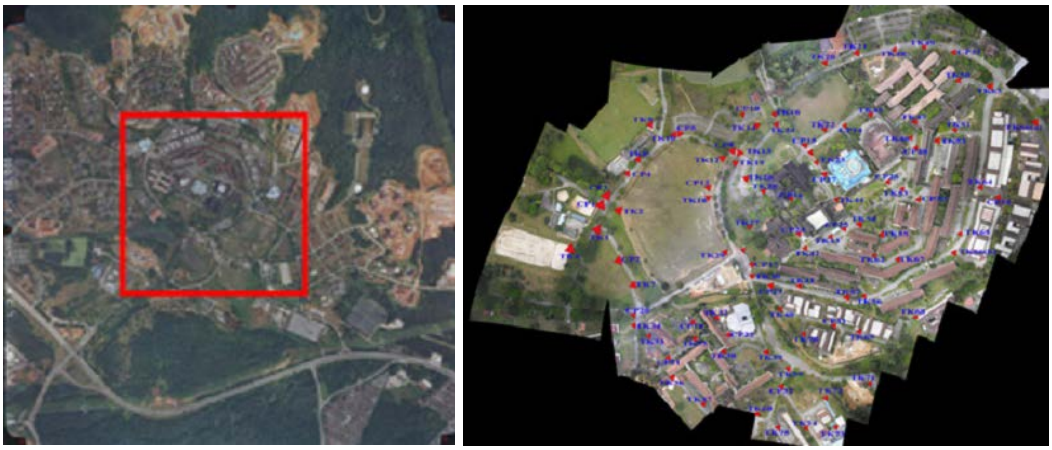

(a) (b)

Figure 2-18. Digital Imagery of UTM Campus (a) Aerial Photograph of Study Area at UTM, Malaysia (b) An Uncontrolled Mosaic (Ahmad and Samad 2010)

Irizarry et al. (2012) used a small-scale drone equipped with a video camera that used image capturing as well as real-time videos at a construction site. They proposed that a high-resolution camera, vocal interaction, and autonomous navigation were some of the ideal features of a drone system that allows safety inspections at construction sites (Irizarry et al. 2012).

Siebert and Teizer (2014) compared different survey techniques based on the expected error and the area to be covered (Figure 2-19). They developed a UAV system to survey landfills and earth moving operations of a pavement project. It is comprised of a lightweight copter having a range of 4 km and a flight time of 18 min. The limitation of having the UAV travel a shorter distance in one flight is compensated by the federal regulations, which allow UAVs to operate only under

line-of-sight (LOS). A flight control unit (FCU) and an inertial measurement unit (IMU) were used to assist in navigation and alignment, respectively. The FCU along with the onboard GPS and magnetic compass facilitate the movement of the UAV through predefined waypoints. The Digital WPL file governing the flight path through the waypoints can be uploaded to the UAV wirelessly. This file has a provision to specify the time required to capture photos at each waypoint (Siebert and Teizer 2014).

A modified Mikrokopter Flight Planning Tool (MK FPT) was used to minimize manual interference in framing the flight path. The UAV traversed through the waypoints at an altitude of 75 m and captured images, with a longitudinal and transverse overlapping of 60 and 40%, respectively. A 3-D model from the collected data was generated using AgiSoft PhotoScan software. A computer with Intel Core i7, 64 GB RAM and Windows 7(64 bit) processed 100 images in 1 hour. Error analysis was conducted by comparing target coordinates (position and height), which were measured using a tachymeter and actual coordinates obtained from the surface model developed by the photogrammetric approach. This study suggested that using high-resolution cameras along with more longitudinal and traversal overlap will minimize errors. They also acknowledged the difficulty in collecting data during wind gusts higher than 25 mph (Siebert and Teizer 2014).

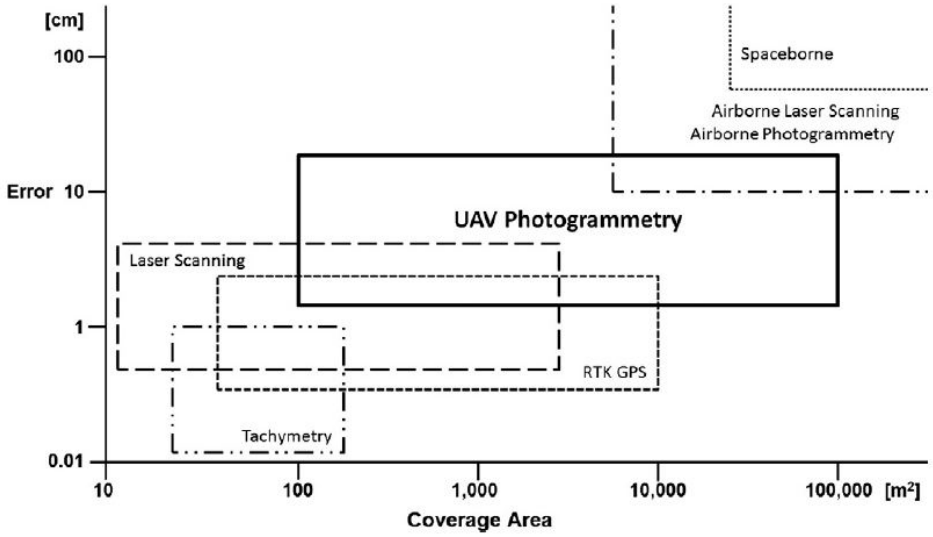

Figure 2-19. Potential UAV Application Areas in Surveying Tasks (Siebert and Teizer 2014)

Details of various previous studies on using UAVs related to infrastructure assets segregated as pavements, bridges, railways, and other infrastructure assets are provided below.

2.5.1 UAV Applications in Transportation Studies

Doherty et al. (2000) presented the applications of the UAVs in transportation related areas done under Wallenberg Laboratory for Information Technology and Autonomous Systems (WITAS) in Linkoping University (LiU), Sweden. Due to the multi-disciplinary nature of the WITAS Unmanned Aerial Vehicle Project, different departments in LiU collaborated to research on fully autonomous UAVs for gathering the traffic and road information. They used a Vertical Takeoff and

Landing Systems (VTOL) mounted with either digital or infrared cameras to collect traffic patterns involving overtaking and U-turns (Doherty et al. 2000).

Frew et al. (2004) used a modified Sig Rascal radio-controlled airplane to demonstrate the vision based autonomous following of road. Vision systems are small in size and lightweight due to its passive type of data collection and processing. They process the natural scenes in the field and measure the relative distance and orientation between aircraft and road. This approach was planned to help in road data collection in areas where Global Positioning System (GPS) is unavailable. They encountered disparities in vision-based and GPS measurements of the UAV due to their assumption of zero roll (Frew et al. 2004).

Zhang (2008) used a computer stationed on the ground for real-time communication with the UAV. Flight position was continuously monitored and control commands were sent to the onboard navigating assembly. The image acquisition system was calibrated and then used for data acquisition. The unpaved road condition data was collected by maintaining the UAV at about 50 m above ground. Wash boarding or the corrugation effect on unpaved roads was represented by closely spaced valleys and ridges formed in the captured images. Severity of wash boarding was assessed depending upon the number and width of the ridges. Attempts were also made to develop algorithms for extracting the automatic pavement condition data from the collected images (Zhang 2008).

University of Washington collaborated with the US Department of Transportation (US DOT) explored the capabilities of UAVs as an avalanche condition identification tool, especially over the slopes near state highways located on mountainous terrains. They acknowledged the requirement of obtaining a project specific Certificate of Authorization (COA) permission to fly from Federal Aviation Administration (FAA). In an effort to reopen the avalanche prone road section, WSDOT opted for the low cost alternative of using MLB BAT UAV during initial trial and identified the avalanche-prone trigger zones and snow chutes. They also identified the limitation of using a fixed wing aircraft, in an urban area, requiring a 100-foot long flat road surface to land. Hence they opted for a rotary wing UAV i.e. R-Max in their second test to follow a preprogrammed waypoints to conduct a survey of terrain conditions along a road prone to an avalanche event (McCormack and Trepanier 2008).

Herold et al. (2008) provided a case study that involves road distress interpretation from the imaging spectrometry obtained using unmanned aerial vehicles (UAV). However they also acknowledged the then prevailing barriers for using UAVs for civilian purposes (Herold et al. 2008). Lin and Saripalli (2012) detected roads from aerial images of a desert. A histogram-based thresholding algorithm was developed to detect the road region. Additionally, a line detection algorithm was used to refine the detected road area (Lin and Saripalli 2012).

Zhang and Elaksher (2012) discussed a helicopter based digital imaging system for collecting pavement condition data over unpaved rural roads. This system is comprised of a UAV furnished with a digital camera, on-board computer, GPS receiver, inertial navigation system (INS), and a geomagnetic sensor. An onboard computer assists in navigation by coordinating the GPS and INS together. The ground control station (GCS) transmits signals to activate the camera at preset locations. The steps in the developed system include calibration of the camera, image orientation, 3D model development, and assessing the unpaved road condition from the models as shown in Figure 2-20. Construction of a 3D model (as shown in Figure 2-21) by matching the points in two adjacent images was discussed in detail. An accuracy up to 5 mm was observed when the data extracted from the images was compared with the data obtained from a manual survey (Zhang and Elaksher 2012).

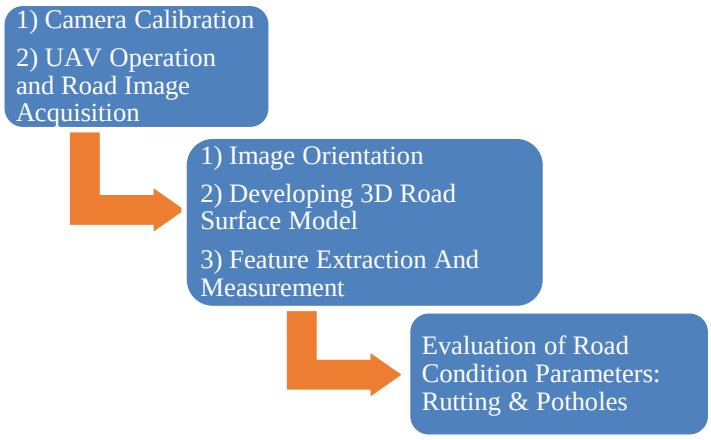

Figure 2-20. Flowchart of Unpaved Road Condition Evaluation System (Zhang and Elaksher 2012)

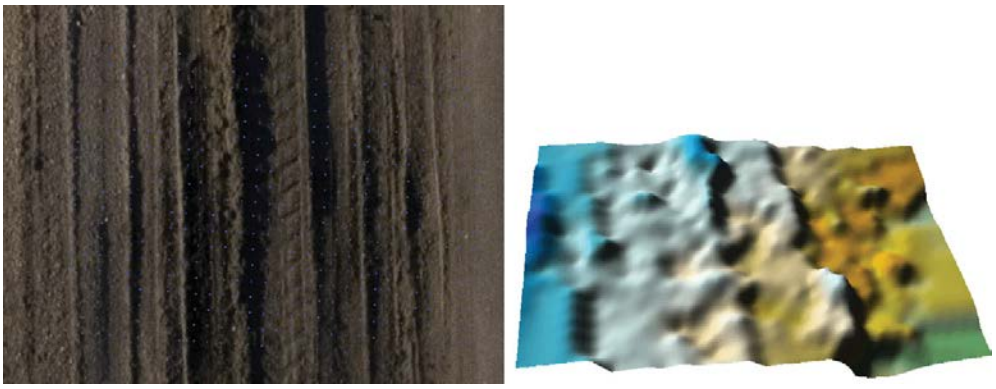

(a) (b)

Figure 2-21. Road Condition Assessment (a) Rutting on an Unpaved Road (b) A Reconstructed 3D Model of the Rut Area (Zhang and Elaksher 2012)

According to a special report on drones in Asphalt, the magazine of the Asphalt Institute (2016), the University of Vermont partnered with the Vermont road agency and used a UAV to monitor the rivers adjacent to roadways. This study

was focused to prevent the pavements from flooding and other moisture related pavement failures (Asphalt Institute 2016). Other agencies also used UAVs in conjunction with thermal imaging cameras to detect the pavement cracks on a bridge as shown in Figure 2-22. Thermal imaging largely depends upon the time at which the images were captured (Asphalt Institute 2016).

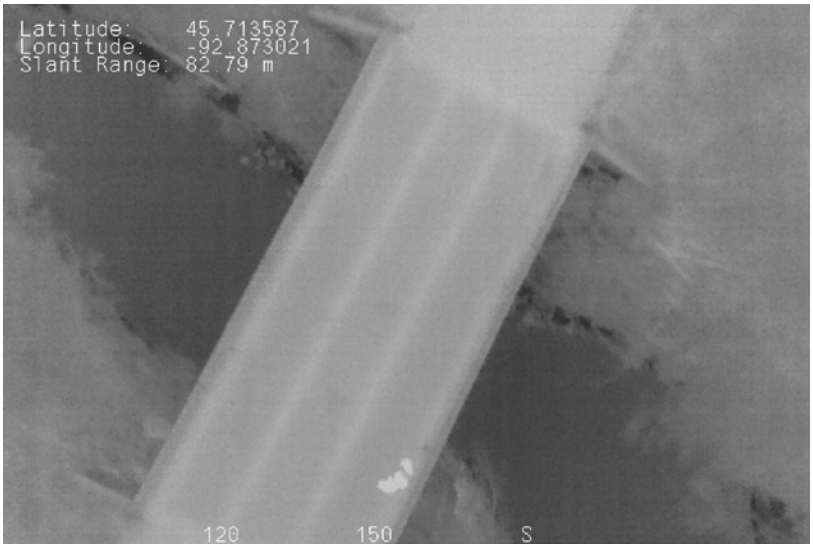

Figure 2-22. Thermal Image Captured by UAV (Asphalt Institute 2016)

Brooks et al. (2015) discussed 3-D models generated using the bundle adjustment principle as shown in Figure 2-23. These models form the basis for extracting the elevation details of each point using Agisoft PhotoScan software (Brooks et al. 2015). These elevations can be used to calculate the cross slope, rutting, volumetric calculations and other pavement related features. Rut volume calculations can be used to assess the cost of materials required for repair and

rehabilitation of ruts. Cutting and filling calculations made use of the data collected by the UAV, which assists in the cost estimation of pavement construction.

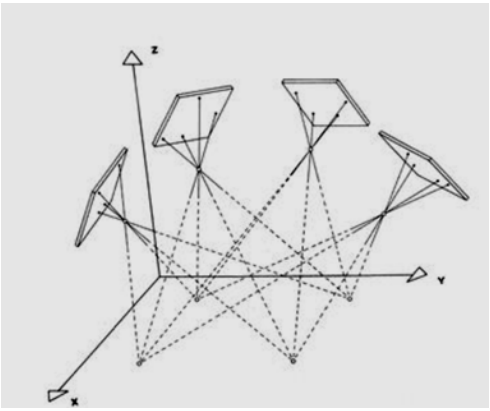

Figure 2-23. Bundle Adjustment to Generate 3D Model (Brooks et al. 2015)

Pereira and Pereira (2015) demonstrated embedded image processing systems for automatic crack recognition using UAVs. They emphasized on identifying the different types of mortar cracks on facades using aerial inspection. Segmentation by edge detection and particulate filter are the two crack identifying algorithms discussed by Pereira and Pereira (2015). Different crack images were used to calibrate the crack identifying algorithms and tested those with simulated mortar cracks on façade (Pereira and Pereira 2015).

Díaz-Vilariño et al. (2016) evaluated the suitability of unmanned aerial photogrammetry for measuring road runoff. D8 algorithm was used to estimate the flow direction of the run off. They compared the run off data from DEMs obtained from photogrammetry data with the light detection and ranging (LIDAR) dataset as

ground truth and concluded that reasonable accuracy could be obtained using UAV photogrammetry (Díaz-Vilariño et al. 2016).

Marinelli et al. (2017) presented the work on identifying the horizontal alignment from the road data images collected from mobile terrestrial and aerial remote sensing platforms. Those images were subjected to edge extraction and feature recognition in Matlab to identify the horizontal alignment (Marinelli et al. 2017). Another study also studied feasibility of using drones for evaluating the effectiveness of soil treatment methods on performance of the pavement using UAV collected data (Puppala et al. 2018c).

2.5.1.1 UAVs for Traffic Related Studies

Of late, traffic monitoring had been the most common application of UAVs related to transportation infrastructure. Shastry and Schowengerdt (2002) developed a methodology to extract parameters of traffic flow from the aerial data collected. They used an aerial platform mounted camera to overcome the drawbacks of a stationary mounted camera like vehicle occlusion, changing light conditions, and other factors. They extracted the vehicle trajectory by extracting the temporal data from the spatio-temporal data obtained aerially (Shastry and Schowengerdt 2002).

Kaaniche et al. (2005) conducted a vision system based traffic surveillance using UAVs. UAV was flown in a predefined paths along a list of waypoints identified by the GPS coordinates with an uncertainty of 10 m. The videos of the traffic were collected to obtain various characteristics of traffic such as vehicle

counts, speed, flow rate, and density. They demonstrated identification of the vehicles using the common fate law on the aerially collected data (Kaaniche et al. 2005).

Coifman et al. (2006) demonstrated UAVs for collecting roadway usage data, which was otherwise, a laborious task using conventional practices. They had flown a BAT III technology UAV assembled with a payload of two video cameras over the surroundings of The Ohio State University covering many intersections and a freeway. Video images were relayed to the ground station in real-time, during the course of the flight.

Several applications like determination of Level of Service (LOS) of the road, Average Annual Daily Travel (AADT), Origin Destination (OD) flows and documentation of intersection travel patterns from the aerially collected data were realized from their work. LOS was measured using the traffic density (vehicles/km) and AADT (vehicles/hr). Queues, signal timings, arrival rates, and turning movements were excerpted from the aerial collected data (Coifman et al. 2006).

Butenuth et al. (2009) used a LDR 3K camera system integrated in a ZEISS aerial camera mount coupled with navigation system on UAV to monitor the traffic. The central camera was positioned with nadir view and the other two cameras were having a tilt of 35°. This setup was to obtain higher field of view even at lower altitudes. Vehicle detection and tracking were differentiated in their work to identify non-moving vehicles. Vehicle tracking from the aerial images using

normalized cross-correlation and velocity and trajectory evaluation were discussed in their work (Butenuth et al. 2009).

Braut et al. (2012) researched on using airborne videos for developing OD matrices at complex intersections. OD matrix comprises of the number of vehicles going from each intersection entry to each intersection exit. They stated that using trained workers at the complex intersections can be time consuming and costly as it requires the use of helicopters for aerial data collection. They evaluated the performance of the data collected from the camera mounted on a hovering UAV and discussed the importance of stabilization of the air-borne video (Braut et al. 2012).

Videos of the traffic within the urban areas were collected using an Unmanned Aerial Vehicle (UAV) due to its non-intervention on the road infrastructure by Salvo et al. (2014a). A quadcopter with carbon fiber body and a compact digital camera placed in nadir view was used to collect the traffic related data as a low cost alternative to traffic related surveys performed with conventional methods. These videos were processed to classify traffic and obtain kinematic quantities of traffic flow that could be used to address congestion (Salvo et al. 2014a).

Zhang et al. (2014) emphasized the importance of traffic information collected by UAVs for smooth operations of Intelligent Transportation System (ITS). They proposed using Dempster-Shafer theory, which is based on information

fusion, and Kalman filter together as the better way of identifying road sections from the videos obtained from UAV (Zhang et al. 2014). Azevedo et al. (2014) demonstrated about the steps involved in the vehicle trajectory identification from the aerial remote sensing data. Initial steps involved image collection and processing followed by algorithms scanning the image pixels for vehicle identification and tracking (Azevedo et al. 2014).

Salvo et al. (2014b) discussed about the computation of gap acceptance at an urban intersection using videos of a probe vehicle collected from an UAV flying at an altitude of above 60 meters. They adopted UAV due to its non-invasive nature on driver's behavior during the data collection. They also mentioned that high spatial resolution, rapid operation, and reduced operating costs could be obtained using the UAVs. Ground control points were placed in the intersection and used to estimate the accuracy of the images. The accuracy of vehicle trajectory recognition from this methodology was estimated by comparing the vehicle speed values obtained from the GPS probe and from the UAV videos. After obtaining a satisfactory match, these videos were used to obtain the acceptable gap adopted by the drivers merging from secondary street to main road at an urban intersection (Salvo et al. 2014b).

Zheng et al. (2015) provided their work on identifying driving patterns of Driving While Intoxicated (DWI) drivers in real time using Unmanned Aircraft System (UAS). The vehicle trajectories are identified from the aerial videos to spot

the erratic drivers. This allows for proactive regulation of erratic driving by the law enforcement officials, thereby reducing DWI-related accidents (Zheng et al. 2015).

Barmpounakis et al. (2016) stated that the collection of visual information over larger networks, such as transportation infrastructure, can be challenging. A comparison of different attributes common between the use of static cameras, and cameras mounted on Manned Aerial Vehicle (MAV) and Unmanned Aerial vehicle (UAV) was provided in their works. In their opinion, installation of stationary cameras fail to provide a clearer idea during an unexpected emergency and can be costly in the end. They mentioned that using a Manned Aerial Vehicle (MAV) for localized inspections such as an accident area might not be feasible due to the cost constraints involved in it (Barmpounakis et al. 2016).

UAVs offer a potential alternative to the earlier practices due to the less time required to be airborne compared to a MAV and operation flexibility offered. Unmanned aerial vehicles score over the stationary cameras as they provide different views to understand more about the infrastructure conditions prevailing on the ground. Unlike the MAVs UAVs can also facilitate a low cost localized inspection be it an intersection or an accident/traffic jammed area (Barmpounakis et al. 2016). Chow (2016) discussed about dynamic UAV-based traffic monitoring using programming algorithm based on Least Squares Monte Carlo simulation (Chow 2016).

Babinec and Apeltauer (2016) considered various errors that can be induced into the data collected by cameras mounted on UAVs and evaluated the position accuracy of objects identified from the aerial data. Later this approach was used for traffic surveillance and monitoring. Based on Monte Carlo Sampling, they developed an accuracy measuring tool (Babinec and Apeltauer 2016).

Guido et al. (2017) identified the versatility of UAVs in monitoring traffic data from videos. They developed an algorithm to identify the vehicles and validated it using a probe vehicle equipped with high accuracy GPS and a control point on its roof. Ground Control Points (GCPs) placed homogeneously around the area helped in correcting the orientation of captured images. All frames from the video were stabilized, converted into grayscale, and then Gaussian-blurring filter was applied to smoothen the video frames. The algorithm was trained by inputting set of true and false images containing the probe vehicle. The speed of the probe vehicle from the aerial video and the GPS sensor were compared with time and have exhibited close match (Guido et al. 2017).

Zeng et al. (2017) developed a hybrid approach for microscopic models to simulate pedestrian behavior at signalized intersections using aerial video data collected in Beijing, China. Trajectories were extracted from the data collected using camera mounted on a quadrotor unmanned aerial vehicle (UAV). Kalman filtering (KF) technique was used to correct the errors in the raw trajectory data. The coordinates in the videos were then georeferenced using featured points. The

model developed was calibrated and compared with two competitive models (Zeng et al. 2017).

Khan et al. (2018) presented their work on automatic identification of traffic flow and shockwave at a signalized four-legged intersection using UAVs. They detected the shockwave based on identifying the critical points in the vehicle trajectory where the motion of the vehicle changes significantly. They also monitored through traffic behavior in addition to the turning traffic (Khan et al. 2018). Kaufmann et al. (2018) conducted research on identifying moving synchronized flow patterns in over-saturated city traffic from the aerial data. UAV was used to record various situations in city traffic and vehicle trajectories were extracted (Kaufmann et al. 2018).

2.5.2 UAV Applications in Bridge Studies

Metni and Hamel (2007) monitored bridges using UAV systems and developed a strategy for autonomous flight using orientation limits (Metni and Hamel 2007). Michigan Tech Research Institute (MTRI) collaborated with Michigan DOT (MDOT) and used five different UAV platforms to evaluate two bridges, two pump stations, two traffic sites, and a roadway asset site. Figure 2-24a shows the rotary type UAV (Bergen Tazer 800 hexacopter), employed by Michigan Tech Research Institute (MTRI) with a camera attached for aerial survey of pavements and bridges. Figure 2-24b shows the captured high-resolution image from a Tazer 800 UAV fitted with a Nikon D800 DSLR camera (Brooks et al. 2015). They reported that

high-resolution pavements were captured by using a Bergen Hexacopter paired with optical and thermal sensors (Figure 2-25).

Two axis gimbals assisted in maintaining the same camera direction during the UAVs movements. In addition, the stability from using six rotors in the hexacopter also contributed to higher quality data. When the connection between the controller and the hexacopter is lost, the on-board GPS feature guides the hexacopter back to the starting point at a travel height of 150 feet (Brooks et al. 2015).

(a) (b)

Figure 2-24. Aerial Data Collection (a) UAV with a Digital Camera; (b) High-Resolution Image from UAV Camera (Brooks et al. 2015)

(a)

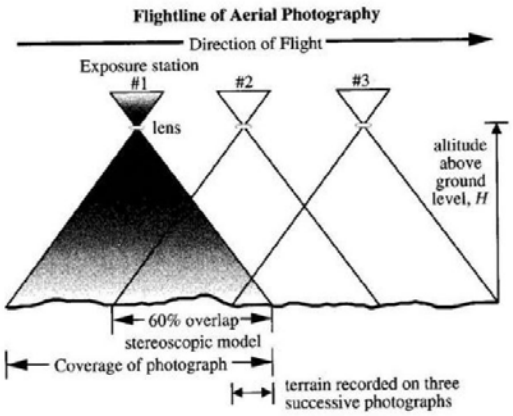

(b)

Figure 2-25. Aerial Bridge Deck Inspection (a) A Bergen Hexacopter Collecting Bridge Condition Data and (b) Stereoscopic Imagery (Brooks et al. 2015)

MTRI also demonstrated the effectiveness of using a rotary wing, DJI Phantom 2, for aerial surveys in challenging areas, such as the locations beneath bridges and in confined spaces (Brooks et al. 2015). The camera (with the ability to take pictures and record videos to micro SD cards with a real-time video link of up to 900 feet) was mounted on the DJI Phantom Vision 2 UAV and used to create photographic inventories of sites such as bridges with hard-to-reach areas. The assessments of the UAV studies, as shown in Figure 2-26, clearly show signs of significant distress in the form of spalling and cracking in the bridge. The results were analyzed and used to identify structural defects (Brooks et al. 2015).

(a) (b)

Figure 2-26. Bridge Condition (a) Bridge Selected for a UAV Assessment, and (b) A High-Resolution Image Showing Spalling and Cracking (Brooks et al. 2015)

The Asphalt magazine also stated that Michigan DOT (MDOT) utilized UAVs to conduct bridge deck inspection. The benefits observed include the increase in safety for their working personnel, and a reduction in time and cost. By using the UAV to conduct the bridge deck inspection in lieu of standard procedures, MDOT saved around $4000, roughly 90% of the cost invested in standard procedures (Asphalt Institute 2016).

2.5.3 UAV Applications in Rail Corridor Studies

Railroad planning requires collecting geographical, meteorological, and other data that could possibly influence decisions regarding selection, construction and use of rail routes. Due to the rapid development in software platforms and reduction in the cost of components such as autopilots for autonomous flights, cameras, and batteries, the availability of UAV-based studies is increasing in commercial markets.

Inspection of the rail corridor is needed to identify conditions (e.g., washouts, rail buckling, and debris accumulation) that could potentially affect the safe operation of the rail line. In addition, it is important to detect encroachment on rail right-of-way. Such data collection becomes more difficult, especially in remote and inaccessible areas. UAVs must be operated within visual line of sight (VLOS) and this poses additional challenges to UAV operations, especially in remote and difficult to access areas.

The use of UAV techniques could provide rapid, cost-effective and high-quality survey data that could be immensely helpful, especially for inspection of railway routes that pass through hilly terrain and have long uninhabited stretches, which is usually the case. In addition, as railroads pass through urban areas, UAV-CRP studies can gather fast and accurate information regarding right-of-way acquisition. Fast and accurate surveys of larger railroads can be performed using fixed wing and full-sized UAVs, which would reduce the freight and train delays, thereby avoiding disruptions to the rail's routine services.

The drone industry is observing a continuous advancement in its technology and associated on-board sensors (Stewart et al. 2014). This enables rail inspectors to use data gathered by the drone to identify defects rather than physically access the track. In colder regions, UAVs can be equipped with infrared sensors and their images can be used to check the switch point heating systems on rail tracks as shown in Figure 2-27 (Stewart et al. 2014). For instance, the Dutch railway

company, ProRail, is using infrared images collected from drone-based cameras to detect frozen switching points; which gives them the information they need to stop rail traffic before accidents can happen (Stewart et al. 2014).

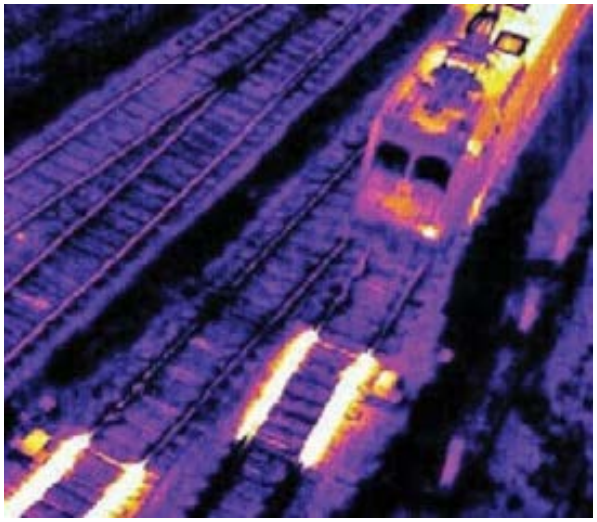

Figure 2-27. Infrared Images from Drone-Based Camera to Detect the Freezing of Switching Points (Stewart et al. 2014)

It should also be noted that the manual procedure of checking the switch points is labor-intensive and can jeopardize the safety of the employees (Stewart et al. 2014). In contrast, the drones' camera-based examinations are not only faster, but require less boots on ground and are injury free since data is remotely collected and processed in the office. Thus, no employees are put on tracks to do actual physical inspections (Stewart et al. 2014).

Germany's national railway company Deutsche Bahn spent over £6 million to remove graffiti on train depots and maintenance facilities. To help prevent such

incidents in the future, the company conducted trial studies using mini drones equipped with infrared cameras to detect trespassers and vandals (Stewart et al. 2014). Such UAV-based inspections can improve and enhance the safety of railway tracks and other railway facilities.

Recently, BNSF Railway collaborated with the Federal Aviation Administration (FAA) to assess the damage to railroad tracks from the record flooding that hit Texas and Oklahoma in 2015. Rail route inspection, as shown in Figure 2-28, was carried out by flying the unmanned aerial vehicles mounted with high-definition video cameras over the flood-affected areas. The high-definition video feed clearly showed areas where the rail line was washed out and locations where excess debris was collected at the foundation of rail bridges (The Association of American Railroads 2015). In addition, the authorities could examine the condition of bridges and quickly deploy maintenance crews to repair damage once the floodwaters receded (The Association of American Railroads 2015).

Figure 2-28. BNSF Railway (Bryan 2015)

Other potential areas of UAV application are in the inspection of rail routes in North America, especially in remote areas where a physical inspection becomes tough in winters due to harsh climatic conditions. BNSF railways are the second largest freight railroad network in North America with approximately 32,500 miles of track to manage and maintain. In May 2015, FAA announced a new project, the Pathfinder program, in collaboration with three leading U. S. companies, namely, Cable News Network (CNN), PrecisionHawk, and BNSF railways (Perlman 2017). Accordingly, CNN works with Georgia Tech University to research visual line of sight (LOS) operations for safely news gathering in urban areas; PrecisionHawk researches agricultural operations for rural areas, flying beyond visual line of sight (BVLOS); and BNSF railways explore command-and-control challenges of using

UAV to inspect the rail system infrastructure, beyond the visual line of sight (Perlman 2017).

In 2015, as a part of FAA's Pathfinder program, the BNSF railways collaborated with Insitu Inc. to conduct inspection of rail infrastructure beyond the visual line of sight using UAV. Figure 2-29 shows a photo of the ScanEagle (UAV) launched at a site near Vaughn, New Mexico to inspect 140 miles of rail track to find any washouts and bridge damage to rail infrastructure (Insitu 2018). The BNSF is currently working to test a complete system for BVLOS, including all the hardware, platforms, software and sensors needed. According to the report by Association of American Railroads (2015), BNSF's role in the Pathfinder Program, involves researching the use of long-range drones, which have the ability to fly hundreds of miles from their operators (The Association of American Railroads 2015).

Figure 2-29. BNSF and Insitu Inc. Launching the ScanEagle UAV for Rail Inspection (Insitu 2015)

Recently in Turkey, a 85-mile long and 1800-ft wide corridor (Figure 2-30a) passing through plains, hills, mountains, and urban areas meant for a high-speed rail network was efficiently surveyed using a fixed-wing UAV shown in Figure 2-30b. The project was subjected to all types of weather conditions and was completed within a small turnaround period of 2 months. The project also involved establishing many ground control points as part of the aerial survey to achieve the desired high precision required in railway planning (Figure 2-30c).

Employment of the UAV technology proved to be quick and enabled the delivery of the final report within three months of project initiation. The project also satisfied the client's minimum accuracy requirement (Diner 2015). The aerial survey also avoided the danger of personnel working along trackside thereby preventing any personal harm; hence, the UAV technique improved safety.

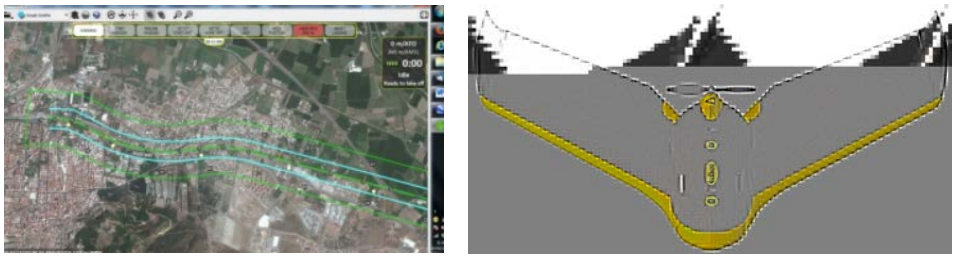

(a) (b)

(c)

Figure 2-30. Aerial Rail Corridor Inspection (a) Railroad Corridor Between Ankara and Azmir, Turkey; (b) Fixed Wing UAV Used in Aerial Survey; and (c) Worker Establishing Ground Control Points (Diner 2015)

UAVs can also be deployed for close visual inspection tasks involving the rail network. High volume and low height rail infrastructure inspection is typically done by crews working under line possession. The use of UAVs to carry out visual inspection reduces the need for interruption to rail services and provides detailed imagery from an elevated viewpoint, which can identify defects that may not be visible from ground level. For low-volume, high-rail infrastructure such as viaducts and bridges, traditionally the inspection access method would be rope access, scaffolding or elevated platforms. The use of UAVs to inspect these structures saves time and expense, and removes inspection personnel from the inherent risk in working at great heights (Stuart 2015).

2.5.4 UAV Applications for Volumetric Studies

Accurate volumetric calculations are required to determine rock cuts along the railroads. Traditional surveying methods are laborious, time-consuming, and subjects surveyors to safety risks. The resultant surveys are also less accurate. Lightweight UAVs can be flown at lower altitude and because they are equipped with a variety of sensors, including digital camera to record high quality still images or high definition videos taken from different angles, their accuracy is greater than previously possible. Furthermore, the stereo-imagery can be used to generate three-dimensional (3D) point clouds and create a digital surface model (DSM).

Appropriate image analysis software can be used to process and visualize the overlapping imagery data as accurate 3D models of the area of interest. Both rock cuts and stockpile volume can be accurately determined from this technique in a relatively safer, cheaper, faster, and more accurate manner. However, the accuracy with which measurements can be obtained from such 3D models will depends on resolution of images taken. GeoCue Group, a software solution company, has recently developed new image processing algorithms to create more accurate 3D models that can prevent overlapping images of stockpile or rock cut areas. From these 3D models, accurate volumetric computations can be done using software developed by GeoCue Group.

2.5.5 UAV for Other Civil Engineering Applications

Niethammer et al. (2012) used a radio-controlled mini quadcopter UAV mounted with a visible range camera to monitor a landslide in Super-Sauze, France. They evaluated the capability of UAVs to capture desiccation cracks, fissures, and displacements on the landslide surface. The images were processed and stitched to obtain an orthomosaic and digital terrain models (DTMs) of the landslides (Niethammer et al. 2012). Horizontal displacement of around 7 to 55 m was obtained by comparing two orthomosaics of the landslide data collected in 2007 and 2008. Niethammer et al. (2012) acknowledged the need to research on reducing the time required for data processing.

Construction site, monitoring is one of the common application of UAVs in civil engineering field. Figure 2-31 shows the view from the UAV that was used to monitor a construction site on a closed section of highway. This inspection was performed to assess transportation assets and traffic conditions (Brooks et al. 2015).

Figure 2-31. View from the UAV Used for Construction Site Monitoring (Brooks et al. 2015)

UAVs also find their applications in the construction management tasks specifically for project progress monitoring, job site logistics, evaluating safety conditions, and quality inspections. Irizarry and Costa (2016) discussed about various applications and the Unmanned Aerial Systems (UAS) regulations in Brazil and United States. A DJI Phantom 2Vision, a low cost UAS, was used by Irizarry and Costa (2016) for the image collection of construction sites. Project personnel working at the site were provided with a questionnaire consisting of four sections related to demographic information, reviewing the information from the asset images, level of agreement about the usefulness of the asset images, and comparison with current methods. They provided a rough cost estimate of tasks involved with the unmanned aerial flight operations. Prior to the new regulations by FAA in 2016, obtaining a Certificate of Authorization (COA), to fly in the restricted airspace, was charged around $6000 to $9000 by the data collection

operators per COA. They also recommended the importance of educating the workers about the use of these aerial data collection methods, as it was observed that some of the workers stopped working to view the flying aircraft (Irizarry and Costa 2016).

Tatum and Liu (2017) presented their work on using UAVs that are reliable and cost effective within the construction industry. Construction companies capture aerial photographs of the construction activity for not only monitoring the project progress but also for innovative advertising techniques. They discussed about the previous works done using UAVs for surveying, inspection, and safety/security monitoring. They also circulated a survey questionnaire to 69 companies to obtain a conscience on different topics like year-of-UAV-adoption, applications of UAVs, cost of using UAVs, and risk mitigation using UAVs. The outcome of those surveys indicated 57% of the respondents indicated that using UAVs had provided cost avoidance and 42% of the respondents agreed that using UAVs had a positive schedule impact on their projects (Tatum and Liu 2017).

Howard et al. (2018) provided the details regarding the use of UAVs for military, recreational, public sector, commercial, and construction purposes. Due to the relatively newness of the UAV technology, assessments of safety during its field use were not on par with the technological advancements. There might be some work place hazards caused and avoided using UAV, hence an awareness about these details would help in effective implementation of this technology. They

proposed that a database of the UAV related injuries would help in mitigating those situations in the future considering it advantages of providing worker's safety in many ways (Howard et al. 2018).

Tziavou et al. (2018) presented their work on aerial mapping of a coastal area using fixed wing and rotary wing UAVs. They concluded that the level of detail of geological maps obtained from the aerial orthomosaics is comparable with that of the traditional methods. UAVs took five times less time to collect the same detail compared to that of traditional ways. They also observed that the data collected from rotary wing UAV is more detailed relative to that of the fixed wing aerial data (Tziavou et al. 2018).

2.6 SPECIAL AREAS OF UAV APPLICATIONS

According to previous studies on pavements, several factors, including accuracy of the data, quality of data and data management form, must be considered for optimal UAV based pavement data collection. Some of these findings are provided below:

2.6.1 Accuracy of the Data

The quality of images changes with respect to the camera, drone position, conditions and other parameters are all important and this information must be correct. According to Ellenberg et al. (2015) the accuracy of the camera can be evaluated by taking a white paper containing lines of a known thickness. Images of the paper are placed at varied distances from the UAV and are captured by a camera

mounted on the UAV and the thickness of lines in the captured image are compared to the original thickness to measure the accuracy of the camera.

Images captured by UAVs might exhibit non-uniform stretching of the image, also known as distortion. The curved appearance of actual straight lines in the captured image showcases the radial distortion. This can be corrected using the multi-plane calibration method using images in distinct orientations placed at various distances away from the UAV & camera assembly. Keeping the camera parameters constant, these corrections will then be applied to the images collected in the field (Ellenberg et al. 2014).

2.6.2 Quality Management of Field Surveys

Quality management of UAV-based field surveys is a key aspect when dealing with highly variable pavement data. Shekharan et al. (2006) points out that agencies without a quality management plan tend to under or overestimate maintenance and rehabilitation needs (Shekharan et al. 2007). Pierce et al. (2013) asserts that collecting high quality data avoids the costs associated with inferior data quality. Additional expenditure incurred due to poor quality data involves recollecting, reprocessing, or rerating data costs (Pierce et al. 2013). Effective pavement management systems depend on the quality of the pavement condition data collected. Quality data assists in making timely decisions regarding rehabilitation work and reduces the life cycle cost of the pavement.

According to McGhee (2004), agencies must formulate quality assurance plans that include qualification and training for the data collection personnel, calibration and maintenance of the equipment, validation sections, and additional checks. Sufficient care needs to be taken while collecting data using unmanned aerial vehicles.

Rathinam et al. (2008) discussed the discrepancies in the data collected by the UAV following a predefined set of GPS points called waypoints. They demonstrated the efficiency of UAV data collection by assembling a positioning sensor. It generated a closed loop response by comparing the cross-sectional profile generated in the learning step with the real time scanned lines of the road surface. This feedback response assists in regulating the location error of UAV with respect to the road surface, while collecting the data. Hence, positioning sensors are needed if waypoints are sparsely distributed. Developing UAV-CRP technology, based upon quality assurance plans (Figure 2-32) may avoid the costs related to the poor data quality.

Figure 2-32. Data Quality Management Cycle (Pierce et al. 2013)

2.6.3 Data Management.

Thousands of gigabytes (GB) of data generated after surveying road sections can overload a data acquisition system in place. Efficient data management systems are required on board as the amount of data increases with the quality of the images collected. Most of the time, a dedicated work place is used to store data about data (i.e., metadata). It describes the content, quality, location, condition, and other characteristics of the data. Sometimes metadata (i.e., other relevant information regarding the road section) may give an estimate about the possible cause of specified distress and assist in arriving at possible solutions. Great volumes of generated data can be handled efficiently by equipping the system with higher processors.

Notably, the above three factors related to data and quality of UAV surveys are crucial for proper characterization of pavement distress conditions that will be input into the pavement management information system (PMIS) database. As noted earlier, condition rating scores need to be determined for the entire roadbed miles and this condition score needs to be collected once a year. Due to cost and time limitations posed by this requirement, agencies rate one lane for each roadbed and considers this lane representative of all lanes for the specific roadbed.

If proven as a viable tool for pavement condition rating surveys from the present research investigations, the present UAV studies offer an excellent opportunity for DOTs to overcome some of the present limitations. As this tool can provide survey results in a quick and safe manner and the data can be analyzed and stored in electronic format to be checked as needed. Also, since the data is collected on an annual basis, the results could show the prevailing conditions at a site that might have contributed to pavement distresses in a more systematic manner and this will certainly enhance our understanding of pavement performance (materials, environment and loading conditions) thereby leading to better strategies of pavement management.

But, huge amounts of data generated would be a disadvantage if proper data management policies are not followed. There are many commercial cloud data storage platforms offering services to handle large data, exploring those options by exercising discretion in selection would prove to be very helpful.

2.7 DISASTER MANAGEMENT AND RECONNAISSANCE SURVEYS

In the past decades, frequency of disasters have been on the rise. There is a need for adopting strategies that are efficient and safe. Hurricane is one of the major disasters where UAVs could be used to efficiently collect the data.

Storms can form easily over warm water bodies located near to the equator. The surrounding air swirls in to compensate for the lower air pressure created by the rise of warm air above those water bodies. This wind flow creates an eye and gradually grows into a storm. When the speed of the outer rotating winds of a storm attain a minimum of 39 mph, it is termed as a Tropical Storm. When the speed of the winds exceed 74 mph, it is termed as Tropical Cyclone or Hurricane (Erickson 2018).

Tropical Cyclones originate frequently from the Atlantic basin, and, less frequently, from the central North Pacific Ocean. Their names are selected from a six-year rotating list of names, updated and maintained by the World Meteorological Organization (WMO) (NOAA 2018). Hurricane is classified by the Maximum Sustained Wind Speed defined as the speed of the winds that occur for a minimum time period of 1 minute and at a standard meteorological altitude of 10 m (33 ft) in unobstructed area above the ground. Hurricanes are classified into five types basing upon the Maximum Sustained Wind Speed shown in Table 2-2 (Landsea 2006).

Table 2-2. Saffir-Simpson Hurricane Wind Scale (Erickson 2018)

Category	Wind Speed (mph)	Damage Level	Storm Surge (feet)
1	74-95	**Minimal**	**4-5**
2	96-110	**Moderate**	**6-8**
3	111-129	**Extensive**	**9-12**
4	130-156	**Extreme**	**13-18**
5	157 or higher	**Catastrophic**	**19+**

The hurricane mechanism feeds on the warm moist air as shown in the Figure 2-33. These hurricanes die down as they move over to the land, due to the unavailability of the same energy provided by warm ocean water bodies. But most of the cases, the hurricane intensity would have helped it to travel great distance over land and already resulted in great damage before it ceased. There are satellites monitoring the occurrence of these natural disasters to warn and reduce the enormity of loss. Two Geostationary Operational Environmental Satellites (GOES) jointly managed by the NASA and the National Oceanic and Atmospheric

Administration (NOAA) to assist the meteorologists in observing and predicting the weather (Erickson 2018).

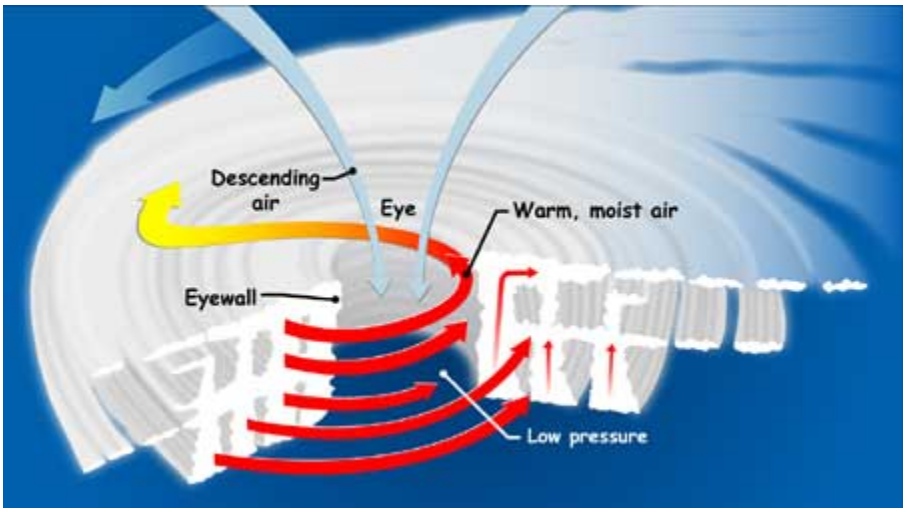

Figure 2-33. Mechanism of Hurricane from the Slice of Eye (Erickson 2018)

Category 4 Hurricane made landfall in Houston Metropolitan area on August 25, 2017 and inflicted serious damage. The diameter of the hurricane was 280 miles and wind speed was around 130 mph, as shown in Figure 2-34. Though the winds died down in few days, the Rainfall-triggered flooding had caused catastrophic damage due to inundation (CNN News 2017). This has been recorded as the second most costly hurricane to make landfall in the United States after 1900. Due to this being once in a 500-year flood, two reservoirs exceeded their limit and breached causing inundation of most parts in Houston. Some areas in the Houston metropolitan area witnessed more than 50 inches of rain, according to National Weather Service (Gallagher et al. 2017).

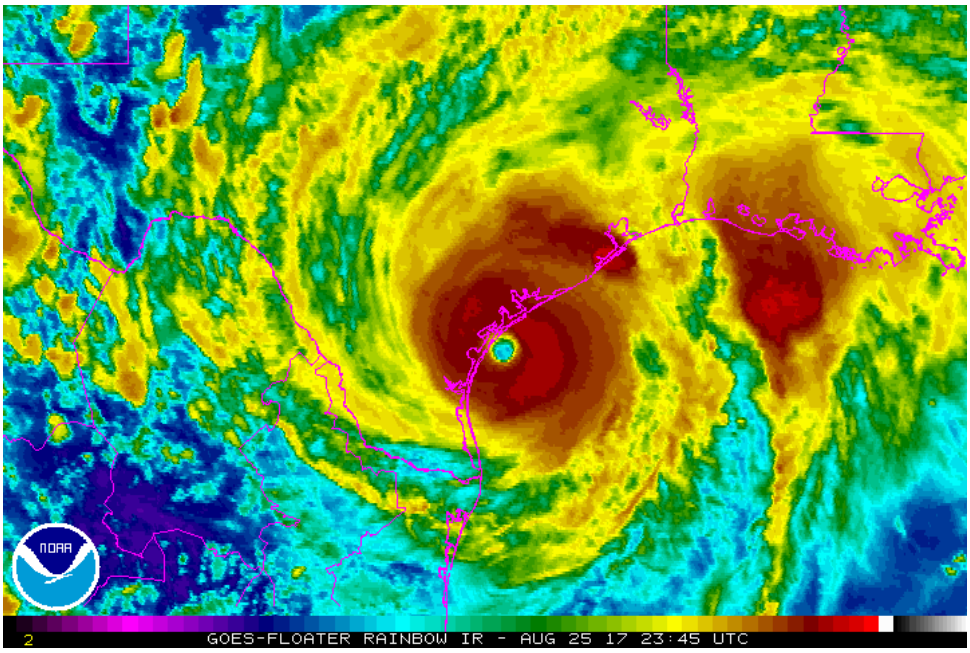

Figure 2-34. Hurricane Harvey's Landfall over Rockport, Texas, as a Category 4 Storm (Wurman and Kosiba 2018)

A geophysicist also claimed that the city sank by couple of centimeters due to the weight of flood water over one third area of Houston (Huber et al. 2018). More than 13 million people and 185k homes were affected by the flood water (Gallagher et al. 2017). When the floodwaters receded, all the sodden furniture, clothing, and other household objects piled up on the streets as debris. It was approximated to 8 million cubic yards of debris in Houston alone. The debris need to be cleared as it poses a risk to public health. Although Houston did not experience the following Hurricane Irma but its rescue efforts suffered due to the diversion of resources (CBS news 2017).

2.7.1 UAVs for Disaster Management

The potential of UAVs as an inspection tool during and after a disaster is enormous, as it compensates for the shorthanded city agencies by efficiently collecting the data in a safe and quick manner.

Ezequiel et al. (2014) demonstrated the applications of UAVs for assessment and infrastructure development after a disaster. They provided a detailed workflow of data collection that includes flight planning and data acquisition, data processing, and data delivery. Case study data collected during different natural disasters were provided. Image analysis was used to differentiate the coconut plantations from the forest area thereby providing an assessment of land use in the Samar and Leyte islands. However, the accuracy is questionable as there was no ground truth measurements established in this research (Ezequiel et al. 2014).

2.8 SUMMARY

The chapter described UAVs, remote sensing, and photogrammetry-related information in the first few sections. These are followed by various UAV applications in many civil infrastructure fields, and all these early studies provided some preliminary information for present field studies. The main idea of this literature review is to show that UAVs can provide quick survey results for bridge, pavement, railway tracks, runways, and other infrastructure in a safe and quick manner. This means that this methodology can provide a valuable tool for TxDOT

for performing annual field surveys with limited personnel; hence, UAV-CRP technology can result in substantial savings for the state DOT in these survey-related expenses. Still, there are some research-related questions on the validity of the UAV interpreted results versus traditional measurements. These questions can be answered with more field surveys and analyses of results in a broader scale analysis.

CHAPTER 3: TOTAL SYSTEM ERROR ANALYSIS

3.1 INTRODUCTION AND BACKGROUND

Calibration defines the accuracy and quality of measurements recorded by a device (Tempcon 2018). Like every measurement system, calibration checks, including measuring the accuracy of the UAVs and the visible light camera assembly, need to be thoroughly checked and evaluated. Unfortunately, sparse literature details were available on UAV-CRP studies, partly due to this being a relatively new method for an advanced infrastructure health monitoring application and therefore limited by the adoption issues in transportation infrastructure monitoring due to regulatory concerns.

A comprehensive set of calibration procedures using the sparsely available literature as well as discussions with subject matter experts on UAVs, surveying, photogrammetry and civil infrastructure have been devised as part of this research. The goal of these calibration checks is to minimize any uncertainty in imagery measurements by ensuring the accuracy of the total data collection system thereby assisting in high-quality infrastructure data collection (Congress et al. 2018).

This chapter covers the need for comprehensive calibration checks for UAV-CRP technology and parameters that are necessary for infrastructure inspections. The following sections provide the objectives and methodologies followed to obtain data results. The methodologies contain step-by-step guidelines for performing various calibration checks in both laboratory and field based UAV-

CRP studies. Subsequently, the data results are analyzed and used to obtain best field practices conducive to obtaining high quality infrastructure monitoring data. These calibration checks and the UAV-CRP technology results are proven valuable in obtaining high quality three-dimensional (3D) models of civil infrastructure data as is evident from pavement infrastructure data provided in the later sections.

3.2 UAV-CRP CALIBRATION OBJECTIVES AND CHECKS

Camera calibration parameters, including focal length of camera lens and principal point offset, as well as radial and tangential distortion coefficients, are often considered and evaluated using a sufficient number of ground control points. These calibration parameters were computed by operating UAVs at different field environmental conditions. Ground checkpoint coordinates were considered and used in calculating the root mean square error (RMSE) values in latitude, longitude, and altitudes of original point locations in the field and their respective locations in the generated model. These comparisons are used to estimate and evaluate the accuracy of the generated three-dimensional dense point cloud model.

Figure 3-1 presents UAV equipment and accessories used in this research, which includes an Aibotix hexacopter UAV system and several accessories such as the GNSS surveying unit and a high definition camera attached with 20 mm lens (Figure 3-1). Though all the equipment used in this UAV research are high quality and off-the-shelf products, still there is a necessity to test the compatibility of these equipment when involved with the aerial infrastructure monitoring and field

assessment. Before collecting the infrastructure data, a comprehensive set of checks were planned and executed using the total system comprising of the UAV and other accessories to evaluate the quality of data provided by the UAV-CRP technology.

(a) (b) (c)

Figure 3-1. UAV-CRP Technology Accessories (a) Hexacopter (b) GNSS Unit (c) Digital Camera with 20mm Lens

In the UAV-CRP studies, imaging analysis is typically performed on the infrastructure photographs collected from the UAV platform. Images collected are then used to develop 3D infrastructure models. It is necessary to check and evaluate various parameters that will influence UAV based image collection as the final 3D models might be influenced by the imagery collection. These parameters include geotagging of the images, camera parameters such as focal length of the lens and monitoring of environmental field conditions including thermal and wind conditions at the site, as well as other image related distortion errors. A comprehensive understanding and then evaluation of any potential errors would help in assessing and ultimately enhancing the quality of image collection that will

provide a complete understanding of the infrastructure imaging analysis and health monitoring assessment steps performed subsequently.

3.2.1 Equipment Details

3.2.1.1 Aibot X6 V2 Hexacopter by Aibotix

Figure 3-2 presents the Aibot X6 system produced by Aibotix and Leica Geosystems distributes and provides technical assistance. Table 3-1 provides a summary of technical features of the X6 presented here.

Figure 3-2. Components of Aibot X6 V2 Hexacopter (Source: Leica Geosystems)

Table 3-1. Technical features of Aibot X6 V2 hexacopter (Source: Aibotix)

Length/width	1.05 m (3.4 ft)
Height	0.45 m (1.5 ft)
Construction	Carbon fiber composite (CFK)
Dead weight	3,400 g
Take-off weight	4,600 g – 6,600 g
Maximum payload *	2,000 g – 3,200 g
Maximum speed *	40 km/hr
Maximum flying height *	3,000 m density altitude
Flight time *	Up to 30 minutes
Operating temperature	-20 to 40 degrees Celsius
Positioning	GPS/RTK
Control	Manual and autonomous
Batteries	2x 5,000 mAh Lithium-Polymer

*Dependent on payload and conditions

The Aibot X6 hexacopter is designed for a wide range of applications including surveying, infrastructure monitoring, precision agriculture and other areas. Underneath the hexacopter, green LED lights in the front and red LED lights in the back assist in determining its orientation during flight. It has six motor and propeller pairs enclosed in a lightweight composite airframe to handle high winds. It also consists of ultrasonic and barometric sensors that assist in maintaining

altitude hold at a safe distance above the ground. The LVP antenna relays the video signals to the digital live video display unit (DLVP). Top and bottom servo gimbals on the copter accommodate and hold different types of sensors. The multi-cable geo-box triggers the camera in accordance with either the flight plan or intervalometer. The X6 has four legs that assist in takeoff and landing operations.

3.2.1.2 Trimble R8 GNSS unit

This unit consists of a receiver, as shown in Figure 3-1b, compatible to work in base only, rover only, or base and rover configurations. Coordinates of the ground control and check points are obtained by post-processing the collected data at the respective ground points.

3.2.1.3 Sony Alpha 6000

A normal DSLR camera, as shown in Figure 3-1c, was used in this research and the settings adopted during the data collection are presented as follows:

- Lens Focal Length : 20.0 mm
- Shutter Speed : 1/800
- Image Sensor Width : 23.5 mm
- Image Sensor Height : 15.6 mm
- ISO : Auto
- Aperture : f2.8

The camera is triggered by the multi-cable geo-box depending upon either the flight plan or the intervalometer. Images and videos can be recorded by

plugging the HDMI cable into the camera. All inspection features of the infrastructure can be monitored in real-time using the Digital Live Video Display unit (DLVP) positioned at the ground station.

3.2.2 Camera Calibration Parameters

Most of the modern cameras follow the simple pinhole camera model where the light reflected from the inspecting object enters through the aperture and forms a sharp image on the sensor (Scratchapixel 2.0 2018). Focal length (f), as shown in Figure 3-3a, is defined as the optical distance from the point where light rays converge at the lens to the camera sensor (Berkenfeld et al. 2018; Martin 2012). Two types of lenses, prime and zoom lens, are categorized by constant and varying focal lengths, respectively. Theoretically, the principal point is the intersection of the optical axis and the center of the camera sensor, as shown in Figure 3-3b, and also the origin of the camera coordinate system (Simek 2013). The deviation of the actual principal point from the theoretical principal point is termed as the principal point offset (C_x, C_y).

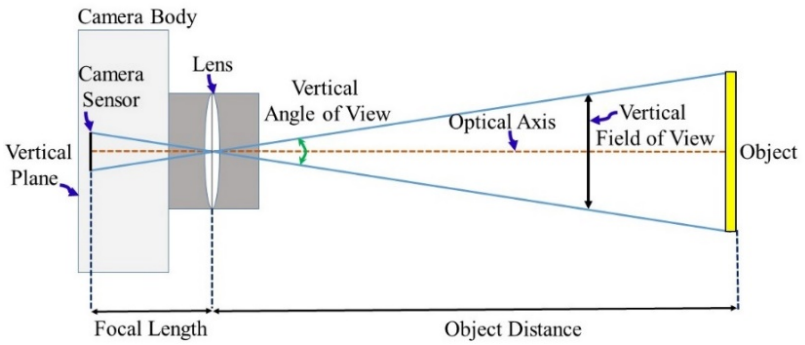

(a)

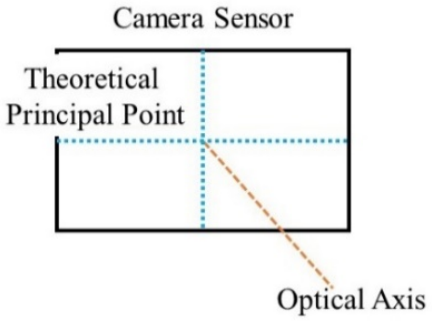

(b)

Figure 3-3. Calibration Parameters (a) Focal Length and (b) Principal Point

Due to the variance in manufacturing and positioning of the lens, there are two types of distortions including radial and tangential distortions, respectively. Radial distortion can be observed when the straight lines appear curved in the images (Mathworks 2017; University of Cologne 2017). There are two types of radial distortion: barrel distortion (or positive radial distortion) appears when lines appear to curve inwards, and pincushion distortion (or negative radial distortion)

appears where lines appear to curve outwards, as shown in Figure 3-4 (University of Cologne 2017).

Barrel distortion occurs when the field of view of lens is larger than the size of the camera sensor, making straight lines curve inwards in an attempt to fit the information. Pincushion distortion occurs because the field of view of lens is smaller than the size of the camera sensor, curving straight lines outwards in an attempt to fit the information (Mansurov 2018). Tangential distortion, on the other hand, occurs when the lens, sensor and vertical plane are not in parallel alignment, as shown in Figure 3-5 (Mathworks 2017). Radial distortion coefficients (k_1, k_2, k_3); and tangential distortion coefficients (p_1, p_2) are the calibration parameters considered related to distortion.

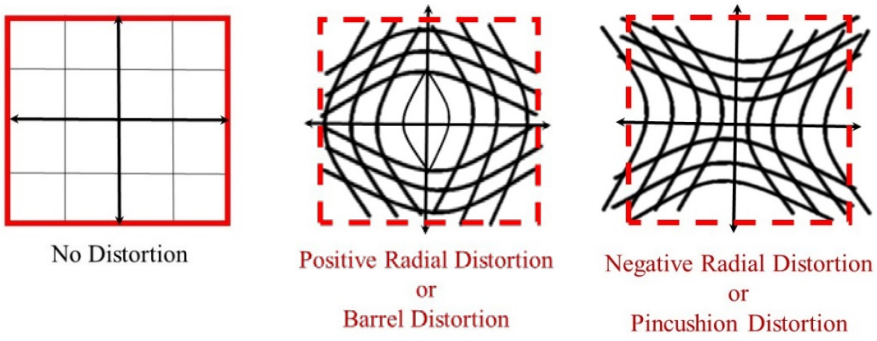

Figure 3-4. Different Radial Distortion Scenarios

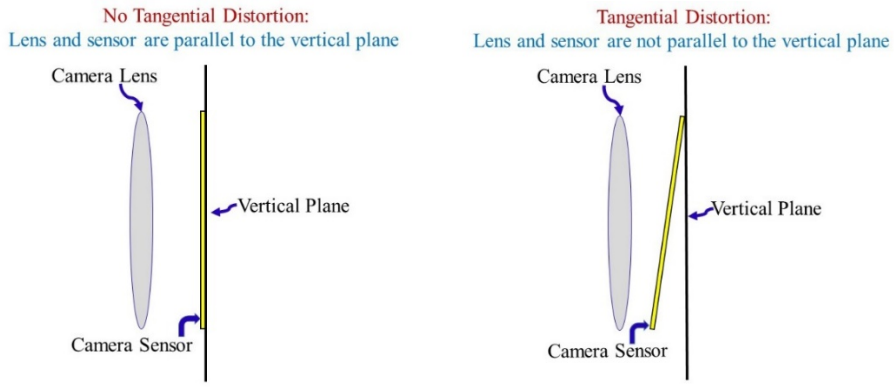

Figure 3-5. Different Tangential Distortion Scenarios

Camera calibration parameters related to various image features, as shown in Figures 3-4 and 3-5, are considered and fully addressed in both indoor and outdoor analyses on camera calibration parameters. Parameters addressed are focal length (f); principal point offset (C_x, C_y); radial distortion coefficients (k_1, k_2, k_3); and tangential distortion coefficients (p_1, p_2).

Ground sampling distance (GSD) can be obtained by dividing the product of flight height (F_H) and sensor width (S_W) with the product of focal length (f) and number of pixels per image width (N_I), as shown in Eq. 2. Provided there is good resolving power of the camera, smaller GSD often result in better quality data. Hence, using a higher focal length for the same flying height, sensor dimensions, and number of pixels per image will result in a better GSD. Varying flying height will also affect the ground sampling distance thereby affecting the quality of data. Hence an appropriate flight altitude adopted for the corresponding level of data quality acquired using a camera with specific focal length.

$$GSD = (F_H * S_W) / (f * N_I) \quad \text{Eq. (2)}$$

According to Smith et al. (2014a), the drafting committee of the American Society for Photogrammetry and Remote Sensing (ASPRS)'s Positional Accuracy Standards for Digital Geospatial Data, the quality of the 3D models obtained from the imagery are not solely dependent upon focal length, principal point offset, and distortion coefficients. Other factors such as amount of imagery overlap, quality of the GPS signal, density of ground points, flight altitude, and others will also influence the accuracy of 3D models (Smith et al. 2014a). All of the parameters discussed above play an important role in the image capture as any errors of these parameters will result in erroneous three-dimensional point cloud models in subsequent engineering analysis.

The present research addresses the variance of 3D model errors with variance in calibration parameters, flight altitude, overlap, atmospheric conditions, and location accuracy as a part of the infrastructure image measurements using the UAV platform. The following sections provide a holistic approach adapted by this research to assess individual unit performance in combination with the platform and external environmental variables associated in the imagery collection.

3.2.3 Calibration Objectives

Comprehensive calibration studies were devised and conducted on the hexacopter UAV and camera accessory components to address the following objectives and

evaluate any errors in the imagery and interpreted data collected by the UAV-CRP technology:

I. To study the variation in accuracy of geotagging images

II. To study the variation in the focal length of camera lens

III. To study the thermal effects on camera lens

IV. To study the nonlinear errors like radial and tangential distortion errors

V. To evaluate the 'Structure from Motion' (SfM) errors, and

VI. To analyze resolution and resolving power of the system

Various calibration parameters related to above specific objectives are computed by various workflows discussed in the following sections.

3.3 STEP-BY-STEP METHODS FOR CALIBRATION CHECKS

Figure 3-6 presents an outline of the steps involved in the total system error procedures followed in this research. As a part of the analysis, researchers calculated calibration parameters of the camera mounted on a tripod in indoor ambient conditions as well as the camera mounted on UAV in outdoor flying conditions. On the outdoor flight collected data, the root mean square error (RMSE) values in latitude, longitude and altitude of the actual checkpoint positions in the field, and the estimated checkpoint positions of the model are calculated and evaluated to validate the accuracy of the 3D models of infrastructure.

Results are analyzed and discussed with respect to flight altitude, atmospheric conditions, image overlap, and georeferencing. The total system error

analysis attempted here focuses on how the variance in different factors discussed by Smith et al. (2014a) influence the accuracy of the 3-dimensional dense point cloud model of infrastructure that is ultimately produced. All these parameters obtained are tabulated appropriately for comparison and accomplishing the objectives.

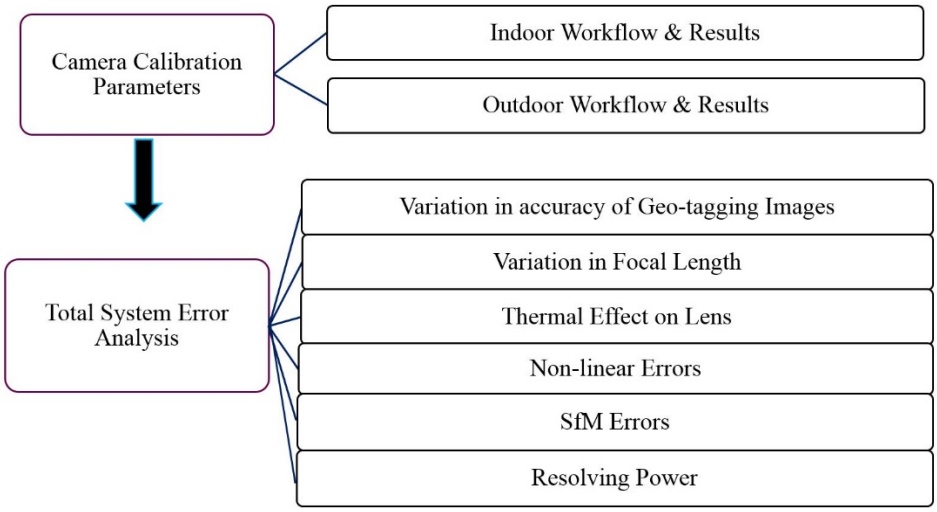

Figure 3-6. Flow Chart Depicting the Step-by-Step Method for Calibration Checks

3.3.1 Indoor Workflow

Indoor workflow analysis was conducted to study the deviation of camera parameters from the manufacturer specifications. These analyzed results were used to compare and determine the acceptance of the parameters obtained in the field. The steps involved in indoor workflow were performed as presented in the following section:

A minimum of three images of the checkerboard as shown in Figure 3-7 were first captured. Agisoft Lens Software, which is based on Brown's distortion model, was used for analyzing the images. This software has inbuilt algorithms to check the straightness of the checkerboard lines and identify the inner square corners of the checkerboard in the collected images. After uploading all images, poor quality images were screened according to a quality number provided by the software and removed after manual inspection. Desired camera calibration parameters that need to be measured were established and then a calibration function was executed in the image analysis. After completion of this process, camera calibration parameters can be exported as an XML file. These parameters for every iteration are tabulated for further comparisons in addressing each of the above objectives.

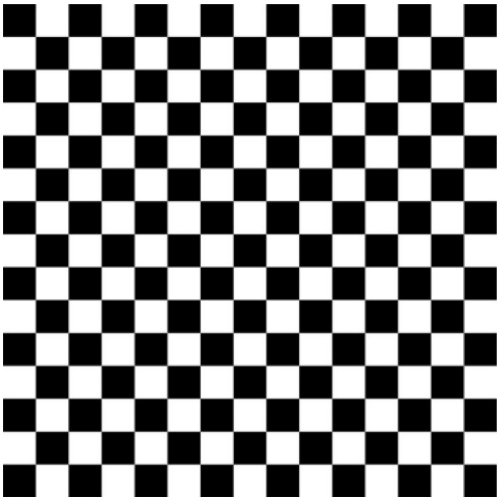

Figure 3-7. Checkerboard Image Used for Indoor Calibration Analysis

3.3.2 Outdoor Workflow

Outdoor analysis was conducted to address the changes in camera calibration parameters and then evaluate the RMSE values between latitude, longitude and altitude parameters of original points' location in the field and their respective location in the generated model with respect to different flight altitudes, atmospheric temperatures, lens temperature and other factors. For this purpose, a parking area outside the UT Arlington campus was used as a test site location for operating UAV flights at three different altitudes of 40 m (132 ft), 30 m (98 ft), and 22m (72 ft). The steps involved in performing outdoor workflow are presented in the following:

The detailed procedure includes establishing ground points spread over the field area, as shown in Figure 3-8a. Ground points consists of ground control points (GCPs) that help to build the 3-dimensional (3D) dense point cloud model and checkpoints (CKs) which are used to evaluate the accuracy of the 3D dense point cloud model generated. Availability of a high accuracy GNSS unit determines the number of GCPs required for achieving a dense point cloud of an infrastructure image with an optimum accuracy.

A flight plan with an adequate amount of longitudinal and lateral overlaps was created to cover the infrastructure area under inspection, as shown in Figure 3-8b. The image data was then collected by autonomously traversing the UAV

through the waypoints as shown in Figure 3-8c. Autonomous navigation facilitates repeatable and reproducible infrastructure monitoring data.

In Figure 3-8c, two consecutive images captured from the drone are observed to have a longitudinal overlap marked in yellow and two adjacent images captured along two adjacent flight legs have a lateral overlap that was marked in purple. Three sets of longitudinal and lateral overlaps equaling to 80% & 60%, 70% & 50%, and 60% & 40% respectively were selected and studied for each flight altitude.

The Global Navigation Satellite System (GNSS) was connected to the nearest base station after logging all the necessary details into the GNSS NTRIP caster manager (Networked Transport of Radio Technical Commission for Maritime Services via Internet Protocol). After the field tasks including UAV flights and image data collection were completed, the image data was geotagged using real time kinematic (RTK) based GNSS data. However, there was also another option for geotagging the images using post processing kinematic (PPK) based GNSS data. The PPK data could only be accessed after the base station is updated with the satellite constellation data, which typically could take couple of days after the flight operation. Consequently, this research used RTK data, which offers quick access to high quality UAV location data in real time and was accessed immediately after completing the UAV flight mission.

The geotagged images were uploaded into Agisoft PhotoScan software and these images were paired using a high quality alignment, as shown in Figure 3-8d. The text file comprising of the original coordinates of GCPs were inputted into the software, and these control points were then manually located in the captured images, as shown in Figures 3-8e and 3-8f. The model was corrected based on the differences between GCP locations generated in the model and the locations that were manually identified. The camera images were then optimized to generate the camera calibration parameters that were utilized during infrastructure imaging and related performance data collection.

The camera calibration parameters of the model inspected at a particular flight altitude, overlap, atmospheric temperatures, and other parameters were determined and then exported as a text file for further comparisons. These calibration parameters were used by Agisoft PhotoScan software to process the point cloud generation, mesh and texture rendering, and ortho-rectification. A fully navigable Digital Elevation Model (DEM) was then generated along with the three-dimensional dense point clouds, mesh and orthomosaics. Dense point cloud model and orthomosaic files of the model were exported in LAS and TIFF file formats, respectively for further processing.

These dense point cloud and the orthomosaic files were imported into LP 360 software, a commercial software that can be utilized to analyze three-dimensional point clouds collected from aerial sensors. A text file comprising of

the actual checkpoint coordinates were imported into the software to mark the position of each check point on the 3D model depending upon the respective latitude, longitude, and altitude values of each check point. The accuracy of the generated 3D model was inferred from the RMSE values calculated between latitude, longitude, and altitude values of the original point coordinates in the field and their respective locations marked manually on the generated 3D model as shown in Figure 3-8g and 3-8h. The pink square in the Figure 3-8h represents the estimated location of the checkpoint on the model generated from the imported checkpoint coordinates file and the green cross represents the actual location of the checkpoint manually located on the generated 3D model.

The camera calibration parameters, 3D model, orthomosaic, and the RMSE values denoting the accuracy of the models were generated for different flight altitudes, overlaps, and atmospheric temperatures for comparison purposes. The following sections cover analysis and discussion of these results.

(a) (b)

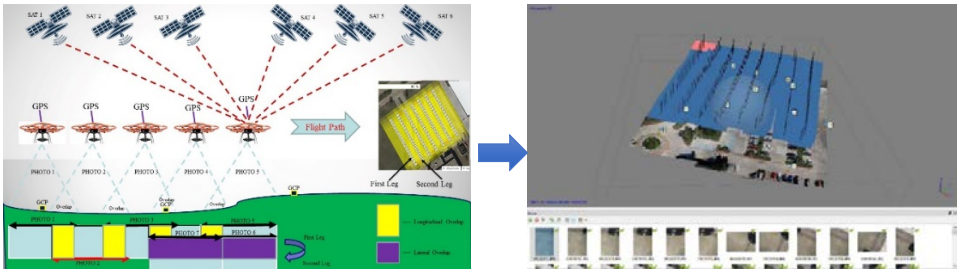

(c) (d)

(e) (f)

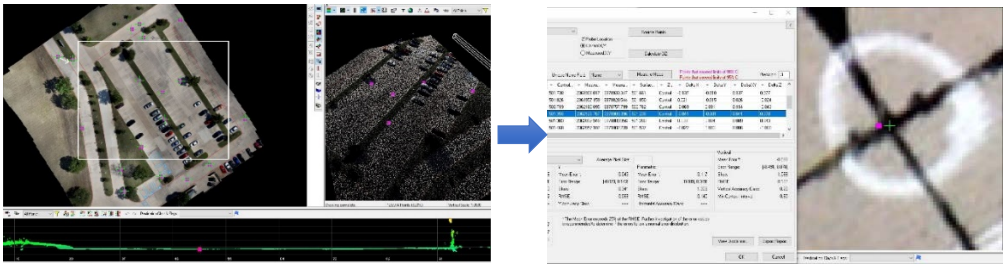

(g) (h)

Figure 3-8. Outdoor Workflow Details (a) Process of Setting-Up Ground Points; (b) Flight Plan Comprising of Adequate Overlap and Waypoints Information; (c) Data Collection Through Autonomous Navigation and Identification of Longitudinal and Transverse Overlap in Aerial Images; (d) Pairing of Geotagged Images with High Quality Alignment; (e) Manual Location of GCPs Over the

Inspection Area; (f) Close-up View of Manually Marked GCP Represented by a Green Flag; (g) Estimated Position & Actual Position of Check Points Marked Over the Infrastructure Model; (h) Close-up View of Estimated Position of Check Point Represented by Pink Square and Actual Position of Check Point Represented by Green Cross

3.4 ANALYSIS OF TEST RESULTS AND DISCUSSION

Data collected from both workflows were analyzed in the following sections to address the specific objectives of performing total system error analysis:

3.4.1 Variation in Accuracy of Geotagging Images

Even though the UAV is navigated with the help of a geographical positioning system (GPS), location details provided by GPS could be less accurate. Therefore, there is a need for considering a more accurate way of obtaining the elevations at which the images were captured. Advent of the global navigation satellite system (GNSS) had offered research team an accurate way of estimating the location of the UAV while capturing images. The ability to process the GNSS location data either in Real Time Kinematic (RTK) or Post Processed Kinematic (PPK) offers certain flexibility while operating in remote areas where there could be a problem accessing the base station. The GNSS cap can be mounted on the UAV during the image capture process to facilitate the collection of both RTK and PPK based data for geotagging the images.

RTK system typically works in real-time through a radio-link established between the antenna connected to the GNSS cap on the UAV and a base station on the ground. When the base station is far from the UAV antenna to access, then a temporary base station will be created and connected to the main base station through internet. RTK assists in accurately geo-tagging the images immediately after the completion of the flight surveys. The data stored in the GNSS cap along with the PPK data from the base station is used to geotag the flight images as well. However, the drawback of PPK data being accessible only after couple of days, when satellite data was updated at the respective base station, prompted the use of RTK geotagging results.

In this research, RTK geotagging accuracy was compared with the accuracy offered by GPS based geotagging. This helped in evaluating the type of geotagging method that needs to be used to obtain accurate infrastructure monitoring data. A lightweight rope was used so the weight of the rope will not influence the flying capability of the UAV hexacopter used in this research, shown in Figure 3-9.

Figure 3-9. Flying UAV Attached with a Lightweight Rope Marked with 1-meter Intervals

A 12-meter long lightweight rope was marked at 1-meter intervals and tied to the bottom of the camera gimbal. The UAV was flown in manual mode to trigger the camera at every 1-meter altitude levels. After the UAV took off from the ground elevation of 152.93 m, ten images were collected at 1-meter altitude intervals. The captured images were immediately geotagged after the completion of the flight using RTK data and GPS data for comparison provided below.

Table 3-2 presents approximate elevations (second column) above which the photo was taken, both RTK geotagged, and GPS geotagged image elevation data shown in the third, and fifth columns, respectively. The RTK data can be

observed to have an error ranging from -0.06 m to 0.08 m (column 4). The GPS geotagged data appears to have a much larger error ranging from -2.85 m to -4.63 m (column 6). Some of the errors in the RTK geotagged data can be accounted for by the differences in distances between the starting point of the cable and the camera sensor and any slight bends in the lightweight rope due to wind at the site during surveys.

Considering these factors, the accuracy levels provided by RTK geotagging of the images is deemed acceptable. This check has ensured that it is possible to collect infrastructure data and build an accurate 3-D dense point cloud models for analysis when RTK geotagging images are used for such model generation.

Table 3-2. Comparison of Elevations of Images Geotagged from RTK GNSS and GPS Data

Image	**Estimated Original Elevation (m)**	**RTK GNSS Elevation (m)**	**RTK Elev. – Est. Original Elevation (m)**	**GPS Elevation (m)**	**GPS Elev. – Est. Original Elevation (m)**
1	153.93	153.99	0.06	151.08	-2.85
2	154.93	154.93	0.00	151.66	-3.27
3	155.93	155.87	-0.06	152.18	-3.75
4	156.93	156.89	-0.04	152.95	-3.98
5	157.93	158.01	0.08	153.91	-4.02

6	158.93	158.96	0.03	154.68	-4.25
7	159.93	159.92	-0.01	155.43	-4.5
8	160.93	160.93	0.00	156.41	-4.52
9	161.93	161.91	-0.02	157.30	-4.63
10	162.93	162.97	0.04	158.49	-4.44

Where RTK is Real Time Kinematic; GNSS is Global Navigation Satellite System; GPS is Global Positioning System; RTK Elev. is Elevation from the RTK GNSS data from UAV's GNSS unit; GPS Elev. is Elevation from the GPS data from UAV's GPS unit; and Est. Original Elevation is Estimated Original Elevation of each image with 1 meter increments above the base elevation.

3.4.2 Variation in the Focal Length of the Camera

The objective of this calibration check is to study and address changes in focal length of the camera lens and any errors associated in generating the three-dimensional dense point cloud model from camera imagery. First, indoor data were collected, and the indoor camera calibration parameters were then obtained following steps discussed herein related to indoor workflow. Table 3-3 presents variations of focal length measurements in ambient indoor conditions maintained at 21°C (70°F). These results show that the focal length remained constant and close to the manufacturer focal length of 20 mm in all the indoor trials.

Table 3-3. Indoor Camera Calibration Parameters Obtained in Various Trials

Parameter	Trial 1	Trial 2	Trial 3	Trial 4
f (mm)	20.23	20.23	20.26	20.27
C_x (Pixels)	−48.19	−42.69	−47.10	−47.84
C_y (Pixels)	−21.31	−31.27	−16.15	−16.28
k_1	−0.18	−0.19	−0.18	−0.18
k_2	0.17	0.18	0.17	0.16
k_3	−0.03	−0.05	−0.03	−0.02
p_1	0.00	0.00	0.00	0.00
p_2	0.00	0.00	0.00	0.00

Where f is focal length; (C_x, C_y) is principal point offset; k_1, k_2, and k_3 are radial distortion coefficients; and p_1, and p_2 are tangential distortion coefficients

Outdoor calibration data collection was performed on UAV flights operated at three different flight altitudes, 40 m (132 ft), 30 m (98 ft), and 22 m (72 ft), respectively, and the outdoor camera calibration parameters were obtained using images collected from these flight surveys in the field. All the outdoor flights were performed with 80% longitudinal overlap and 60% lateral overlap, respectively. The atmospheric temperature values were collected from the weather applications available over internet. Variations in focal length with changes in atmospheric temperature along with their RMSE values are presented in Table 3-4.

Focal length values measured from outdoor studies, shown in Table 3-4, did not vary much at a given flight altitude, suggesting that outside prevailing ambient conditions during data collection did not have much influence on the camera lens calibration parameters. The RMSE values of the points in the generated three-dimensional model compared to the original field points in the X, Y, and Z directions, are also small.

Table 3-4. 3D Model RMSE Values Corresponding to Data Collected at Three Flight Altitudes Operated At Three Atmospheric Temperatures

Flight Altitude of 40 m (132 ft) with 80% & 60% Overlap Set			
Parameter	Trial 1 (32°C)	Trial 2 (33°C)	Trial 3 (36°C)
Focal length (mm)	20.42	20.71	20.47
X RMSE (cm)	3.4 [0.11]	2.1 [0.07]	3.7 [0.12]
Y RMSE (cm)	2.4 [0.08]	1.8 [0.06]	2.4 [0.08]
Z RMSE (cm)	4.6 [0.15]	4.3 [0.14]	5.2 [0.17]
Flight Altitude of 30 m (98 ft) with 80% & 60% Overlap Set			
Parameter	Trial 1 (32°C)	Trial 2 (33°C)	Trial 3 (36°C)
Focal length (mm)	20.47	20.66	20.43
X RMSE (cm)	3.0 [0.10]	2.7 [0.09]	4.0 [0.13]
Y RMSE (cm)	2.4 [0.08]	1.8 [0.06]	2.7 [0.09]
Z RMSE (cm)	4.6 [0.15]	3.4 [0.11]	5.2 [0.17]
Flight Altitude of 22 m (72 ft) with 80% & 60% Overlap Set			

Parameter	Trial 1 (32°C)	Trial 2 (33°C)	Trial 3 (36°C)
Focal length (mm)	20.60	20.50	20.43
X RMSE (cm)	−3.0 [−0.10]	−2.7 [−0.09]	−3.7 [−0.12]
Y RMSE (cm)	1.8 [0.06]	1.8 [0.06]	2.1 [0.07]
Z RMSE (cm)	5.2 [0.17]	4.6 [0.15]	5.8 [0.19]

Where RMSE is Root Mean Square Error and RMSE values in feet are provided in [ ]

From the above analysis and results, it is noted that the focal length slightly varied with changes in UAV flight altitude, and flying operating conditions. When compared with the manufacturer specifications, the change in focal length in field conditions is between 2% and 3.5%, which is small and insignificant. Focal length changes that occurred in the field conditions did not influence the accuracy of the dense point model when these images were used in the subsequent analysis. This was also evident from the RMSE values in the X, Y, and Z directions, as provided in Table 3-4. Hence, the prevailing atmospheric conditions during the data collection did not influence the present UAV-CRP system and its data collection.

3.4.3 Thermal Effect on Lenses

In this calibration check, the objective is to study the influence of outside thermal temperatures on the focal length of a camera using localized lens temperature measurements. The following steps were performed to study and observe any

changes associated in the focal length of the camera with change in lens temperature. Only outdoor studies were performed as a part of this check, which includes UAV flight operations at three different flight altitudes: 40 m (132 ft), 30 m (98 ft), and 22m (72 ft). The task includes collecting images and measuring the localized camera lens temperature after each flight using an infrared thermometer. The outdoor camera calibration parameters were obtained using steps described in the section related to outdoor workflow. Lens temperature was measured using the Fluke 59 MAX infrared thermometer, as shown in Figure 3-10.

Figure 3-10. Fluke 59 MAX Infrared Thermometer

All the outdoor flights for this objective were performed with 80% longitudinal and 60% lateral overlap, respectively. RMSE values for corresponding 3D models were calculated and included in the analysis. Table 3-5 presents the variation of focal length with lens temperature in field conditions.

Table 3-5. 3D Model RMSE Values Corresponding to Three Flight Altitudes Operated at Three Atmospheric and Lens Temperatures

Flight Altitude of 40 m (132 ft) with 80% & 60% Overlap Set			
Parameter	Trial 1 (32°C)	Trial 2 (33°C)	Trial 3 (36°C)
Focal length (mm)	20.42	20.71	20.47
Lens Temp (°C)	33.2	33.8	40.6
X RMSE (cm)	3.4 [0.11]	2.1 [0.07]	3.7 [0.12]
Y RMSE (cm)	2.4 [0.08]	1.8 [0.06]	2.4 [0.08]
Z RMSE (cm)	4.6 [0.15]	4.3 [0.14]	5.2 [0.17]
Flight Altitude of 30 m (98 ft) with 80% & 60% Overlap Set			
Parameter	Trial 1 (32°C)	Trial 2 (33°C)	Trial 3 (36°C)
Focal length (mm)	20.47	20.66	20.43
Lens Temp (°C)	33.2	36.6	39.3
X RMSE (cm)	3.0 [0.10]	2.7 [0.09]	4.0 [0.13]
Y RMSE (cm)	2.4 [0.08]	1.8 [0.06]	2.7 [0.09]
Z RMSE (cm)	4.6 [0.15]	3.4 [0.11]	5.2 [0.17]
Flight Altitude of 22 m (72 ft) with 80% & 60% Overlap Set			
Parameter	Trial 1 (32°C)	Trial 2 (33°C)	Trial 3 (36°C)
Focal length (mm)	20.60	20.50	20.43
Lens Temp (°C)	32.1	39	37.6
X RMSE (cm)	3.0 [0.10]	2.7 [0.09]	3.7 [0.12]

Y RMSE (cm)	1.8 [0.06]	1.8 [0.06]	2.1 [0.07]
Z RMSE (cm)	5.2 [0.17]	4.6 [0.15]	5.8 [0.19]

Where RMSE is root mean square error in cm and RMSE values in feet are provided in [ ]

The data collection was conducted to observe the influence of field atmospheric and corresponding lens temperature on the accuracy of 3D models. The focal length values did not vary much with respect to the lens temperature at a given flight altitude. All three-temperature conditions did not show any appreciable impacts on the accuracy of 3D models, suggesting that the camera and lens accessories are appropriate for performing imaging studies as per their specifications.

3.4.4 Non-linear Errors

The objective of this calibration check is to study and assess any changes in the distortion parameters of the camera lens and the errors generated in the three-dimensional dense point cloud modeling from potential distortion in the captured images.

The following steps were performed in outdoor conditions during UAV studies at three different flight altitudes: 40 m (132 ft), 30 m (98 ft), and 22 m (72 ft). Once image data were captured, the camera calibration parameters were obtained, using the earlier described steps on outdoor workflow. All the outdoor flights were performed with 80% longitudinal and 60% lateral overlap. Table 3-6

presents the variation of distortion parameters with atmospheric temperature in the field conditions along with RMSE values determined at all three flight altitudes.

Table 3-6. 3D Model RMSE Values and Distortion Coefficients Corresponding to Three Flight Altitudes Operated at Three Atmospheric Temperatures

Flight Altitude of 40 m (132 ft) with 80% & 60% Overlap Set			
Parameter	Trial 1 (32°C)	Trial 2 (33°C)	Trial 3 (36°C)
k_1	−0.17	−0.17	−0.17
k_2	0.13	0.13	0.13
k_3	0.01	0.03	0.01
p_1	0.00	0.00	0.00
p_2	0.00	0.00	0.00
X RMSE (cm)	3.4 [0.11]	2.1 [0.07]	3.7 [0.12]
Y RMSE (cm)	2.4 [0.08]	1.8 [0.06]	2.4 [0.08]
Z RMSE (cm)	4.6 [0.15]	4.3 [0.14]	5.2 [0.17]
Flight Altitude of 30 m (98 ft) with 80% & 60% Overlap Set			
Parameter	Trial 1 (32°C)	Trial 2 (33°C)	Trial 3 (36°C)
k_1	−0.17	−0.17	−0.17
k_2	0.13	0.13	0.12
k_3	0.02	0.02	0.02
p_1	0.00	0.00	0.00
p_2	0.00	0.00	0.00

X RMSE (cm)	3.0 [0.10]	2.7 [0.09]	4.0 [0.13]
Y RMSE (cm)	2.4 [0.08]	1.8 [0.06]	2.7 [0.09]
Z RMSE (cm)	4.6 [0.15]	3.4 [0.11]	5.2 [0.17]
Flight Altitude of 22 m (72 ft) with 80% & 60% Overlap Set			
Parameter	Trial 1 (32°C)	Trial 2 (33°C)	Trial 3 (36°C)
k_1	-0.17	-0.17	-0.17
k_2	0.13	0.12	0.12
k_3	0.02	0.02	0.02
p_1	0.00	0.00	0.00
p_2	0.00	0.00	0.00
X RMSE (cm)	0.3 [0.01]	2.7 [0.09]	3.7 [0.12]
Y RMSE (cm)	1.8 [0.06]	1.8 [0.06]	2.1 [0.07]
Z RMSE (cm)	5.2 [0.17]	4.6 [0.15]	5.8 [0.19]

Where k_1, k_2, and k_3 are radial distortion coefficients; p_1, and p_2 are tangential distortion coefficients; RMSE is root mean square error and RMSE values in feet are provided in [ ]

Based on the results reported in the above Table 3-6, the distortion coefficients remained the same and negligible, indicating no distortion of images in all flights at different field conditions and operating altitudes. Overall, higher overlap in longitudinal and lateral directions also contribute to reducing the effect of distortion of the images on the 3D models. This can also be inferred from the small RMSE values in X, Y, and Z directions of the 3D model. For this reason, it

can be stated that this calibration check is acceptable for the total system used in this research, and no impact on dense point cloud generation is anticipated during infrastructure monitoring applications of UAV-CRP technology.

3.4.5 Structure from Motion (SfM) Errors

This SfM calibration check is to estimate any errors between actual and estimated positions in the three-dimensional dense point cloud model and assess structure from motion related errors in the analysis. This objective provides information about the influence of flight-related movements or shaking on the dense point cloud models generated from the image data collected.

Outdoor data collection was performed at three different flight altitudes: 40 m (132 ft), 30 m (98 ft), and 22 m (72 ft), with three different overlaps. Analysis was performed using the earlier described steps in the section related to outdoor workflow to study the effects of varying flight altitude and overlaps on the captured results. The RMSE values were calculated for the respective conditions and represented as the SfM errors of the developed three-dimensional dense point cloud model. Two scenarios, provided below, are considered to evaluate the SfM errors.

The first scenario provides the variation in flight altitude with a constant overlap, i.e., 80% longitudinal and 60% lateral overlap for all three flight altitudes: 40 m (132 ft), 30 m (98 ft), and 22m (72 ft). The results corresponding to two atmospheric temperatures 32°C (90°F) and 35.6°C (96°F) were provided in Table 3-7.

The second scenario provides the variation in longitudinal and lateral overlap at constant flight altitude. Results obtained from three sets of longitudinal and lateral overlap (80% & 60%), (70% & 50%), and (60% & 40%) maintained at each flight altitude 40 m (132 ft), 30 m (98 ft), and 22m (72 ft) are provided in Table 3-8.

Table 3-7 presents the SfM errors obtained at different flight altitudes at 32°C (90°F) and 35.6°C (96°F) atmospheric temperatures, respectively.

Table 3-7. 3D Model RMSE Values Corresponding to Two Atmospheric Temperatures Prevailing at Three Different Flight Altitudes

Atmospheric Temperature of 32°C			
Parameter	Flight Alt.-1 (22 m)	Flight Alt.-2 (30 m)	Flight Alt.-3 (40 m)
X RMSE (cm)	3.0 [0.10]	3.0 [0.10]	3.4 [0.11]
Y RMSE (cm)	1.8 [0.06]	2.4 [0.08]	2.4 [0.08]
Z RMSE (cm)	5.2 [0.17]	4.6 [0.15]	4.6 [0.15]
Atmospheric Temperature of 35.6°C			
Parameter	Flight Alt.-1 (22 m)	Flight Alt.-2 (30 m)	Flight Alt.-3 (40 m)
X RMSE (cm)	3.7 [0.12]	4.0 [0.13]	3.7 [0.12]
Y RMSE (cm)	2.1 [0.07]	2.7 [0.09]	2.4 [0.08]
Z RMSE (cm)	5.8 [0.19]	5.2 [0.17]	5.2 [0.17]

Where RMSE is root mean square error in cm and RMSE values in feet are provided in [ ]

Table 3-8 presents the SfM errors obtained by varying three sets of overlap (i.e., 80% & 60%; 70% & 50%; and 60% & 40%) represented as three trials: 1, 2, and 3, respectively, at each flight altitude.

Table 3-8. Structure from Motion (SfM) Errors Corresponding to Three Flight Altitudes Operated at Three Sets of Longitudinal and Lateral Overlap

Flight Altitude of 40 m (132 ft)			
Parameter	Trial 1	Trial 2	Trial 3
Longitudinal overlap (%)	80	70	60
Lateral overlap (%)	60	50	40
X RMSE (cm)	2.1 [0.07]	1.5 [0.05]	1.2 [0.04]
Y RMSE (cm)	1.8 [0.06]	2.1 [0.07]	2.4 [0.08]
Z RMSE (cm)	4.3 [0.14]	4.6 [0.15]	4.3 [0.14]
Flight Altitude of 30 m (98 ft)			
Parameter	Trial 1	Trial 2	Trial 3
Longitudinal overlap (%)	80	70	60
Lateral overlap (%)	60	50	40
X RMSE (cm)	4.0 [0.13]	3.0 [0.10]	3.4 [0.11]
Y RMSE (cm)	2.7 [0.09]	2.1 [0.07]	2.1 [0.07]
Z RMSE (cm)	5.2 [0.17]	5.2 [0.17]	6.0 [0.20]
Flight Altitude of 22 m (72 ft)			
Parameter	Trial 1	Trial 2	Trial 3

Longitudinal overlap (%)	80	70	60
Lateral overlap (%)	60	50	40
X RMSE (cm)	3.7 [0.12]	3.0 [0.10]	3.4 [0.11]
Y RMSE (cm)	2.1 [0.07]	2.1 [0.07]	2.4 [0.08]
Z RMSE (cm)	5.8 [0.19]	5.2 [0.17]	5.5 [0.18]

Where RMSE is root mean square error in cm and RMSE values in feet are provided in [ ]

At a given flight altitude, it takes more flight time to collect the data with a higher overlap set (i.e., 80% in longitudinal and 60% in lateral direction) compared to other lower overlap sets. Overall, 80% and 60% overlaps in the longitudinal and lateral direction, respectively, are regarded as the optimal overlap levels needed to obtain the required level of image data quality and to avoid the formation of any gaps in the model triggered by a no picture event by the camera during the field operations. The data provided above have shown minimal SfM errors.

All the RMSE values obtained in all the objectives discussed in above sections were observed to be less than 6 cm. According to the New ASPRS Positional Accuracy Standards for Digital Geospatial Data (Smith et al. 2014b) for non-vegetated areas, the horizontal accuracy is classified by the square root of sum of the squares of RMSE values in X and Y direction. Vertical accuracy is classified based upon the RMSE in Z direction. Accuracy of the horizontal data obtained in

all above sections is better than horizontal accuracy class of 5-cm and accuracy of the vertical data is very close to the vertical accuracy class of 5-cm.

3.4.6 Analyze Resolution and Resolving Power of the Total System

The objective of this final calibration check is to study and address both resolution and resolving powers of the total system representing UAV studies with a visible light camera. The following steps were performed as a part of the calibration check to measure the resolution and resolving power of the camera. The analysis was conducted in both indoor (as shown in Figure 3-11a) and outdoor facilities (as shown in Figure 3-11b). Typically, this analysis is performed using a Siemens star image. The Siemens star is a spoke-pattern imaging target that helps in determining the spatial resolution of the camera (Horstmeyer et al. 2016). This research considered a 16-cycle Siemens star, as shown in Figure 3-11c, with each spoke representing a cycle. This is a simple way of estimating the resolution by identifying the distance of the distinguishable dark area portion of each cycle from the center.

Siemens star used is shown in the Figure 3-11c, and this star image contains black and white windmill blade shapes with a center. This image was printed with 0.9 m (35 in.) X 0.9 m (35 in.) dimensions for laboratory and field studies. Siemens star imaging was performed with a mounted camera in three different scenarios: 1) Camera mounted on a tripod in indoors; 2) Camera mounted on the UAV in indoor

flights, as shown in Figure 3-11a; and 3) Camera mounted on the UAV in outdoor flights, as shown in Figure 3-11b.

(a) (b)

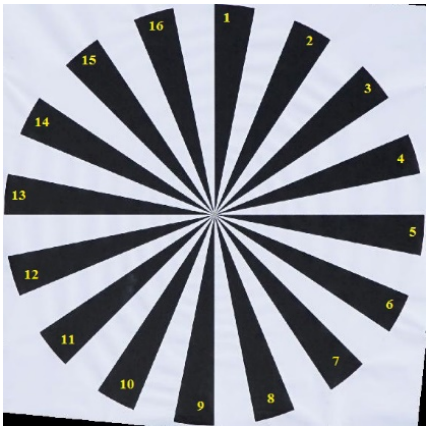

(c)

Figure 3-11. Capturing Siemens star in Different Scenarios (a) UAV Flight Indoors (b) UAV Flight Outdoors with (c) Marked Center and Cycles in Siemens Star

After capturing the Siemens star images under the different scenarios mentioned above, the following steps were performed on the captured images. First, the center was identified by marking the center squares with red and yellow colors, as shown in Figure 3-12. Second, the sixteen cycles in the Siemens star were marked as shown in Figure 3-11c. Resolution was computed by dividing the 0.9 m (35 in.) diameter of Siemens star with the number of pixels occupied by the Siemens star in either length or breadth direction. Number of relatively light colored pixels from center to the recognizable dark colored tip of each cycle near to the Siemens star center were counted from Figure 3-12.

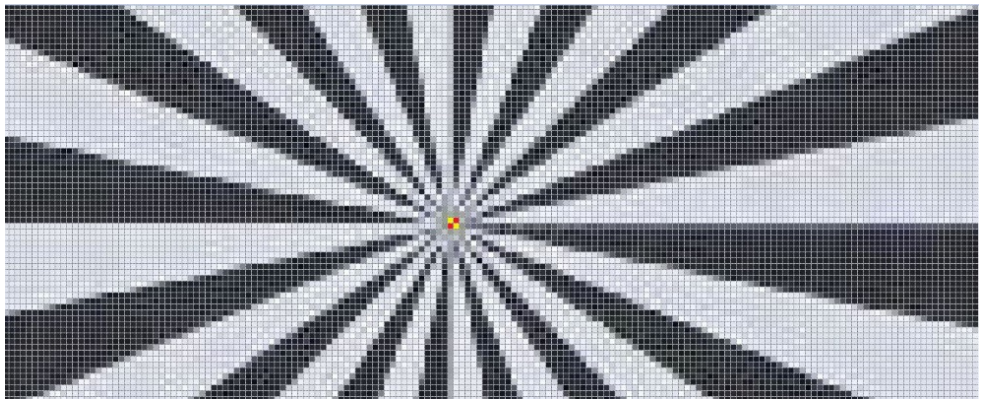

Figure 3-12. Zoomed in View of the Siemens Star Center Used to Count the Number of Light Colored Pixels from Center to the Recognizable Dark Colored Tip of Each Cycle

A matrix that includes the distance from the Siemens star center to the distinguishable dark area portion of each cycle from the center was prepared. All the measured distance values are used to obtain an average value. The average

distance value obtained above is multiplied with the resolution value to obtain the resolving power of the total system, and these results are shown in Table 3-9.

Table 3-9. Resolving Power of the Camera Mounted on Stationary and Aerial Platforms at Three Different Distances from the Siemens Star

Scenario	Trial-1 (Distance – 1.8 m)	Trial-2 (Distance – 4.3 m)	Trial-3 (Distance – 6.1 m)
Tripod Mounted Camera- Indoor	0.2 cm	0.6 cm	0.9 cm
Indoor Flight	0.2 cm	NA	NA
Outdoor Flight	0.4 cm	0.7 cm	1.2 cm

From the results shown in Table 3-9, the resolving power of the camera mounted on a tripod indoors appears slightly better than the other two scenarios. This can be attributed to absence of vibrations due to the camera's stationary position on the tripod and ambient conditions during the data collection. However, it can be observed that the resolving power of the camera mounted on drone outdoors is relatively comparable to those of the camera mounted on the tripod and drone indoors. Having a servo gimbal on the unmanned aerial platform reduces the vibrations induced during the flying operations. This might have helped in acquiring good resolving power with a diminutive blur. This final check confirms that the resolving power of the total system used in the UAV-CRP studies is suitable for infrastructure data collection in the field.

As seen from the earlier sections, the UAV-CRP system used in this research has provided an error free imagery of the infrastructure that in turn has provided an accurate three-dimensional infrastructure dense point cloud. This research knowledge gained was applied in collecting the pavement infrastructure data as provided in the subsequent section.

3.5 SUMMARY

This chapter covers comprehensive calibration checks on a UAV platform and camera used at different flight altitudes, different overlap sets, and environmental conditions. Indoor and outdoor workflows were elaborated to guide the engineering fraternity to evaluate their UAV systems. All these calibration checks helped in validating the compatibility of UAV and camera sensor accessories in providing high quality infrastructure images that were valuable engineering analyses.

The above calibration checks and results lead to the observation that the present UAV platform and camera accessories can provide photogrammetry data of high quality and excellent repeatability. This research is expected to provide a comprehensive idea to UAV users about validating the accuracy of their aerial imaging systems used for infrastructure monitoring.

CHAPTER 4: INFRASTRUCTURE MONITORING

4.1 DATA REPRESENTATION

The following infrastructure data was collected and the results were analyzed in the following sections to address the UAV applications on the state of infrastructure including pavements, bridges, rail corridor and volumes of construction material stockpiles. The site locations are provided in the Figures 4-1 and 4-2.

I. Pavement condition data was collected at the following three sites:

- TxDOT Cedar Park Campus, Austin, Texas
- TxDOT District Headquarters, Fort Worth, Texas
- US Highway 82 in Sherman , Paris District, Texas

II. Construction material stockpile volume data was collected at three sites:

- TxDOT Cedar Park Campus, Austin, Texas
- TxDOT District Headquarters, Fort Worth, Texas
- TxDOT Area Office, Decatur, Texas

III. Bridge infrastructure condition data was collected at one site:

- SH 360 Extension, Mansfield, Texas

IV. Rail infrastructure condition data was collected between Alpine-Presidio region:

- Rail Road Crossing site, at railway milepost MP 1027.22
- Rail Bridge site, at railway milepost MP 1019.5
- Washout site, at railway milepost MP 1001.5

- Rock-Cut site, at railway milepost MP 1008.1

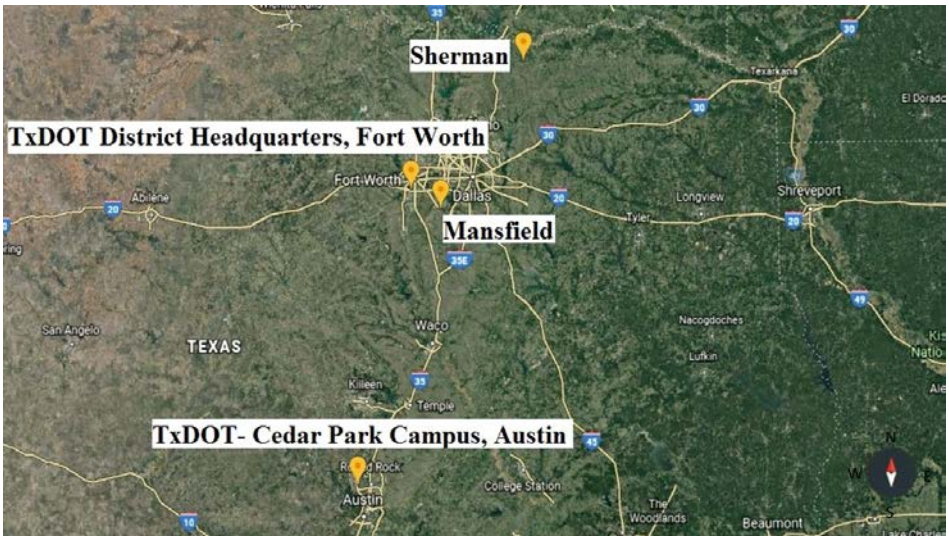

Figure 4-1. Location of the Infrastructure Data Collection Sites

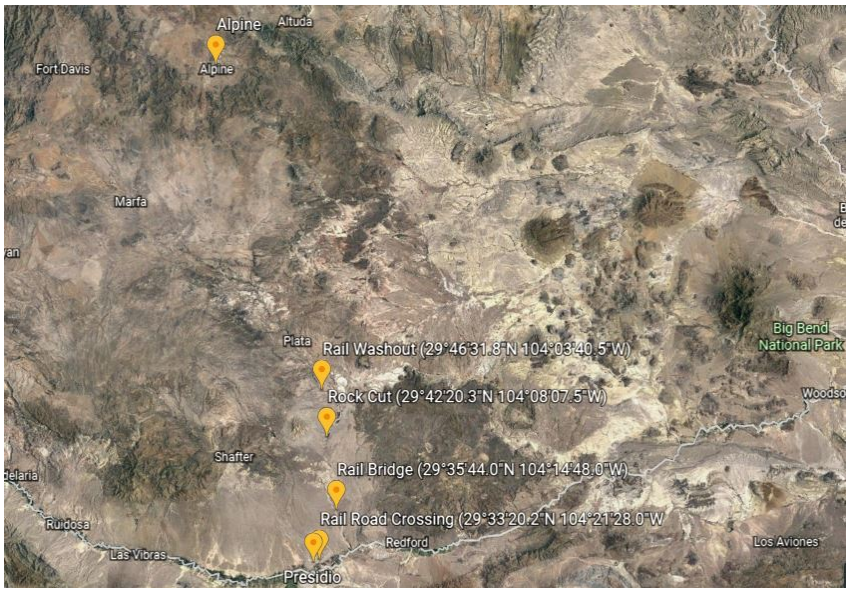

Figure 4-2. Location of Data Collection Sites between the Alpine - Presidio Region

The data from the above locations were analyzed and presented in four categories: pavement condition assessments, stockpile volume calculations, bridge inspection and rail corridor studies. The following sections cover each of these categories:

4.2 PAVEMENT FORENSICS

Measuring pavement characteristics and/or distress using traditional methods can be subjective and time consuming. The last few decades have witnessed paradigm shifts in pavement distress monitoring from inspectors conducting windshield surveys to vehicles mounted with automatic laser scanners. However, data capture using laser mounted land vehicles is affected by the shadows and moving vehicular traffic. There is also a terrestrial scanner like LiDAR system, which provides high accuracy data although consuming more time.

Compared to the past, in recent years there has been a phenomenal rise, propelled by technology advancements, in the application of drones. Growing intrigue towards employing unmanned aerial vehicles (UAVs) for frequent data collection was a driving force behind this research project. UAVs coupled with high quality camera lenses and global navigation satellite system (GNSS) devices have the scope to collect survey-grade data with a fewer ground control points (GCPs). They present a rapid, accurate and economical alternative for data collection systems. UAVs offer repeatability and reproducibility of data collection and help in monitoring change in assets regularly. As pavement distress starts to develop,

drones can be used to identify it earlier and give scope to proactive maintenance, thereby increasing the service life of the pavement.

Detailed data collection involves laying down ground points that include ground control points (GCPs) and check points (CKs) spread over the field area. A flight plan is then devised with adequate longitudinal and lateral overlaps to cover the required area under inspection. Availability of a highly accurate GNSS determines the number of GCPs required for optimum accuracy. Captured images from UAV surveys can be georeferenced using GNSS data accessed either by real time kinematic (RTK) techniques or post processing kinematic (PPK) techniques. A GNSS RTK cap is connected to the nearest base station via internet after logging in all the necessary details. All images will be stamped with time and location using a geo-box attached to the camera. Highly accurate geotagged images are then fed into the Agisoft PhotoScan software, where poor quality images can be removed. Applying photogrammetry techniques to the input images, the software processes the image alignment, point cloud generation, rendering of mesh & texture, and ortho-rectification. We can develop fully navigable digital elevation models (DEM) in addition to dense point clouds, mesh and orthomosaics.

These dense point clouds and orthomosaics are imported into the LP 360 software and CK coordinates are used to estimate the accuracy of the model. Differences between the actual position, located manually in the software, and estimated position, are located by the inputted coordinates of the CK, read in terms

of the X, Y and Z RMSE of the model. For any object under inspection, a toe (i.e., a bounding line) is formed by joining points that confine the object under inspection. The area enclosed within the toe is referred to as the base area and the point cloud data within the base represents the object. Those imported files can also be viewed at different angles to extract the toe and compute the object parameters desired in any 3D image analysis software.

4.2.1 Pavement Inspection Study Areas

Initially, a demonstration of UAV data collection capabilities was conducted in front of the TxDOT officials in TxDOT Cedar Park Campus, Austin. Apart from the regular UAV research flights in a parking lot at UTA, this was the first field visit site where the Aibot X6 was flown and a live video was shown to a larger audience. The view of the camera mounted on the drone was relayed onto two TV screens connected to the digital live video display (DLVP) for the convenience of the officials seated far from the data collection area and witnessing the drone capabilities. In addition to the inspection of the pavement site at Cedar Park Campus, the volumetric data of the two detention ponds and a sand stockpile on the campus were also collected.

After a safe and successful demonstration of initial UAV flights, this research collected the photogrammetry data of pavement stretch inside the TxDOT district headquarters in Fort Worth. Aerial data was also collected at the US Highway 82 site in Sherman, Texas to inspect a section of the highway and the

Farm to Market (FM) road adjacent to it. The draft of the TxDOT Flight Operations Manual (FOM) guidelines were followed and validated during this field visit. All these locations are shown in Figure 4-1.

4.2.2 Pavement Condition Data

Many factors influence pavement conditions and contribute to their distress with time. Expansive soils cause differential settlement due to heaving and it can be detected using aerial technologies (Puppala et al. 2018c). Analyses of the collected pavement condition data by UAV-CRP studies are presented in the following sections:

4.2.2.1 Pavement characteristics

UAV-CRP technology can be used to measure various other characteristics of pavements that help in assessing the ride quality and safety conditions offered to the road user. International roughness index (IRI) is calculated using the Golden car method that feeds on the longitudinal elevation profile of the pavement section. UAVs may be used to collect the longitudinal elevation profile by flying away from the pavement section with an inclined camera facing towards the pavement section. In the event of rain, cross-slope of the pavement is important to ensure that there is ample drainage. The ultimate goal is that there is no ponding or stagnant water on or near the pavement; this will prevent hydroplaning from impeding the available skid resistance. It also prevents moisture intrusion into underlying expansive subgrades and thereby mitigates differential movements of pavement (Mohammad

et al. 1995; Puppala et al. 2011, 2013). At turns, it is also necessary to check if there is sufficient transverse slope i.e. super elevation providing necessary centripetal force for a safe turn.

In this research, the UAV was flown adjacent to US 82 Highway located near Sherman, Texas. Cautionary signs, as shown in Figure 4-3, were placed on both directions of the highway during studies, according to guidelines from the TxDOT FOM.

Figure 4-3. Cautionary Sign Ahead of Drone Operating Area

No traffic regulations were imposed while collecting the data from the drone flying away from the pavement. Both the longitudinal and transverse slopes of the pavement were calculated from the same pavement data collected at multiple flight altitudes at 20 ft and 75 ft, respectively. The UAV was flown at a safe distance of 10 ft away from the pavement section. Hence, the camera angle was obliquely inclined towards the pavement while flying at 20 ft high and in the nadir position while flying at 75 ft high; this was to ensure full transverse coverage of the

pavement site. Due to the vegetation on the pavement shoulder, a large wooden plank was placed to serve for landing and take-off. Data collection was only conducted on one side of the pavement due to the obtained permissions for this. However, data collection on both sides would offer a more comprehensive data analysis and interpretation.

The images were processed to obtain 3D dense point cloud model and orthomosaic, as shown in Figure 4-4. Accuracy analysis was performed on the model developed from the images, using the checkpoint (CK) coordinates placed on the pavement. The RMSE values in X, Y, and Z directions of points in the model are 0.1 ft (3 cm), 0.2 ft (6 cm), and 0.1 ft (3 cm), respectively. Accuracy of horizontal data obtained is close to horizontal accuracy class of 5-cm and vertical data obtained is better than vertical accuracy class of 5-cm.

Figure 4-4. Orthomosaic of US 82 Highway Section

4.2.2.1.1 Longitudinal slope

Dense point cloud models obtained from the UAV-CRP technology were used to obtain the elevation profiles along the pavement surface. For a detailed data representation, the longitudinal slope profile was estimated by placing points along

two wheel paths, parallel to the pavement centerline, for each lane. According to AASHTO PP 69-16, the inner wheel path of the lane was defined as a line parallel to the lane centerline and at a distance of 0.875 m left of the centerline. The same standard defined the outer wheel path as the line parallel and at a distance of 0.875 m right from the lane centerline, as shown in the Figure 4-5. By taking the leverage offered by the dense point cloud model, points were placed at 1 cm intervals along the longitudinal direction of the pavement.

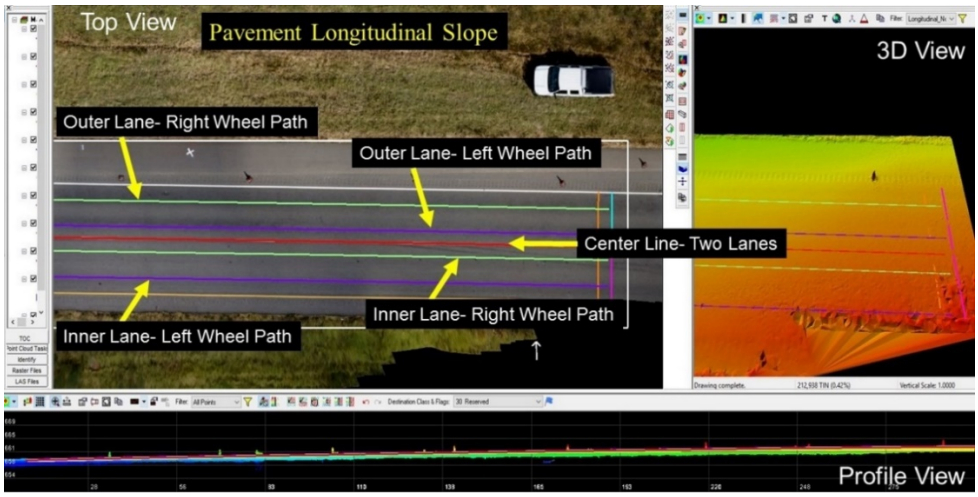

Figure 4-5. Pavement Longitudinal Slope along Two Wheel Paths of Each Lane

More than 10,000 points were placed within the 300 ft stretch, along the five paths shown in Figure 4-5

1. Outer Lane- Right Wheel Path (shown in Figure 4-6)
2. Outer Lane- Left Wheel Path (shown in Figure 4-7)
3. Center Line- Two Lanes (shown in Figure 4-8)
4. Inner Lane- Right Wheel Path (shown in Figure 4-9) and

5. Inner Lane- Left Wheel Path (shown in Figure 4-10)

The starting point of the inspection stretch was considered the datum point and the difference in the elevation of all other points from the datum point was plotted to understand the longitudinal profile. All five paths provided information on the varying longitudinal profiles of the pavement section.

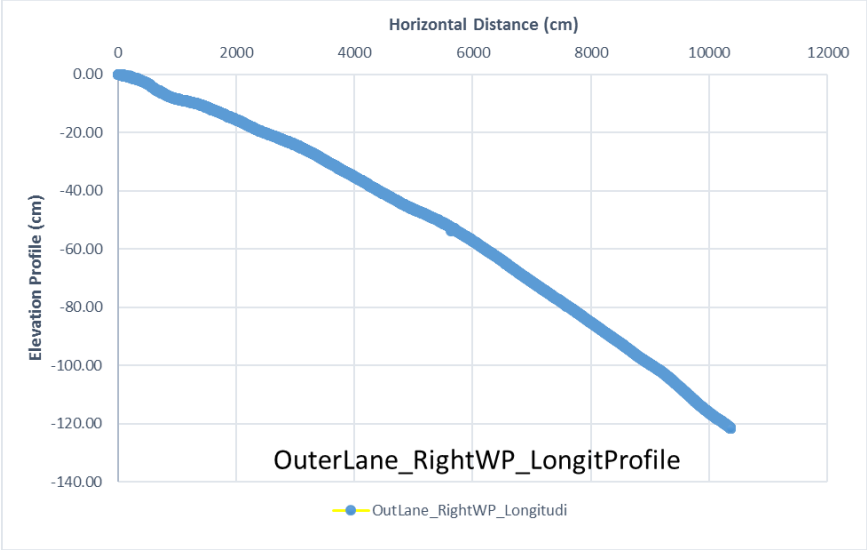

Figure 4-6. Longitudinal Profile along Right Wheel Path of Outer Lane

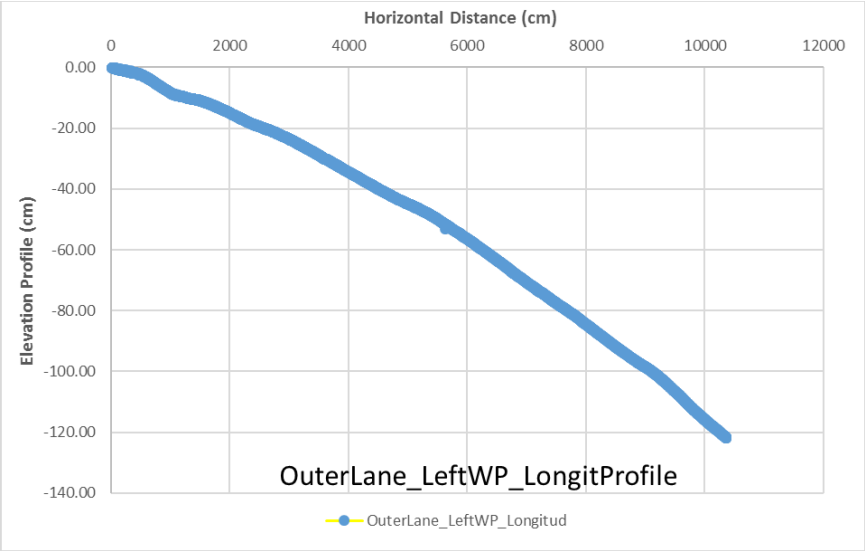

Figure 4-7. Longitudinal Profile along Left Wheel Path of Outer Lane

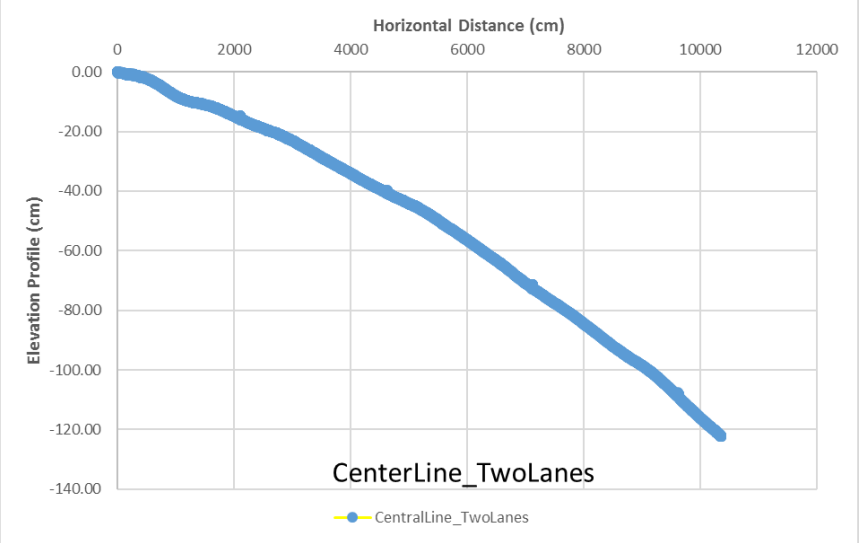

Figure 4-8. Longitudinal Profile along Centerline of Two Lanes

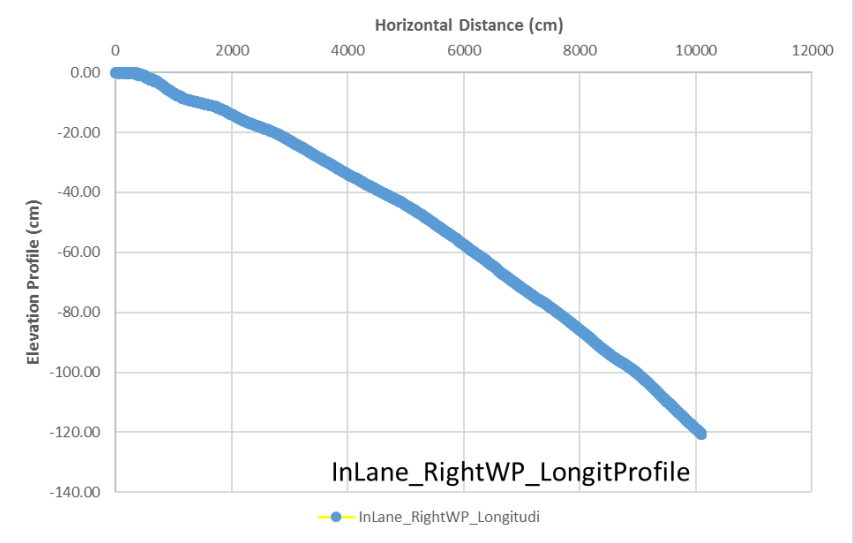

Figure 4-9. Longitudinal Profile along Right Wheel Path of Inner Lane

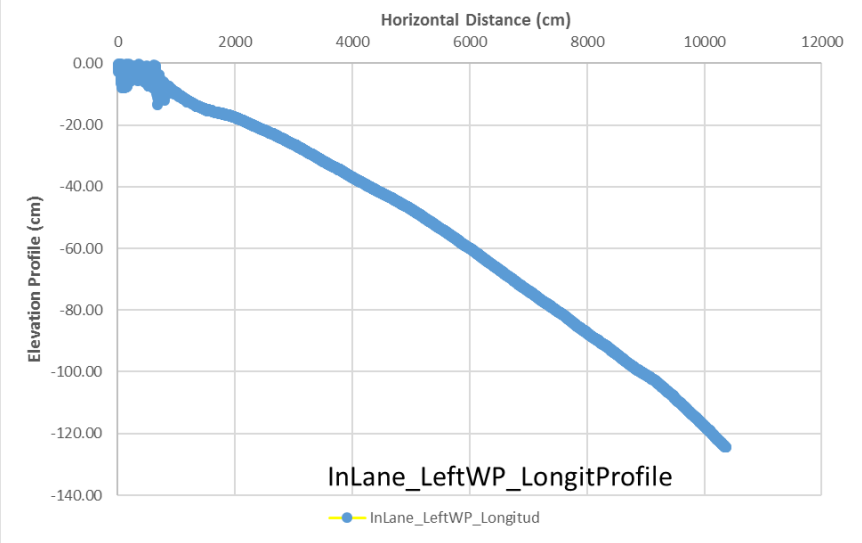

Figure 4-10. Longitudinal Profile along Left Wheel Path of Inner Lane

All the longitudinal profiles along the five paths shown in the Figures 4-5 to 4-10 were converted into International Roughness Index (IRI) values. IRI values were used to estimate and compare the riding comfort experienced by the road

users. The elevation profile of the outer lane collected by TxDOT using the standard profiler was inputted into ProVAL software to obtain an IRI value of 1.44 m/km (91 in/mi). The IRI values can be obtained along any selected path, including standard wheel paths, within the UAV-CRP data collection area.

For comparison purposes, IRI values from the same stretch of the pavement segment, along the right and left wheel paths of both outer and inner lanes were computed from the UAV-CRP collected data. After inputting the elevation profiles of the left and right wheel paths of outer lane shown in Figures 4-6 and 4-7 into ProVAL software, the average IRI value obtained along the outer lane wheel paths was 1.46 m/km (92 in/mi). Subsequently with the elevation profiles of the left and right wheel paths of the inner lane shown in Figures 4-9 and 4-10, the average IRI value obtained along the inner lane wheel paths was 1.65 m/km (104 in/mi).

The IRI values obtained using the elevation data from the profiler and the UAV-CRP technology studies showed an excellent match. This also may pave the way for using UAV-CRP technology to identify critical pavement stretches depending on the distress parameters and IRI. Costly traditional methods may be further conducted only on these critical stretches, which not only saves time but also economical. More studies may ensure a better understanding of this approach.

4.2.2.1.1.1 Digital Elevation Model (DEM) and Contour Maps

Digital Elevation Model (DEM) and the contour maps of US Highway 82, as shown in Figures 4-11 and 4-12, indicate the relative elevation differences and the possible

drainage path of water in the event of rain. This type of data visualization offers a quick idea in estimating the elevation of the objects under inspection. The road section can be observed to be sloping downwards along the direction of travel (indicated by the black arrows) starting from right side, with higher elevation indicated by the deep green color, towards the lower elevation indicated by aqua color on the left side of Figure 4-11.

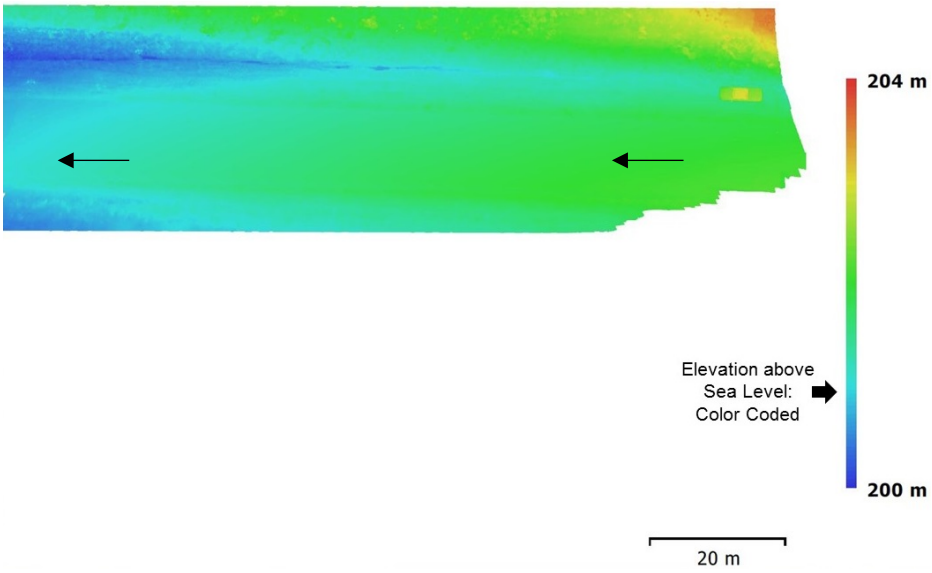

Figure 4-11. DEM of US Highway 82 Section

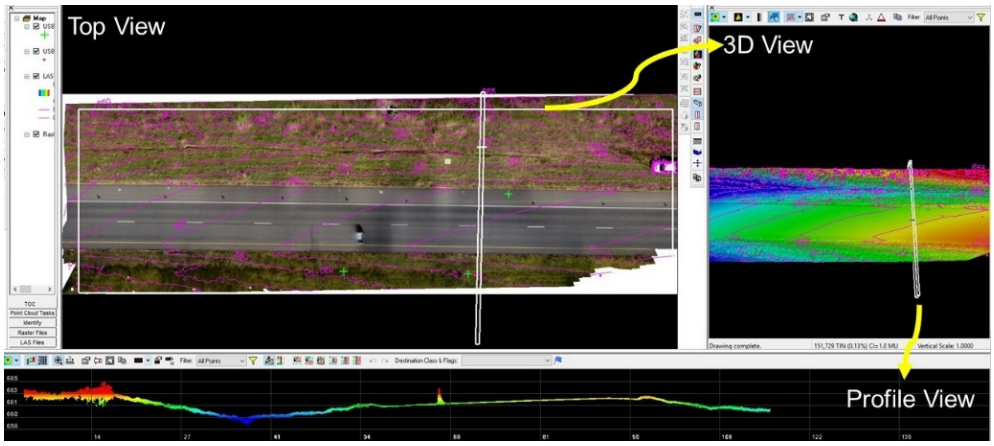

Figure 4-12. Contour Map of US Highway 82 Section

Pavement data was also collected on a nearby road connecting FM 1752 and west bound US highway 82. A multiple flight paths were adopted with 20 ft and 75 ft as operating flight altitudes. The GCP was used to develop the model and CK coordinates were used to estimate the quality of the model in terms of RMSE values in X, Y, and Z directions. The RMSE values in X, Y, and Z directions are 0.06 ft (1.8 cm), 0.07 ft (2.1 cm), and 0.02 ft (0.6 cm) respectively. Accuracy of horizontal data obtained is close to horizontal accuracy class of 2.5-cm and vertical data obtained is better than vertical accuracy class of 1-cm.

Due to the vegetation on the shoulder of the pavement, a large wooden plank was placed to serve for both landing and takeoff. Data collection was only conducted on one side of the pavement due to the research stage of this project. All photos were processed to obtain a 3D dense point cloud model and orthomosaic, as shown in Figure 4-13.

Figure 4-13. Orthomosaic of the Road Connecting FM 1752 and West Bound US Highway 82, Paris District, Texas

DEM and contour map of the nearby road connecting FM 1752 and west bound US 82 Highway in the Paris district provided an idea of the drainage flow patterns at the site (as shown in Figures 4-14 and 4-15).

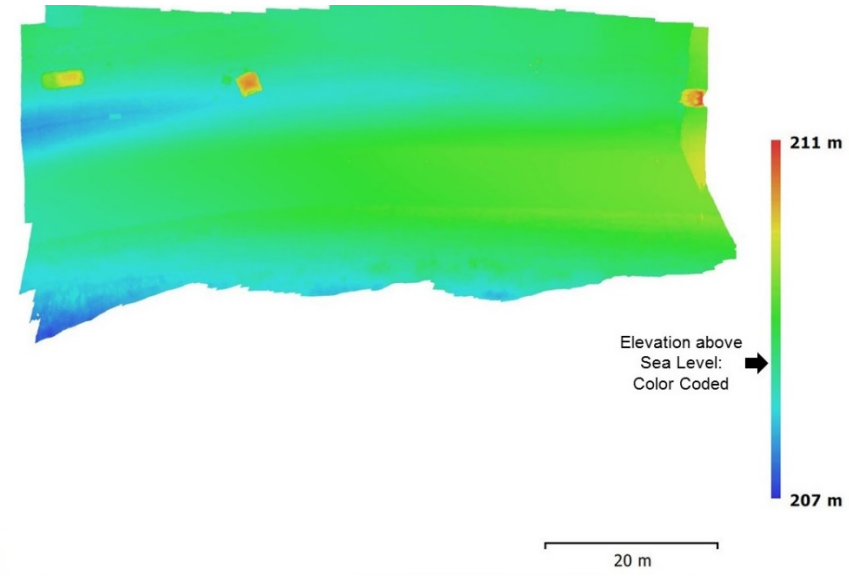

Figure 4-14. DEM of Road Connecting FM 1752 and West Bound US Highway 82, Paris District, Texas

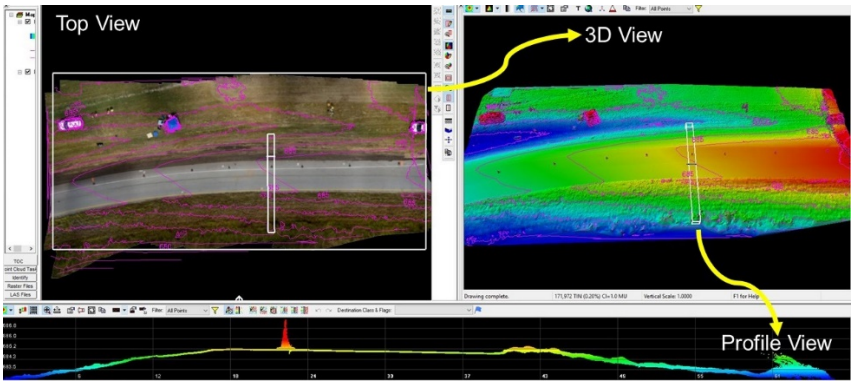

Figure 4-15. Contour Map of Road Connecting FM 1752 and West Bound US Highway 82, Paris District, Texas

4.2.2.1.2 Transverse slope

Due to the availability of dense point cloud models, the cross slope of the pavement was calculated at desired longitudinal spacing on the pavement section. For better

representation, the cross slope was computed with points placed, across the pavement, in the transverse direction at 1 cm intervals. Transverse direction was selected according to AASHTO PP 70-10 (AASHTO, 2014), which defines a transverse line as a line that deviates less than 10° to the perpendicular line of the pavement centerline.

The transverse slope was calculated at 30 ft intervals along the longitudinal direction of the pavement. The cross slope sections provided in Figure 4-16 show a slope of 3.2% sloping towards the shoulder (indicated by the green colored arrows in the top and profile views). This can also be observed in the profile section view provided, where the white and yellow pavement markings and the centerline of two lanes can be seen at the bottom of Figure 4-16. It shows that the shoulder of the pavement, over which the traffic cones are placed, was at a lower altitude compared to the other side of the pavement in the transverse direction.

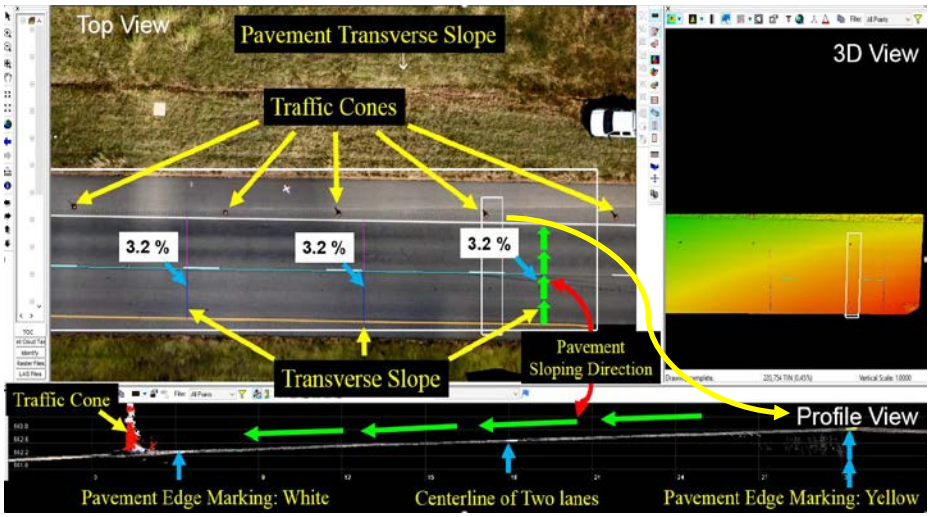

Figure 4-16. Transverse Slope Computed Along Three Paths

For comparison with traditional purposes, Faros X 330 Terrestrial LiDAR was used for the collection of pavement data. Data collected from the terrestrial LiDAR was also processed to compare the cross slope values as shown in Figure 4-17. The length of the line selected over the pavement is 293.30 in. and the elevation difference of the two points was 9.42 in. The transverse slope of 3.2% obtained from the LiDAR data matched the value obtained from UAV-CRP data analysis. This exercise demonstrated that the cross slope measurements could be computed using UAV-based photogrammetry studies, which can be used as a part of Quality Control (QC)/ Quality Assurance (QA) works.

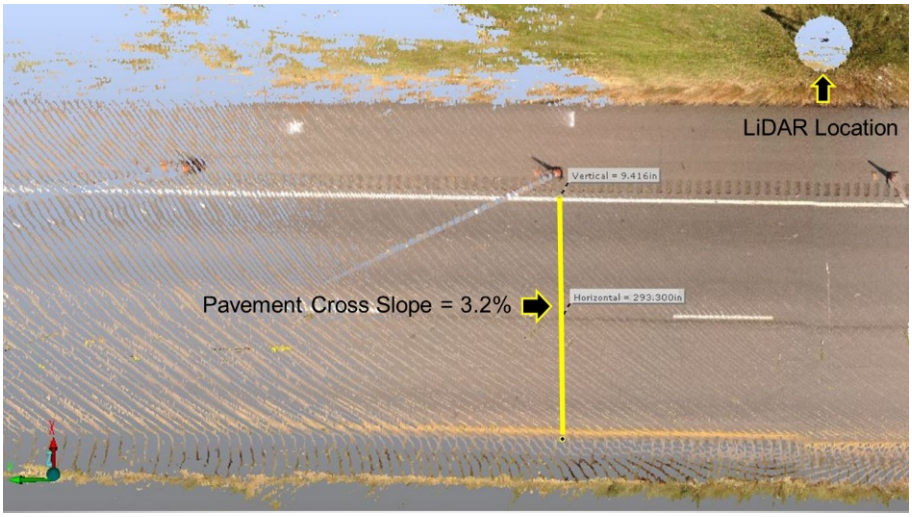

Figure 4-17. Transverse Slope Computed from LiDAR Data

Analysis of the pavement characteristics data collected from UAV-CRP methodology proved efficient and accurate. This methodology helped in transforming the present subjective inspections to objective methods by providing repeatable and reproducible data.

4.2.2.2 Pavement Edge Distress

The pavement data collected over the road section inside the TxDOT campus during the UAV field demonstration event held at TxDOT Cedar Park Campus, Austin was analyzed for distress. There was no vehicular traffic inside the TxDOT campus at the time of UAV surveys, as the employees were advised to park their vehicles in a separate facility. This provided an opportunity to perform flight operations directly over the pavement at lower heights and collect high quality nadir

images. There was an on-grade curb inlet located near to the outlet drainage point as seen in the Figure 4-18.

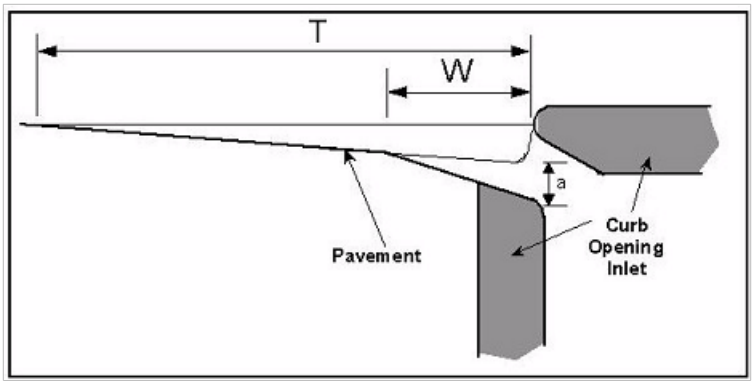

Figure 4-18. Curb Opening Inlet Drain (TxDOT 2018)

The UAV-CRP data of the pavement was collected by flying an operation directly over the pavement site at a flight altitude of 20 ft and the data was analyzed to study various pavement features. The curb inlet, shown in Figure 4-18, was typically provided to drain the runoff water accumulated on the pavement. Figures 4-19 (a-d), depict various zoom-in levels of the orthomosaic of the same pavement section exhibiting minor edge distress near the on-grade curb inlet.

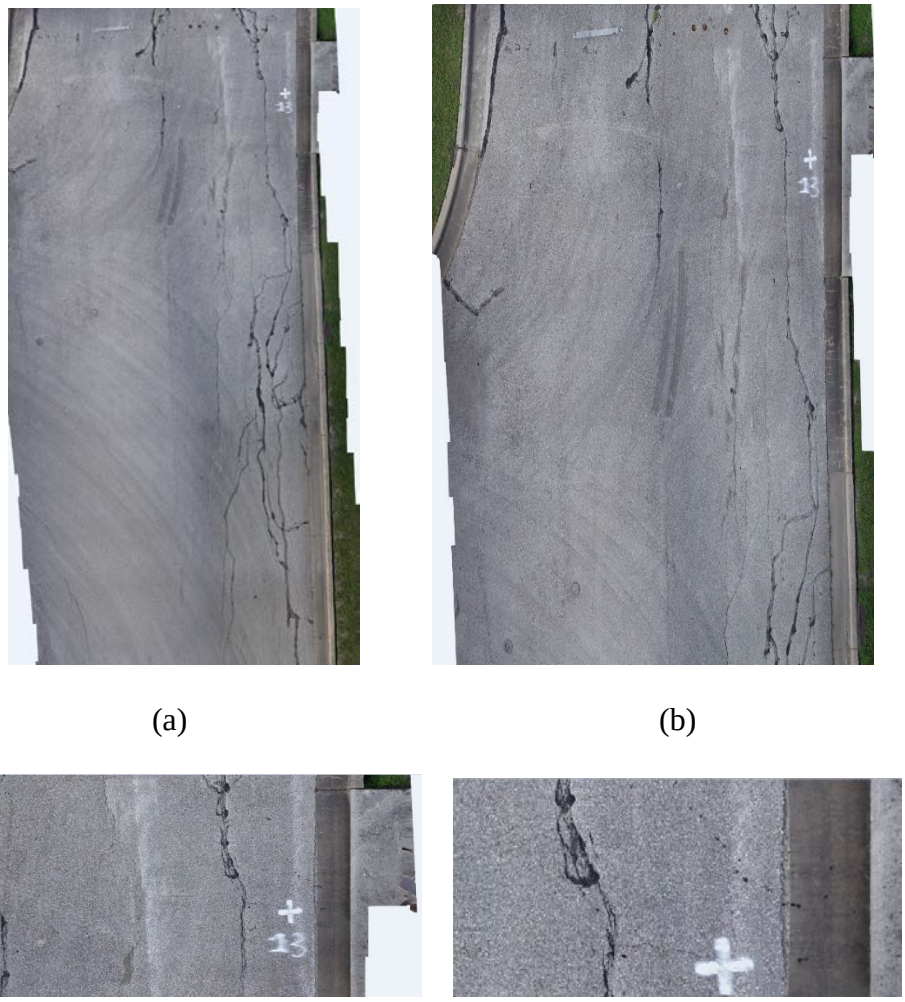

(a) (b)

(c) (d)

Figure 4-19. Various Zoom in Levels of Orthomosaic of the Pavement Stretch TxDOT Facility Austin

Researchers identified minor edge distress near the curb inlet from the 3-dimensional data shown in Figure 4-20. The 3D view of the white rectangular box located in the top view is provided on the right hand side of the Figure 4-20. Profile view of the rectangular cuboid in the 3D view is presented at the bottom of the

Figure 4-20. Engineers should be able to delineate the distress levels, within the red rectangles in all views, and observe the distress features. The depth of the distress was estimated as 0.4 in.

This visualization analysis and approach can be used to estimate the features of other distress like rutting and pot holes that are covered in the subsequent sections.

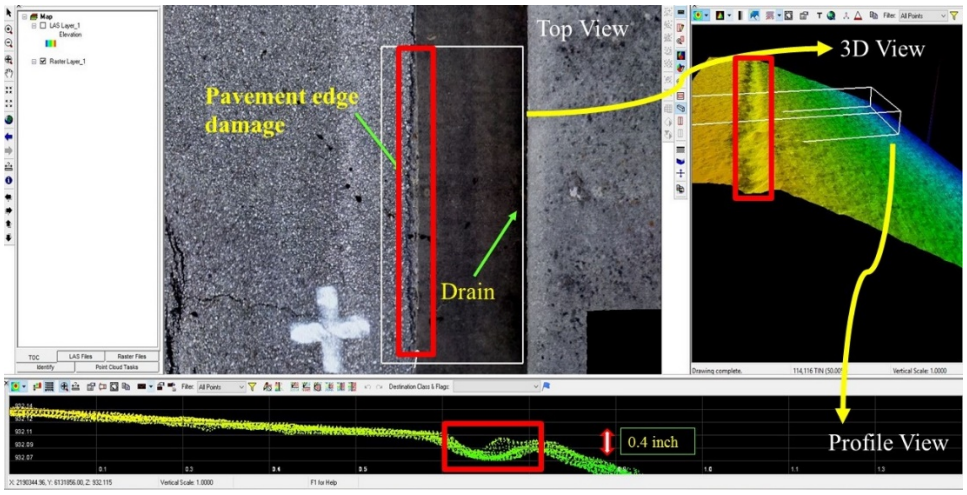

Figure 4-20. Pavement Edge Distress, Top View, 3D View and Profile View

4.2.2.3 Pavement Cracking

Figure 4-19 presents cracks detected on a pavement section that were sealed in order to prevent the weakening of pavement sub layers due to percolation of water. Proper sealing will fill and bond the cracks, thereby preventing moisture intrusion and mitigating pavement deterioration. The pavement section shown in Figure 4-19 features cracks seal coated with asphalt emulsion as well as minor cracks that might have developed after sealing, shown in Figure 4-21a. The orthomosaic

developed from the collected images was processed to identify the pavement crack dimensions. The total length and average width of longitudinal crack shown in Figure 4-21a are 3.4 ft (40.7 in.) and 0.03 ft (0.35 in.), respectively. The percentage of pavement-cracked area was computed as 1.2%.

Pavement data was also collected on a service road connecting FM 1752 and west bound US 82 Highway. A multiple flight path was adopted with 20 ft and 75 ft as operating flight altitudes. The orthomosaic was analyzed to find total length and average width of the longitudinal cracks as shown in Figure 4-21b were 37.8 ft (453.9 in.) and 0.03 ft (0.36 in.), respectively. The percentage of pavement-cracked area was computed as 0.1%. This information along with assumed crack depth will be helpful in estimating the quantity of seal coat material required.

(a) (b)

Figure 4-21. Estimating Pavement Crack Dimensions (a) TxDOT Site in Austin and (b) Service Ramp near US Highway 82

4.2.2.3.1 Cracked Areas

Pavement crack related data was collected at a flight altitude of 80 ft AGL inside the TxDOT district headquarters in Fort Worth, as shown in Figure 4-22. Coding algorithms were used to identify the minor cracks shown in Figure 4-22d. These cracks were hard to detect, for the naked eye, from the images shown in Figure 4-22. It is important to identify minor cracks, as identifying them early will prevent them from becoming major cracks over time.

The general procedure and workflow of the Python script designed to calculate the areas of regions of cracks in asphalt is provided below. There are many steps involved in cracked area recognition but out of all those, only images of four important steps were provided below. The program begins by loading the image specified by the path inputted in the command call if that image exists and can be read. The loaded image was stored initially as a 3-channel RGB image, as shown in Figure 4-22a. The image was then converted to grayscale to ignore unwanted colored elements. Next the image was processed using an inverse binary threshold followed by a series of Gaussian blurs, dilations, and binary thresholds to clump together the groups of cracks and remove the unwanted pixels. Then all the small isolated contours, defined as group of white pixels that were not attached to the groups of cracks are removed from the image. The remaining contours representing the main areas of cracks were then dilated and filled so they are solid white.

At this point, the contours generally represent the area of the cracks, but in order to produce a more accurate area, the process was applied again by performing a bitwise OR operation on the current image and the original image to get an image with only the original pixels in the selected contours and white pixels everywhere else. This image then undergoes a very similar process as that described for the initial analysis of the image till the inverse binary threshold, but then the image was eroded by the same amount that it was dilated in the initial process, as shown in Figure 4-22b. Then the image consisting of contours that represent the area of the cracked regions was obtained and the areas of these contours are then calculated, as shown in Figure 4-22c.

Another bitwise OR operation was applied with the current image and the original image to display the original pixels in the cracked regions and their corresponding number of pixels, as shown in Figure 4-22d. The number of pixels obtained 299273, 505678, and 59932, respectively starting from top in clockwise direction, are multiplied with pixel area of 22.2 mm^2 to obtain the cracked area as 6.6 m^2, 11.2 m^2, and 1.3 m^2, respectively.

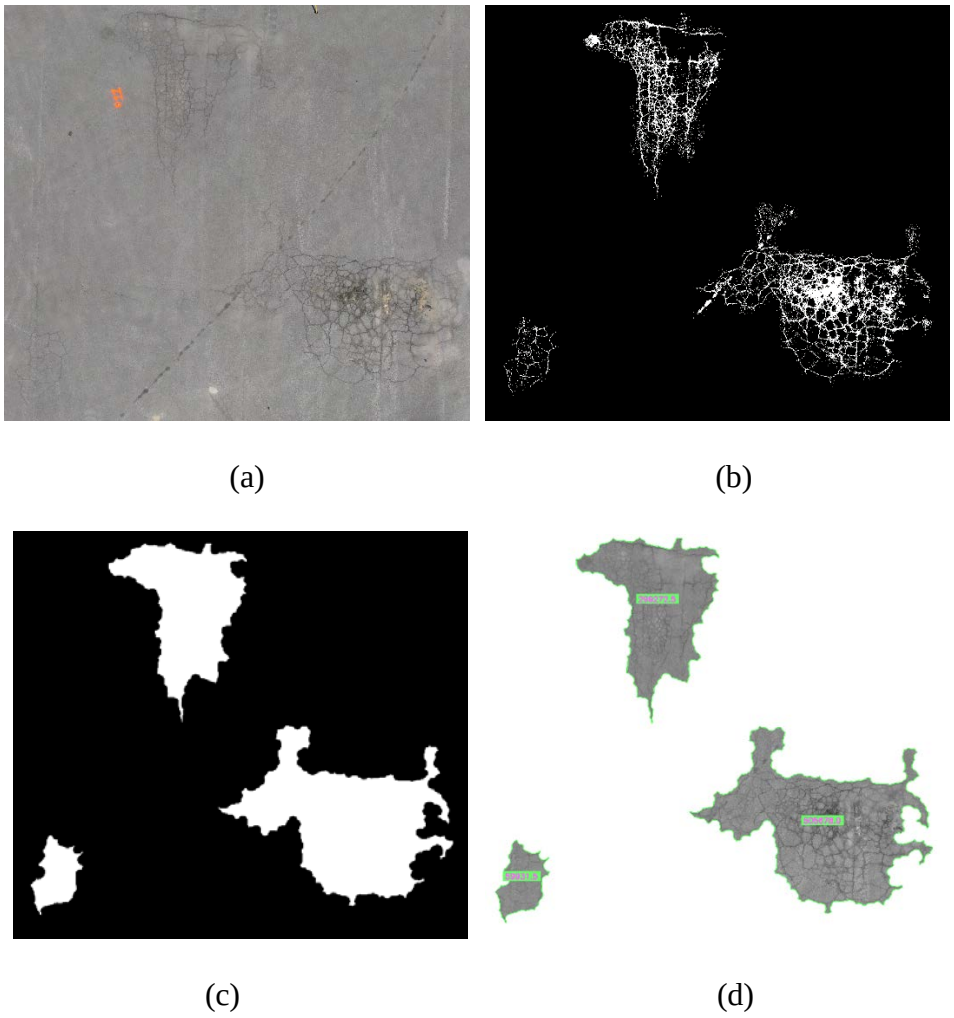

(a) (b)

(c) (d)

Figure 4-22. Workflow of Algorithms to Detect Cracked Areas

Proactive repairs of minor cracks would therefore enhance the longevity of the pavements. Also, entry of debris, water, and other unwanted materials can be further prevented by properly sealing minor cracks and thereby preventing them from transforming into major distresses. The extent of distress marked in Figure 4-22d helps in planning the proactive maintenance procedures required to slow down the pavement deterioration process. This information can be a valuable input to the

pavement condition index (PCI), which has a threshold value used by agencies to decide on the pavement rehabilitation and preservation works.

4.2.2.3.2 Crack Sealing

Even though, the presence of vegetation is a minor problem but it indicates the condition of the sealing applied to cracks. As mentioned in earlier sections, proper sealing of cracks will be crucial in increasing the service life of the pavement. The UAV-CRP data collected at Cedar Park campus identified growing vegetation in cracks indicating deterioration of pavement seal coatings, as shown in Figure 4-23. Deterioration of seal coats provided the space for the growth of unwanted vegetation.

The presence of growing vegetation can accelerate pavement deterioration, if left unchecked. By using color recognition algorithms on the UAV-CRP collected data, engineers will be able to spot the vegetation growth and alert the road agencies to take necessary actions. These practices come under the good maintenance measures required to preserve pavement life and maintain road conditions.

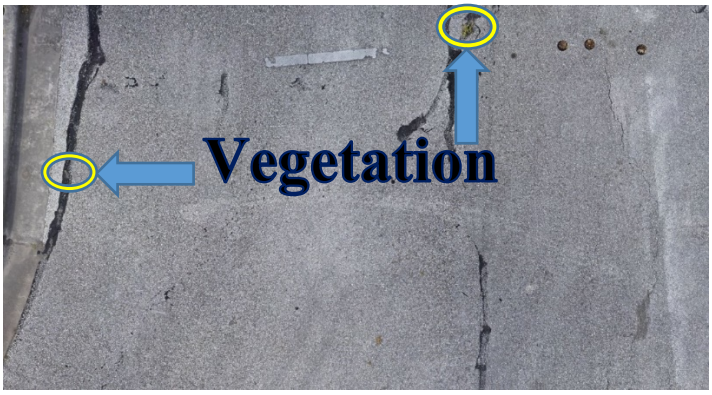

(a)

(b)

(c)

Figure 4-23. Pavement Crack Seal Condition (a) Identifying Vegetation Growth on Pavements (b) Zoomed in Vegetation over Left of Pavement Image (c) Zoomed in Vegetation over Top of the Pavement Image

4.2.2.4 Permanent Deformation or Rutting

Researchers identified multiple distresses in the pavement data collected inside the agency facility in Fort Worth, Texas. The distress located in front of the vehicle

shown in Figure 4-24 was identified from the UAV-CRP technology data and attributed to permanent deformation.

Figure 4-24. Multiple Pavement Distress

The image data was used to develop dense point cloud models and orthomosaics to analyze distress features. The extent and depth are among the important distress features that were identified in this research. Figure 4-25 shows the depth of permanent deformation that contributed to the cracking of the pavement. It should be noted that the permanent deformation or settlement is not directly under the wheel path; this settlement may be contributed by weak layers underlying the paved section.

The pavement top layer was devoid of the support from the underlying layers and led to excessive cracking. The depth of the distress was estimated to be 0.3 ft (3.36 in.); this helps in assessing the severity of the distress. The cracking

area identified in Figure 4-24 and the distress features identified in Figure 4-25 help to decide if a pavement needs quick rehabilitation measures.

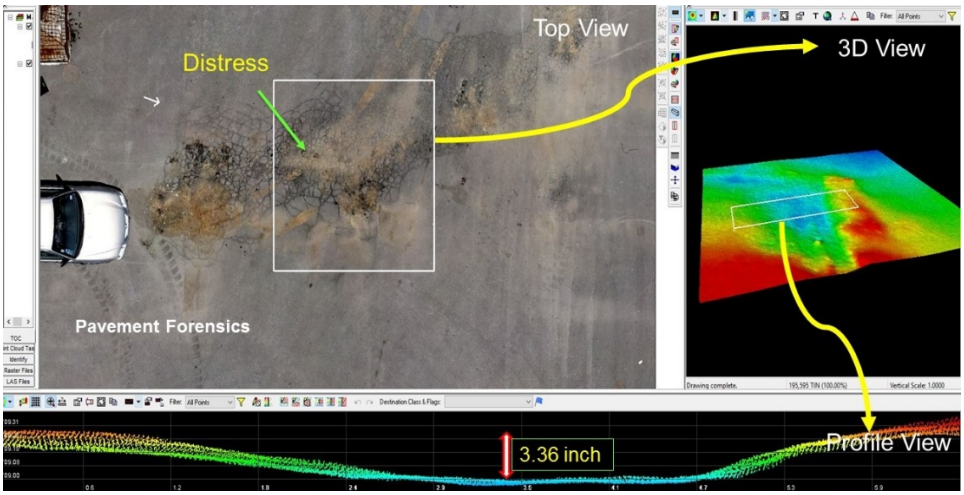

Figure 4-25. Permanent Deformation Induced Cracking

Availability of quick and efficient methodology such as unmanned aerial vehicle – close range photogrammetry (UAV-CRP) will help in planning for early recognition of these distresses and the subsequent proactive maintenance of the distressed pavements. This would not only reduce maintenance costs over the long run, but would also enhance pavement-riding conditions.

4.3 CONSTRUCTION MATERIAL STOCKPILES

UAV-CRP methodology was also utilized to collect the accurate volumetric data of the pavement construction material in the stockpiles in two locations: TxDOT District Headquarters at Fort Worth and TxDOT area office in Decatur as shown in Figure 4-26. Accurate inventory of each material stockpile helps in better planning for construction activities. This research also demonstrated the differentiation of

material types in the stockpiles, depending upon the appearance, mixed in a single stockpile.

Figure 4-26. Location of the Construction Material Stockpiles

4.3.1 TxDOT District Headquarters, Fort Worth

Two stockpiles inside the TxDOT District Headquarters, Fort Worth facility were captured at a flight altitude of 75 ft AGL using UAV-CRP technology. The two stockpiles that were mixed at one corner were delineated depending upon the complexion and the volume of material in each stockpile was calculated. The volumes were estimated to consist of 804.3 yd^3 of fine sand material and 54.5 yd^3 of coarse sand material, respectively, as shown in Figure 4-27.

The ground truth measurement for the volume of fine sand was provided by the TxDOT officials and was around 820 yd^3. The flatness of the pavement underneath the stockpiles also helped to achieve a volume estimation accuracy of 98%. However, if the stockpiles are stacked up on an undulated surface, even the

UAV-CRP technology that captures the accurate surficial properties may result in erroneous interpretations. The present traditional methods have similar limitations in properly estimating volumes in such cases as well. This aspect still needs further investigation.

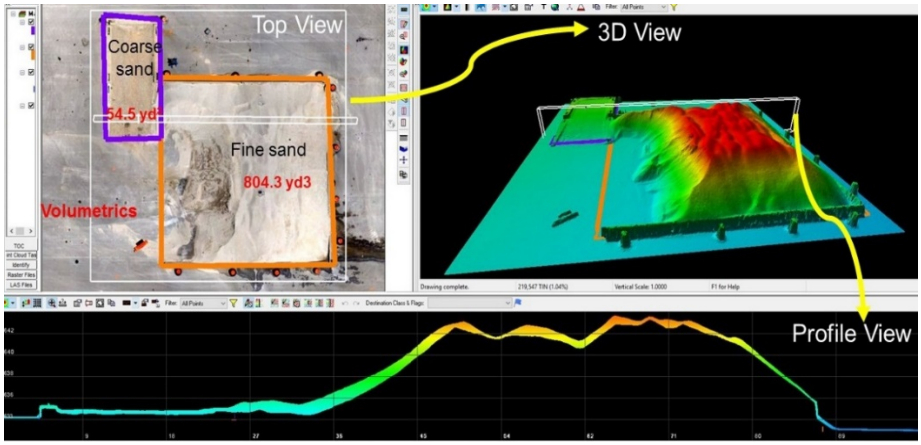

Figure 4-27. Stockpile Volumetrics of Pavement Construction Materials

DEM of the whole area provides an idea about the relative elevation of the surficial features of the TxDOT Fort Worth campus, as shown in Figure 4-28. The circular objects with clear elevation difference, denoted by a red arrow on the right side of Figure 4-28, were identified as the silos present inside the facility as shown below.

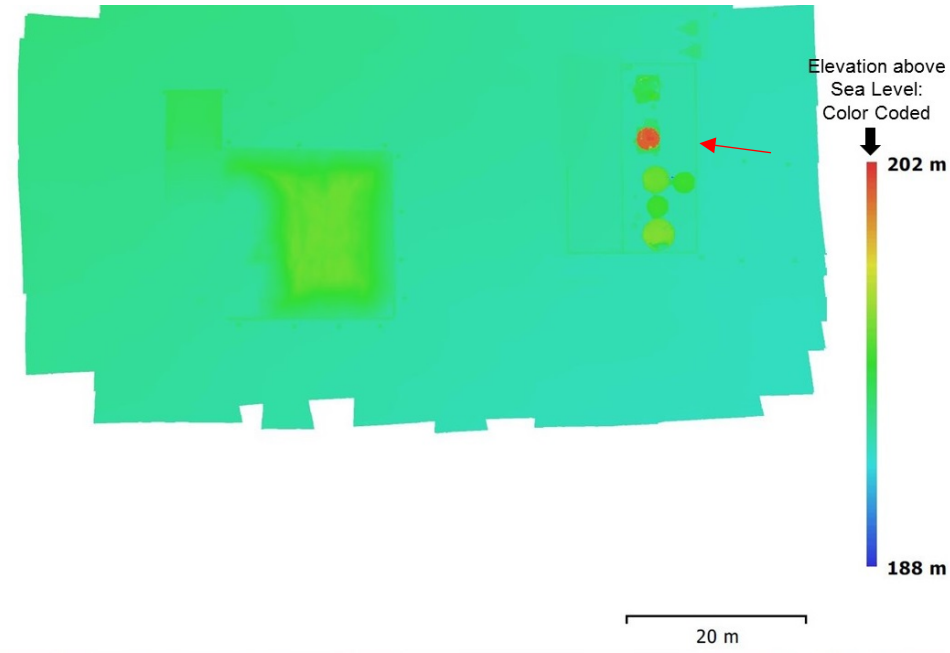

Figure 4-28. DEM of Sand Stockpiles in Fort Worth, Texas

In addition to volumetric calculations, the pink colored contour lines (shown in Figure 4-29) of the stockpiles add another dimension to the understanding of the surveyor and workers while removing the stockpile materials, resulting in a safe excavation.

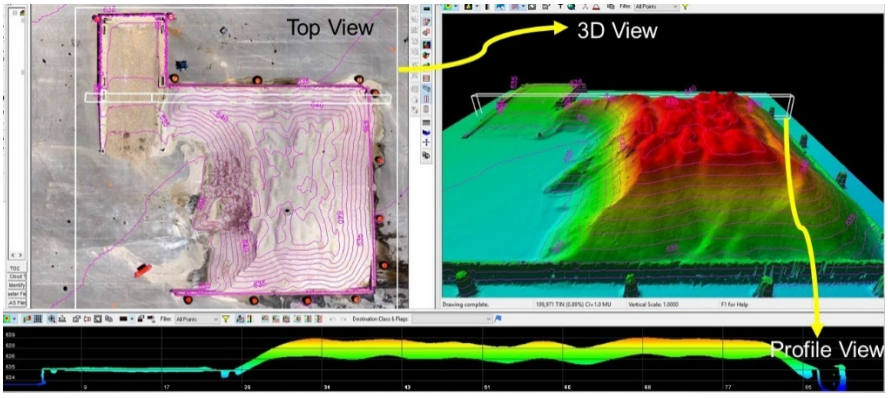

Figure 4-29. Contour Lines over Sand Stockpiles in TxDOT Fort Worth

Obtaining the contours using traditional methods would have resulted time-consuming and also unsafe for the workers to climb on those stockpiles without knowing the stability of such surfaces. Using UAV-CRP technology, all these data outputs could be obtained by analyzing the same dataset collected during the mission flights.

4.3.2 TxDOT Area Office, Decatur

The next stockpile assignment was at the TxDOT area office in Decatur that included a huge recycled asphalt pavement (RAP) stockpile in addition to small coarse and fine sand stockpiles. The RAP stockpile was almost 30 ft high with a large base area. The UAV-CRP data of the stockpile was collected using a pre-planned flight plan covering the area with 80% longitudinal and 60% lateral overlap. High quality aerial images collected at a flying height of 90 ft (provided in the Figure 4-30) shows that there are RAP materials with different asphalt content evident through the complexion of the material. Upon examining the images from the stockpiles, it was noted that this RAP stockpile was composed of mixed material, as shown in Figure 4-30. Dark colored material indicate RAP extracted from top pavement layers and light-colored material depicts RAP extracted from underlying pavement layers. In some instances, this data is important as the presence of excess binder on the aggregates might be unfavorable for some purposes. Assuming the land beneath the stockpile was flat, the three types of RAP material were delineated in Figure 4-30 by white, aqua, and orange colored

boundaries. The respective material volumes starting from left to right are 1857.6 yd^3, 2239.5 yd^3, and 1455.3 yd^3, respectively.

The ground truth volumetric measurement of the whole stockpile provided by the TxDOT officials was 5547 yd^3 and the total volume obtained from the UAV-CRP methodology was 5552.4 yd^3, which resulted in an error of 0.1% of the ground truth value. Considering the benefits offered such as safety provided (working personnel need not walk over steep slopes), the efficiency (collecting the data within 10 minutes), and accuracy provided, the UAV-CRP technology is deemed appropriate and acceptable.

For comparison purposes, the volume of the small RAP stockpile, delineated by the purple boundary, beside the huge stockpile was calculated from UAV-CRP technology and using traditional methods. Using traditional methods, the Triangular Irregular Networks (TIN) surface was developed by collecting the coordinates of the finite points over the stockpile and interpolated to find the volume of stockpile as 101.4 yd^3. The single flight data comprising of both the large and small stockpiles was used to estimate the volume of the small stockpile as 104 yd^3. Error in this case was found to be around 2.5% of the value obtained using traditional GPS methods. There is also a chance that the UAV-CRP methodology offers accurate volumetric numbers, owing to its ability to accurately capture the surface undulations when compared to the traditional way of interpolating.

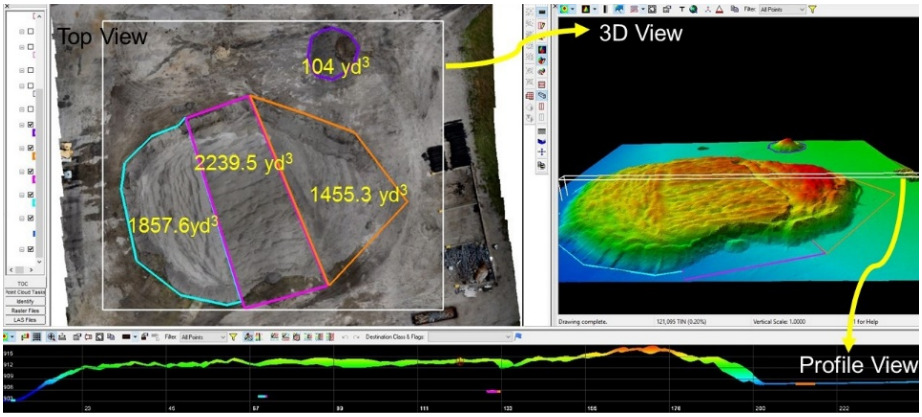

Figure 4-30. Mixed RAP Stockpile

The DEM of the whole area provides an idea about the relative elevation of the surficial features of the TxDOT Decatur campus, shown in Figure 4-31. The rough estimation of material volume in the storage bays, indicated by a red arrow in the bottom right corner of the Figure 4-31, can also be considered as a part of regular inventory inspection conducted by UAV-CRP technology. It also gives an estimate of the steepest and unstable slope of the stockpile, thereby assisting in planning for excavating and transporting the stockpile material.

.

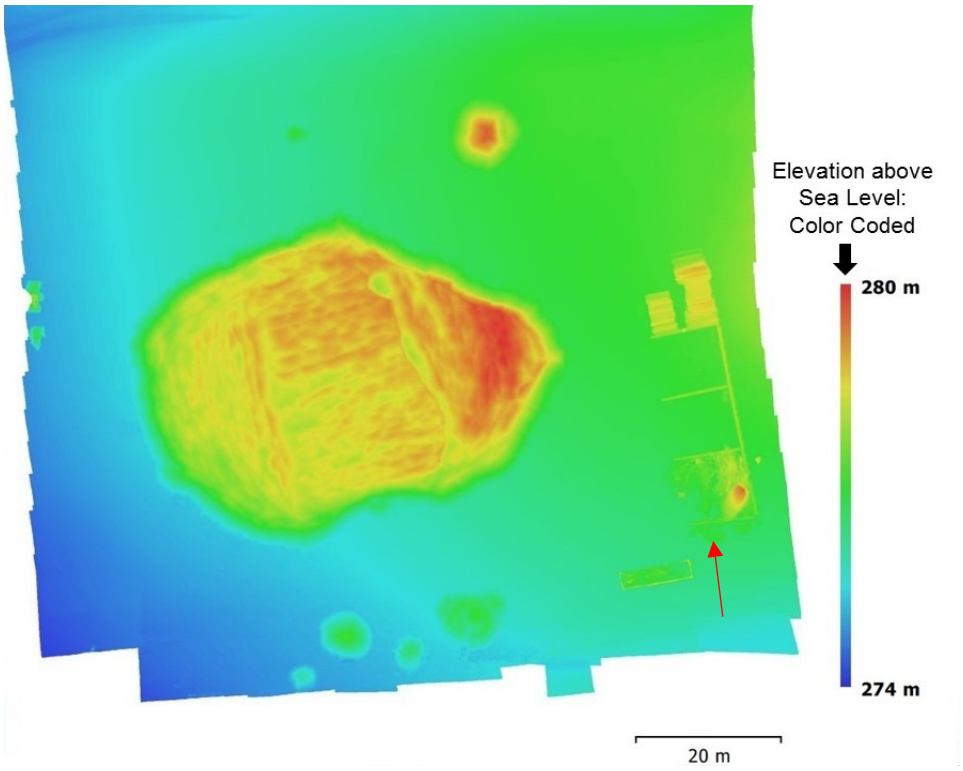

Figure 4-31. DEM of RAP Stockpile in Decatur, Texas

There were also other stockpiles distributed within the TxDOT campus at Decatur, Texas. UAV-CRP technology was used to capture all the features of the 20,000-yd^2 area by flying the UAV at 80 ft AGL. The volume of stockpiles were computed as shown in Figure 4-32. The volume of the two RAP stockpiles and one sand stockpile delineated by the aqua, red, and blue boundaries are 532.6 yd^3, 207.4 yd^3, and 967.6 yd^3, respectively.

If the same flight plan is used to collect the data every few days, it helps in conducting timeline monitoring of change in stockpile volumes. This approach can also be executed at the road construction site as a quality control (QC) check

assisting the road agency by letting them know how much material is being utilized in the construction, which can be compared to the amount of work in progress. By using this approach, inventory checks of any facility becomes safe, efficient, and economical.

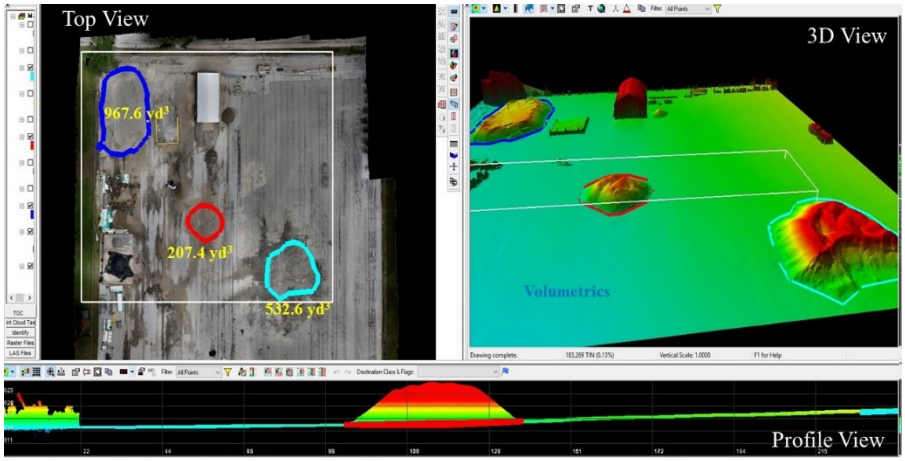

Figure 4-32. Inventory data collection that includes multiple material stockpiles

The DEM of the whole area provides an idea about the relative elevation of the surficial features of the TxDOT Decatur facility, shown in Figure 4-33. The rough estimation of the material volume in the storage bays (as indicated by a red arrow in the bottom left corner of the Figure 4-33) can also be estimated as a part of the regular inventory inspection as conducted by the UAV-CRP technology.

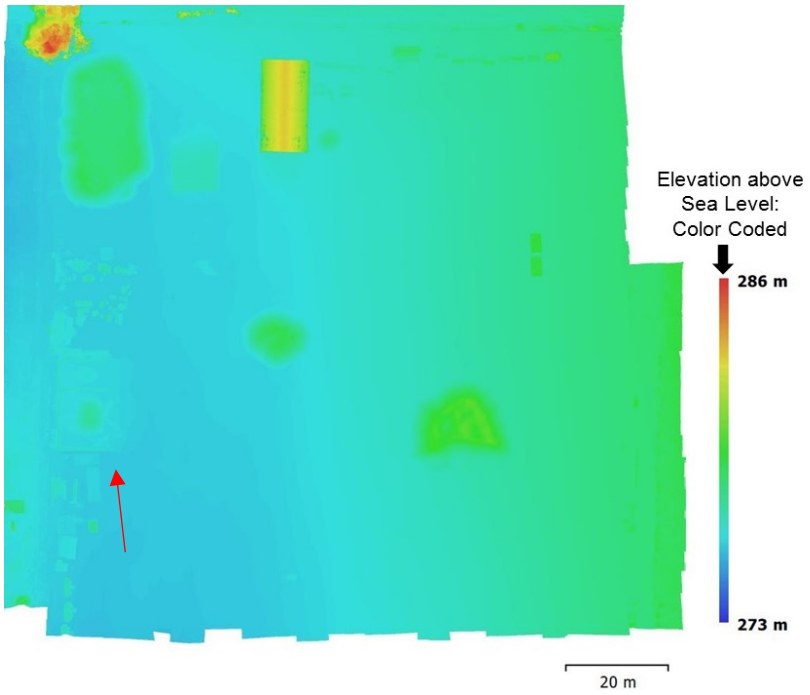

Figure 4-33. DEM of Multiple Stockpiles in Decatur, Texas

In addition to the volumetric calculations, the pink colored contour lines (shown in Figures 4-34 and 4-35) of the stockpiles add another dimension to the understanding of the surveyor. Overall, UAV analyses of stockpiles can provide the data to TxDOT in various forms, which can be used for volumetric assessments in periodic inventory estimations. In addition, slope contours can be used to assess the stability of stockpiles such that there will not be any stability failures of stockpiles during unloading operations.

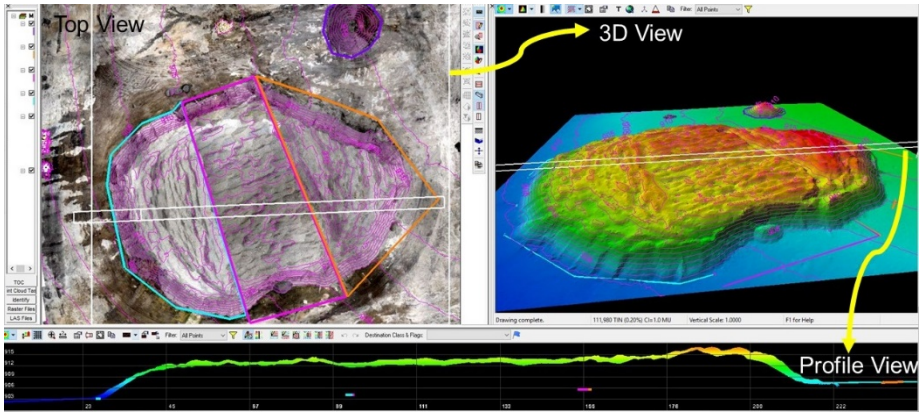

Figure 4-34. Contour Lines on the Stockpile Data Collected at Decatur

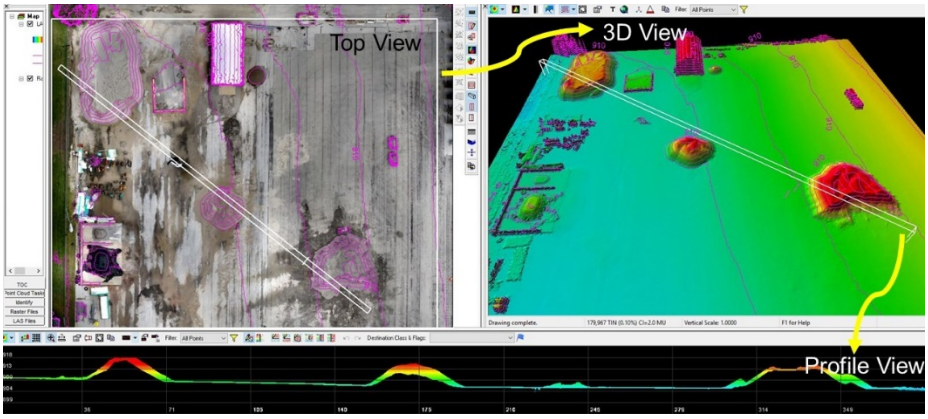

Figure 4-35. Contour Lines on the Multiple Stockpile Data Collected at Decatur

Estimation of stockpile volumes using UAV-CRP technology has proven to be a valuable tool due to both accuracy and safety elements. It is essential that agencies start using this tool for construction site monitoring and stockpile volume assessment on a timely basis.

4.4 BRIDGE MONITORING

A bridge inspection was carried out on a newly constructed bridge, not yet opened for traffic. This new bridge is an extension of State Highway or SH 360 located at 32.523034 N, 97.083709 W, in Mansfield, Texas. The Aibot X6 and DJI Phantom 4 were used for flight operations to conduct the 360° bridge inspection, which included superstructure and substructure data collection.

4.4.1 Bridge Inspection Investigations

Inspection was conducted on a newly constructed 20 ft high and 700 ft long bridge of SH 360, not yet opened to traffic, located in Mansfield, Texas. A comprehensive 360° bridge inspection was conducted that included cameras mounted on the bottom gimbal covering the bridge deck and on the top gimbal covering underneath the bridge deck in separate missions. The DJI Phantom quadcopter was also used for capturing the 4K video of the entire bridge infrastructure. Superstructure was inspected based on the condition of the deck, approach slab, railings, and joint conditions. The substructure was inspected for the condition of the beams, soffits, bearings, wing walls, abutment, pile and cap, as well as the pile footing.

The following UAV configurations (i.e. bottom gimbal and top gimbal) were used during superstructure and substructure inspections, respectively (as shown in Figure 4-36).

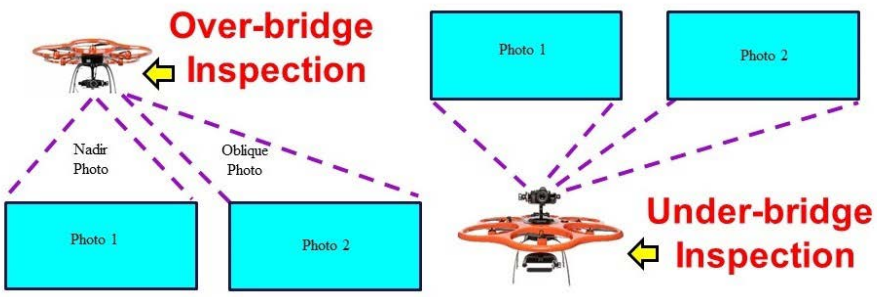

Figure 4-36. UAV Configurations used for Bridge Superstructure and Substructure Inspection

GCPs that were used to build the 3D dense point cloud model of the bridge and CKs were laid on the bridge deck prior to the flight operations. Flight plans with multiple flight altitudes were then conducted to capture the details of the bridge deck and to cover the surroundings of the bridge within the stipulated time. Higher altitude flight was helpful in covering the adjacent bridge features, which did not warrant a high quality detail. CKs were later used to check the accuracy of the model: The X, Y, and Z RMSE of the model estimated from the analysis are 0.09 ft (2.7 cm), 0.04 ft (1.2 cm), and 0.23 ft (7.0 cm), respectively. Accuracy of horizontal data obtained is close to horizontal accuracy class of 2.5-cm and vertical data obtained is better than vertical accuracy class of 10-cm. The orthomosaic of the bridge deck is shown in the Figure 4-37. The DEM of the bridge is also provided in the Figure 4-38.

Figure 4-37. Orthomosaic of the Bridge Deck of SH 360 located in Mansfield, Texas

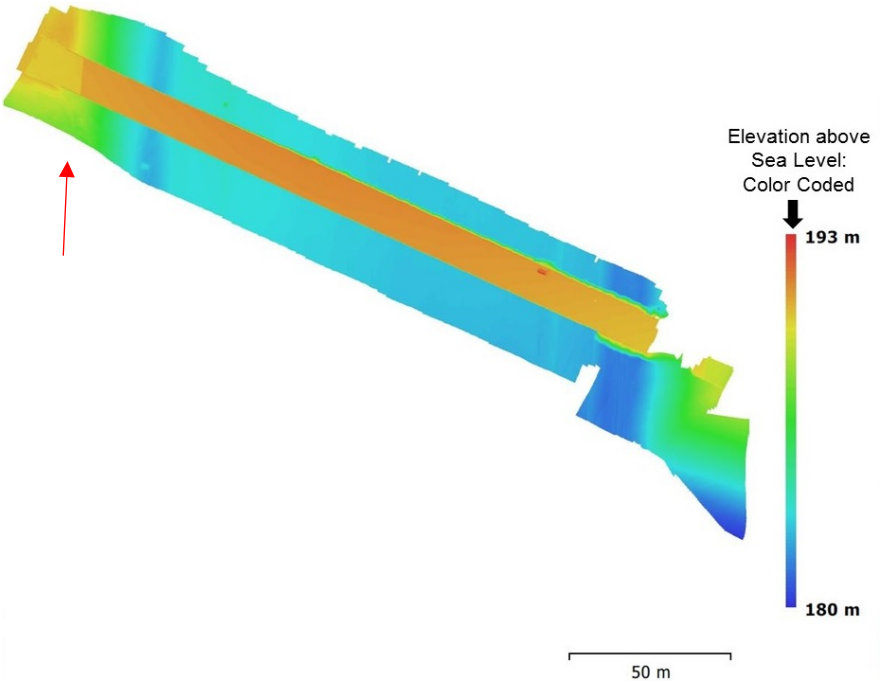

Figure 4-38. DEM of the Bridge of SH 360 located in Mansfield, Texas

The orange colored rectangle in the DEM represents the bridge deck. The colored elevation bar, located at the right side of the Figure 4-38, also indicates that there is an elevation difference of 20 ft (6 m) between the bridge deck and the surrounding ground. The elevation difference between the ground and the deck appears reduced near the abutments where the soil embankment slopes, represented by a green colored area indicated by a red arrow at the top left corner of Figure 4-38. Contour lines shown in Figure 4-39 add another dimension to the understanding of the engineer as they depict different elevation levels of the infrastructure.

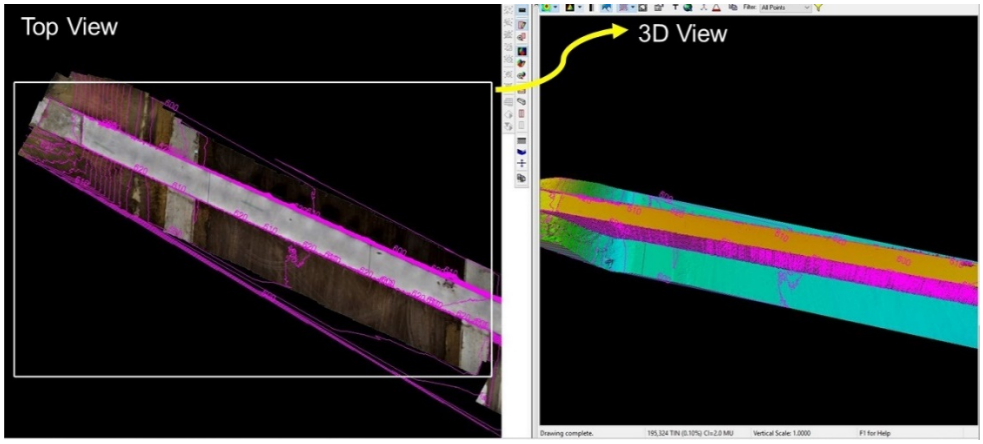

Figure 4-39. Contour Lines on the Bridge Deck and the Surrounding Ground

4.4.1.1 Bridge Superstructure Inspection

Being a newly constructed bridge, a few places on the bridge superstructure were marked with black tape of known dimensions to evaluate the performance of UAV-CRP technology measurements compared to ground truth measurements (a few markers are shown in Figure 4-40). In addition, the width of two joints was

measured using a ruler and the results were compared with the measurements made from the visualization model generated from the UAV collected data, as shown in Figure 4-41.

Figure 4-40. Taped Markers and Joint Width Locations on the Bridge Deck

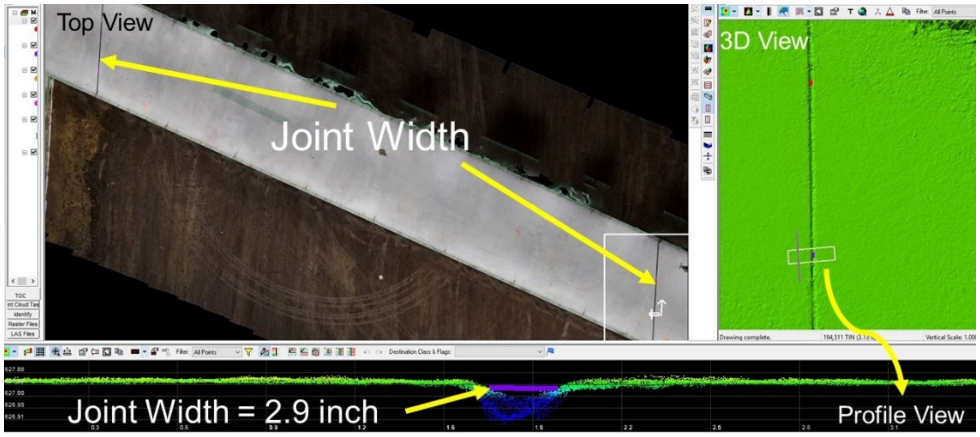

Figure 4-41. Joint Width Sections at Two Joints on the Bridge Deck

Taped markers were placed at seven random locations, as shown in Figure 4-42, to compare accuracy of UAV-CRP measurements using ground truth measurements and these results are provided in Table 4-1.

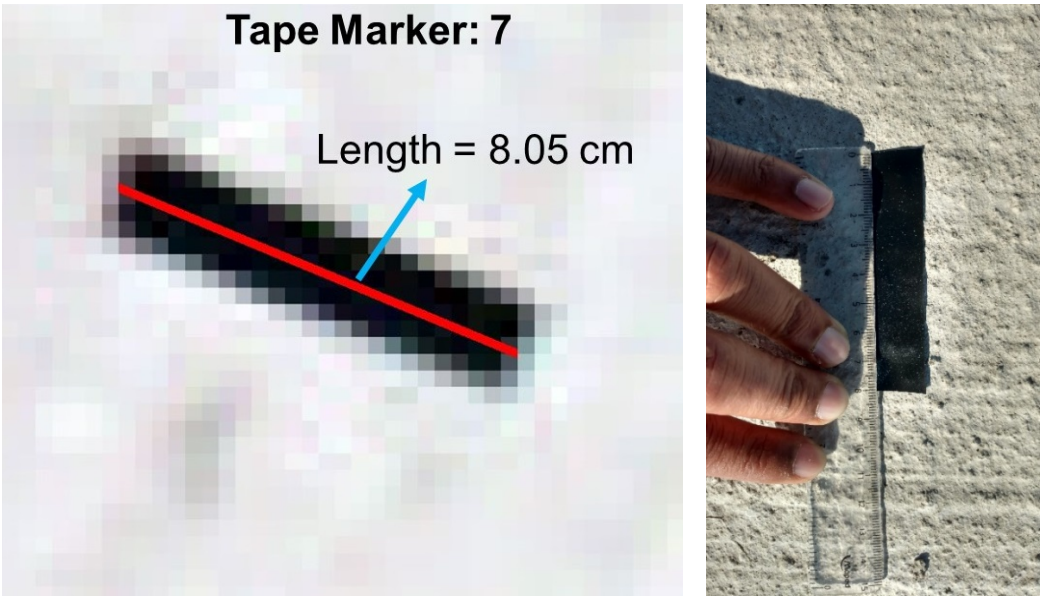

(a) (b)

Figure 4-42. Measurements made on Marker No. 7 using (a) UAV-CRP Measurements (b) Length Measured Using Ruler

Table 4-1. Taped Marker Length Comparison between UAV-CRP Data Measurements and Ground Truth Measurements

Marker Number	UAV-CRP Data Measurements (cm)	Ground Truth Measurements (cm)	Absolute Error (%)
1	10.56	10.80	2.2
2	8.94	8.85	1.0
3	8.49	8.50	0.1
4	9.68	9.70	0.2
5	9.56	9.60	0.4
6	8.87	8.90	0.3
7	8.05	8.00	0.6

Except for the maximum error value, i.e., 2.2%, all the remaining errors are less than 1%, indicating the high quality of the UAV-CRP data was collected and analyzed in this infrastructure monitoring.

The joint width at four sections of the model generated from UAV-CRP data was measured on the bridge deck, two at each joint, and compared to a ruler measured value of 7.4 cm (shown in Figure 4-43 and Table 4-2).

Figure 4-43. Ground Truth Measurement of Joint Width

Table 4-2. Joint Width Comparisons between UAV-CRP Data Measurements and Ruler Measurements

Joint Width Section	UAV-CRP Data Measurements (cm)	Ground Truth Measurements (cm)	Absolute Error (%)
1	7.14	7.40	3.5
2	7.46	7.40	0.8
3	7.36	7.40	0.5
4	7.49	7.40	1.2

The UAV-CRP methodology can be applied to conduct monitoring of changes in joint widths over a certain period. By flying closer to the surface of the

bridge, the condition of the joint filler can also be closely detected. This was however not evaluated in this research.

4.4.1.2 Under-bridge Inspection

The drone configuration with the top gimbal, as shown in Figure 4-36, was used to perform under-bridge inspections at the same bridge. The pilot and the primary visual observer were stationed below the bridge; the UAV was flown under along the bridge's longitudinal direction. Lack of GPS forced the pilot to operate in manual flight mode while inspecting underneath the bridge. Each bridge span, the distance between two bridge columns, was monitored during each flight. The secondary visual observer was placed at a safe offset distance away from the bridge columns to inform the pilot when the UAV came alarmingly close (less than 6 ft) to the columns. The TxDOT bridge inspector accompanying the UTA research team was able to monitor the camera visuals live on a DLVP throughout the inspection. Inspector inputs were passed on by the primary visual observer to the pilot, who maintained line of sight of the UAV throughout the flight. Because the bridge was newly constructed, it did not exhibit much damage. However, moisture staining was observed underneath the bridge beams, shown in Figure 4-44.

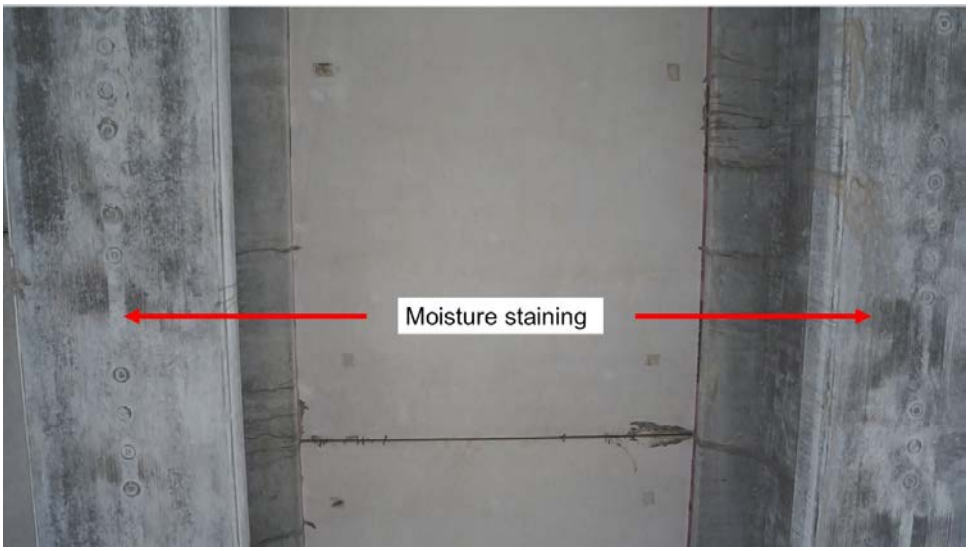

Figure 4-44. Moisture Staining Underneath the Bridge Beams

The bearings, pier cap, permanent metal deck forms (PMDF), and other substructure features can be identified from the bridge inspection studies conducted, as shown in Figure 4-45. PMDF structures are placed to keep the thickened end slabs in place and hence plays a key role in the structural integrity of the bridge. There was no appreciable distress observed in the inspection because this was a new bridge, which had not yet been opened to traffic. However, inspections on in-service bridges may reveal distresses like cracking and spalling of concrete bridge elements, rusting of PMDF and other metal parts, damages in the bearings and pile caps, and other surficial distress.

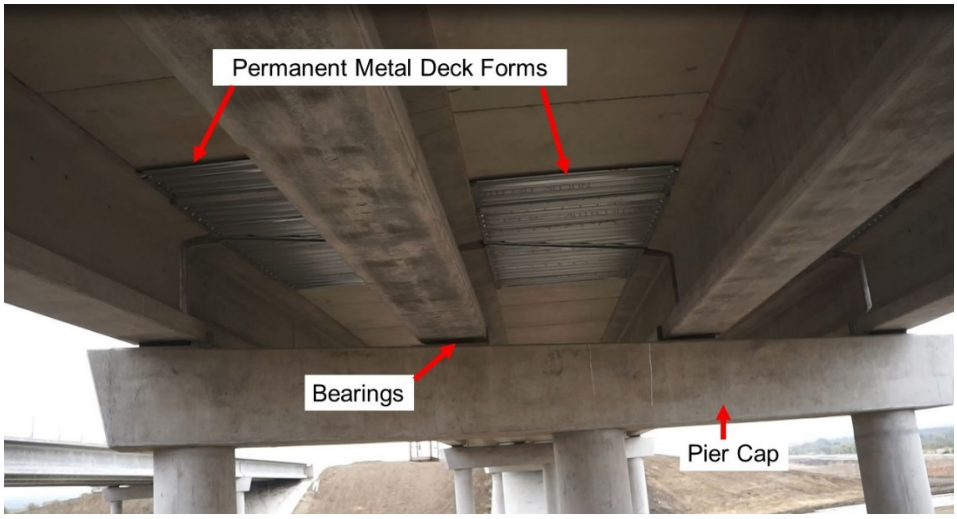

Figure 4-45. Under-bridge Inspection Featuring Bridge Substructure Elements

The stills from the 4K videos were helpful in capturing the side views of the bridge that included the columns, pier caps, bearings, and other bridge elements shown in Figure 4-46. The condition of the bearing pad and the bearing seat can be inspected by zooming on those elements as shown in Figure 4-47. These images can also help in identifying the surficial condition of the outer beams.

Figure 4-46. Side View of the Bridge Substructure Elements

Figure 4-47. Zoomed in Images Depicting the Condition of the Bearings and Pier Cap

Increased safety when accessing hard to reach areas is an important benefit as noted from the bridge studies presented in this report. Under-bridge inspection, that would have been done using a snooper truck stationed and obstructing traffic over the pavement, can be accomplished in less time with minimal traffic disruption by using a UAV.

4.5 RAIL CORRIDOR

4.5.1 Rail Corridor Inspection Study Areas

Due to the research phase of using UAVs for various infrastructure applications, a decommissioned rail track corridor was selected to provide a chance to concentrate on evaluating the data collection capability of UAVs. This rail track used to receive high traffic during the 1800s and presently in decommissioned state. This provided an opportunity to demonstrate the feasibility of using aerial data for track maintenance.

Two UAV flying teams, one from the University of Texas at Arlington (UTA) and the other from Michigan Technological Research Institute (MTRI) traveled to the Alpine-Presido region, Texas along with two TxDOT employees to conduct rail corridor inspection studies at four separate locations. The group used two Ford F250 crew cab trucks, as shown in Figure 4-48, equipped with hi-rail gear for operating over rail tracks to visit the rail corridor sites. The locations and their nearest mileposts' (MPs') numbers are listed below.

- Rail Road Crossing site, at railway milepost MP 1027.22

- Rail Bridge site, at railway milepost MP 1019.5
- Washout site, at railway milepost MP 1001.5
- Rock-Cut site, at railway milepost MP 1008.1

Figure 4-48. Ford F250 Crew Cab Truck Equipped with Hi-Rail Gear

The locations of the data collection sites in the Alpine-Presidio region were selected based on the idea of employing drones for various applications. Before the start of every day for field data collection, there was a TxDOT briefing on safety protocols, followed by a discussion of fieldwork objectives by the UT Arlington team. Personal protective equipment (PPE) was mandated for everyone taking part in the field operations.

4.5.1.1 Railroad Crossing Mapping Surveys

A railroad crossing, located in Presidio, Texas, was the first of the data collection sites visited. The location coordinates of this site can be identified as 29.555607610

N, 104.357767373 W. Observations during the initial reconnaissance surveys indicated that the decommissioned rail track had accumulated a large volume of debris. The objective of this location visit was to map the railroad at grade crossing area that extended to at least 60 meters in all directions from the center point of the crossing. For comparison studies, a terrestrial LiDAR survey was first conducted, and then a close-range photogrammetry study was performed with a UAV.

Traffic flow was unobstructed for the most part and was only regulated while covering the central part of railroad crossing area from two terrestrial LiDAR scan surveys spanning 15 minutes each, using two flagged workers standing on either end of the inspection road area. A Faros X 330 LiDAR with resolution of ¼ and quality of 4× was used considering the level of detail required, distance from the railroad crossing, and the available time. Four spheres, three on one side and one on other side of the road along the rail line, were placed to assist in stitching of two LiDAR scans together (shown in Figure 4-49a).

UAV data collection was performed by UAV platform, Aibot X6 hexacopter, as shown in Figure 4-36. Railroad crossing area extending 60 m length in each of the four directions from the center of the crossing location was measured with a tape and marked by placing a traffic cones. Six ground points, four ground control points (GCPs) and two ground check points (CKs) were laid using Trimble R8 as shown in the Figure 4-49b.

(a) (b)

Figure 4-49. Railroad Crossing (a) Lidar Scanning, and (b) Collecting the Ground Points Information

Flights were planned in such a way to avoid flying over the adjacent private area in the north-west part of the site shown in Figure 4-50. The dense point cloud model, high quality orthomosaic, and digital elevation model (DEM) pictures are shown in Figures 4-50(a-c), respectively. The orthomosaic was obtained after building mesh and rendering texture to the dense cloud points that can be observed by the sharpness exhibited by the orthomosaic compared to dense point cloud model. DEM offers an overview of the elevation of the objects with in the area read from a color-coded elevation bar, shown in figure 4-50c.

They are the imaging analysis outputs obtained from 342 photos collected during two flight plans executed at an altitude of 85 ft, spanning 10 minutes each. Throughout the data collection, real time video of the camera view was displayed on the digital live video display (DLVP) unit. The orthomosaic obtained was

helpful in setting up the sight triangles and the DEM was useful in determining if there are any obstructions within the sight triangle.

(a) (b)

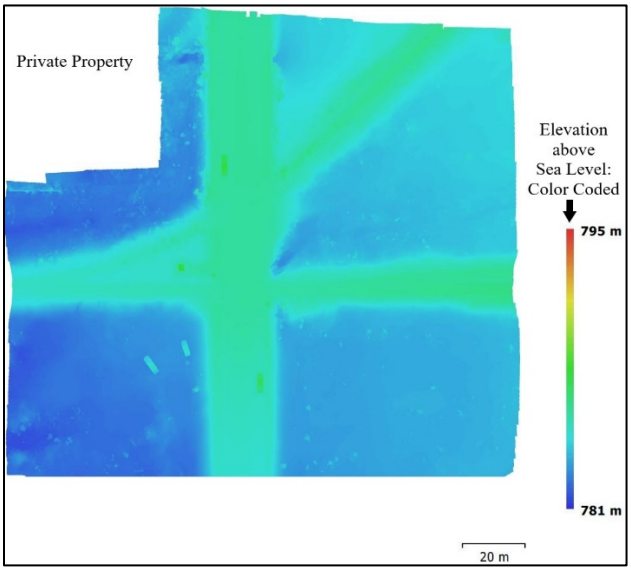

(c)

Figure 4-50. Railroad Crossing (a) Dense Point Cloud Model (b) High Quality Orthomosaic (c) Digital Elevation Model (DEM)

It is important to validate the accuracy of any model developed from collected images. Four ground control points (GCPs) were used in obtaining the dense point cloud models, and the accuracy of the model in the X, Y, and Z directions was estimated using two check points (CKs). Root Mean Square Error (RMSE) values in X, Y, and Z directions are 0.78 ft (2.4 cm), 0.17 ft (5.2 cm), and 0.05 ft (1.4 cm), respectively. Accuracy of horizontal data obtained is close to horizontal accuracy class of 5-cm and vertical data obtained is better than vertical accuracy class of 2.5-cm.

The measurements obtained from the terrestrial LiDAR and the UAV-CRP data were compared to evaluate the accuracy of the data captured using UAV. The spacing between the outer ends of the two rails was calculated from both the data collected from terrestrial LiDAR and UAV-CRP, as shown in Figures 4-51 and 4-52, respectively.

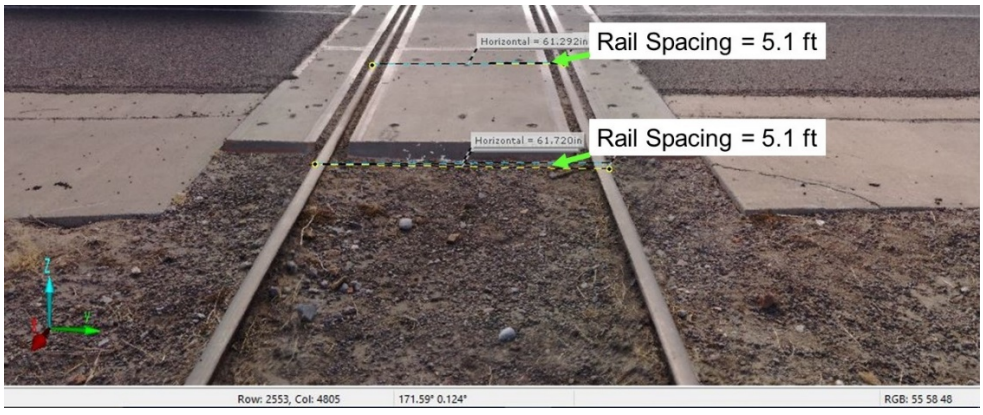

Figure 4-51. Rail Spacing Measured from Railroad Crossing Data Collected Using Terrestrial LiDAR

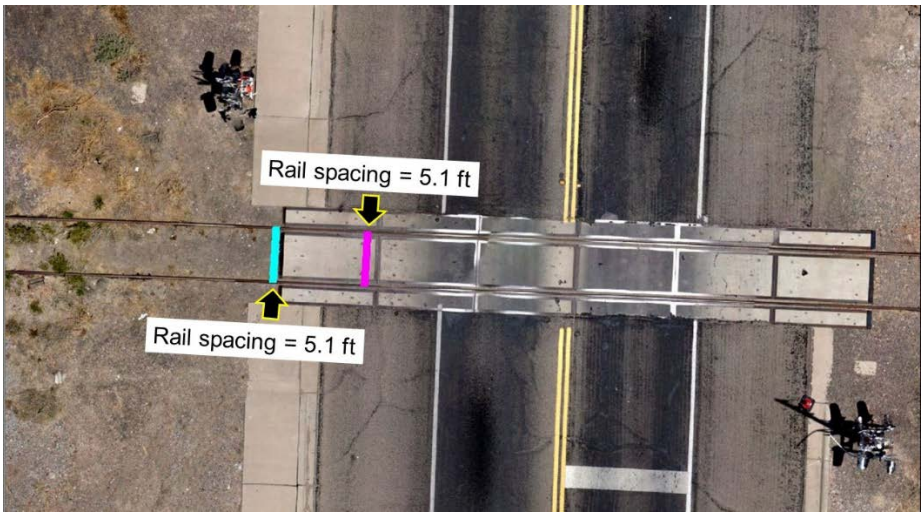

Figure 4-52. Aerial View of Rail Spacing Measured from Railroad Crossing Data Collected Using UAV-CRP

The nearest rail spacing measurement in the LiDAR data, as shown in the Figure 4-51, is represented by the aqua line drawn in UAV-CRP data, as shown in Figure 4-52. The farthest rail spacing measurement in the LiDAR data, shown in Figure 4-51, is represented by the pink line drawn using UAV-CRP data, as shown in Figure 4-52. Considering the terrestrial LiDAR data as the benchmark, the percentage error in lengths measured by the UAV-CRP data compared to the LiDAR data monitored is recorded as 0.7% and 0.3%, respectively. This analysis indicates that the UAV-CRP data can accurately detect several rail track features at a rail corridor. With this assurance of accuracy, the railroad corridor data was analyzed for different features and results are presented in the following:

4.5.1.1.1 Rail Corridor Feature Identification: Vegetation, Debris and Rusting

The output models from the UAV-CRP technology were analyzed based on their ability to cover several rail corridor problems. UAV-CRP offers a uniform scale in the orthomosaics, which assisted in pinpointing the areas of debris, rusted rail sections, and vegetation encroachment areas as they appear in the field (as shown in Figures 4-53a and 4-53b). Submergence of rail ties under debris can also be identified in the zoomed orthomosaic view of the rail track section shown in Figure 4-52. This information is needed for the proper maintenance of rail track, which is essential to safe railway operations.

(a) (b)

Figure 4-53. Rail Track Condition Assessment (a) Vegetation Encroachment and (b) Rusted Rail Sections

4.5.1.1.2 Obstruction Identification within the Sight Triangle of Rail Road Intersection

The elevation information of the area obtained from the digital elevation model (DEM) is useful in identifying any potential obstruction or encroachment within the sight triangles formed, as shown in Figures 4-54(a–d). Each of these figures

displays three views: a top view, 3D view, and profile section view. A yellow triangular toe with its two sides parallel to the centerline of the pavement and centerline of the rail line was formed at grade with the pavement. The length of the two legs of the triangle was obtained by calculating the stopping sight distance corresponding to the allowable vehicular speed on the pavement. The two sides meet orthogonally, and their other ends are joined by the hypotenuse of the triangle.

Analysis was performed using cut and fill volumetric calculations, where the toe triangle formed in the level field with the pavement serving as the horizontal partition between the cut and fill sections. Cut was represented by the black regions where there are objects above the level of the pavement section and fill is represented by red regions where there are no objects above the level of pavement. The black regions are inspected closely to identify potential obstructions laying within the sight triangle.

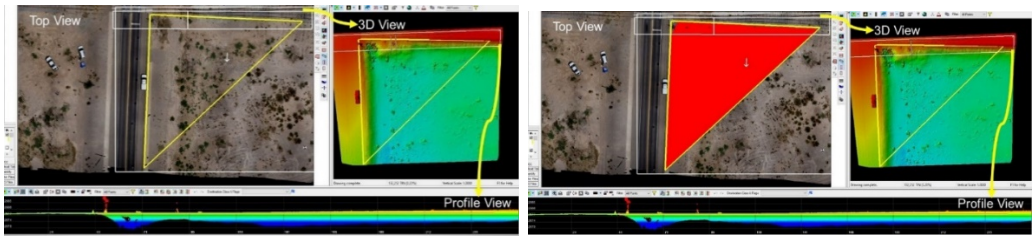

(a) (b)

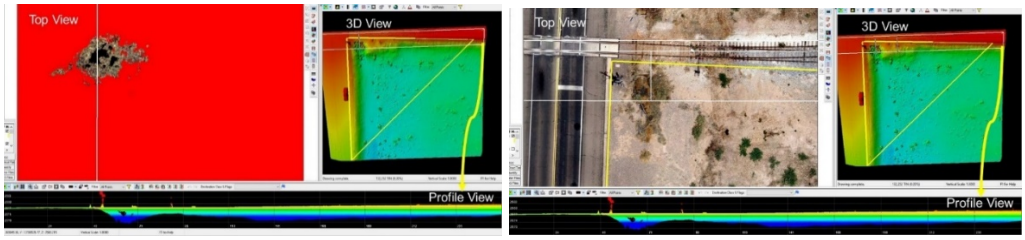

(c) (d)

Figure 4-54. Obstruction Analysis (a) Sight Triangle Formed by the Toe, (b) Sight Triangle Area Marked Red and Black, (c) Inspecting the Black Regions near the Orthocenter of the Sight Triangle, (d) Inspecting Black Region Representing Vegetation Protruding Above the Level of the Sight Triangle

The yellow toe triangle was formed as shown in Figure 4-54a and analyzed for potential obstructions to line of sight within the yellow sight triangle. In Figure 4-54b, the red region in the top view shows the area without any obstructions. The small black pockets near the orthocenter, zoomed in Figure 4-54c, represent the objects above the level of the pavement and within the sight triangle. With closer inspection in Figures 4-54c and 4-54d, the black regions were formed due to the vegetation growing above the level of the sight triangle. The sectional profile view at the bottom of each picture shows that the elevation of the vegetation is not great enough to deem it as a harmful obstruction within the sight triangle.

4.5.1.1.3 Elevation profile near to tracks

The comfort of those who drive over the Nation's streets and highways is an important factor when estimating the condition of any pavement. An attempt was

made to estimate the discomfort experienced as indicated by IRI values from the UAV-CRP collected data. The MTRI team collected photogrammetry data using a Nikon D810 camera mounted on a Bergen hexacopter to determine the ride smoothness at railroad crossings. The assembled drone configured for research and weighs just over 11 pounds including the payload costs $5,000. The 3D digital elevation model (DEM) and the orthomosaic (shown in Figures 4-55(a)–(c)) were used to calculate the elevation details.

The MTRI team measured the elevation profile at four sections across two specific rail crossings (as shown in Figure 4-55). After extracting the elevation profiles of those sections using ArcGIS Desktop, the elevation values were imported into ProVAL to determine the IRI of each section at its respective crossing, with the depression areas representing the rail tracks removed. This resulted in IRI values in the range of 9.12 to 12.31 m/km (578 to 780 in/mi), which needs further inspection along the whole pavement stretch.

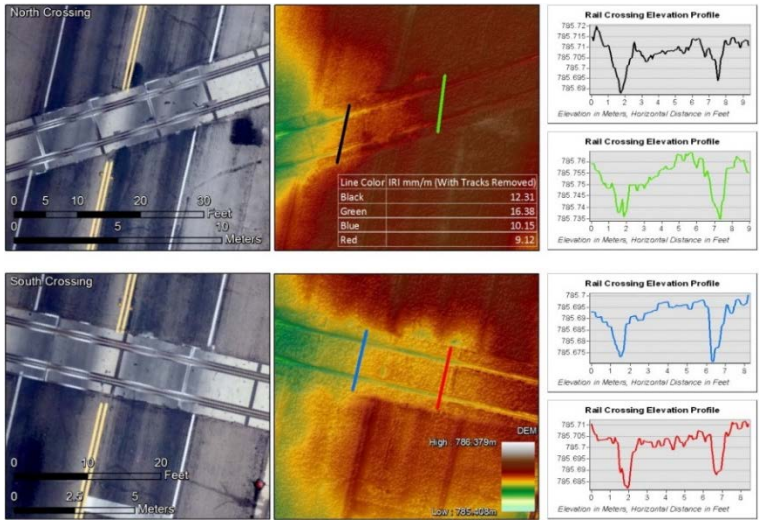

(a) (b) (c)

Figure 4-55. Aerial Mapping Products of Railroad Crossing (a) Orthomosaic, (b) DEM and (c) The Elevation Profile of Four Sections

4.5.1.2 Railway Bridge

The UAV inspection teams comprising UTA and MTRI team visited a railway bridge located at coordinates, 29.59554545 N, 104.2466614 W. A 360° rail bridge inspection was accomplished using top and bottom gimbals mounted on the UAV. The bottom gimbal on the Bergen hexacopter and DJI phantom was used to capture the top and side views of the bridge. The top gimbal on the Aibot X6 hexacopter, as shown in Figure 4-56, was used in conducting the under-bridge inspection.

Figure 4-56. UAV with Camera Mounted on Top Gimbal Flying Towards the Bridge for Inspection

4.5.1.2.1 Rail Bridge: Super and Substructure Inspection

A TxDOT bridge inspector accompanied the UTA and MTRI research team to supervise the inspection. Throughout the under-bridge inspection, the bridge inspector accessed the live relay of the camera's view on the digital live video display unit (DLVP) monitor and passed on the information needed to inspect the bridge elements that are of importance to TxDOT. This under-bridge inspection not only helped to identify missing rivets and bolts but also the presence of the rusted sections and rotten tie members, as shown in Figure 4-57. This drone inspection was also safer for the TxDOT workers who traditionally collect this information walking on a wooden platform placed 70 ft above ground level just below the 1500

ft long bridge. During our UAV inspection, research team identified the heavily distressed walking platform shown at the bottom of Figure 4-57 and Figure 4-58a. Some of the elements identified included rail ties, bridge girders, plates, rivets, bridge columns, and other rail elements.

Figure 4-57. Under-bridge View Displaying Missing Rivets, Rotten and Rusted Bridge Elements

The stills from the 4K quality videos of the bridge's top and side views were used to identify the damaged ties and railings, and the condition of the plates and rivets on the bridge columns as shown in Figure 4-58(a–d).

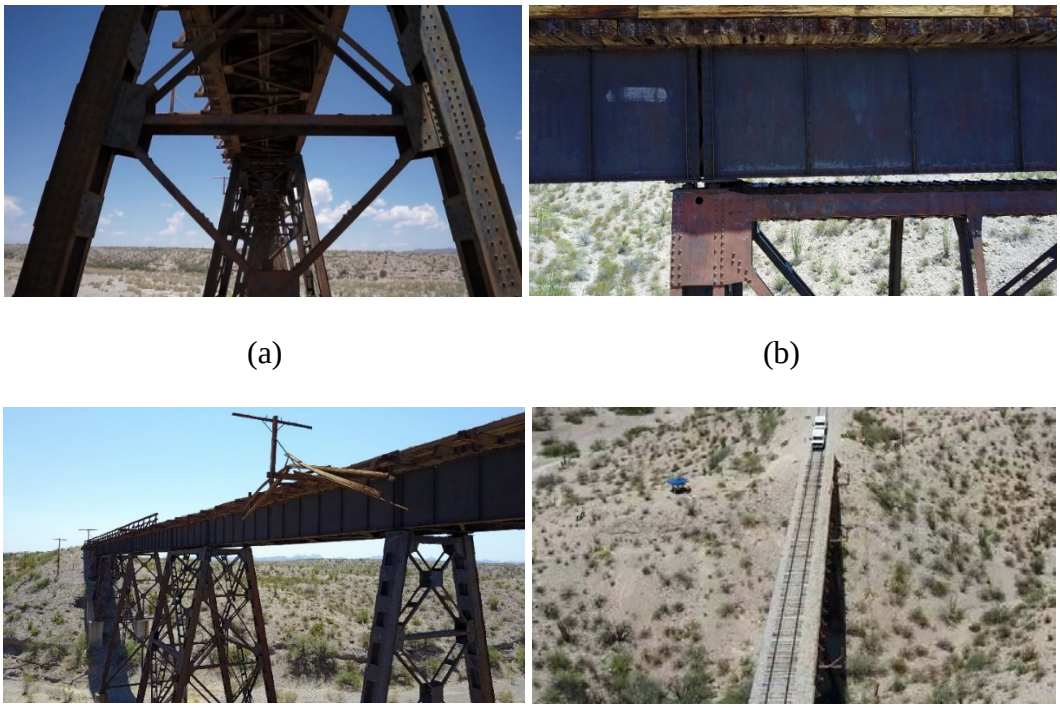

(a) (b)

(c) (d)

Figure 4-58. Rail Bridge Inspection (a) Bridge Column Inspection (b) Side View of the Bridge Girders (c) Damaged Railings (d) Top View of the Railway Line

4.5.1.2.2 Thermal Imaging

The UTA and MTRI team used FLIR Vue Pro thermal camera mounted on the Bergen hexacopter and collected visible range digital imagery with a Nikon D810 used in the small Phantom 3A and Mavic Pro quadcopters. Six survey-grade GPS-based ground control points were laid on the bridge and at the ends of the bridge. The thermal data was used to detect the improper alignment of rail ties indicated by stark differences between the temperature of a tie from that of the surrounding debris, as shown in Figures 4-59a and 4-59b. We can also apply algorithms to detect

if a tie is missing or buried under the debris. We can also differentiate between good and damaged ties using the thermal data, which showcase their ability to conduct heat differently.

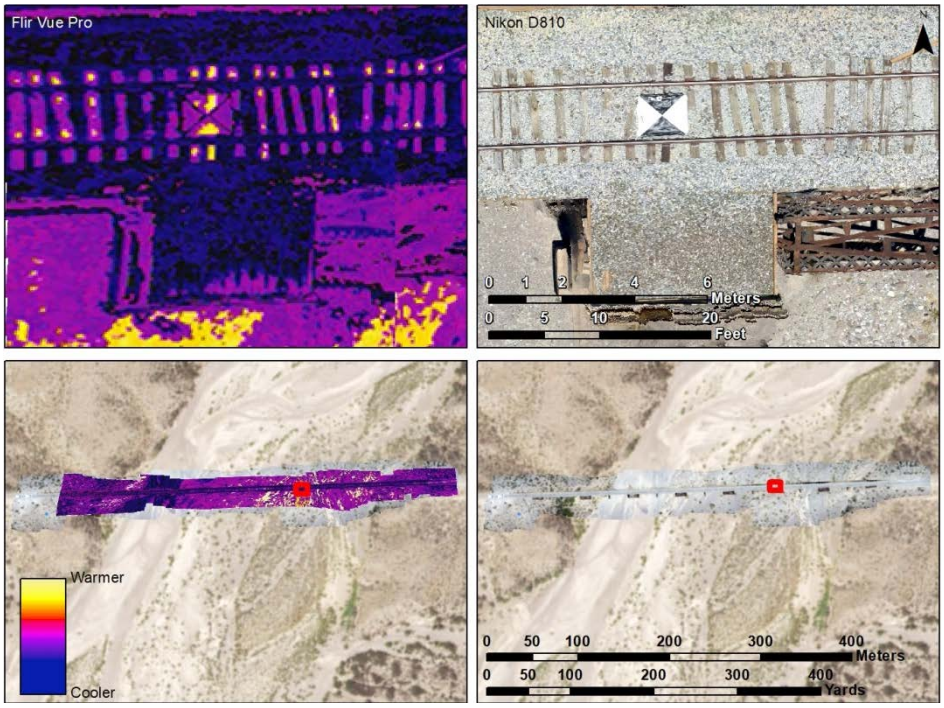

(a) (b)

Figure 4-59. Aerial Data of Rail Bridge (a) Thermal data from Flir Vue Pro Camera (b) Orthoimage from Nikon D810 Camera

Figure 4-60 shows how the pixel values of each tie in the thermal imagery can be extracted to indicate the relative temperatures of the ties. This can then be compared with the optical imagery to show how tie brightness affects temperature; darker ties with more creosote are usually warmer than bright ties. This analysis is

useful for an automated identification of older ties with more creosote that might need replacement.

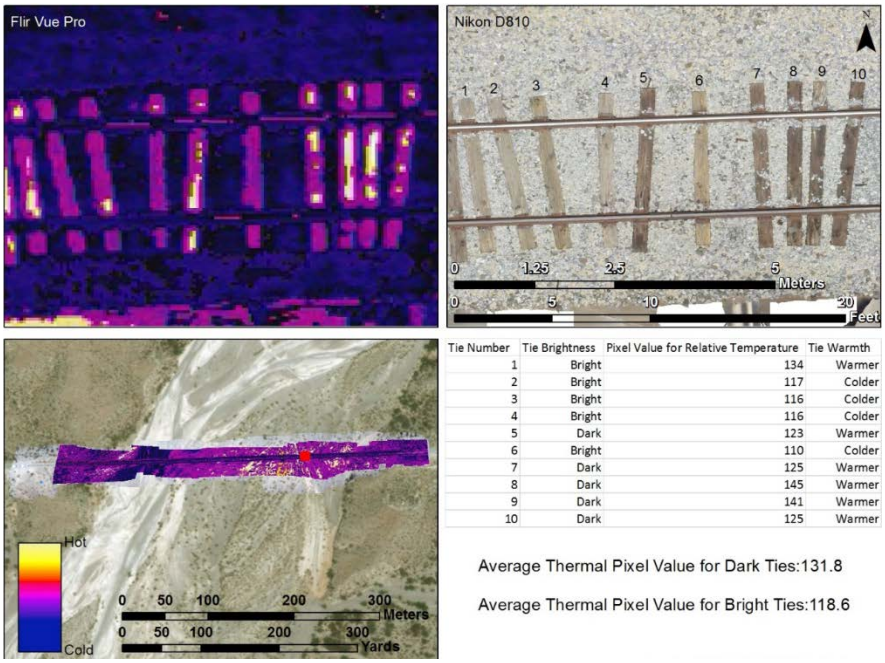

Tie Number	Tie Brightness	Pixel Value for Relative Temperature	Tie Warmth
1	Bright	134	Warmer
2	Bright	117	Colder
3	Bright	116	Colder
4	Bright	116	Colder
5	Dark	123	Warmer
6	Bright	110	Colder
7	Dark	125	Warmer
8	Dark	145	Warmer
9	Dark	141	Warmer
10	Dark	125	Warmer

Average Thermal Pixel Value for Dark Ties:131.8

Average Thermal Pixel Value for Bright Ties:118.6

Figure 4-60. Relative Brightness Linked With Temperature to Identify Older Ties Needing Replacement

4.5.1.2.3 Bridge Bearing Condition Inspection

The UTA and MTRI research team also demonstrated the use of 4K video (equivalent to 8.8 MP resolution) in conducting bridge inspection. Over a period of 4 minutes and 46 seconds, 1000 feet of bridge fascia were flown at 30 fps 4K video, which is the same as taking 8,580 continuous images of the bridge. This video capture was also repeated for the other side of the bridge. The TxDOT inspector also expressed interest in inspecting the condition of the bridge bearings. Hence,

the individual frames from the 4K video were extracted and merged together to create detailed side views of the bridge bearings (as shown in Figure 4-61). Providing this kind of rapid video inventory capability can help to inspect hard-to-access parts of bridges in a very short amount of time.

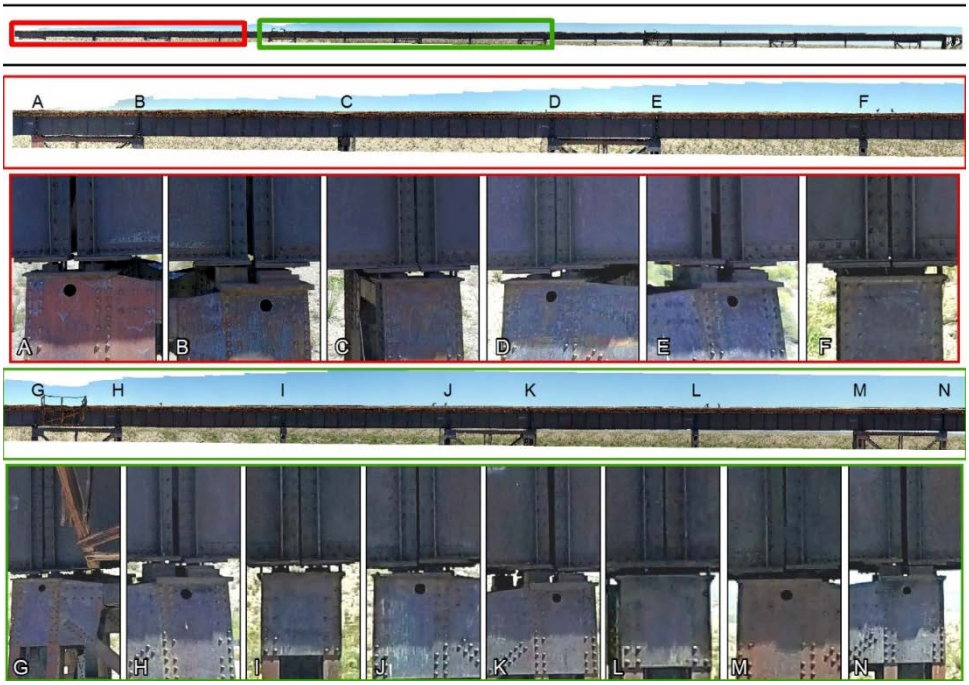

Figure 4-61. Bridge Bearing Inventory Created from 4K Video Stills Collected by a Mavic Pro Small Quadcopter UAV

These videos and the images were helpful in assessing the condition of the railway track located in a remote area of Texas.

4.5.1.3 Railway Washout

The UTA and MTRI inspection team visited the washout area underneath the rail track located at 29.77550326 N, 104.06125797 W. A drainage path leading to the

washout had been observed during the initial inspection of the site. For ground truth comparisons, the width of the washout was found manually at different sections along the length of the washout, as shown in Figure 4-62a. Damaged ties/sleepers were marked to assess the detection capability of 3D models developed from the UAV-collected data.

A LiDAR scan was performed using the Faros X 330 LiDAR at the washout site. A resolution of ¼ and quality of 4x were selected considering the level of detail required as well as the distance from the washout and the available time, as shown in Figure 4-62b. Subsequently, five ground control points were set up using Trimble R8. The Bergen hexacopter was flown over the washout site.

(a) (b)

Figure 4-62. Inspection of Washout (a) Manual Measurement of Washout Width, and (b) LiDAR Scanning at Washout underneath the Rail Track

The UAV data was analyzed to develop orthomosaic and 3D dense point cloud models that not only help estimate the extent of the washout, but also identify the drainage path that contributed to it, as shown in Figure 4-63.

Figure 4-63. Aerial view of Drainage Path That Contributed to the Washout

Ground truth measurements were made and compared with LiDAR (as shown in Figure 4-64) and UAV collected data measurements are shown in Figure 4-65.

Figure 4-64. Washout Width Measured Using Data Collected from Terrestrial LiDAR

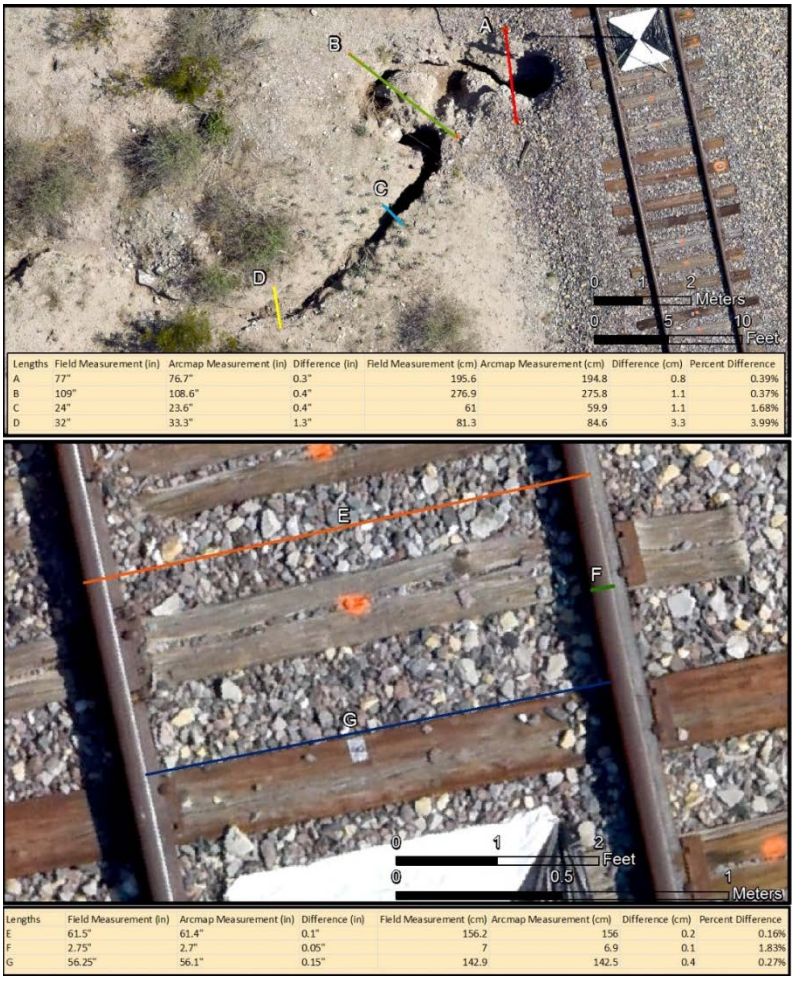

Lengths	Field Measurement (in)	Arcmap Measurement (in)	Difference (in)	Field Measurement (cm)	Arcmap Measurement (cm)	Difference (cm)	Percent Difference
A	77"	76.7"	0.3"	195.6	194.8	0.8	0.39%
B	109"	108.6"	0.4"	276.9	275.8	1.1	0.37%
C	24"	23.6"	0.4"	61	59.9	1.1	1.68%
D	32"	33.3"	1.3"	81.3	84.6	3.3	3.99%

Lengths	Field Measurement (in)	Arcmap Measurement (in)	Difference (in)	Field Measurement (cm)	Arcmap Measurement (cm)	Difference (cm)	Percent Difference
E	61.5"	61.4"	0.1"	156.2	156	0.2	0.16%
F	2.75"	2.7"	0.05"	7	6.9	0.1	1.83%
G	56.25"	56.1"	0.15"	142.9	142.5	0.4	0.27%

Figure 4-65. Measurements of Washout Width and Rail Spacing from UAV Data

The error between the measurements from the Terrestrial LiDAR and the UAV-CRP data at Section A is 0.1%. Comparisons of the drainage path width and washout obtained from the ground truth measurements and the measurements from UAV-CRP data are shown in Figure 4-65 and indicate an error of 0.4%, 0.4%, 1.7%, and 4% at sections A, B, C, and D, respectively. Comparisons of rail spacing measurements from the ground truth and the UAV-CRP data show an error of 0.2%,

1.8%, and 0.3% at Sections G, E, and F, respectively. These errors are small indicating that UAV-CRP data and analyses provide the measurements matching ground truth values obtained from traditional methods.

4.5.1.4 Rock Cut

The rail line passing through a rock cut located at coordinates 29°42'20.3"N, 104°08'07.5"W was visited by the inspection team. Unstable rock slopes, rock fall debris, and damaged ties were among the problems identified on this rail infrastructure. Stability of rock cuts is warranted for safe operation and preservation of any infrastructure asset that passes through hilly terrain. A proper assessment of the stability of cuts could result in planning for measures reducing the damage caused by potential landslides during hazardous disasters such as earthquakes and hurricanes. The UAV-CRP methodology assists in collecting such data in a safe and efficient manner. UAV operations were performed on a rail line passing through one of the rock-cut sections in the Alpine-Presidio region, Texas. A LiDAR scan was performed using the Faros X 330 LiDAR at the rock cut site. A resolution of ¼ and quality of 4× were selected considering the level of detail required, distance from the rock walls, and the available time.

Subsequently, an attempt to set up five ground control points using Trimble R8 failed as the site was 30 miles away from the base station and covered with soil on both sides. Here, radio communication issues with the real-time kinematic (RTK) broadcast signals prevented collection of GPS data. The UAV was taken

off from the box (as shown in Figure 4-66a) due to the unavailability of a flat ground surface and high wind gusts. The Aibot X6 hexacopter was flown at multiple flight altitudes manually due to the variations in the ground profile, wind speed, and bird threat in this remote area of Texas. The copter was flown away from the wind tunnel effect created by the rock walls on either side of the cut. While maintaining the copter's line of sight data was collected as the area, being covered was monitored in real-time using a live video display unit (DLVP).

Servo gimbal was not only useful in damping the vibrations caused due to flying in windy conditions but also in collecting nadir and oblique images. Oblique images were helpful in creating an accurate representation of the uneven slope surfaces of the rock walls. Geotagged images were used to generate a high-quality 3D dense point cloud model, as well as a digital elevation model (DEM), and orthomosaic, shown in Figure 4-66b and 4-66c. These files are used to obtain different views as shown in Figure 4-66b.

(a) (b)

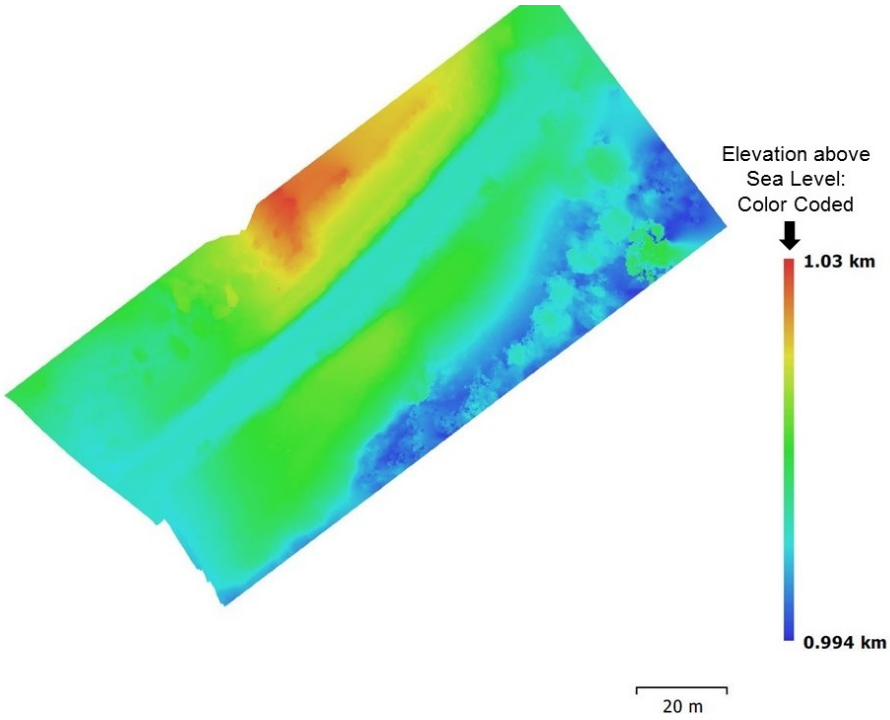

(c)

Figure 4-66. Rock Cut Inspection (a) Setting up the UAV Take off Point on a Box, (b) Rock Cut Shown in Different Views (c) DEM of the Rock Cut

Data collected from the terrestrial LiDAR and the UAV are analyzed to compare the accuracy of the UAV data, shown in Figures 4-67 and 4-68. The nearest rail spacing measurement in LiDAR data, shown in Figure 4-67, is represented by the aqua line drawn in UAV data, shown in Figure 4-68. The farthest rail spacing measurement in LiDAR data, shown in Figure 4-67, is represented by the orange line drawn in UAV data, as shown in Figure 4-68.

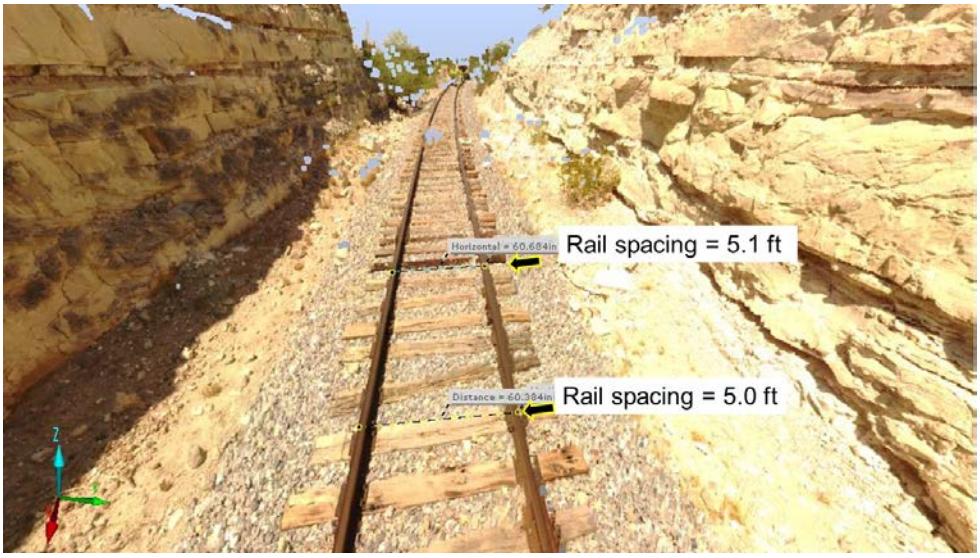

Figure 4-67. Rail Spacing Measured At Rock Cut Using Data Collected from Terrestrial LiDAR

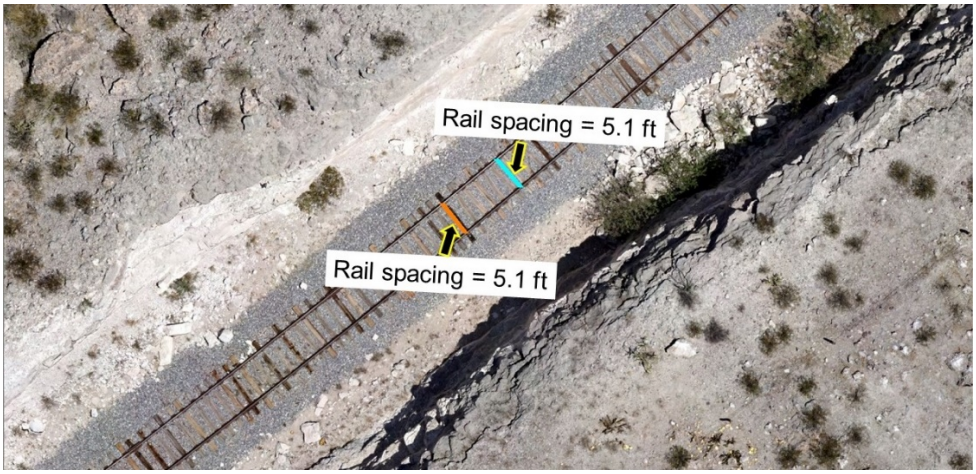

Figure 4-68. Aerial View of Rail Spacing Measured at Rock Cut Using Data Collected from UAV-CRP Technology

Considering the terrestrial LiDAR data as the benchmark, the percentage error in aqua and orange lengths measured by the UAV are recorded as 0.4% and

0.7%, respectively. This analysis indicates that the UAV-CRP data could accurately capture several features of rock cut. Further results from the rock cut are presented in the following sections:

4.5.1.4.1 Rock Slope Stability Analysis

All three views including top (or plan view), 3D view, and profile section views of the railway infrastructure passing through a rock cut are presented in Figure 4-66b. These different view perspectives can help identify the most critical rock slopes and plan stabilizing measures in case the slopes appear to be too close to a failure state as shown in Figures 4-69 and 4-70. The debris on the track is made up of rocks that rolled down from the rock outcrops, which is simulated in the two- and three-dimensional models for a more realistic field experience representation. Also, potential rock debris volume estimation can be performed to help plan debris removal after the occurrence of rock slides.

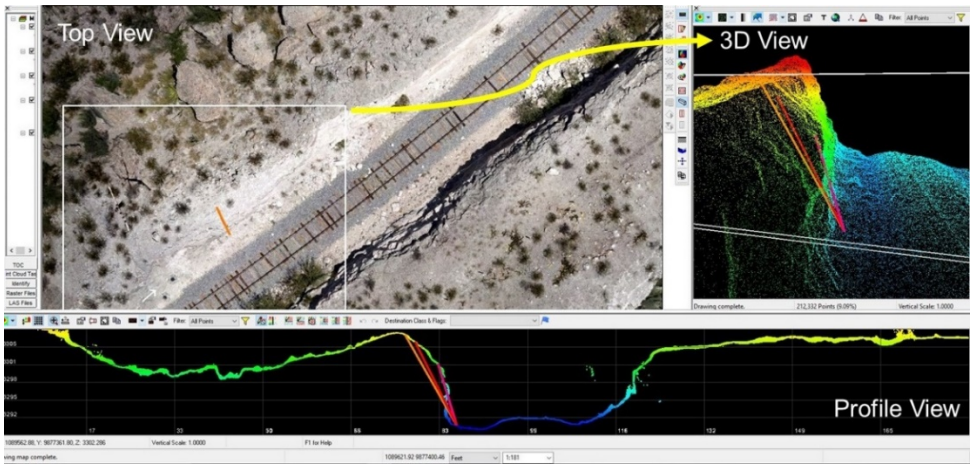

Figure 4-69. Slope Stability Analysis of the Rocks at One Location

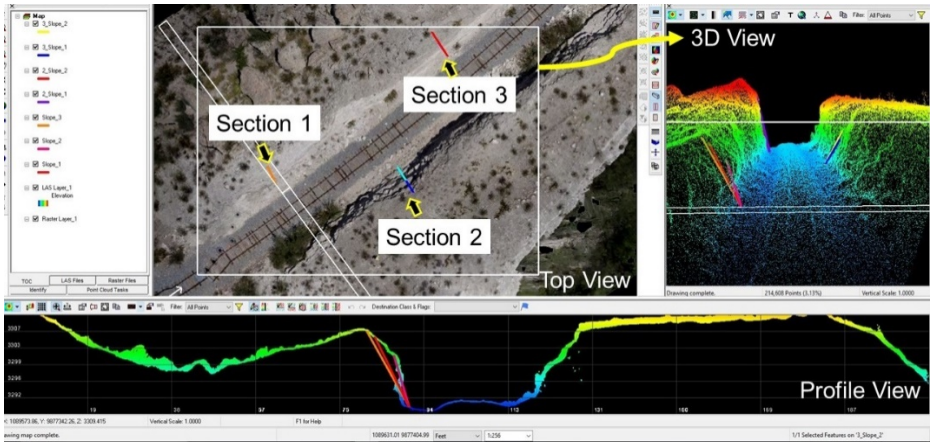

Figure 4-70. Slope Stability of the Rocks at Multiple Locations along the Infrastructure

Slope stability information was presented at three locations (two on left and one on right side of the track), in the rock slope section as shown in Figure 4-70. For Section 1, the slopes (presented as tangent slope angles) connect each of the three points on the slope region with the point located on the toe of the slope of the left rock slope as shown in Figure 4-69, are 3.3, 2.0, and 1.7, respectively. Similarly, the slopes connecting the point on the slope toe and the points on the crest on the slope section (only two slopes are drawn here) were calculated at two other locations depicted in Figure 4-70. The slopes for Section 2 on the right rock slope are 2.0 and 1.8. The slopes for Section 3 on the left rock slope in are 4.5 and 3.0.

This information will be input into any slope stability software with the availability of rock material properties at the site, engineers will be able to perform

slope stability assessments of the rock cut sections. Any unstable slopes will then be reviewed and strengthened.

4.5.1.4.2 Debris Detection on Rail Lines

The two sky-blue lines, in the top view of the photo image shown in the Figure 4-71, represent the rail tacks. Two red lines on either side of the track, as shown in the 3-D view on the top right of Figure 4-71, were formed as the toe lines at the level of the rails 9 ft each from the nearest rails.

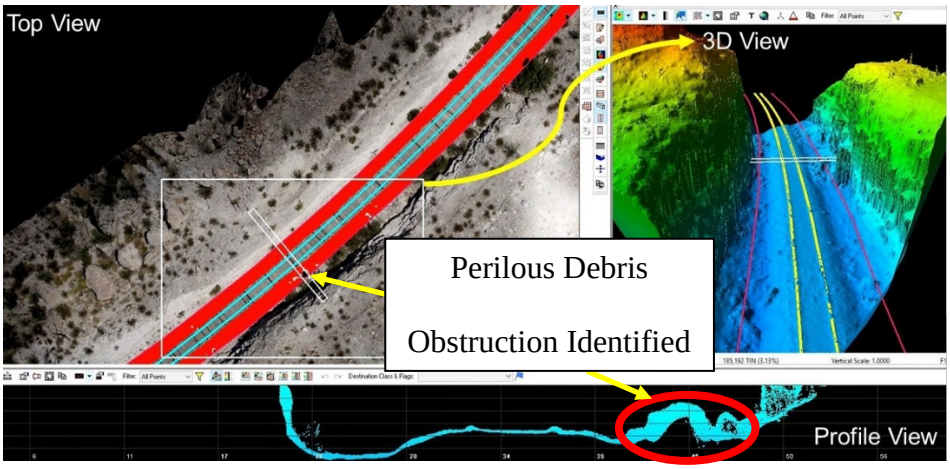

Figure 4-71. Perilous Debris Obstruction Identification within the Permissible Vicinity of Rail Infrastructure

The cut and fill volumetric method was used to find any possible rock falls that are above the level of the rails and could pose a potential danger to the smooth movement of the rail traffic on the infrastructure. The toe formed level with the rails serves as the horizontal partition between the cut and fill. Cut is represented by black regions where there are objects above the level of the rails and fill is

represented by red regions where there are no objects above the level of rails within the region between the toe and the rails.

The red regions around the rail lines, represented by the sky-blue color, denote the areas where there is no potential obstruction from rock debris accumulated near the rail lines due to unstable rocks. The black regions, pointed out by the yellow arrow in the top view of Figure 4-71, represent the rock debris above the rail levels. This can also be inspected on the right side of the rail track shown in the profile section view, highlighted by the red oval, at the bottom of Figure 4-71. This data will be very useful in areas with unstable slopes or with slopes that are not easily accessible. In addition to all the data collected, damaged or rotten ties can also be counted by observing the number of dark ties visible in the top views of images presented in Figures 4-69, 4-70, and 4-71.

4.5.1.4.3 Thermal Imaging

The UTA and MTRI team collected the aerial data at another rock cut site with only one rock wall and a valley on the other side. A Nikon D810 mounted on the hexacopter was used to collect visible range images and Flir Vue Pro to gather the thermal data. This data was used to develop the orthomosaics that help in further evaluations. Thermal imaging, visible range orthomosaics, and DEMs as shown in Figures 4-72(a)–(c), can be used to identify the improper alignment of rail ties indicated by stark difference between the temperature of a tie from that of the surrounding debris and also sliding debris. Research teams can also apply

algorithms to detect if the tie is missing or buried under the debris and also to differentiate between good and damaged ties using the thermal data that highlights the variability in thermal properties of damaged and healthy ties.

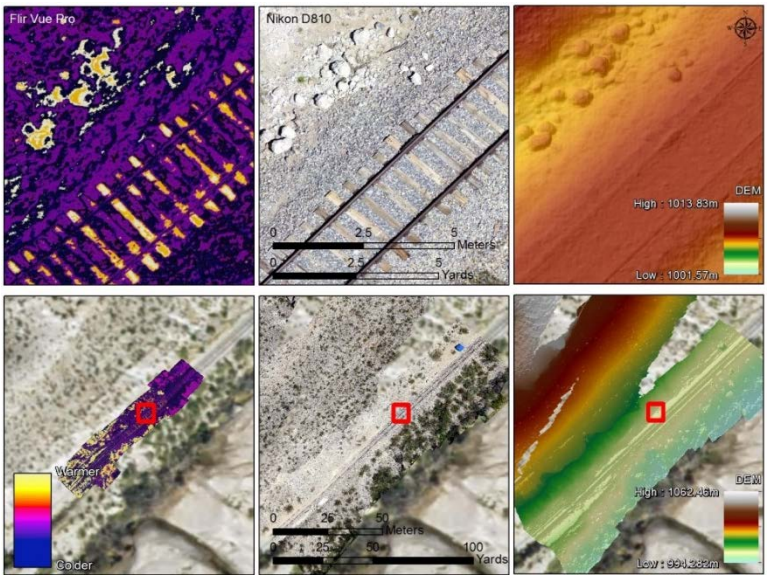

(a) (b) (c)

Figure 4-72. Aerial Data of Rock cut (a) Thermal Imaging (b) Orthomosaic (c) DEM

4.5.1.4.4 Erosion Detection

Aerial data collected by UTA and MTRI team was processed to obtain elevation data that can be used to detect erosion around rail ties, as shown in Figure 4-73. The ties were protruding out, without any substantial support to hold the rails in place. This is detrimental to safe rail operations. Eight rail ties were selected and the respective elevations of top face of each tie from the bottom of the ground were measured from UAV-CRP data and a tape for comparison purposes.

All measurements were within 1.61 cm of their field values, as close as 0.80% (8.89 cm vs. 8.82 cm) although one area had 6.35 cm vs. 4.80 cm. As field measurements were only recorded within the nearest ½ in., it is possible that the measurements from the remote sensing results might be accurate. This research also demonstrates that the UAV-CRP data can be used in the detection of missing ballast support for ties due to erosion. This process can likely be automated to find areas of ballast fouling and other problems along rail lines.

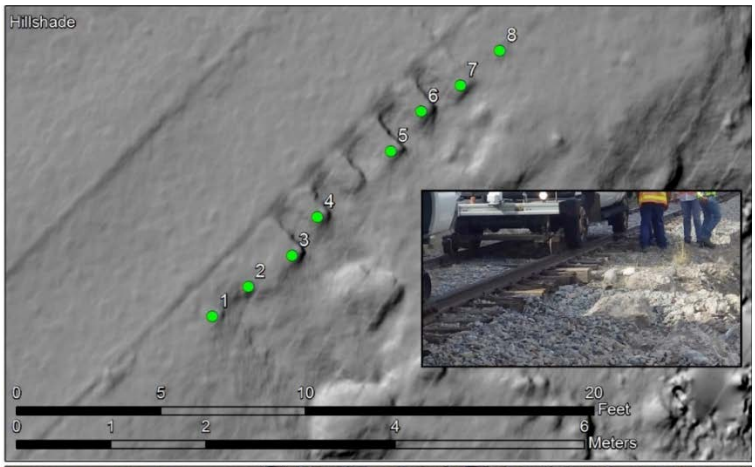

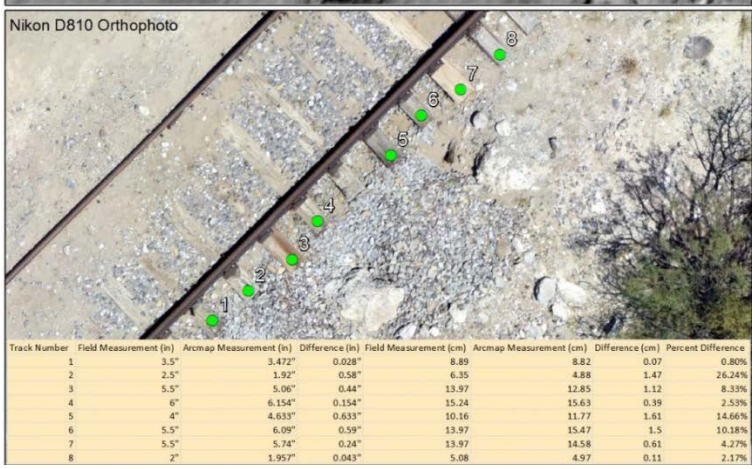

Track Number	Field Measurement (in)	Arcmap Measurement (in)	Difference (in)	Field Measurement (cm)	Arcmap Measurement (cm)	Difference (cm)	Percent Difference
1	3.5"	3.472"	0.028"	8.89	8.82	0.07	0.80%
2	2.5"	1.92"	0.58"	6.35	4.88	1.47	26.24%
3	5.5"	5.06"	0.44"	13.97	12.85	1.12	8.33%
4	6"	6.154"	0.154"	15.24	15.63	0.39	2.53%
5	4"	4.633"	0.633"	10.16	11.77	1.61	14.66%
6	5.5"	6.09"	0.59"	13.97	15.47	1.5	10.18%
7	5.5"	5.74"	0.24"	13.97	14.58	0.61	4.27%
8	2"	1.957"	0.043"	5.08	4.97	0.11	2.17%

Figure 4-73. Detection of missing ballast support for the ties due to erosion

4.6 SUMMARY

UAV-CRP technology collected data offer a comprehensive idea on the distress features including permanent deformation to cracking patterns in pavements, spalling to bearing condition of bridges, and washout to buckling of rail lines. Various infrastructure condition assessments including transportation to geotechnical infrastructure health monitoring were possible and these applications were performed and fully addressed in this research.

Pavement images were collected and processed to build different photogrammetric models. These models were analyzed for different distress like cracking, permanent deformation, pot holes, and other serviceability parameters. International roughness index (IRI) and transverse slope were measured using traditional profilers and terrestrial LiDAR to compare with UAV-CRP technology. Although a good match was obtained between the IRI values using the traditional methods and UAV-CRP technology, there is need for conducting more validation studies.

UAV-CRP technology have shown good correlation with the measurements from terrestrial LiDAR. Python programming language was used to identify the cracked region basing upon different filters applied on the pixel intensity based images. Pavement construction material stockpiles were also estimated using UAV-CRP technology and have shown an excellent match with the traditional methods. UAV-CRP technology have provided the stockpile information quick, safe and

efficient manner compared to conventional techniques. Bridge structure was inspected for obtaining the condition of superstructure and substructure elements. Top gimbal and bottom gimbal cameras were used in separate flights to conduct a 360° bridge inspection.

Railway corridor inspections on the decommissioned rail line in the Alpine-Presidio region have shown that data collection using UAV-CRP technology is quick, safe, and accurate compared to the traditional way of data collection. In this dissertation research many important features that might affect the working of railroad crossing had been identified using this new technology. Various superstructure and substructure elements of the rail bridge were safely inspected. Washout location has also been identified along with the drainage path leading to the erosion of soil underneath the track. Information pertaining to the stability of rock cuts were also obtained using this technology. UAV-CRP technology studies have provided information critical to the safety of road and rail users.

CHAPTER 5: DISASTER MANAGEMENT OPERATIONS

5.1 INTRODUCTION

Recently the frequency of disaster occurrence has gone up and it created the need for exploring tools and equipment that help in various disaster management operations. UAVs had provided scope to monitor places that cannot be easily accessed by humans, especially during the time of disasters. Mounting different sensors also helps in inspecting the situation, in an innovative view which otherwise would not be possible with a naked eye. In this dissertation research, UAVs were explored for reconnaissance surveys during and after the Hurricanes. They were mounted with a visible range camera and the condition of the infrastructure in addition to the debris stockpile information.

5.2 HURRICANE HARVEY DETAILS

Large amounts of debris was generated from Hurricane Harvey that struck the state of Texas, USA in 2017. As a part of National Science Foundation (NSF) RAPID study, UT Arlington studied the use of UAV-CRP technology for the estimation of stockpile volumes of debris generated from the inundated household items. This chapter describes the framework followed to estimate debris piles and pavement condition using UAV-CRP technology related data collection.

Research team visited various sites in the City of Beaumont, Texas including a landfill site and the debris piles stacked up on the streets, as part of reconnaissance survey to select appropriate sites for data collection. Due to the

research nature of the study, with an intention to collect more data in the available time, the sites were selected in such a way that the streets have continuous debris piles in the vicinity. DJI Phantom Advanced 4 is built with front obstacle avoidance sensors that help in maneuvering in complex places such as arterial roads covered with poles, trees, and other obstacles. Due to the obstructions posed by the trees and buildings, all the UAV data collection was done in a manual flight mode to have better control of flight operations. Remote pilot in command (RPIC) had flown the copter within the line of sight throughout the flights and the visual observer was able to click pictures looking at the screen providing the views from the camera mounted on the drone.

5.3 UAV AND ACCESSORIES USED

DJI Phantom Advanced 4, as shown in Figure 5-1, was used due to its compactness and higher flight time. It can be operated autonomous as well as in manual flight mode. It has a 20 MP inbuilt camera with adjustable aperture size from F2.8-11.

Figure 5-1. DJI Phantom Advanced 4

5.4 DEBRIS SITE INFORMATION

The sites were selected in such a way that they fall under the class G airspace according to Federal Aviation Authority (FAA). UAV was flown at eight different sites that included flights covering one or multiple stockpiles. The eight debris stockpile sites selected are located at 11800 Carpenter Road, 9902 N Major Dr, 7695 San Anselmo St, 11080 Sherwood Dr, 11130 Fairfield Dr, 11195 Forest Glen, 11135 Forest Glen, and 12700 Tan Oak Ln, Beaumont, Texas, respectively shown in Figure 5-2. All these areas under unrestricted flying zones, falling under class G airspace, are numbered as Site 1, 2, 3, 4, 5, 6, 7, and 8. Sites 1, 2, 4, 5, and 7 consisted of single debris stockpile each; Site 6 consisted of two debris stockpiles; and sites 3 and 8 consisted of three debris stockpiles each.

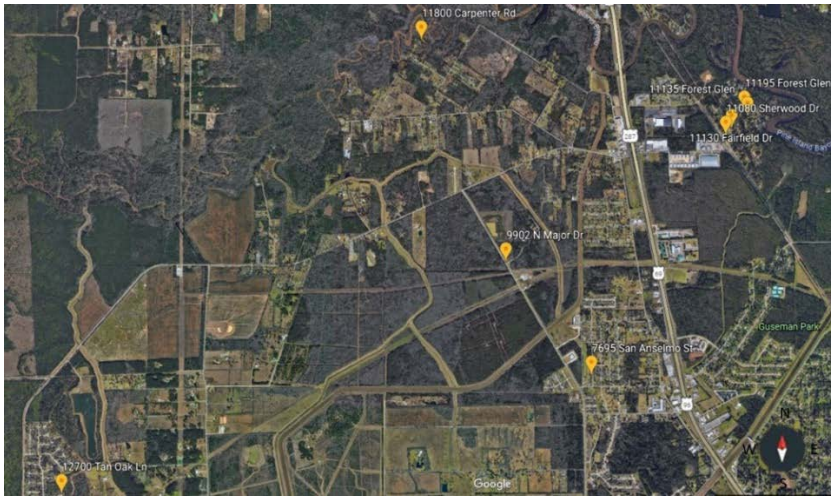

Figure 5-2. Locations of Eight Debris Piles Located in Beaumont, Texas (Map data © 2018 Google)

5.5 DATA COLLECTION AND ANALYSIS

All the staff participating in the research were required to wear Personal Protective Equipment (PPE) while performing the UAV data collection procedures. Traffic cones were placed at the boundary of the inspection area projecting on to the roadway but there was no traffic control as the UAV was flown off from the pavement. Due to the early days after the disaster had occurred, these arterial roads mostly had the slow moving garbage truck traffic that can be easily spotted. The UAV was taken off from a flat surface and flown in multiple flight legs parallel to the longest side of the debris stockpiles. Whenever a passing vehicle was spotted and informed by one of the visual observers, the drone was flown away to a safe distance from the pavement and hovered still to continue the data collection after the vehicle passed.

Each stockpile was covered in three longitudinal legs due to the smaller width of the stockpiles and the lower flight altitudes adopted. First leg of the UAV flight was selected in such a way that it is couple of feet away from the edge of the stockpile and the pictures were manually taken in such a manner that noticeable objects on the stockpile were identified on the monitor and ensured that they are captured in at least four images in the longitudinal direction. At the end of the longest stockpile leg, the UAV was flown laterally to reach the central plane of stockpile and the procedure adopted for adequate longitudinal overlap coverage

during the first leg was followed along the center line of the stockpile, parallel to the first leg.

The third leg was flown along couple of feet away from the edge of stockpile to obtain adequate lateral overlap as well. Whenever the stockpile width was higher, an extra leg was introduced in the middle for acquiring better quality data with higher overlap. These procedures were followed for the data collection at all eight debris sites discussed below

Despite of lacking the ability to penetrate the surface of debris stockpiles, the UAV-CRP provides an accurate estimation of the irregular outer surface from the 3-dimensional dense point cloud model. Using the orthomosaic, a boundary was created by joining the points around the debris stockpile and the base of the debris stockpile was formed between these points. Both these views offered by the 3-dimensional dense point cloud model and the orthomosaic are combined to measure the distances in three dimensions.

Most of the debris stockpiles were piled up on the side of the streets where the land was sloping, hence, the elevation of the ground under the debris stockpile is interpolated between elevations of two boundary points. The volume was calculated by estimating the dense point cloud points above the base and enclosed within the boundary marked. These procedures were followed for estimating the volume of each debris stockpile at all eight site locations provided below.

5.5.1 Debris Site 1

The first debris stockpile was inspected near to the location 11800 Carpenter Road, Beaumont, Texas. The only stockpile inspected at this location composed of the sodden household objects dominated by the furniture. There was no vehicular traffic during the data collection hence the UAV was taken off from the adjacent hard surface. Following the procedure explained in earlier sections, the single stockpile was inspected in a manual flight. The images captured were processed in image analysis software to develop 3-dimensional dense point cloud model, orthomosaic and digital elevation model (DEM). Orthomosaic offers a better 2-dimensional scaled view to estimate the horizontal distances in the model.

Additional depth perception offered by the color-coded elevation in DEM will help in a quick and rough estimation of the volumetric numbers, shown in Figure 5-3. The color-coded bar in the DEM of the collected data represents the highest elevation point on the debris pile by dark red and the lowest elevation point in the collected data by dark blue. This gives an estimate of the relative elevations of the surrounding areas i.e. the area where the debris stockpile was formed is sloping downwards as we move away from the pavement. Using the procedures discussed above, 3-dimensional dense point cloud model and the orthomosaic obtain the volume of the debris stockpile was obtained as 2,230 ft^3.

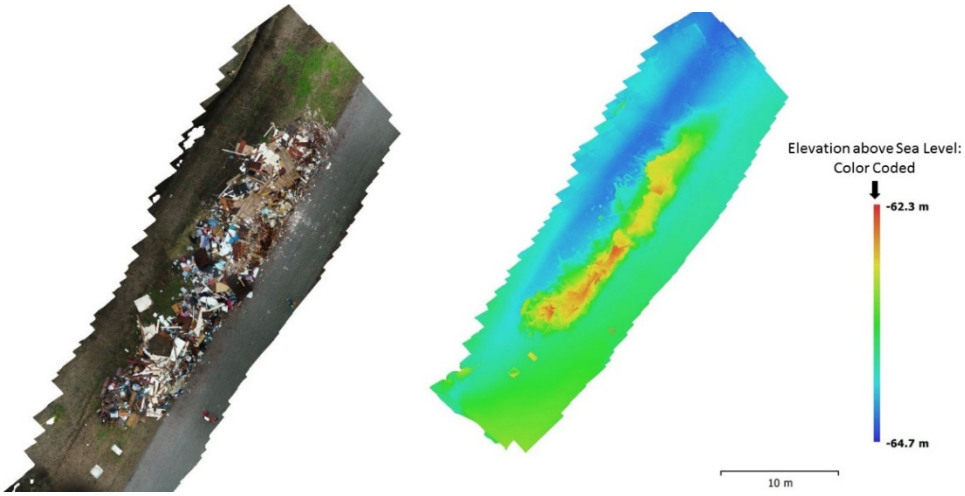

(a) (b)

Figure 5-3. Site 1 Data (a) Orthomosaic (b) Digital Elevation Model (DEM)

5.5.2 Debris Site 2

The second debris stockpile site was inspected near to the location 9902 N Major Drive, Beaumont, Texas. There is only one debris stockpile inspected at this location that composed of mostly the construction rubble and sodden wooden furniture. There was moderate traffic on the adjacent pavement. Even though there were no appreciable obstructions posed by the nearby trees, UAV was flown manually to interrupt immediately after spotting a vehicle and resume the data collection after the passing of vehicle.

All the images were collected and processed according to the procedures explained above to generate the 3-dimensional dense point cloud model, orthomosaic and digital elevation model (DEM), as shown in Figure 5-4. The color coded bar in the DEM of the collected data represents the highest elevation point

on the debris pile by red and the lowest elevation point in the collected data by dark blue. This gives an estimate of the relative elevations of the surrounding areas i.e. the area adjacent to the pavement over which the debris stockpile was formed appears to slope downwards away from the pavement. Using the 3-dimensional dense point cloud model and orthomosaic, the volume of the stockpile was obtained as 380 ft^3.

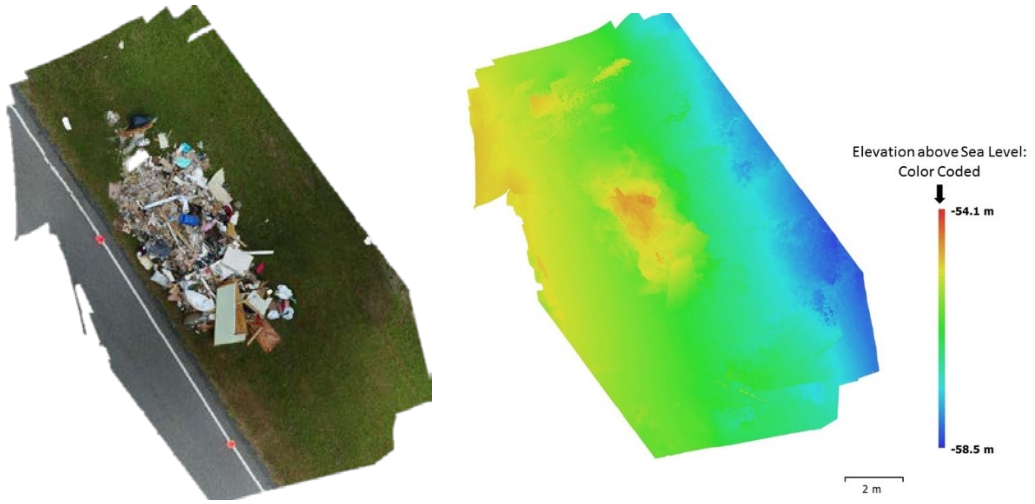

(a) (b)

Figure 5-4. Site 2 Data (a) Orthomosaic (b) Digital Elevation Model (DEM)

5.5.3 Debris Site 3

The third debris stockpile site was inspected near to the location 7695 San Anselmo St, Beaumont, Texas. There were three debris stockpiles piled on both sides of the pavement and these were predominantly composed of construction rubble and sodden wooden furniture. There was no traffic during the data collection on the San Anselmo Street, however, due to the debris location's proximity to the T

intersection with Willis Lane, an additional visual observer was employed for spotting the traffic from Willis Lane turning into San Anselmo Street.

The UAV was flown manually due to excessive obstructions posed by the trees. The flight path was planned in such a way that all three debris stockpiles were covered in single flight mission at that location. This gave an opportunity to even collect the data pertaining to the arterial pavement in and around the debris piles, as it gave an opportunity to assess the infrastructure condition after the natural disaster.

All the images were collected and processed according to the procedures explained above to generate the 3-dimensional dense point cloud model, orthomosaic and digital elevation model (DEM), as shown in Figure 5-5. The two stockpiles on the right side of the pavement in Figure 5-5a are marked as 3a, 3b, and the debris pile on the left side of the pavement is marked as 3c. The color-coded bar in the DEM of the collected data represents the highest elevation point on the debris pile by red and the lowest elevation point in the collected data by dark blue. This gives an estimate of the relative elevations of the surrounding areas i.e. the debris stockpile was formed over the area sloping downwards in the direction away from the adjacent pavement. Using the 3-dimensional dense point cloud model and orthomosaic, the volume of the three stockpiles are obtained and these are 676 ft^3, 104 ft^3, and 28 ft^3, respectively.

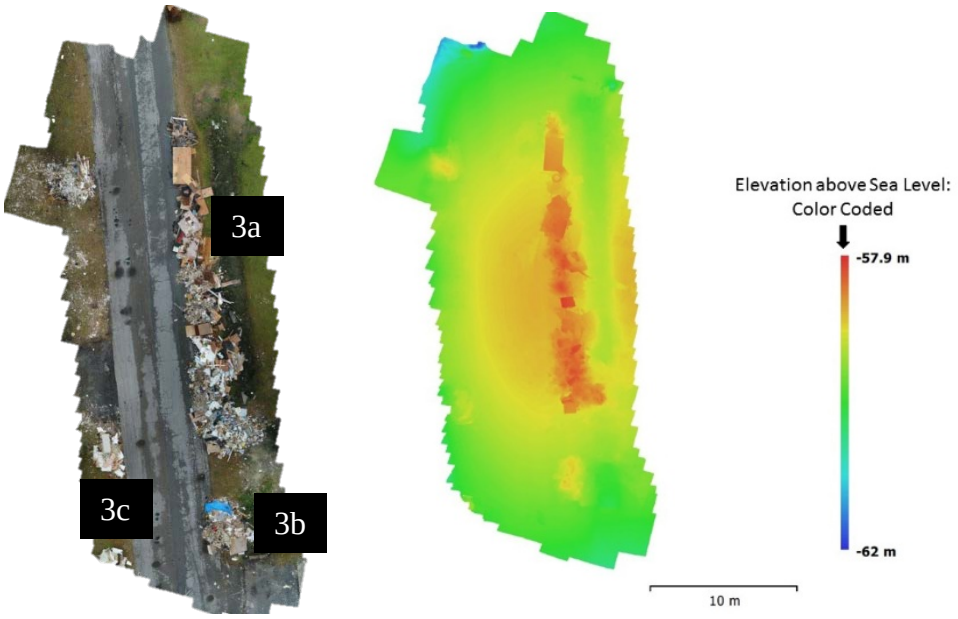

(a) (b)

Figure 5-5. Site 3 Data (a) Orthomosaic (b) Digital Elevation Model (DEM)

5.5.3.1 Pavement Infrastructure Condition

The Rutting or excessive permanent deformation is a common type of flexible pavement distress transpired due to deformation of either due to poor asphalt mix properties or the underlying base and subgrade layers or both (Puppala et al. 2003, 1999, 2011). Improper design standards, poor pavement construction practices, and higher vehicular traffic than designed are some of the factors contributing to the deformation of asphalt mix layer. Underlying pavement layers' deformation can be observed immediately after a rainy season, causing floods to inundate the whole pavement right of way. The stagnant water permeates into the underlying pavement layers and reduces the shear strength causing the deformation of underlying layers.

Excessive rut depths can also contribute to water stagnation that impedes the friction necessary for skid resistance. Pavement rut depth needs to be measured to ascertain the suitability of pavement conditions for road users. Traditional methods use a straightedge placed over two pavement contact areas across the rut and a gauge to measure to measure the rut depth as the distance between bottom surface of straightedge and the deformed pavement surface (ASTM E1703/E 2005). This is a tedious procedure as it requires frequent position change of the instrument and also requires more personnel to perform the traffic control operations and follow other safety protocols. UAV-CRP technology offers a quick way of assessing the rut depth with no or minimal traffic restrictions.

The research team used the UAVs to map the pavement infrastructure condition in Beaumont, Texas, immediately after Hurricane Harvey in 2017. This hurricane triggered floods, which inundated Houston and many other cities along the coastal region. One of the infrastructure sites that was inspected had pavement sides piled up with debris generated from the household items to walls from damaged residences, as shown in the top view of the Figure 5-6.

The 3D view presents the color-coded elevation of pavements and surroundings covered under the outer cyan colored rectangle in the top view, as indicated by yellow arrow in Figure 5-6. The red color in 3D view indicates the crest of the debris pile and the pavement is indicated by green and yellow colored area on the left side of the debris pile. Lowest point in the collected data indicating

the sloping ground on the other side of the pavement opposite to the debris pile location was indicated by dark blue color in the 3D view as shown in Figure 5-6. Color coded elevations can also be seen in the profile view of the pavement provided in Figure 5-6.

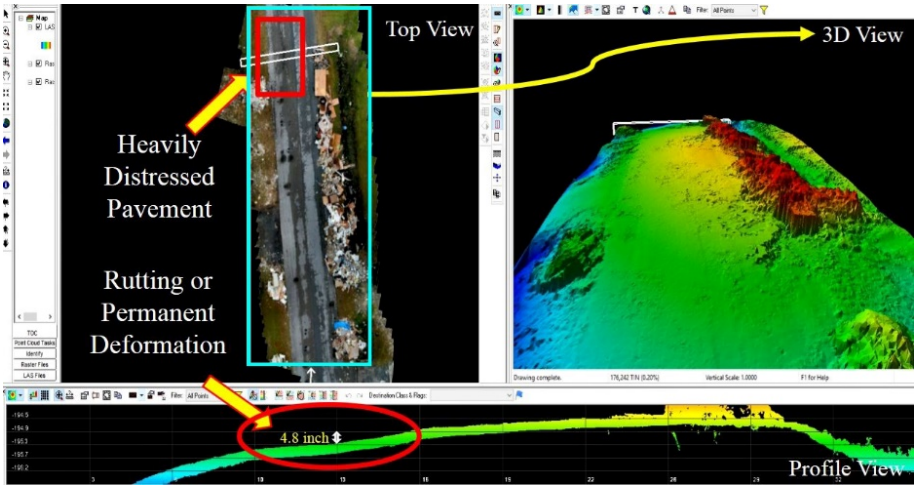

Figure 5-6. UAV-CRP Technology Data Identifying Rutting of Pavement Section Immediately after Hurricane Harvey

While collecting data, the research team physically identified permanent deformation conditions at the pavement locations marked within red colored rectangle in the top view and red colored ellipse in the profile view of the Figure 5-6. After processing the images and building models, they were analyzed for determining the extent of distress. The sectional view of the pavement at the small white rectangle shown in the top view was provided in the profile view of the Figure 5-6. The depth of the rutted portion from dense point cloud was estimated as 12.20 cm (4.80 in.), which matched with the depth measurements taken from field

surveys. The UAV-CRP technology provided a quick and accurate way of estimating the rutting depth in addition to providing other pavement related information.

During these studies, it was also realized that the aerial technology not only helps in estimating the debris but also assesses the condition of the adjacent pavements affected by inundation caused by hurricane triggered rainfall events. These aerial surveys are multi-purpose as they do not require separate traditional methods for estimating the condition of pavement infrastructure and debris volumes. Same photogrammetry data collected from UAV is analyzed for multiple attributes.

5.5.4 Debris Site 4

The fourth debris stockpile site was inspected near to the location 11080 Sherwood Dr, Beaumont, Texas. Only one stockpile composing of sheet rock waste, sodden couches and carpets in addition to the furniture was inspected at this location. This was located parallel to a railway line and does not have any tree obstructions. The debris was located around pavement and the adjacent areas, and hence extra precaution was taken by having visual observers due to the presence of moderate traffic activity while performing the UAV surveys and data collection operations.

All the images were collected and processed according to the procedures explained above to generate the 3-dimensional dense point cloud model, orthomosaic and digital elevation model (DEM), as shown in Figure 5-7. The color

coded bar in the DEM of the collected data represents the highest elevation point on the debris pile by red and the lowest elevation point in the collected data by dark blue color. This gives an idea of the relative elevations of the surrounding areas i.e. the debris was piled over an undulated pavement surface formed due to excessive cracking, indicated by light yellow color in the DEM. Using the 3-dimensional dense point cloud model and orthomosaic, the volume of the stockpile was obtained as 907 ft^3.

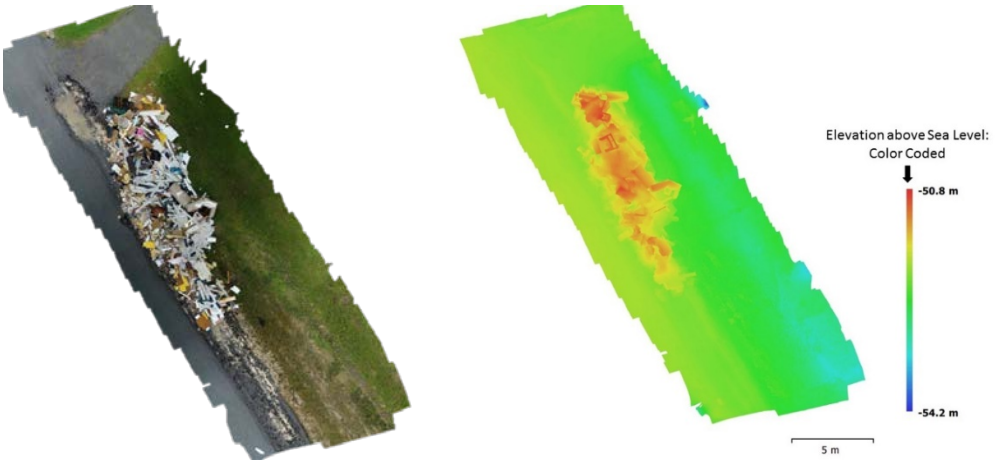

(a) (b)

Figure 5-7. Site 4 Data (a) Orthomosaic (b) Digital Elevation Model (DEM)

5.5.4.1 Pavement cracking

The aerial data of debris collected was also able to capture the pavement distress shown in Figure 5-8. This data was collected immediately after the hurricane and there was no prior data of the pavement condition was available with the research team. Hence, google maps were accessed to obtain the images of the exact same

location before the hurricane. Unfortunately, the last image of the same location was captured in January 2013. Nevertheless, they were studied for understanding the reasons for this excessive cracking failure of the pavement as shown in Figure 5-8. Although not many cracks were identified but a sealed crack and a developing crack, barely noticeable, were identified from those google images.

(a) (b)

Figure 5-8. Google Map Street Images of Sherwood Dr Looking towards Tram Rd, Beaumont, Texas Captured in January 2013 (a) Sealed Cracks (b) Developing Cracks (Map data © 2018 Google)

The aerial data was analyzed for estimating the present condition of distress as shown in Figure 5-10. A maximum depth of distress was calculated as 2.4 in. along the 80 ft length of distress identified quickly from aerial data shown in Figures 5-9 and 5-10.

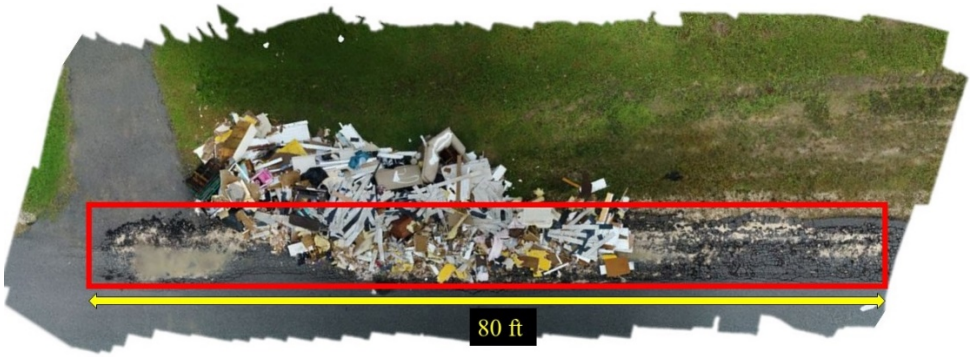

Figure 5-9. Pavement Distress Highlighted in the Orthomosaic of the Debris Site

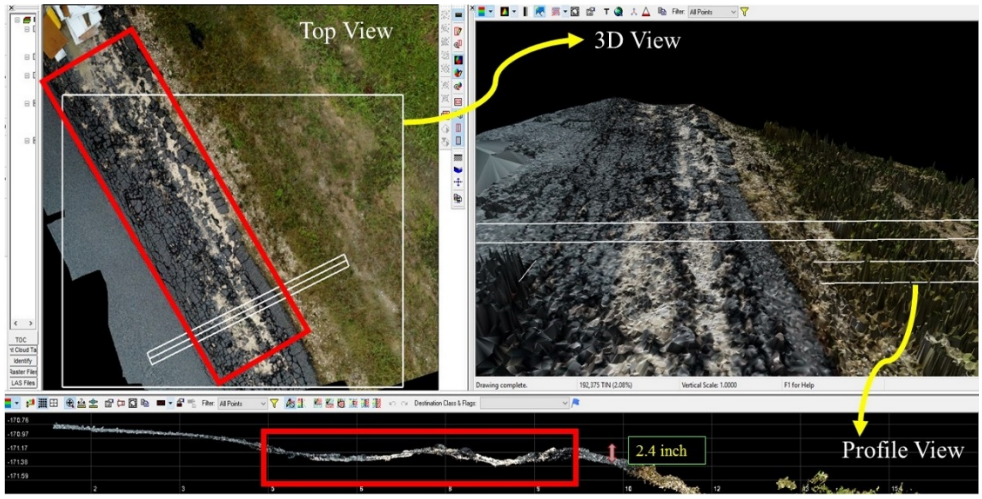

Figure 5-10. Different Views of the UAV-CRP Data Displaying the Extent of Distress

This author opines that this site has problems with underlying pavement layers as evidenced from the google images captured in 2013. Although it is observed to have some sealed cracks from the previous images as shown in Figure 5-8a, new cracks had also been observed to develop which can be seen in Figure 5-8b. The seepage of water through these fresh cracks, traffic volume, and other

factors affecting pavement stability might have triggered this failure. This research also acknowledges that the distress had occurred due to the absence of an affordable monitoring tool that could have provided scope for frequent proactive monitoring at low cost and helped in planning for preventive maintenance. UAV-CRP technology offers high quality data images of the pavement compared to google images and would help in monitoring the distress propagation over a period. This alerts the road agencies about the need for pavement maintenance before it deteriorates to such a condition that mandates rehabilitation of the whole pavement structure.

5.5.5 Debris Site 5

The fifth debris stockpile site was inspected near to the location 11130 Fairfield Dr, Beaumont, Texas. This site location had only one stockpile comprising of the waste generated from window panels, sodden mattresses, and broken wooden pieces. There was not much of vehicular traffic during the data collection but the tree density forced the research group to opt for manual flight. All the images were collected and processed according to the procedures explained above to generate the 3-dimensional dense point cloud model, orthomosaic and digital elevation model (DEM), as shown in Figure 5-11. The color-coded bar in the DEM of the collected data represents the highest elevation point on the debris pile by red and the lowest elevation point in the collected data by dark blue. This gives an estimate of the relative elevations of the surrounding areas i.e. the smaller width debris was

piled over a flat surface and there is a ditch, represented by blue color, adjacent to the stockpile and away from the pavement. Using the 3-dimensional dense point cloud model and orthomosaic, the volume of the stockpile was obtained as 847 ft^3.

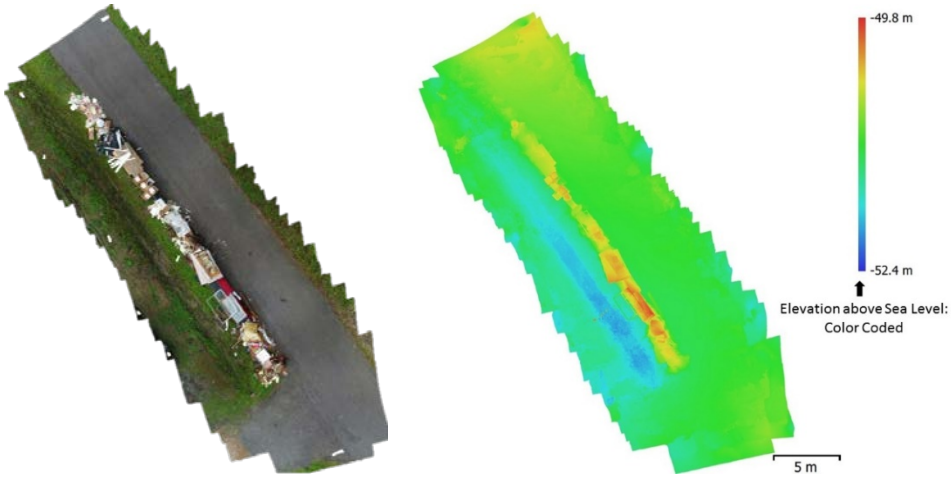

(a) (b)

Figure 5-11. Site 5 Data (a) Orthomosaic (b) Digital Elevation Model (DEM)

5.5.6 Debris Site 6

The sixth debris stockpile site was inspected near to the location 11195 Forest Glen, Beaumont, Texas. There are two debris stockpiles comprising of clothes, wooden furniture, refrigerators, and boxes at this site location. Manual flight was adopted to cover the both stockpiles due to the tree obstructions. There was not much traffic during the data collection. All the images were collected and processed according to the procedures explained above to generate the 3-dimensional dense point cloud model, orthomosaic and digital elevation model (DEM), as shown in Figure 5-12. The top and bottom stockpiles at this site location in Figure 5-12a are marked as 6a

and 6b, respectively. The color-coded bar in the DEM of the collected data represents the highest elevation point on the debris pile by red and the lowest elevation point in the collected data by blue. This gives an estimate of the relative elevations of the surrounding areas i.e. the debris stockpile 6a is having higher elevation compared to debris stockpile 6b which has larger base area. Using the 3-dimensional dense point cloud model and orthomosaic, the volume of the two stockpiles were obtained as 982 ft^3 and 1280 ft^3.

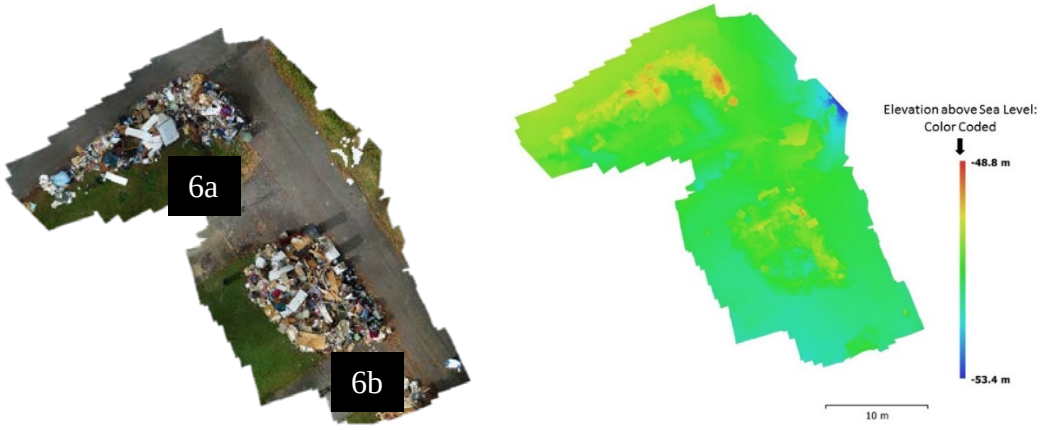

(a) (b)

Figure 5-12. Site 6 Data (a) Orthomosaic (b) Digital Elevation Model (DEM)

5.5.7 Debris Site 7

The seventh debris stockpile site was inspected near to the location 11135 Forest Glen, Beaumont, Texas. The only stockpile at this location composed of sheet rock waste, broken wooden panels, furniture, and stuffed up trash bags. There was not much traffic and the presence of tree obstructions made the research team to adopt manual flight mode. All the images were collected and processed according to the

procedures explained above to generate the 3-dimensional dense point cloud model, orthomosaic and digital elevation model (DEM), as shown in Figure 5-13. The color coded bar in the DEM of the collected data represents the highest elevation point on the debris pile by yellow and the lowest elevation point in the collected data by blue. This gives an estimate of the relative elevations of the surrounding areas i.e. the debris was piled over a surface sloping downwards away from the pavement. Using the 3-dimensional dense point cloud model and orthomosaic, the volume of the stockpile was obtained as 1,839 ft^3.

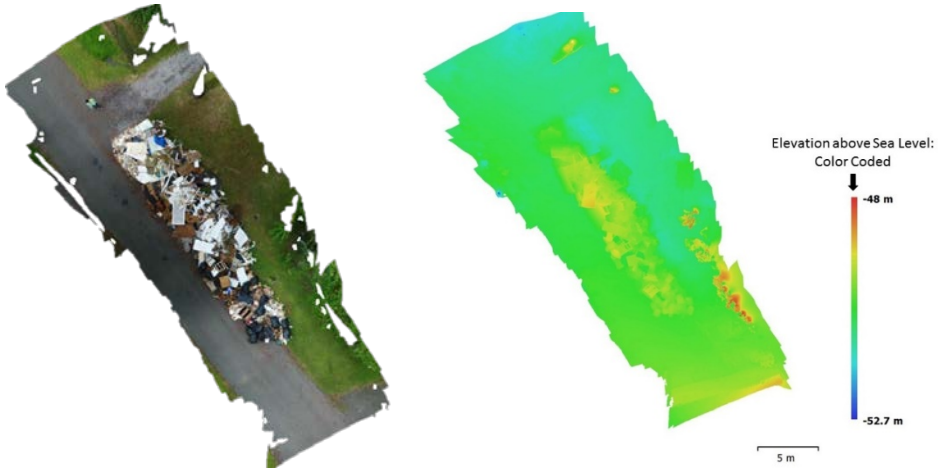

(a) (b)

Figure 5-13. Site 7 Data (a) Orthomosaic (b) Digital Elevation Model (DEM)

5.5.8 Debris Site 8

The eighth debris stockpile site was inspected near to the location 12700 Tan Oak Ln, Beaumont, Texas. The three stockpiles are located at the end of the Tan Oak Lane. They mostly comprised of sheet rock waste, broken wooden furniture and

other sodden household items owing to their proximity to the residential houses. During the data collection, there was no vehicular traffic on this street as the stockpiles were located the dead end of the street. All the images were collected and processed according to the procedures explained above to generate the 3-dimensional dense point cloud model, orthomosaic and digital elevation model (DEM), as shown in Figure 5-14. The three stockpiles in the Figure 5-14a are identified in clockwise direction as 8a, 8b, and 8c, respectively. The color-coded bar in the DEM of the collected data represents the highest elevation point on the on the adjacent house roof by red and the lowest elevation point in the collected data by blue. This gives an estimate of the relative elevations of the surrounding areas i.e. the debris stockpile were stacked in front of the houses. Using the 3-dimensional dense point cloud model and orthomosaic, the volume of the three stockpiles were obtained as 1,400 ft^3, 1,564 ft^3, and 687 ft^3, respectively.

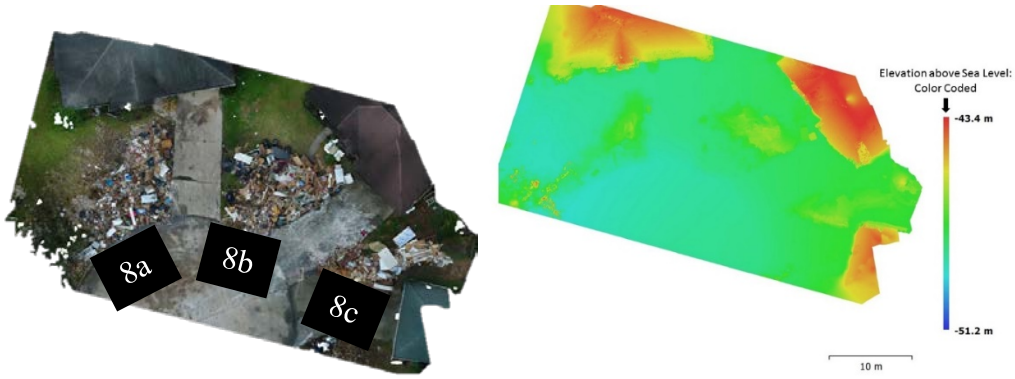

(a) (b)

Figure 5-14. Site 8 Data (a) Orthomosaic (b) Digital Elevation Model (DEM)

All the debris volumetric information including location, number of stockpiles and aerial images at each location, and volumes are tabulated in Table 5-1. At debris site-3, volumes of 3a, 3b, and 3c; site-6, volumes of 6a and 6b; and at site-8, volumes of 8a, 8b, and 8c are provided in an order in the fifth column of the Table 5-1.

Table 5-1. Volume of Stockpiles Estimated using UAV-CRP Data Collected at Each Debris Site

SNO.	Site Location & Comments	Coordinates	No. of Images	Volume (Cubic Feet)
1)	Debris Site – 1 (One Stockpile)	30.1819 , -94.2037	127	2,230
2)	Debris Site - 2 (One Stockpile)	30.1604 , -94.1991	79	380
3)	Debris Site - 3 (Three Stockpiles)	30.1491 , -94.1896	164	676 & 104 & 28
4)	Debris Site - 4 (One Stockpile)	30.1730 , -94.1748	116	907
5)	Debris Site - 5 (One Stockpile)	30.1732 , -94.1737	81	847
6)	Debris Site - 6 (Two Stockpiles)	30.1754 , -94.1721	131	982 & 1280
7)	Debris Site - 7 (One Stockpile)	30.1749 , -94.1716	81	1839
8)	Debris Site - 8 (Three Stockpiles)	30.1381 , -94.2486	220	1400 & 1564 & 687

5.6 SUMMARY

The frequency of natural disasters with higher intensity has risen up in the recent times and this warrants the use of new technology to inspect the debris generated quickly, efficiently, and safely. During these studies, it was also realized that the aerial technology not only helps in estimating the debris but also to assess the condition of the adjacent pavements affected by inundation caused by hurricane triggered rainfall. These aerial surveys are multi-purpose as they don't require separate traditional methods for estimating the condition of pavement infrastructure and debris volumes. Same photogrammetry data collected from UAV is analyzed for multiple attributes. UAV-CRP technology offers scope to collect more data with less boots on the ground, which is the case immediately after a disaster.

CHAPTER 6: COST ANALYSIS

6.1 INTRODUCTION

Due to the growing need of infrastructure agencies for acquiring quality data in less time, it would not be an exaggeration if UAVs are forecasted to be part of every agencies' inspection procedures in the near future. This is possible mainly due to the safety elements and cost effectiveness associated with this method when compared to traditional methods. According to Association for Unmanned Vehicle Systems International (AUVSI), this claim is also supported by the forecasted phenomenal investment of $5 billion in U.S. commercial drone sector by 2025 (Mccarthy 2015).

Cost analysis is a very important step of any emerging technology, as all the benefits provided will be nullified if the costs involved could not justify its use. This step is crucial in evaluating the feasibility of using UAV-CRP technology for the practical applications in infrastructure sector. The sections below provide a detailed information on costs involved with this innovative technology. Various companies related to civil engineering, surveying and mapping, UAV operations, and others were contacted to obtain various aerial inspections related cost information. The details are provided as below

A short questionnaire related to tasks that can be performed by the commercial unmanned aerial vehicle (UAV) vendors for transportation infrastructure was drafted and emailed to several UAV companies. The

questionnaire is provided in the Appendix-A. Responses and details are provided in the following section.

6.2 VARIOUS DETAILS ABOUT THE UAV DATA COLLECTION COMPANIES

Details about the companies that were surveyed about various details pertaining to infrastructure monitoring using UAV-CRP technology are provided here.

6.2.1 Background of Companies Surveyed

The research team focused on contacting vendors with backgrounds in transportation infrastructure and surveying practices. Because few companies responded, the observations noted in this section are limited, since they are solely based on information provided by the respondents. The lack or limited responses is attributed to the fact that only a few major companies are capable of providing a wide range of service.

Many are either expanding or acquiring skillsets in this dynamic fast-growing field. Responses were therefore hindered by the limited experiences of the vendors in the transportation infrastructure arena. This is to be expected, as the US DOT Federal Aviation Administration (FAA) exemption was not initiated until 2016. This exemption was issued as a “Final Rule setting forth standards for operation and certification of small-unmanned aircraft systems. Known as the RIN 2120– AJ60, the most notable exemptions were expressed as follows:

> "Small UAS operators may request waivers of operational rules applicable to small UAS, requirements such as the requirement to maintain visual line of sight and yield right of way to manned aircraft, as well as prohibitions on operations over people and in certain airspace" (From Federal Register, Vol. 81, No. 148 / Tuesday, August 2, 2016 / Notices,
>
> US DOT Office of the Secretary, [Docket No. DOT–OST–2016–0131].

Hence, more time is needed to find vendors that can provide infrastructure services based on the new freedoms and opportunities for UAV users that apply for and are granted the needed waivers.

Researchers noted that this observation is valid in many states around the U.S.A., as evidenced by the researcher's knowledge acquired from the UAV panel and works at the recent 2018 Transportation Research Board's (TRB's) annual conference in Washington, DC. It should be noted that many DOT agencies are focusing on research related to infrastructure applications while exploring the development of policies and guidelines.

The majority of companies that responded focused on pipelines and other linear infrastructure inspections. They provide traditional commercial surveying services that include setting up ground control points (GCPs) and a base station for real time kinematic (RTK) data. Most of the responding companies use both fixed-wing and multirotor UAVs to conduct inspections of larger areas with the former and localized inspections with the latter. Companies having varied sensors, ranging

from digital single-lens reflex (DSLR) cameras to mobile LiDAR sensors were selected and surveyed to study and understand their experience using these different sensors. All surveyed companies lacked experience in conducting UAV inspections with the ground sampling distance (GSD) required to detect pavement distress.

6.2.2 Equipment Used

Almost all of the companies used a Trimble unit for setting up GCPs and a base station for RTK data. The UAV companies that were contacted were mostly using visible-range camera-related photogrammetry, although a few companies were also exploring infrared range (IR) cameras and mobile LiDAR sensors. Normalized difference vegetation index (NDVI) cameras have been used extensively by companies performing precision agriculture-related inspections. Most of the companies that were contacted does not possess a top gimbal camera capable of conducting under-bridge inspections.

Most respondent companies possess both rotary wing and fixed wing UAVs. Companies involved in data collection of large areas use fixed wing UAVs due to their higher flight times and operating speeds. Companies dealing with smaller inspection areas, e.g., localized inspections use rotary wing UAVs.

Companies utilize visible range cameras and LiDAR sensors mounted on UAVs to provide 3D dense point cloud models, which can be exported as orthomosaics, DEMs, and DTMs. These models help analyze and detect the features of infrastructure or utility elements under inspection. Infrared (IR) cameras

provide thermal reflectance data of elements under inspection. Different sensors are used depending upon the client, site, and inspection-type requirements.

6.2.3 Survey Parameters

Though there are growing applications of UAVs, such as sensor-based UAV inspections, most of the UAV inspection companies in the past were working in only one or two niche areas and were not exploring other potential application areas mainly due to FAA regulations. Due to the US DOT FAA 2016 UAV exemptions (titled ‘Department of Transportation Federal Aviation Administration; DOT/FAA854 Requests for Waivers and Authorizations Under 14 CFR part 107,’’ commonly referred to as RIN 2120– AJ60), many companies have now started acquiring UAVs and sensors for performing different tasks, including infrastructure studies.

Companies have already been conducting large-scale UAV inspections, such as assisting in pipeline inspections, electrical line inspections, monitoring the crop health distributed over a large area, stockpile volumetric calculations, and other applications. However, most of the UAV companies lack the civil engineering expertise or background that is required to analyze the remotely collected data from an engineering perspective, while other companies do not have the appropriate equipment that is required to collect the precision data. All companies collect data by operating UAVs at higher flight altitudes that result in a larger ground sampling distance (GSD). However, companies also expressed an interest in acquiring

equipment necessary for conducting inspections with smaller ground sampling distances (GSDs) if there are potential opportunities to expand their UAV services.

All but one of the companies who responded to the questionnaire have conducted UAV inspections as a part of subcontracting works. Most of these companies have limited experience in inspecting pavement infrastructure. One company had experienced in conducting small-scale UAV operations for TxDOT before no-fly restrictions were imposed. Part of those operations included stockpile volumetric calculations, clay cap inspections, landfill monitoring, detention pond inspections, and drainage mapping. One UAV application that most of the companies were able to provide was the estimation of the stockpile volumetric of materials. However, none of them provided details of error percentages when compared to ground truth-values.

One of the applications conducted by most of the UAV companies contacted was the mapping of pipelines, closely related to roadway mapping. Most companies will need to acquire additional precision sensors to conduct meaningful pavement and other infrastructure inspections.

6.2.4 Parameters of Deliverables

The collected images from the camera/LiDAR are geotagged and stitched/registered to generate 3D dense point cloud models, orthomosaics, digital elevation models (DEMs), and digital terrain models (DTM). Most of the companies deliver output file formats that can be inputted into standard 3D

modeling analyses and 3D printing software. Some companies will overlay other information, such as thermal or vegetation index, over the primary orthomosaics developed from the visible range camera.

The above outputs need to be inputted into imaging analysis software in order to inspect the infrastructure element under scrutiny. Due to the lack of an established engineering viewpoint, most companies were not able to perform comprehensive analysis of models and provide only qualitative deliverables such as images and videos of infrastructure. For most company personnel responding to our questionnaire, imaging was no more important than any of the other tasks involving calculation of lengths, elevations, and volumetric estimations. The majority of these companies have not provided information on automated detection of infrastructure distress.

The present requirement of the clients is to have a resolution ranging from a couple of centimeters to a decimeter. This also reduces the size of the output files. Bigger files can be stored in the cloud, a service that many firms offer, charging a standard price per gigabyte (GB). Despite possessing the hardware to handle data larger than the current trend, a few companies claimed that they had not received a client request for better resolution models than the above-specified numbers.

6.2.5 Cost Details

Most of the companies have a range of prices for each deliverable, depending upon the magnitude of the area or object under inspection and the time required to

process the data with the required quality level. The rate of charge for data collection, deliverables, technician salaries, and other expenses seems to reduce with an increase in the scope and magnitude of work and the repetition of the work at the same location.

Some companies were not able to provide a cost estimate for the infrastructure-related UAV inspections due to limited or no experience in handling such projects. Nevertheless, the companies that provided rough cost estimates did so by providing a price-per-hour or price-per-day rates. Companies did not explicitly specify a direct increase in cost for higher detailed surveys, but instead provided a higher charge for the operations due to the increase in the number of flights. Due to the in-house capability of all companies to set up ground control points (GCPs), the estimated cost of setting up ground control points ranged from $200 to $1000 depending on the number of GCPs required for the specified accuracy. The cost of services for companies that charge cost-per-day rates ranged from $2000 to $5000 per day, while the cost of services for companies that charge based on the costs-per-hour ranged from $150 to $350 per hour.

Depending upon various operation attributes, such as inspection time, site complexity, and difficulty level of the inspection, FAA rates for hiring a certified UAV remote pilot in command (RPIC) generally range from $185 to $500 per hour. Rate for visual observer generally ranges from $85 to $300 per hour. The companies that seemed to be capable of complex operations based their cost

estimates on a cost-per-day schedule. In addition to the operating costs, a standard per diem charge, ranging from $150 to $250 per day, needs to be paid to the operators if the work period is more than 8 hours long. Most of the surveyed companies were not interested in conducting challenging tasks like under-bridge inspections.

6.2.6 Surveys Summary

The researcher had attended many conferences related to UAVs (AUVSI 2017, UAV EXPO 2017 & 2018) and transportation infrastructure (TRB 2018). Based on the current state of practice in transportation sector and the responses from the companies to the questionnaire provided in the Appendix-A, this research determined that the UAV state of practice is still relatively new for those involved in infrastructure evaluation projects. Thus, an in-depth infrastructure inspection is an early development stage compared to the more mature current state of practice among those who provide field surveys and stockpile volumetrics. Many of the surveyed companies are traditional inspection companies that have just recently started working with UAVs, while others are newer companies that primarily work with UAVs. All of the participating companies are familiar with general surveying methods, such as utilizing differential GPS equipment for setting GCPs and using base stations to collect RTK data for imparting more accuracy in these studies.

Majority of these companies seem to work on their present client requirements and hence planned to expand their application diversity. The present

application areas mostly focus on pipeline inspections, stock pile measurements, cut and fill measurements, mining surveys, slope stability, elevations and drainage mapping, detention pond measurements, electric grid inspections, solar panel area surveys, vegetation inspections, and others. The future application areas they intend to work on include pavements, railways, and bridge decks. However, none of these companies showed any interest in conducting inspections of hard-to-reach areas, like under-bridge inspections.

The identified companies, who preferred fixed-wing UAVs due to their greater flight time and operating speeds, were more focused on capturing data over very large areas. Many of their application areas, such as pipeline inspections, involve long linear surveys up to several miles each. Due to the time required, many of the companies often opted for fixed-wing UAVs to collect the features of linear objects, such as pavements, rail lines, and bridge decks. Based on the research experience, the author acknowledges that a multirotor is more useful in conducting localized inspections, such as under-bridge inspections, in addition to collecting substantial ground area data per flight while operating under the line of sight of the remote pilot in command (RPIC).

Some respondent companies used ground sampling distance (GSD) in their work, but found that a couple of centimeters to decimeters of GSD is not conducive to conducting in-depth infrastructure inspections. In order to meet the Transportation agencies' requirements of collecting infrastructure data, UAV

companies will need to operate at lower altitudes and use higher quality UAVs with more advanced camera accessories to get high-resolution images. A small number of companies have advertised that they can achieve the GSD required to identify cracks on infrastructure.

6.3 RETURN ON INVESTMENT OF UAV-CRP TECHNOLOGY

Various topics related to the return on investment (ROI) for using UAV-CRP technology for infrastructure monitoring. ROI analysis provides details about the benefits of using this innovative technology. The ROI analysis presented here is based on similar framework used by Texas Department of Transportation. Benefit areas identified in this research are of two types: qualitative and economic. The qualitative benefits are non-monetary as it is realized that the high level of UAV-CRP applications with its continual advancements in knowledge and management. The research based on economic benefits lies in the money saved as the new technology gets the job done more quickly, more accurately, and at less cost. The present research defines UAV-CRP based on its features and functions, which yield benefits in nine different areas illustrated in Figure 6-1.

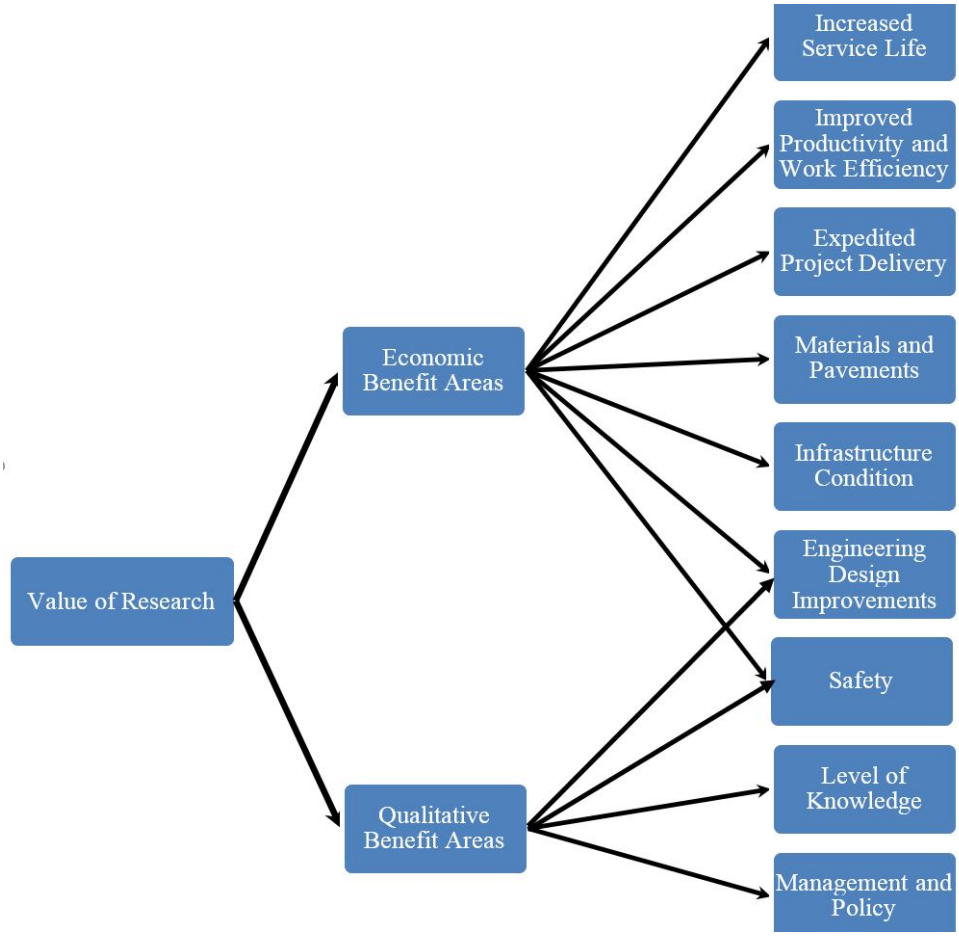

Figure 6-1. Major Focus Areas

6.3.1 Benefit Areas

Five areas have exclusive quantitative benefits, two areas have qualitative benefits, and two others have both quantitative and qualitative benefits. The following sections describe each of these benefit areas in detail:

6.3.1.1 Increased Service Life

Different types of distress in pavements including longitudinal and transverse cracking, rutting or permanent deformation, alligator cracking, and other distress

data need to be collected to assess the pavement condition. Pavement characteristics like longitudinal slope, transverse slope, and sight distances at crossings also need to be collected to monitor the changes in the pavement design parameters. The quality of collected data measuring distress and pavement characteristics plays a key role, since repairs are performed based upon pavement health condition. Traditional methods of assessment are subjective, time consuming, and can delay decision making on rehabilitation strategies.

The unmanned aerial vehicle system-close range photogrammetry (UAV-CRP) used in this research, has the potential to collect similar pavement distress data in a relatively shorter period and in a safer manner. The data obtained from UAV-CRP operations were used to quickly perform analysis and identify pavement sections that require immediate repairs. Pavement characteristics like longitudinal slope, transverse slope, and sight distances at crossings were also calculated to monitor changes or deviations from the initial design values. Due to the proactive monitoring leading to preventive maintenance, the annual pavement maintenance cost can be reduced and the service life of the structure is extended when using UAV-CRP instead of traditional methods.

6.3.1.2 Improved Productivity and Work Efficiency

This project successfully demonstrated that the UAV-CRP technology could be used to survey large areas with fewer personnel in a short amount of time, leading to improved work productivity. The large amounts of quality data obtained from

one set of UAV-CRP operations can be analyzed for multiple infrastructure parameters, which would otherwise have required multiple traditional surveys. Thereby, adopting timely UAV-CRP surveys will improve the efficiency of infrastructure inspections.

6.3.1.3 Expedited Project Delivery

Collection of inspection data in the field using UAV-CRP technology requires a minimal amount of time. UAV-CRP collection procedures replace multiple traditional surveys with fewer flights that collect multiple parameters, which will reduce delays in project time. The data can be processed and analyzed quickly, reducing the turn-around time and leading to expedited project planning and delivery. Continuous monitoring of construction procedures using UAV-CRP technology helps in executing construction steps according to design plan and delivers the project in time. This will prevent any penalty costs incurred due to delays in construction.

6.3.1.4 Materials and Pavements

Assessing the performance of materials and pavements in field conditions is an important application area for UAV-CRP technology. Researchers often study novel materials that can be used either in bases/sub-bases or pavement surface materials to produce resilient pavements and rail track systems with the potential to experience less distress. Examples of materials used in pavements include modified asphalt concrete, cement concrete materials, as well as novel chemically

treated sub-soils to stabilized aggregate bases. Performance of these materials in mitigating pavement distress is often the focus of new research. The UAV-CRP studies will provide an excellent opportunity to evaluate these potentially transformative materials by providing high quality field monitoring data, which can lead to widespread incorporation of materials that will enhance pavement performance in field conditions.

The UT Arlington research team monitored vertical settlements underneath an approach slab supported by a hybrid geo-foam embankment section at a bridge site (Shafikhani et al. 2017). Deformations were monitored from field instrumentation technologies facilitated by both horizontal inclinometers and LiDAR surveys (Shafikhani et al. 2017). These traditional methods are stationary and thus take more time to collect whole data. The use of UAV-CRP technology for deformation monitoring enables the rapid collection of reliable deformation data. Such data collected repetitively over time can provide an assessment of the geofoam system's efficiency in reducing the vertical settlement of approach slab pavements. Hence, the use of UAV-CRPs for the research evaluation of various types of innovative materials in field test sections would help DOT agencies to implement successful materials and pavements into practice. This alone could potentially save millions of dollars in annual maintenance costs and hence lead to a stronger and more resilient pavement infrastructure.

UAV-CRP methodology was also successfully used to determine the volume of pavement material stockpiles, with good matching of ground truth measurements obtained with traditional methods. This helps in planning the pavement construction and reduces wastage of stock material. During asphalt pavement construction, UAVs equipped with thermal cameras can also be used to monitor the temperature of asphalt laid and plan the compaction procedure. This helps prevent the micro cracking formed during compaction of cold asphalt mix and hence increases the pavement durability.

6.3.1.5 Infrastructure Condition

The health of various transportation infrastructure, including but not limited to highways, bridges, and railway corridors, could be monitored efficiently and quickly by using UAV-CRP technology. The safely obtained data and accurate assessments provided could contribute to the extensive use of this technology to complement traditional monitoring methods for infrastructure health condition monitoring in the near future.

6.3.1.6 Engineering Design Improvements

This research demonstrated that UAV-CRP technology could be used to collect the characteristics of transportation infrastructure like longitudinal slope, transverse slope, and sight distances, and compare them to minimum design standard. The results of these studies and comparisons of UAV-CRP methods with traditional methods can improve the safety and comfort to those who drive the roads under

consideration. This type of quick data collection procedure helps identify the need for any design improvements. Future advancements in sensor hardware technologies can provide data that will be beneficial to assessing engineering designs.

6.3.1.7 Safety

The major advantage of UAV-CRP technology is that it can lead to safer operations in the field. Compared to traditional surveys, UAV-CRP technology requires minimal traffic control for performing field operations. Unlike traditional surveys where the crew or the inspecting vehicles have to operate on the pavement, UAV-CRP technology results in less interference with traffic as the pilot and the flying drone are operated at a safe distance away from the pavement or near bridge infrastructure. This will help in avoiding work-related accidents and related costs while providing safety for road users. The safety offered by UAVs in accessing hard-to-reach areas, such as underneath bridges for under the bridge inspection stands out as one of the most important benefits of this new technology.

6.3.1.8 Management and Policy

This research generated a questionnaire, which was used in this work to obtain the responses of different UAV operators who use drones as part of their inspection and survey business. We focused on those who used their UAVs to inspect transportation infrastructure, but as noted in earlier chapters, the field is so new due to past restrictions that were not lifted until 2016, finding a large number of

respondents was impossible. All the UAV operator responses (who were referred to as vendors and sometimes surveyors) and the practical experience gained while collecting UAV field data contributed to formulating policies for different UAV operations involving transportation agency's infrastructure assets.

Current traditional methods used to collect data pertaining to pavement inspections, railway corridor inspections, and rock cut volumetrics are time consuming and can delay the decision-making process. Data collected through UAV-CRP technologies can be processed quickly and represented in a user-friendly manner, assisting both project managers and policy makers in developing sound planning, decision-making, and efficient operations management.

6.3.1.9 Level of Knowledge

This research was initiated in response to the sparse amount of academic knowledge available in the literature on UAV-CRP usage in assessing transportation infrastructure. As this research study progressed, the researchers were able to learn and compile more theoretical and practical knowledge pertaining to the UAV topics under study. The analysis of the data collected by the UAV-CRP technology also offers a new dimension to the understanding. This knowledge is being disseminated on various national and international platforms to increase the level of knowledge of engineers, practitioners, the public, and decision makers. This report on UAVs is one such attempt to expand the present literature on UAV research related to infrastructure studies.

Developing UAV operations-related procedures, guidelines, and initial applications for surveying pavements and railway corridor operations will propel agency personnel, including surveyors, engineers, and technicians towards the usage of UAVs for the various tasks outlined in this research. The high-quality and reliable data collected will be analyzed and used by the agencies in making sound and rational decisions related to infrastructure assessment, distress management, asset management, and resource allocation strategies.

6.3.2 Intangible Assets

Several intangible benefits are also identified from the UAV-CRP operations as provided below:

1. Patents, copyrights, and licenses
2. Non-compete agreements
3. Favorable financing
4. Trained and assembled workforces
5. Contracts
6. Leasehold interests
7. Unpatented proprietary technology
8. Trademarks/Trade names

UTA research and expansion of knowledge regarding UAV applications will lead to workshops and training sessions that will benefit DOTs and other infrastructure agencies in conducting infrastructure monitoring and asset

management studies. Some of the above benefit topics either will directly or indirectly connect to this wider dissemination of this knowledge.

6.4 COST ESTIMATES

This section deals with the cost analyses of various technologies basing on the data collected from different vendors and the compilation of the costs and time periods for conducting UAV inspection tasks during this research.

The cost analysis presented here focuses on four of the major application areas, further subdivided into seven subtasks that are presented in the sections below. Both qualitative and economic analyses are conducted in the following four major application areas of UAV-CRP technology: inspection of different types of highway pavement, bridge site investigations, stockpile volumetric studies, and railway corridor studies. Certain assumptions were made with respect to potential benefits in each of these areas. During the execution of the research tasks, more details on the true benefits, along with quantitative and qualitative information, were collected. This section has been updated based on the wealth of experience gained by the research team throughout the research and prepared to contribute to a new understanding of the return on investment associated with using UAV-CRP technology compared to traditional methods.

6.4.1 Pavement Inspection

Currently, visual surveys and profiler studies, as well as other non-destructive studies, are conducted by various DOTs to assess pavement conditions, which in

turn can be used for formulating pavement rehabilitation strategies. Pavement condition includes the distress data as well as the geometric design characteristics like longitudinal slope, transverse slope, and sight distances at crossings.

Based on email communications with the TxDOT Maintenance Division, the annual cost of visual inspections is estimated to be approximately $2.5M per 90,000 miles of roadbed in Texas. Visual surveys are relatively cheaper when compared to UAV applications; however, they are also operator sensitive, meaning that the final assessments may vary from person to person and from location to location. After the visual inspections, critically rated sections will be inspected for various pavement characteristics.

The limitations of the visual surveys warrant a rational methodology for a uniform assessment of pavement characteristics across the state. TxDOT uses semi-expensive to expensive methods, such as ground penetrating radar (GPR), LiDAR surveys, and other laser-based surveys for collecting pavement distress information including cracking, rutting or permanent deformation, and other pavement characteristics that can be visualized or scanned.

In the present dissertation work, the possibility of obtaining high quality photogrammetry details of the pavement condition using UAV-CRP methodology was explored. It should be noted that the focus of this research included high-speed roads consisting of both urban and rural interstate highways, freeways, and expressways. Considerable cost savings in expenditures using UAV survey

methods were observed, as these procedures provided quick data with less traffic regulations.

Based on the available surveying vendor information, traditional surveying of the pavements for acquiring all characteristics was estimated as $3 per linear foot, which translates to approximately $3,000 for a 1,000-ft long pavement section. This traditional survey was assumed to provide both the extent of pavement distress, and pavement characteristics such as longitudinal and lateral slope analysis. Assuming that this operation takes 1.5 hours, the cost of expenditures for a registered professional land surveyor (RPLS) and technician for this in-the-field survey is about $165/hour and $70/hour, respectively.

Assuming two flagged staff will be required for traffic control, the payments for the two-flagged staff members for the whole job would be close to $150. The total expenditure of traditional methods involving the survey cost and personnel wages would be $3,503 (the sum of $3,000, $353 and $150). In addition, there will also be an additional traffic delay cost that arises while regulating the freight and passenger traffic, which is not considered in this study to be on the conservative side.

A highway pavement nearly 1000 ft long can be inspected using UAV-CRP technology for data collection in a 30 min period, involving multi altitude flights and no major traffic control operations. Videos of the pavement site in 4K format can be collected in another 10 minutes. UAV capital recovery and operation costs,

GCP setup costs, as well as mobilization costs would average $800 per pavement site.

The approximate costs for flight operations, including expenses of a three-member team comprised of one pilot, and two visual observers, would be around $400 and post processing of data including visualization analysis and final deliverables, which include a report along with videos, would be $1,500. Hence, the total approximate cost would be close to $2,700 per pavement site survey. However, this cost varies depending upon the travel distance to the pavement site, additional per diem costs, number of pavement lanes, complexity of the site (might warrant extra visual observers), type of deliverables, inclement weather conditions, and other factors.

Even though the cost of traditional surveys conducted to measure cross slope, longitudinal slope, sight distance, and extent of distress is assumed to be on the lower side, considerable savings will be generated from the ability of UAV-CRP technology to collect pavement distress identification information, which includes the three basic pavement types; asphalt concrete-surfaced; jointed (plain and reinforced) Portland cement concrete; and continuously reinforced concrete.as found in the FHWA Distress Identification Manual for the Long-Term Pavement Performance Program (Miller and Bellinger 2014). Thus, the UAV-CRP technology can capture all of the pavement distress and characteristics in a single

flight as compared to the need of multiple traditional surveys needed to collect the same data.

Using UAV-CRP technology over traditional methods would, therefore, result in the quantitative benefit of a 23% cost savings. A major quantitative benefit of UAV-CRP technology is the reduction of traffic delays from traffic controls during traditional field surveys thereby avoiding the loss of productive time for the road users.

By extrapolating the potential 1000-ft cost savings for the high-speed urban and rural interstate highway roads in the state of Texas using UAV-CRP technology, anticipated cost savings for the 16,319 urban and rural interstate lane miles (miles reported in (FHWA 2014)), to be $69.2M. This number will even be higher if all the 675,580 total lane miles of state highways, FM roads and other roads in Texas are included for pavement inspection studies using UAV-CRP technology. Again, a conservative reduction factor of 4 to account for variance due to pavement types that will be surveyed and adaptation by districts is assumed. This implies that a cost savings of $17.3M would be realized with UAV-CRP based pavement ratings studies. Again, these expenses are for the evaluation of the entire pavement system in the state of Texas and may be spread throughout several years.

Major indirect benefits of using UAV-CRP technology over traditional methods are minimized fuel consumption costs and reduced high emissions due to idling of the traditional survey-dedicated vehicles during traffic control. We also

anticipate other indirect benefits with UAV-CRP studies, as described below. Safety of the traffic users can be ensured by eliminating possible rear-end accidents during traffic control situations, which can occur due to sudden reduction in vehicle speeds while conducting traditional visual surveys for pavement forensics.

Continuous monitoring of new pavement construction sites with UAV-CRP technology will provide existing pavement characteristics that can be checked with minimum design standards. This approach gives scope for performing timely maintenance if the design characteristics are found to be deteriorated. The palpable data obtained from the analysis of UAV-CRP data increases the level of knowledge of engineers, practitioners and leaders thereby making the decision-making process easier. The derived data and prompt analysis will lead to more robust field operations at a node (or a given site), or at the network level (district level). All benefits will lead to more realistic assessments of pavement distress conditions and appropriate pavement management strategies.

6.4.2 Bridge Inspection

According to the TxDOT's "Report on Texas Bridges As of 2016" prepared by the Bridge Division of TxDOT, there were 53,875 bridges in Texas (TxDOT Bridge Division 2016) at that time. These bridges must be inspected regularly once in two years to assess their condition. Bridges were classified as good or better (GB) structure, structurally deficient (SD) structure, functionally obsolete (FO) structure, sub-standard for load only (SSLO) structure, load-posted bridge, and land-locking

bridge depending upon the condition. 80 % of the inspected bridges were classified as good or better (GB) structures. Bridge inspection includes monitoring of approach slabs from superstructure elements to substructure elements. The sections below constitute a brief overview of the cost analysis conducted for various tasks involved in bridge inspections.

A 360° bridge inspection was conducted using UAVs with different configurations involving cameras mounted on the top and bottom gimbals for under-bridge and bridge superstructure data collection, respectively. Monitoring the bridge approach slab deformation is also important as the road user's perception of comfort is based upon their experience while traveling on the roads.

Based on the vendor information received from traditional inspection operators, the traditional survey analysis cost for all the features of the bridge deck profile is assumed to be $3 per linear foot; thus, the cost would be $2,700 for a 900-ft long bridge. This traditional survey is assumed to provide both the extent of bridge deck pavement distress, and other characteristics. Depending upon the vendor information, the rate of pay for the bridge inspector and technicians required for the job is assumed as $100 per hour and $50 per hour, respectively. The traditional method of under-bridge inspection involves a snooper truck rented at $1,800 per bridge to collect the substructure condition.

Assuming that the inspection of the superstructure and the substructure requires an average of two 8-hour working days per bridge, the total pay for three

technicians may be calculated as $2,400 for the whole period of inspection. In addition, per diem lodging and food costs close to $150 should be included as well. The total expenditure for conducting traditional methods of bridge monitoring would be approximately $9,400 per bridge (from cost breakdown in this paragraph: $2,700 ($3 per linear foot), + $1,600 (two 8-work day wages for bridge inspector), + $1,800 (truck rental), + $2,400 (two 8-work day wages for three technicians), and $900 (per diem for three technicians)). The expenditure increases further due to transportation costs if the truck is rented from some other location in the United States.

Using UAV-CRP technology, conditions of the bridge deck and the approach slabs of nearly 900 ft long were collected in 30 min data collection procedures involving multi altitude flights. High-definition 4K-quality videos of the bridge sides were collected in another 30 min. Underneath the bridge, all five spans can be inspected in 90 minutes with the bridge inspector viewing the live feed on a digital live video display unit (DLVP) monitor. The UAV capital recovery and operation costs, ground control points (GCP) setup costs, as well as mobilization costs would be approximately $1,000 per bridge site. The approximate costs for flight operations, including a three-member team comprised of one pilot, and two visual observers, would be around $1000 and post processing of the imaging data including visualization analysis and final deliverables including a report and videos would be $2,000. Hence, the total approximate cost for performing a UAV-CRP

inspection would be close to $4,000 per bridge. However, this cost varies depending upon the travel distance to the site, additional per diem costs, number of bridge spans, complexity of the site (might warrant extra visual observers), type of deliverables, inclement weather conditions, and other factors. Using UAV-CRP technology over traditional methods would result in a quantitative benefit of 58% in cost savings.

Other quantitative benefits of UAV-CRP technology can be realized from avoiding traffic delays as it does not warrant any traffic restrictions on the overpasses, a requirement while conducting the under-bridge inspection using a snooper truck under traditional methods.

A major indirect benefit that can be observed is the safety provided by the UAV-CRP technology while conducting the under-bridge inspection. Another indirect benefit of UAV-CRP technology is the potential reduction in accidents associated with bump problems. UAV-CRP technology assists through early detection of deterioration resulting in proactive repairs of bridge bump issues, thereby providing a safer ride for road users and probable savings in future maintenance costs.

It should be noted that these reports provide more comprehensive bridge rating data than approach slab settlement alone, and this information could be input into other bridge rating surveys. Live video relayed on the monitor during the inspection and the videos post inspection will increase the knowledge of the

inspector pertaining to the bridge infrastructure. UAV-CRP analysis data includes bridge distress such as spalling, cracks, rusting, bridge approach settlement or permanent deformation data, and other pavement features.

By using UAV-CRP methods over traditional methods, the approximate cost savings of performing annual bridge surveys of 9,698 bridges would be $52.4M, based on 2016 TxDOT Bridge report (TxDOT Bridge Division 2016) stating that 18% of Texas bridges were not rated under the good or better category and are considered to be prime candidates for bridge surveys using UAV-CRP technology. This number represents a high approximate value and assumes all bridge surveys are done with UAV-CRP technologies.

A conservative reduction factor of 4 is assumed to account for the variability of bridge types; hence, an approximate cost savings of $13.1M is obtained as an estimate of bridge infrastructure ratings. The research team believes that the UAV-CRP technology will provide direct and quick assessments of annual bridge ratings as demonstrated in the present research. Further research and future validation studies are needed to further assess true savings of this technology.

6.4.3 Railway Corridor Inspection

Railway corridor inspection includes the cost analysis for data collection of railroad crossings, track failures, rail bridge, rock cut volumetrics and encroachment detection. Typically, the rail corridor inspection survey is performed with ground crew for site-specific areas. The inspection crew use mobile LiDAR via hi-rail

vehicles to survey a railway line to detect washouts, rail buckling, and other track asset conditions. As per the Federal Railroad Administration (FRA) track inspection guidelines, the allowable railway track speeds may have to be reduced to account for track inspections.

Many accidents occur at grade railroad crossings across the United States. Poor sight distance is one of the primary causes; hence, frequent mapping and monitoring of grade railroad crossings eliminates the costly alternative of providing grade-separated railroad crossings. Rail bridge inspections need to be conducted regularly to prepare condition-rating reports. The maintenance and functionality of rail infrastructure passing through a rock cut depends upon the stability of rock slopes and the detection of rock fall debris on rail tracks. The rail tracks can be inspected for failures using sensors mounted on the hi-rail vehicles.

Currently, obstructions within sight triangles at railroad crossing and volumetric calculations of debris at rock cuts can only be estimated from multiple traditional surveying tasks. Appropriate use of UAV-CRP technology for the inspection of various rail corridor sites have been successfully demonstrated in this research.

6.4.3.1 Railroad Crossings

At railroad crossings, the presence of obstructions can result in many problems such as accidents. Traditional methods utilize total station and other survey equipment used for obstruction identification, which can consume more time while exposing

surveyors to perilous conditions. Frequent disruptions to highway and rail traffic also contribute to traffic delays and emission costs. The tedious and operator-sensitive nature of conventional methodologies justify the search for a new methodology that offers detailed mapping information while providing considerable savings in man hours and surveying costs. This project demonstrated a practical solution by using UAV-CRP methodology that collects high-quality image data using principles of photogrammetry and within a shorter time than the conventional techniques.

As per Federal Railroad Administration (FRA) 2009 statistics, there are 9,817 railroad grade crossings in the state of Texas and many of them interact with TxDOT pavement infrastructure (TxDOT 2011). The following assumptions were made in calculating annual expenditures of mapping the at-grade railroad crossings using traditional surveys. Based on the surveying vendor information, the traditional way of surveying the pavement and the rail sections is assumed to be $3 per linear feet and it amounts to $2,400 for a railroad crossing area with 400 ft of pavement and 400 ft of railway track. This traditional survey is assumed to provide both pavement and rail characteristics. The flag staff would be required to collect the data for 4 hours at a total cost of $400. The total cost for mapping at grade railroad crossings is calculated as the sum of the surveying expenditure, including flagged staff wages, and cost of expenditure for Registered Professional Land Surveyors (RPLS) and technicians for this job, which is about $165/hour and

$70/hour, respectively. Thus, the total cost would be close to $3,740 (sum of $2,800 and $940).

At railroad crossings, the UAV-CRP technology collects the distress data, the obstructions in sight triangle data, and encroachment identification data in the same flight operation. At grades, railroad crossing data was collected in 30 minutes. The sum of the UAV capital recovery and operation costs, GCP setup costs, as well as mobilization costs would be approximately $800 per at-grade railroad crossing site. The approximate costs for flight operations including a two-member team comprised of one pilot, and one visual observer would be around $300 and post processing of data including visualization analysis and final deliverables including a report and videos would be $2,000. Hence, the total approximate cost using UAV-CRP technology would be close to $3,100 per at-grade railroad crossing visit. However, this cost varies depending upon the travel distance to the site, additional per diem costs, number of pavement lanes and rail lines, complexity of the site (might warrant extra visual observers), type of deliverables, inclement weather conditions, and other factors. These rates will be considerably reduced when a more substantial area requires inspection.

Using UAV-CRP technology over traditional methods results in the quantitative benefit of 17% in cost savings. A major quantitative benefit of using UAV-CRP technology at grade railroad crossings is the ability to collect more data in fewer flights compared to the traditional methods. If UAV-CRP technology is

adopted for inspecting the 9,817 at-grade railroad crossings in the state of Texas, it can result in savings of $6.3M. A reduction factor of 4 is used since transportation agency may inspect only a fraction of these crossings with this UAV-CRP technology. Hence, this would result in approximately $1.6M in cost savings for monitoring Texas railroad crossings to plan for enhancing the safety around these crossings.

Using UAV-CRP technology to map at-grade railroad crossings will assist transportation agency personnel in making rational decisions related to providing appropriate grade-separated railroad crossings. Including the traffic counts, in conjunction with accurate mapping of the crossings, UAV-CRP technology can also assist in planning possible expansions/diversions of the highway sections in the future.

6.4.3.2 Rail Track Inspection

The annual expenditure for railway corridor inspections using traditional methods is calculated using data provided by TxDOT Rail Division staff and certain assumptions made are explained in the following section. In 2012, there were approximately 10,469 rail miles in the State of Texas (TxDOT Rail Division, 2016). Based on the surveying vendor information, the traditional way of surveying railway tracks is assumed to cost $3 per linear foot and amounts to $3,000 per 1000 ft of railway track. The total cost invested into mapping a rail track using traditional methods is calculated as the sum of the surveying expenditures, and the product of

the number of workers (assumed to be three) and their time required for mapping rail track (assumed to be 1 hour), with an hourly rate assumed to be $50/hour for personnel. The total cost of field surveys would be close to $3,150 (sum of $3,000 and $150).

UAV-CRP technology is anticipated to gather all the information required for a railway corridor inspection remotely without disrupting trains or delaying their travel time. UAV-CRP technology collects the rail track distress data, debris data, and tie condition data all in the same flight operation. The rail track data of 1000 ft was collected using UAV-CRP technology in 20 minutes. UAV capital recovery and operation costs, GCP setup costs, as well as mobilization costs would be approximately $800 per railway track site. The approximate costs for flight operations, including a three-member team comprised of one pilot, and two visual observers, would be around $400.

Additionally, post processing of data, including visualization analysis and final deliverables, which include a report and videos, is estimated to cost $1800. Hence, the total approximate cost of UAV-CRP technology would be close to $3,000 per 1000 ft of rail track inspections. However, this cost varies depending upon the travel distance to the site, additional per diem costs, number of rail lines, complexity of the site (might warrant extra visual observers), type of deliverables, inclement weather conditions, and other factors. The cost will be reduced if a larger inspection assignment is needed based on economy of scale. We can also expect

that the use of UAV-CRP technology in rail corridor inspections will save expenditures related to the use of hi-rail inspection vehicles, overtime wages due to delays, and the additional costs of emissions.

Using UAV-CRP technology over traditional methods results in the quantitative benefit of 4.8% in cost savings. Major quantitative benefits of using UAV-CRP technology for inspection arises from its ability to collect data on track conditions, encroachment problems, and debris in the same flight. If the UAV-CRP technology is used to inspect 10,469 rail miles in the state of Texas, the estimated savings are around $8.3M for track operations and other track studies. A reduction factor of 4 is used since transportation agency may inspect only a fraction of the rail lines with this UAV-CRP technology. Hence, this would result in approximately $2.1M in cost savings for monitoring rail lines. It should be noted that majority of these rail miles are managed by rail operating companies in Texas.

Major indirect benefits of conducting UAV-CRP studies for mapping rail tracks include assisting agency personnel in proactively monitoring rail infrastructure and providing long-term safe traveling conditions to rail freight and passenger traffic based on improved maintenance and immediate intervention when a problem is detected. Another indirect benefit is the enhancement of safety elements while performing UAV operations in remote sites or locations that are swampy, have dense vegetation or have the highly arid soil found in deserts.

6.4.3.3 Rail Bridge Inspection

According to the data provided by TxDOT Rail Division (2016), there are approximately 400 railway bridges in the state of Texas. Traditional bridge inspection consists of a hands-on visual observation with a qualified inspector, operator, and other crewmembers. Safety equipment, ladders, and under-rail bridge inspection vehicles are used to inspect inaccessible railway bridge regions. The following information is obtained from TxDOT Rail Division's Texas Rail Plan Update (TxDOT Rail Division, 2016), as well as information based on calculations made in this research developed to determine the annual expected benefits of UAV-CRP technology implementation in rail bridge inspection.

Salaries for bridge inspectors and operators are $5.5k and $2k per week, respectively. Costs of an under-bridge inspection unit and its insurance are $5.5k and $500, respectively. Approximate costs incurred on bridge inspections based on a 40-hour work week are the sum of weekly salaries for the bridge inspector, operator, and crew as well as the costs of the under-bridge inspection unit and safety equipment used during operation. This research very conservatively assumes that it takes 2.5 working days (20 hours) to conduct a 360° inspection of a 1000 ft rail bridge using traditional methods. Approximately two bridges can be inspected within a normal workweek (40 hours). We anticipate these costs for traditional surveys to be around $13.5k per week. The approximate cost for each 1000 ft rail bridge would be around $6,750.

Bridge inspections can be conducted remotely using UAVs with low safety risks in a short time period. Using UAV-CRP technology, bridge deck images and videos, including above-and-below assessments of the bridge being inspected, can be collected in a 90-min data collection process involving multi altitude flights. UAV capital recovery and operation costs, GCP setup costs, as well as mobilization costs approximately $1,000 per rail bridge site.

The approximate costs for flight operations including a three-member team comprised of one pilot, and two visual observers would be around $600 and post processing of data including visualization analysis and final deliverables including a report and videos would be $2,000. Hence, the total approximate cost would be close to $3,600 per bridge per visit. However, this cost varies depending upon the travel distance to the site, additional per diem costs, number of rail lines, complexity of the site (might warrant extra visual observers), type of deliverables, inclement weather conditions, and other factors.

When performing the rail bridge inspections using UAV-CRP technology, we will not require an additional crew, additional safety equipment, or the expensive conventional under-bridge inspection unit used by current road-bound practitioners. Presence of a bridge inspector is also optional as the videos are available to provide an in-field view. Thus, the cost of these items can be saved. Using UAV-CRP technology over traditional methods result in quantitative benefits representing a 47% cost savings. It also does not warrant any expensive

safety equipment required for accessing the under-bridge elements. For all the railway bridges in the state of Texas, the total amount saved by conducting UAV-CRP inspection is based on an estimate of 400 bridges served with $3,150 saved per bridge, which would be approximately $1.3M. A conservative reduction factor of 4 is assumed to account for the variability of bridge types; hence, an approximate cost savings of $300k is obtained as an estimate of rail bridge infrastructure ratings

The indirect benefits from this methodology are that it can be used to inspect bridges that are not easily accessible, and it does not require costly safety equipment for field operations. It also gives an option to review the videos and go through them closely to inspect all the elements that are not typically covered or offered by traditional methods.

6.4.3.4 Rock Cut Surveys

Rail infrastructure passing through rock cuts needs continuous monitoring of the rock slopes for safe operation. Traditional surveying techniques are time consuming and perilous to the working staff, due to the steepness of the rock slopes. Because of the complexity involved, the accuracy of the surveying data collected also tends to be reduced. The traditional survey estimates of rail track condition, amount of debris on track, and slope stabilities can only be done through different surveying tasks. Assuming the average cost of performing traditional methods to collect all the data is $4 per ft; thus, the cost of using traditional methods to survey a 1000 ft rail track stretch within an open rock cut is $4,000. This traditional survey

is assumed to provide the rock slope information, presence of any debris obstructions, and other rail features. Expenditure for 4 technicians and the 90 minutes required for operation is estimated as $300. The total cost using traditional methods would be $4,300.

At a rock cut site, UAV-CRP technology collected the rail track distress data, debris data, tie condition data, and the stability of rock cut slopes, all in the same flight operation. The data of 1000 ft rail track was collected using UAV-CRP technology in 30 minutes. UAV capital recovery and operation costs, GCP setup costs, as well as mobilization costs would be approximately $800 per railway rock cut site. The approximate cost for flight operations, including a three-member team comprised of one pilot, and two visual observers, would be around $400 and post processing of data, including visualization analysis and final deliverables including a report and videos, is $2,000. Hence, the total approximate cost of inspection using UAV-CRP technology would be close to $3,200 per 1000 ft of rail track through a rock cut. However, this cost varies depending upon the travel distance to the site, additional per diem costs, number of rail lines, complexity of the site (might warrant extra visual observers), type of deliverables, inclement weather conditions, and other factors.

The UAV-CRP cost will decrease if a larger inspection assignment is needed based on economy of scale. For example, if three bridges are close enough to be assessed in one day, a notable discount can be assessed based on the size of the project, the proximity of the structures served, and the full-time use of an 8-hour day for all the personnel involved.

Using UAV-CRP technology over traditional methods results in the quantitative benefit of 25.6% in cost savings. It also does not warrant any expensive safety equipment required for accessing the dangerous sloping areas on the rock slope. Major indirect benefits using UAV-CRP technology can be seen from the increased safety conditions and efficiency provided while collecting the data. This data can be used to understand infrastructure conditions and prolong service life.

6.4.4 Construction Material Stockpile Volumetrics

A Comparison of volumetric analysis of construction material stockpiles by traditional survey methods and UAV-CRP technology is provided. For conventional methods, small stockpiles with flat slopes are easier and safer to evaluate compared to steeper and larger stockpiles. Increase in the size of a stockpile increases the magnitude of danger and error obtained from these methods. UAV-CRP technology can be used to obtain large stockpiles data accurately with less personnel required.

Based upon the surveying vendor's data, the cost of estimating a 5,500-cubic-yd stockpile using traditional methods is estimated to be $1500. The rate for

Registered Professional Land Surveyor (RPLS) is about $165 per hour and the technician would normally get $70/hour. Assuming this procedure takes an hour, the total expenditures for conducting volumetric measurements using traditional methods would be $1,735 per 5,500-cubic-yd of stockpile material.

Using UAV-CRP technology, information pertaining to a 5,500-cubic-yd stockpile can be collected using 15-min data collection procedures involving multi altitude flights. UAV capital recovery and operation costs, GCP setup costs, as well as mobilization costs would be approximately $500 per stockpile site. The approximate costs for flight operations, including a three-member team comprised of one pilot, and two visual observers, would be around $300 and the post processing of data including visualization analysis and deliverables for final report, would be $600. Hence, the total approximate cost of inspection using UAV-CRP technology would be close to $1,400 per 5,500-cubic-yd of stockpile material. However, this cost varies depending upon the travel distance to the site, additional per diem costs, number of stockpiles needed to be estimated, complexity of the site (might warrant extra visual observers), type of deliverables, inclement weather conditions, and other factors.

The rate of charge will come down if a larger inspection assignment is needed. Using UAV-CRP technology over traditional methods result in a quantitative benefit of 19% in cost savings. UAV-CRP technology also does not warrant any expensive safety equipment required for accessing the dangerous

sloping areas on the stockpiles. This technology can be extensively used to calculate the volume of material stockpiles during construction and is expected to generate more benefits.

Major indirect benefits can be seen from the improved safety and accuracy provided while collecting the data. This data can be used to gather accurate inventory information and plan construction activities accordingly. Digital elevation models (DEM) and contours obtained from this UAV-CRP technology will be helpful in safely planning the loading and unloading activities of stockpiles.

6.5 COMPILATION OF MONETARY VALUES

Based on the assumptions and calculations provided in the above sections, Table 6-1 summarizes the approximate total cost savings obtained by using UAV-CRP technology as compared to the traditional methods. These cost savings realized in this analysis of the above areas are approximate and are based on certain assumptions. Safety operations is one major area where using UAV-CRP technology can enhance the field survey operations and infrastructure assessments.

Table 6-1. Monetary Values Resulting from Using UAV-CRP Technology over Traditional Methods for Different Application Areas

No	Item	Quantity
1.	Approximate cost savings after using UAV-CRP technology in inspecting high speed pavements in Texas	$17.3M
2.	Approximate cost savings after using UAV-CRP technology for inspecting poorly rated bridges in Texas	$13.1M
3.	Approximate cost savings after using UAV-CRP technology to inspect at grade railroad crossings in Texas*	$1.6M
4.	Approximate cost savings after using UAV-CRP technology to inspect rail tracks in Texas	$2.1M
Total Expected benefits from implementing UAV–CRP technology for the above tasks**		$34.1M

Note: * Other railway tasks and stockpiles are not included as appropriate number of each type of infrastructure elements considered was hard to estimate

**Conservative reduction factor of 4 for pavements, bridges, and railways is assumed.

6.6 OTHER POTENTIAL BENEFIT AREAS

In addition to the above infrastructure monitoring tasks, UAV-CRP technology also finds its application in other areas discussed as below.

6.6.1 Asset Management and Remote Area Site Reconnaissance Works

Using UAV-CRP technology for asset management, remote area site reconnaissance, and monitoring works could result in the following benefits:

- Ease of monitoring inaccessible or remote areas
- Increased safety operations
- Money and time saved through inexpensive and time saving procedures
- Improved decision-making in critical asset management using UAV-based data collection

DOT agencies normally spends between $0.1 and $1M per construction project for site reconnaissance studies, based on the scope and area to be examined. In remote and rural areas, including problematic zones (swamps, wetlands, deserts, dense forest regions). These surveys can be expensive and may subject workers to hazardous conditions. UAVs can provide initial reconnaissance data in a short turn-around time that will potentially save millions of dollars annually. UAV reconnaissance data can help districts and area offices in making site-related decisions faster with a much higher safety factor, which will potentially reduce manual operations needed for these studies.

6.6.2 Disaster Response Unit Operations

Disasters often result in devastating consequences and the public agencies often end up short handed in disseminating, coordinating, and rescuing operations. UAVs are in identifying various elements of the inspecting objects during and after the

disaster events. Possible benefits of using UAV-CRP technology for disaster response operations are as follows:

- During natural and manmade disaster situations (floods, forest fires, accidents involving environmental implications, and terrorist situations), districts and areas have to perform preliminary field surveys and make decisions about the closure of roads and bridges to protect people.
- UAV operations will provide live feed data that can be used to make these decisions wisely and quickly
- UAV operations will eliminate most (if not all) safety issues prevailing with the present traditional methods

6.6.3 Real Time Monitoring

Road user cost (RUC) is defined as the estimated daily cost to the traveling public resulting from construction or maintenance work being performed. That cost primarily refers to lost time caused by hazardous conditions. Using UAVs will provide immediate and real time data that can be used to make timely decisions on road and bridge closures, potentially reducing RUCs that depend on the type of road, traffic conditions, motorist costs, and accident-related information. Early closures can lessen or mitigate damages to road and bridge infrastructures and will save human lives.

A conservative estimate of 30% in reductions of construction/maintenance time from the UAV-based decision-making process can be realized. This means

that for a single major construction/maintenance project, the use of UAVs can result in potential cost savings by reducing construction time. The total cost benefits can be several millions of dollars after considering all the larger projects that could be benefitted.

6.7 SUMMARY

Cost analyses of UAV-CRP operations not only indicates its cost effectiveness compared to traditional methods but also provides an idea about the feasibility for conducting frequent inspections that will save a lot of taxpayers' dollars by proactively identifying distress before they transform or inflict an infrastructure with a larger damage.

Implementation of this technology could lead to several millions of dollars in cost savings, with more accurate stockpile volumetric assessments, inexpensive annual inspections of bridges, cheaper site reconnaissance surveys in remote areas, and instant information relay that can trigger emergency responses during natural hazard situations.

CHAPTER 7: BUSINESS GUIDANCE AND POLICY RECOMMENDATIONS

7.1 INTRODUCTION

NCDOT is one of the 10 selectees of Unmanned Aircraft Systems (UAS) Integration Pilot Program-2018 (IPP-2018) shaped by USDOT and FAA. As part of this program, NCDOT will be testing packaged delivery by operating over humans, during night, and beyond visual line of sight (BYVLOS) within a defined airspace (IPP 2018). KDOT is also one among the 10 selectees of Unmanned Aircraft Systems (UAS) Integration Pilot Program (IPP) shaped by USDOT and FAA. Under this program, KDOT is the only agency assigned to evaluate the use of drones for highway and infrastructure management (IPP 2018). In August 2018 under IPP, KDOT with the help of Kansas State University Polytechnic deployed UAS beyond visual line of sight (BVLOS) in rural areas (Lillian 2018). Oklahoma Department of Transportation (ODOT) is using UAS for bridge and other infrastructure inspections (Lercel et al. 2018).

In order to avoid investing in technologies that do not match with agencies' interests, MnDOT suggested the potential UAS users to conduct a return on investment of this technology. MnDOT has conducted UAS operations both in-house and outsourced to external vendors for various projects. MnDOT has initially started using UAS for bridge inspections to overcome the direct and indirect costs involved in traditional bridge inspections. They also reported that using UAS

resulted in improving the efficiency and safety during bridge inspections (Lercel et al. 2018). Although some DOTs have been adopting UAS for agency operations, this research identified that many other DOT agencies' need for guidance and policy recommendations.

Based on the management and practical experience of conducting UAV-related operations performed as a part of the present research, it presents the following viewpoints and policy recommendations for future consideration of the DOT agencies:

7.1.1 General Guidelines

Before applying for a contract bid to carry out UAV operations for DOT agencies, any vendor or consulting agency should have a minimum of 10 hours prior experience in conducting UAV operations in an urban or rural setting. They should demonstrate that the operations follow the guidelines setup in flight operations manual (FOM) of the respective agency and use the survey signs developed as a part of this research. DOT agencies are required to provide necessary traffic control during the inspections. The UAV vendors should be also informed that DOT agencies would not be liable for any kind of claims or disputes arising from the actions of the vendor collecting the data.

7.1.2 Data Collection Activities

Common data collection activities of most survey companies are in agreement with the desired tasks of most DOT agencies. Some companies are capable of collecting

pavement data, rail line data, bridge deck data, stockpile volumetrics, elevation and drainage mapping, embankment data and other data that can be collected using the bottom gimbal camera. The majority of these companies are also capable of traveling and operating in distant remote areas, although some of them focus on a single region.

All of these data collection operations can be outsourced to companies by specifying the required resolving power and accuracy standards. The type of UAV, either rotary or fixed wing type, used for conducting the inspection should not pose any problems as long as the company provides data meeting specified resolving power and accuracy standards. The companies need to deliver standard output deliverables, such as 3D dense point cloud models, orthomosaics, DEMs, DTMs, Vector map data, and any other deliverables, that match the DOT agency requirements.

7.1.3 Analysis and Deliverables

The companies' ability to analyze the outputs from the UAV-collected data from a civil engineering point-of-view is of concern. Many of the companies are familiar with simpler linear measurements and volumetric measurements on the data. However, analyses of the data and interpretation for infrastructure health monitoring prove to be challenging since many companies do not have the necessary background and proper experience to work in these areas. The analysis features also include automatic feature identification, which is clearly lacking in

the commercial consulting sector. This implies DOT engineers may either have to process and interpret the data provided by the vendors themselves, or contract to experts at universities or consulting agencies who will be able to process this data and derive meaningful interpretations. A small number of vendor companies are building partnerships with software companies focused on automated feature detection, but these are not yet available as commercial products or services. Hence, this research proposes that DOT agencies should develop an in-house capability to analyze the deliverables and draw resulting conclusions based on the analysis.

One area of concern is the limited background of vendors in under-bridge inspections. Due to the complexity of the issues involved, this research proposes that DOT agencies should search for vendors that can offer safe and high-quality under-bridge inspection services. This will serve an important need as bridge rating surveys are needed biennially for proper maintenance strategies. It should be noted that there are vendors from different regions that can provide these services, but they may be expensive for the local county commissioners who intend to keep their bridges safe. Again, with time and more work by the local in-state vendors, under-bridge inspection may not be an issue in the near future.

7.1.4 Business Recommendation

Business guidance recommendation for DOT agencies is presented in the following, and this recommendation is based on UAV research experiences, contacts with various traditional surveyors and UAV vendors, and working with

UAV groups from different parts of the country. Application areas include infrastructure imaging, stockpile volumetrics, pavement studies, bridge surveys, rail corridor assessments, emergency response, and other transportation asset management studies. Several factors including FOM, costs of operations, amount of work, liability issues, and benefits of UAVs over traditional methods are considered while making the recommendations.

Three approaches for UAV data collection and analysis were formulated involving two entities i.e. DOT agency and Contractors (classified as the agencies that demonstrated UAV data collection expertise):

- Approach 1 – Only Contractors (commercial and others that demonstrate UAV expertise)
- Approach 2 – Only DOT Internal UAV Group
- Approach 3 – Fusion between DOT UAV Group and Contractors (Hybrid Approach)

In approach 1, UAV-CRP data collection, processing, and data analysis would be performed by UAV contractors or vendors. In approach 2, UAV-CRP data collection, processing, and data analysis would be performed by a UAV group within the DOT. In approach 3, UAV-CRP data collection and processing would be assigned to contractors and data analysis and interpretation would be performed by DOT or by contractors under the supervision of DOT personnel.

Each approach has benefits and limitations as discussed below, are taken into consideration before arriving at a suitable approach that can be adopted for the near future.

7.1.4.1 Approach 1:

The following describes benefits and limitations of approach 1 (Contractors).

7.1.4.1.1 Benefits:

- Readily available UAV platforms and sensors required to conduct the data collection
- Experience in collecting and processing the UAV data

7.1.4.1.2 Limitations:

- Most contractors are not familiar with DOT agencies' Flight Operation Manual (FOM) guidance and hence some training is needed prior to operating over infrastructure under DOTs
- Most contractors lack the civil engineering background while analyzing the UAV collected data
- Most contractors lack a methodology to conduct detailed analysis of the processed UAV data (especially related to pavements, railways and bridges) to provide the state of the condition of infrastructure
- Most contractors lack the experience of collecting UAV data of infrastructure located in an urban environment

7.1.4.2 Approach 2:

The following describes benefits and limitations of approach 2 (DOT Internal UAV Group).

7.1.4.2.1 Benefits:

- Working staff available all over the state
- Possessing the required engineering knowledge to analyze the collected infrastructure data

7.1.4.2.2 Limitations:

- At present, lack the necessary equipment (UAV platforms, sensors and other accessories)
- At present, lack of trained work force in DOTs to conduct the UAV data collection

Due to the above factors in the first two approaches, this research recommends that DOT and contractors work together and complement each other's strengths for performing UAV studies on infrastructure. This approach hereafter termed as approach 3 (Hybrid Approach), should be continued until DOT agencies achieve self-sufficiency in performing UAV-CRP studies, data collection, processing, and analysis.

7.1.5 Decision Matrix

An attempt is made to present different grades of recommendations for each application area in a decision matrix provided in the Table 7-1:

Table 7-1 Decision Matrix of Application Areas and Different Approaches

Application Areas	**Contractors [Approach 1]**	**DOT UAV Group [Approach 2]**	**Hybrid [Approach 3]**
Pavement Studies	3	2	1
Bridge Studies	3	2	1
Rail Corridor Studies	2	3	1
Stockpile Volumetric	2	3	1
Construction Site Monitoring	2	3	1
Emergency Response	2	3	1

Note:

1. The above recommendations are made for the next 10 years
2. The hierarchy of numbers provides an idea about the recommendation for each application area with 1 being the top priority approach and 3 being least priority approach

This research recommends that the approach 3 (Hybrid Approach) to be followed in the initial years to conduct UAV-CRP surveys and monitoring for all the infrastructure application areas. DOT agency overseeing the UAV operations

by contractors in all application areas will not only help in maintaining the quality of the data but will also help DOTs in gaining the experience to conduct the data collection, processing, and analysis.

For pavement and bridge studies, this research recommends that the second preference be given to the DOT UAV group (approach 2) due to engineering expertise that DOT possesses. Also, the inexperience of most of the contractors in collecting, processing, and analyzing precise pavement and bridge data is a major reason for this recommendation. Hence, during the initial years the hybrid [3] approach is recommended as the first preference for these application areas.

Infrastructure condition data post an emergency can be collected, processed and analyzed using the UAV-CRP methodology. Artificial intelligence being not available readily for the image analysis, looking at aerial images and videos would help in the immediate rescue operations. For emergency monitoring, this research recommends that the second preference be given to the contractors (approach 1) due to their experience in collecting the visuals that includes images and videos using UAV-CRP. DOT UAV group (approach 2) is given the third preference due to the shortage of equipment and trained workers for performing UAV-CRP methodology during an emergency. In the initial years, DOT might start with the infrastructure data being collected, processed, and analyzed by the contractors according to DOT requirements and DOT overseeing the operations. Hence, during

the initial years the hybrid approach (Approach 3) is recommended for implementing this UAV application in DOTs.

Resources in the form of staffing and UAV equipment and accessories are needed for DOT to oversee the contractors' works during these initial years. This research recommends two full time staff members to head a new UAV-Infrastructure section and this team should have sufficient background in operating UAVs, surveying and infrastructure engineering fields. Also suggest hiring teams of pilots and observers to perform in-house field UAV studies. Pilots can be part time staff and observers can be trained interns. It is recommended that full time pilots and observers can be gradually hired to work under the new unit leadership.

7.2 SUMMARY

Also, in the near future, it is anticipated that there will be a few more in-state vendors that can provide the services necessary to inspect infrastructures with more awareness and experience in these topics. In addition, other agencies around the country are embracing this new technology and are conducting much-needed research with UAV platforms. All these indicate that the future prognosis of this UAV-CRP technology for infrastructure monitoring will be bright and hence these efforts will help in future cost savings in infrastructure assessments and surveys.

SUMMARY AND CONCLUSIONS

8.1 SUMMARY

In this dissertation research, close range photogrammetry was accomplished using unmanned aerial vehicle (also termed as UAV-CRP) platforms mounted with visible range camera. This methodology helps in remote data collection. Due to its multifaceted benefits, UAV-CRP technology have been explored as a potential infrastructure monitoring tool in the present research and this has been the main objective and focus of this dissertation research.

A comprehensive literature review on UAVs, photogrammetry, traditional monitoring methods, previous studies on UAV applications in Civil Engineering, and latest developments in using UAVs for US DOT agencies have been conducted in the initial chapters. Fixed wing and rotary wing are the two main types of UAVs considered in this research as studies on the hybrid vertical take-off and landing (VTOL) are limited.

Growing demand for the UAV applications was observed from the literature study, also indicated by the fact that as many as 36 DOT agencies have either started using or are researching the feasibility of incorporating UAVs as part of their applications. Various practitioners, researchers, and also engineers have conducted significant amount of research on various UAV applications include monitoring pavements, traffic, landslides, bridges, dams, rail tracks, construction sites, tall structures and stockpile volumetrics.

The main components of UAV-CRP technology include drone equipped with navigation accessories, camera and its accessories, and a gimbal. Even though there are off-the-shelf products available in the market, this study identified a need to evaluate the compatibility of various accessories involved in the data collection procedures. Flight altitude, focal length, longitudinal and lateral overlap of flight, and flight speed affect the quality of the photogrammetry data collected. By varying those parameters, a total system error analysis was conducted on the UAV and other accessories. Methodologies for collecting indoor and outdoor data to achieve the calibration objectives were used to study georeferencing accuracy, effect of different parameters on focal length, distortion, and resolving capacity.

UAV-CRP monitoring had been conducted at sites including various infrastructure assets like pavements, bridges, rail lines, and stockpiles. All the data collection procedures were conducted with research group personnel wearing personal protective equipment and appropriate signs placed ahead of the inspection area on either sides. The infrastructure imagery data was processed to obtain dense point cloud models, orthomosaics, digital elevation models, and contours. These processed outputs were then analyzed for different attributes pertaining to the infrastructure asset under inspection.

Pavement data was collected by flying off the pavement shoulder and with the camera inclined towards the pavement. The pavement data was analyzed for longitudinal and lateral elevation profiles in addition to various distress parameters.

Traditional methods were also conducted to compare the measurements from both the methods. Pavement cracking was identified by algorithms developed in Python programming language. Various functions were ran on the distressed pavement orthomosaic images to identify and calculate the area of distress to help in understanding the condition of the pavement. The volumetric information of the construction material stockpiles had been obtained from the UAV-CRP technology and were compared with traditional surveying methods.

Bridge structure was inspected for superstructure and substructure elements like bridge deck, approach slab, railings, joint conditions, beams, soffits, bearings, wing walls, abutment, pile and cap, as well as the pile footing. Top gimbal mount was used to inspect the underneath of bridge and bottom gimbal mount was used to inspect all other elements. High quality 4K videos were also collected to obtain an idea about the condition of various hard-to-reach areas. The bridge inspector supervising the inspection operations was able to monitor the camera visuals in real-time on a digital live video display (DLVP) unit throughout the inspection.

Different sites along the rail corridor were inspected to evaluate the application of UAV-CRP technology in monitoring the condition of the rail components. At-grade railroad crossing, washout, railbridge, and rock cut are the features inspected using this innovative technology. Different features like rusting of rails, vegetation encroachment, drainage path leading to soil erosion, and tie condition were identified from UAV-CRP collected data. Thermal data was

collected to estimate the health of the ties. Slope information of the rock walls was obtained for analyzing the stability of rock slopes.

UAV-CRP technology had also been used to monitor the debris generated due to the inundation of houses caused by the floods triggered by Hurricane Harvey. In addition to the debris data, infrastructure data pertaining to pavement condition was also collected using UAV-CRP technology to evaluate the distress parameters. Various benefit parameters related to return on investment were considered to conduct cost analysis of this innovative technology.

The aim of this analysis was to evaluate the economic feasibility of using this new technology over the traditional methods. Even though many DOT agencies have started using UAVs, those efforts can be termed as initial developments. This study proposed a few business guidance policy recommendations for the agencies to plan UAV operations for the near future. Benefits and limitations of three approaches were discussed and a decision matrix for different UAV applications was provided.

8.2 CONCLUSIONS

This dissertation study conducted comprehensive work in evaluating the UAV-CRP technology for infrastructure applications and conclusions are provided below.

1. Depending upon the experience gained during the literature study on UAV applications and this dissertation research conducted for evaluating

infrastructure monitoring, rotary wing UAVs better serve the purpose of a localized inspection compared to the fixed wing.

2. All the checks conducted under total system error analysis had ensured that required grade of accuracy could be obtained in the models developed from the imagery data collected in the field. The first check that evaluated the accuracy of geotagging images using RTK data and GPS data validated the high accuracy obtained using RTK GNSS data. This helped the research team in realizing the need for using RTK GNSS data while conducting actual infrastructure studies.
3. Second check examined the variance of focal length in room conditions and field conditions. Indoor results indicated that the focal length remained constant and close to manufacturer specifications. Outdoor results analysis results indicated that the minor variance of the focal length in the outdoor conditions did not induce any substantial errors in the 3D model. The third check proved that, within the temperature range specified by the manufacturer, the focal length of the lens remained within the acceptable range and contributed high quality imaging analysis and 3D models of the infrastructure. Checking lens focal length is a critical step as it is related to the most important feature that is the camera sensor.
4. In the fourth check, zero tangential distortion was recorded, which proves that there was no defect in the camera components. High overlap adopted

also helped in mitigating the radial distortion and obtaining high quality 3D models. The fifth calibration check was about mapping data of an area with more variation in the vertical profile using an aerial mobile platform. Although the optimum flight altitude for data collection is based upon the height of the obstructions in the vicinity, the SfM error analysis provided a comprehensive understanding about the optimum overlap and flight altitude that was adopted during actual field data collection of the infrastructure. The sixth calibration check helped in deciding the particular flight altitude required to identify and distinguish the features under infrastructure survey and inspection with sufficient resolving power of camera.

The above calibration checks and results lead to the observation that the present UAV platform and camera accessories can provide photogrammetry data of high quality and excellent repeatability. This provided confidence in collecting infrastructure monitoring data for making engineering judgements during the subsequent steps of this dissertation research.

5. The UAV-CRP technology successfully inspected the pavements constructed on expansive soils and obtained pavements' characteristics and distress information. Both the longitudinal and transverse elevation profiles of the pavement were analyzed from the same UAV-CRP flight mission data. This UAV based inspection indicates its benefits in terms of higher

safety, lesser workforce and inspection time, and no traffic delay cost compared to two separate traditional inspection methods required for the two attributes discussed above.

6. The UAV-CRP technology also provided a more detailed pavement distress information than the presently used and available traditional methods, and all the distress details collected using UAV-CRP technology could be used to estimate pavement serviceability index (PSI) that helps in assessing the need for pavement rehabilitation.

   Traffic restrictions, a typical sight during most of the conventional inspection methods, were not imposed during the UAV-CRP data collection on the high speed pavement. This innovative data collection procedure also considerably reduced the inspection cost and traffic delay cost. Analysis of the pavement characteristics data collected from UAV-CRP methodology also proved efficient and comparable with traditional methods.

7. Even though the UAV-CRP technology might not match the accuracy level of the laser devices, the UAV-CRP data can be collected and used as a complimentary data collection tool to the traditional methods. Critical pavement sections can be identified by quickly conducting the UAV-CRP technology inspection over the pavement network level and then conduct the costly traditional surveys on those most critical sections identified from the UAV-CRP data analysis.

8. This technology allows for safe data collection of rail infrastructure in hard-to-reach areas such as under bridges, steep slopes, and marshy areas. It has the capability to not only show the washout distress but also an idea about the factors (drainage path leading to it), which is otherwise a time taking task using traditional methods. The rail under bridge inspection had provided a safe access to view the condition of the ties and also the rotten-wooden walking platform that would have been used for regular inspections.

    Due to the emerging nature of this UAV-CRP technology, it is proposed and recommended that UAV-CRP to be used as a complimentary data collection tool to the present traditional methods until common acceptance is obtained among the civil and infrastructure engineering fraternity about solely using UAVs with high quality sensors to perform maintenance studies. Further studies will lead to and ensure such approach in the near future.

UAVs can also be used to collect the infrastructure condition data in addition to helping in rescuing operations during and after the hurricane. UAVs can become a useful tool during disaster management. Cost analysis conducted in this study also assured that millions of taxpayers' dollars could be saved by complementing the traditional data collection methods with UAV-CRP technology in a safe manner.

UAV-CRP technology, owing to its multiple benefits, have gained the impetus for its application in many interdisciplinary fields. Many DOTs have started embracing this technology and realized the benefits. Business guidance recommendations provided in this dissertation suggest that DOT agencies could get benefitted by adapting a hybrid approach for UAV data collection which involves a partnership between DOT personnel and contractors.

8.3 SCOPE FOR FUTURE WORK

This technology being new has opened many avenues that needs further future studies. Below are some of the areas that can be explored:

There is a need to explore UAV data collection by flying beyond visual line of sight (BVLOS), as the future readies up for preprogramming flight plan and launching UAVs remotely. However, this also needs further development and integration with unmanned aerial traffic management (UTM). This can also support drone swarms that can be used for infrastructure assessment before and after a disaster in an efficient manner.

Artificial intelligence and machine learning on the multifaceted UAV image data will automate the processing and analyzing the infrastructure data for various distress. Development of algorithms that automatically feed these data into the pavement maintenance database system (PMDb), bridge maintenance database, and rail maintenance database will be extremely helpful for infrastructure asset management.

The dense point cloud models obtained from UAV data collection can be incorporated with augmented reality and virtual reality to create a whole new experience of visualizing the infrastructure asset condition.

REFERENCES

Abu-Hejleh, N., Hanneman, D., White, D. J., and Ksouri, I. (2006). *Flowfill and MSE Bridge Approaches: Performance, Coast, and Recommendations for Improvements*. Colorado Department of Transportation, Research Branch.

ADOT. (2018). "ADOT gains drones through federal innovation program." <https://www.azdot.gov/media/News/news-release/2018/04/25/adot-gains-drones-through-federal-innovation-program> (Aug. 29, 2018).

Adu-Gyamfi, Y. O., Tienaah, T., Attoh-Okine, N. O., and Kambhamettu, C. (2014). "Functional evaluation of pavement condition using a complete vision system." *Journal of Transportation Engineering*, American Society of Civil Engineers, 140(9), 4014040.

Aggarwal, S. (2004). "Principles of remote sensing." *Satellite remote sensing and GIS applications in agricultural meteorology*, 23–38.

Ahmad, A. (2006). "Digital photogrammetry: An experience of processing aerial photograph of UTM acquired using digital camera." *Asia GIS Conference*.

Ahmad, A., and Samad, A. M. (2010). "Aerial mapping using high resolution digital camera and unmanned aerial vehicle for Geographical Information System." *Signal Processing and Its Applications (CSPA), 2010 6th International Colloquium on*, IEEE, 1–6.

Alvear, O., Zema, N. R., Natalizio, E., and Calafate, C. T. (2017). "Using UAV-based systems to monitor air pollution in areas with poor accessibility."

Journal of Advanced Transportation, Hindawi, 2017.

Archeewa, E. (2010). *Comprehensive studies on deep soil mixing and lightweight aggregates applications to mitigate approach slab settlements*. The University of Texas at Arlington.

Asphalt Institute. (2016). *Improve Safety Save Time Survey Finds a Growing Number of State DOTS are Using Drones to Improve Safety and Collect Data Faster and Better-Saving Time and Money*.

ASTM E1703/E. (2005). "Standard Test Method for Measuring Rut-Depth of Pavement Surfaces Using a Straightedge." ASTM Standards, ASTM International USA.

Azevedo, C. L., Cardoso, J. L., Ben-Akiva, M., Costeira, J. P., and Marques, M. (2014). "Automatic vehicle trajectory extraction by aerial remote sensing." *Procedia-Social and Behavioral Sciences*, Elsevier, 111, 849–858.

Babinec, A., and Apeltauer, J. (2016). "On accuracy of position estimation from aerial imagery captured by low-flying UAVs." *International Journal of Transportation Science and Technology*, 5(3), 152–166.

Barfuss, S., Jensen, A., and Clemens, S. (2012). *Evaluation and development of unmanned aircraft (UAV) for UDOT needs.* Utah. Dept. of Transportation. Research Division.

Barmpounakis, E. N., Vlahogianni, E. I., and Golias, J. C. (2016). "Unmanned Aerial Aircraft Systems for transportation engineering: Current practice and

future challenges." *International Journal of Transportation Science and Technology*, Tongji University and Tongji University Press, 5(3), 111–122.

Bartlett, S., Negussey, D., Kimble, M., and Sheeley, M. (2000). "Use of geofoam as super-lightweight fill for I-15 reconstruction." *Transportation research board 79th annual meeting, Washington, DC*.

Berkenfeld, D., Black, D., Corrado, M., and Silverman, L. (2018). "Focal Length | Understanding Camera Zoom & Lens Focal Length | Nikon from Nikon." <https://www.nikonusa.com/en/learn-and-explore/a/tips-and-techniques/understanding-focal-length.html> (Aug. 11, 2018).

Blank, P., Kirrane, S., and Spiekermann, S. (2018). "Privacy-Aware Restricted Areas for Unmanned Aerial Systems." (April).

Bly, M. (2016). "Unmanned Aerial Systems Are Eyes in the Sky for CDOT Crews —." <https://www.codot.gov/business/process-improvement/lean-case-studies/unmanned-aerial-systems> (Aug. 29, 2018).

Bohman, A. (2018). "Fairbanks drone pilot gets DOT airborne | Local News | newsminer.com." <http://www.newsminer.com/news/local_news/fairbanks-drone-pilot-gets-dot-airborne/article_b5fac6a2-0fd8-11e8-aaa0-474d821fadf5.html> (Aug. 29, 2018).

Braut, V., Čuljak, M., Vukotić, V., Šegvić, S., Ševrović, M., and Gold, H. (2012). "Estimating OD matrices at intersections in airborne video-a pilot study." *MIPRO, 2012 Proceedings of the 35th International Convention*, IEEE, 977–

982.

Briaud, J.-L., James, R. W., and Hoffman, S. B. (1997). *Settlement of Bridge Approaches:(the Bump at the End of the Bridge)*. Transportation Research Board.

Brooks, C., Dobson, R. J., Banach, D. M., Dean, D., Oommen, T., Wolf, R. E., Havens, T. C., Ahlborn, T. M., and Hart, B. (2015). *Evaluating the use of unmanned aerial vehicles for transportation purposes*.

Bryan, ken. (2015). "BNSF | Rails West." <https://railswest.wordpress.com/tag/bnsf/> (Sep. 18, 2018).

Buchinger, D., and Silva, A. G. (2014). "Anomalies detection in asphalt pavements: a morphological image processing approach." *Revista Brasileira de Computação Aplicada*, 6(1), 121–129.

Butenuth, M., Reinartz, P., Lenhart, D., Rosenbaum, D., and Hinz, S. (2009). "Analysis of image sequences for the detection and monitoring of moving traffic." *Photogrammetrie-Fernerkundung-Geoinformation*, E. Schweizerbart'sche Verlagsbuchhandlung, 2009(5), 421–430.

Campbell, J. B., and Wynne, R. H. (2011). *Introduction to remote sensing*. Guilford Press.

Campoy, P., Correa, J. F., Mondragón, I., Martínez, C., Olivares, M., Mejías, L., and Artieda, J. (2009). "Computer vision onboard UAVs for civilian tasks." *Journal of Intelligent and Robotic Systems*, Springer, 54(1–3), 105.

Carey Jr, W. N., and Irick, P. E. (1960). “The Pavement Serviceability-Performance Concept.” *Highway Research Board Bulletin*, 250(250).

Carnie, R. J., Walker, R. A., and Corke, P. I. (2006). “Image processing algorithms for UAV" sense and avoid".” *Proceedings 2006 IEEE International Conference on Robotics and Automation, 2006. ICRA 2006*, IEEE, 2848–2853.

CBS news. (2017). “Cleaning up mountains of trash from Hurricane Harvey could take months - CBS News.” <https://www.cbsnews.com/news/hurricane-harvey-clean-up-texas-houston-trash-garbage/> (Sep. 19, 2018).

CDOT. (2017). “CDOT enters 5-year agreement with drone operators – BizWest.” <https://bizwest.com/2017/10/19/cdot-enters-5-year-agreement-drone-operators/> (Aug. 29, 2018).

Cesetti, A., Frontoni, E., Mancini, A., Ascani, A., Zingaretti, P., and Longhi, S. (2011). “A visual global positioning system for unmanned aerial vehicles used in photogrammetric applications.” *Journal of intelligent & robotic systems*, Springer, 61(1–4), 157–168.

Chaney, K. (2018). “Mississippi DOT Demonstrates How It Uses Drones On Infrastructure Projects.” <https://www.localmemphis.com/news/local-news/mdot-demonstrates-how-it-uses-drones-on-infrastructure-projects/1128951914> (Aug. 30, 2018).

Chow, J. Y. J. (2016). “Dynamic UAV-based traffic monitoring under uncertainty

as a stochastic arc-inventory routing policy." *International Journal of Transportation Science and Technology*, Tongji University and Tongji University Press, 5(3), 167–185.

Christ, G. (2016). "Drone used in turnpike bridge inspection crashes into water | cleveland.com." <https://www.cleveland.com/metro/index.ssf/2016/09/drone_used_in_turnpike_bridge.html> (Aug. 30, 2018).

CNN News. (2017). "Hurricane Harvey aftermath - CNN." <https://www.cnn.com/specials/us/hurricane-harvey> (Sep. 19, 2018).

Coifman, B., McCord, M., Mishalani, R. G., Iswalt, M., and Ji, Y. (2006). "Traffic flow data extracted from imagery collected using a micro unmanned aerial vehicle." *Applications of Advanced Technology in Transportation*, 298–303.

Colomina, I., and Molina, P. (2014). "Unmanned aerial systems for photogrammetry and remote sensing: A review." *ISPRS Journal of Photogrammetry and Remote Sensing*.

Congress, S. S. C., Puppala, A. J., and Lundberg, C. L. (2018). "Total system error analysis of UAV-CRP technology for monitoring transportation infrastructure assets." *Engineering Geology*, Elsevier.

CTDOT. (2015). "ConnDOT: CTDOT to Test Unmanned Aerial Vehicle System (UAV) for Bridge Inspection." <https://www.ct.gov/dot/cwp/view.asp?a=1373&Q=574468> (Sep. 6, 2018).

Daponte, P., De Vito, L., Mazzilli, G., Picariello, F., and Rapuano, S. (2017). “A height measurement uncertainty model for archaeological surveys by aerial photogrammetry.” *Measurement*, Elsevier, 98, 192–198.

Day, D., Homeland, T., Planner, S., State, P., Engineering, T., and Conference, S. (2017). “What is an Unmanned Aerial Vehicle.”

Díaz-Vilariño, L., González-Jorge, H., Martínez-Sánchez, J., Bueno, M., and Arias, P. (2016). “Determining the limits of unmanned aerial photogrammetry for the evaluation of road runoff.” *Measurement: Journal of the International Measurement Confederation*, 85.

Diner, Y. (2015). “Fast Survey of a High-speed Railway Line.” <https://www.gim-international.com/content/article/fast-survey-of-a-high-speed-railway-line> (Aug. 11, 2018).

Dobson, R., Colling, T., Brooks, C., Roussi, C., Watkins, M., and Dean, D. (2014). “Collecting decision support system data through remote sensing of unpaved roads.” *Transportation Research Record: Journal of the Transportation Research Board*, Transportation Research Board of the National Academies, (2433), 108–115.

Doherty, P., Granlund, G., Kuchcinski, K., Sandwall, E., Nordberg, K., and Skarman, E. (2000). “The WITAS Unmanned Aerial Vehicle Project.” *Proceedings of the 14th European Conference on Artifial Intelligence - ECAI 2000*, 747–755.

Dupont, B., and Allen, D. L. (2002). “Movements and settlements of highway bridge approaches.”

Eisenbeiß, H. (2009). “UAV photogrammetry.” ETH Zurich.

Ellenberg, A., Branco, L., Krick, A., Bartoli, I., and Kontsos, A. (2014). “Use of unmanned aerial vehicle for quantitative infrastructure evaluation.” *Journal of Infrastructure Systems*, American Society of Civil Engineers, 21(3), 4014054.

Erickson, K. (2018). “How do hurricanes form? :: NASA Space Place.” <https://spaceplace.nasa.gov/hurricanes/en/> (Sep. 19, 2018).

Estes, C. (2014). *Unmanned Aircraft Use in North Carolina Report to the Joint Legislative Oversight Committee on Information Technology Joint Legislative Transportation Oversight Committee Fiscal Research Division*.

Ezequiel, C. A. F., Cua, M., Libatique, N. C., Tangonan, G. L., Alampay, R., Labuguen, R. T., Favila, C. M., Honrado, J. L. E., Canos, V., and Devaney, C. (2014). “UAV aerial imaging applications for post-disaster assessment, environmental management and infrastructure development.” *Unmanned Aircraft Systems (ICUAS), 2014 International Conference on*, IEEE, 274–283.

Farnsworth, C. B., Bartlett, S. F., Negussey, D., and Stuedlein, A. W. (2008). “Rapid construction and settlement behavior of embankment systems on soft foundation soils.” *Journal of geotechnical and geoenvironmental engineering*, American Society of Civil Engineers, 134(3), 289–301.

FHWA. (2014). “Table HM-60 – Highway Statistics 2013 - Policy | Federal

Highway Administration.” <https://www.fhwa.dot.gov/policyinformation/statistics/2013/hm60.cfm> (Sep. 27, 2018).

Frew, E., McGee, T., Kim, Z., Xiao, X., Jackson, S., Morimoto, M., Rathinam, S., Padial, J., and Sengupta, R. (2004). “Vision-based road-following using a small autonomous aircraft.” *Aerospace Conference, 2004. Proceedings. 2004 IEEE*, IEEE, 3006–3015.

Fu, C., Carrio, A., and Campoy, P. (2015). “Efficient visual odometry and mapping for unmanned aerial vehicle using ARM-based stereo vision pre-processing system.” *Unmanned Aircraft Systems (ICUAS), 2015 International Conference on*, IEEE, 957–962.

Gabrlik, P. (2015). “The use of direct georeferencing in aerial photogrammetry with micro UAV.” *IFAC-PapersOnLine*, Elsevier, 48(4), 380–385.

Gallagher, J. J., Cook, J., and Pearle, L. (2017). “Hurricane Harvey wreaks historic devastation: By the numbers - ABC News.” <https://abcnews.go.com/US/hurricane-harvey-wreaks-historic-devastation-numbers/story?id=49529063> (Sep. 19, 2018).

GDOT. (2014). “TRAFFIC MANAGEMENT: Georgia DOT contemplating drones for traffic control | Roads & Bridges.” <https://www.roadsbridges.com/traffic-management-georgia-dot-contemplating-drones-traffic-control> (Aug. 30, 2018).

Gehrig, M. D., Morris, D. V, and Bryant, J. T. (2004). “Ground penetrating radar for concrete evaluation studies.” *Technical Presentation Paper for Performance Foundation Association*, 197–200.

Gillins, D. T., Parrish, C., Gillins, M. N., and Simpson, C. (2018). *Eyes in the Sky: Bridge Inspections with Unmanned Aerial Vehicles*.

Gonçalves, J. A., and Henriques, R. (2015). “UAV photogrammetry for topographic monitoring of coastal areas.” *ISPRS Journal of Photogrammetry and Remote Sensing*, Elsevier, 104, 101–111.

Guido, G., Gallelli, V., Rogano, D., and Vitale, A. (2017). “Evaluating the accuracy of vehicle tracking data obtained from Unmanned Aerial Vehicles.” *International Journal of Transportation Science and Technology*, Tongji University and Tongji University Press, 5(3), 136–151.

Ha, Q. M., Deville, Y., Pham, Q. D., and Hà, M. H. (2018). “On the min-cost traveling salesman problem with drone.” *Transportation Research Part C: Emerging Technologies*, Elsevier, 86, 597–621.

Haidari, L. A., Brown, S. T., Ferguson, M., Bancroft, E., Spiker, M., Wilcox, A., Ambikapathi, R., Sampath, V., Connor, D. L., and Lee, B. Y. (2016). “The economic and operational value of using drones to transport vaccines.” *Vaccine*, Elsevier, 34(34), 4062–4067.

Haulman, D. L. (2003). *US unmanned aerial vehicles in combat, 1991-2003*. AIR FORCE HISTORICAL RESEARCH AGENCY MAXWELL AFB AL.

Herold, M., Roberts, D., Noronha, V., and Smadi, O. (2008). “Imaging spectrometry and asphalt road surveys.” *Transportation Research Part C: Emerging Technologies*, Elsevier, 16(2), 153–166.

Hill, C. (2016). “Kansas DOT program testing drones for bridge and tower inspections.” <https://www.equipmentworld.com/kansas-dot-program-testing-drones-for-bridge-and-tower-inspections/> (Sep. 18, 2018).

Honkavaara, E., Arbiol, R., Markelin, L., Martinez, L., Cramer, M., Bovet, S., Chandelier, L., Ilves, R., Klonus, S., and Marshal, P. (2009). “Digital airborne photogrammetry—A new tool for quantitative remote sensing?—A state-of-the-art review on radiometric aspects of digital photogrammetric images.” *Remote Sensing*, Molecular Diversity Preservation International, 1(3), 577–605.

Honrado, J. L. E., Solpico, D. B., Favila, C. M., Tongson, E., Tangonan, G. L., and Libatique, N. J. C. (2017). “UAV imaging with low-cost multispectral imaging system for precision agriculture applications.” *Global Humanitarian Technology Conference (GHTC), 2017 IEEE*, IEEE, 1–7.

Horstmeyer, R., Heintzmann, R., Popescu, G., Waller, L., and Yang, C. (2016). “Standardizing the resolution claims for coherent microscopy.” *Nature Photonics*, Nature Publishing Group, 10(2), 68.

Horvath, J. S. (2005). “Integral-abutment bridges: geotechnical problems and solutions using geosynthetics and ground improvement.” *West Virginia*

University, Citeseer.

Howard, J., Murashov, V., and Branche, C. M. (2018). "Unmanned aerial vehicles in construction and worker safety." *American Journal of Industrial Medicine*, 61(1), 3–10.

Hsi, J. (2008). "Bridge approach embankments supported on concrete injected columns." *GeoCongress 2008: Geosustainability and Geohazard Mitigation*, 612–619.

Hu, H., Fernandez-Steeger, T. M., Dong, M., Nguyen, H. T., and Azzam, R. (2010). "3D modeling using LiDAR data and its geological and geotechnical applications." *Geoinformatics, 2010 18th International Conference on*, IEEE, 1–6.

Huber, C., Klinger, H., and O'Hara, K. J. (2018). "2017 Hurricane Harvey: Facts, FAQs, and how to help | World Vision." <https://www.worldvision.org/disaster-relief-news-stories/hurricane-harvey-facts> (Sep. 19, 2018).

Hudson, W. R., Haas, R., and Perrone, E. (2015). "Measures of pavement performance must consider the road user." *9th International Conference on Managing Pavement Assets*.

Hurwitz, D. S., Olsen, M. J., and Barlow, Z. (2018). *Driving Distraction due to Drones*.

Insitu. (2015). "Insitu - Success Stories | Best in Class Insitu Unmanned Aircraft

Systems.” <https://www.insitu.com/success-stories#7> (Sep. 18, 2018).

Insitu. (2018). “Insitu - Commercial Drones | Unmanned Aircraft Systems - Insitu.” <https://www.insitu.com/commercial#5> (Aug. 11, 2018).

IPP. (2018). “Integration Pilot Program Awardees.” <https://www.faa.gov/uas/programs_partnerships/uas_integration_pilot_program/awardees/> (Aug. 28, 2018).

Irizarry, J., and Costa, D. B. (2016). “Exploratory study of potential applications of unmanned aerial systems for construction management tasks.” *Journal of Management in Engineering*, American Society of Civil Engineers, 32(3), 5016001.

Irizarry, J., Gheisari, M., and Walker, B. N. (2012). “Usability assessment of drone technology as safety inspection tools.” *Journal of Information Technology in Construction (ITcon)*, 17(12), 194–212.

Jacobsen, K. (2002). “Calibration aspects in direct georeferencing of frame imagery.” *International Archives of Photogrammetry Remote Sensing and Spatial Information Sciences*, Citeseer, 34(1), 82–88.

Jiang, T., Geller, J., Ni, D., and Collura, J. (2016). “Unmanned Aircraft System traffic management: concept of operation and system architecture.” *International journal of transportation science and technology*, Elsevier, 5(3), 123–135.

Jutkofsky, W., Sung, J., and Negussey, D. (2000). “Stabilization of embankment

slope with geofoam." *Transportation Research Record: Journal of the Transportation Research Board*, Transportation Research Board of the National Academies, (1736), 94–102.

Kaaniche, K., Champion, B., Pégard, C., and Vasseur, P. (2005). "A vision algorithm for dynamic detection of moving vehicles with a UAV." *Robotics and Automation, 2005. ICRA 2005. Proceedings of the 2005 IEEE International Conference on*, IEEE, 1878–1883.

Kanistras, K., Martins, G., Rutherford, M. J., and Valavanis, K. P. (2013). "A survey of unmanned aerial vehicles (UAVs) for traffic monitoring." *Unmanned Aircraft Systems (ICUAS), 2013 International Conference on*, IEEE, 221–234.

Karpowicz, R. (2014). *The Use of Unmanned Aerial Systems for Steep Terrain Investigations*.

Kaufmann, S., Kerner, B. S., Rehborn, H., Koller, M., and Klenov, S. L. (2018). "Aerial observations of moving synchronized flow patterns in over-saturated city traffic." *Transportation research part C: emerging technologies*, Elsevier, 86, 393–406.

Khan, M. A., Ectors, W., Bellemans, T., Janssens, D., and Wets, G. (2018). "Unmanned Aerial Vehicle-Based Traffic Analysis: A Case Study for Shockwave Identification and Flow Parameters Estimation at Signalized Intersections." *Remote Sensing*, Multidisciplinary Digital Publishing Institute,

10(3), 458.

Kish, A., Mui, W., and (U.S.), J. A. V. N. T. S. C. (2003). “Track buckling research.” John A. Volpe National Transportation Systems Center (U.S.).

Kramer, S. L., and Sajer, P. (1991). *Bridge Approach Slab Effectiveness*.

Kuchar, J. K. (2005). “Safety analysis methodology for unmanned aerial vehicle (UAV) collision avoidance systems.” *USA/Europe Air Traffic Management R&D Seminars*.

Lamb, S. (2005). “File:Washout on the RGN.jpg - Wikimedia Commons.” <https://commons.wikimedia.org/wiki/File:Washout_on_the_RGN.jpg> (Sep. 18, 2018).

Landsea, C. (2006). “Tropical Winds Cyclone FAQ.” <http://www.aoml.noaa.gov/hrd/tcfaq/D4.html> (Sep. 19, 2018).

Lanham, M. (2018). “Hot Mix Asphalt Materials, Mixture Design, and Construction.” <https://www.pavementinteractive.org/reference-desk/pavement-management/pavement-distresses/> (Sep. 17, 2018).

Lercel, D., Steckel, R., and Pestka, J. (2018). *Unmanned Aircraft Systems: An Overview of Strategies and Opportunities for Missouri*. Missouri. Dept. of Transportation. Construction and Materials Division.

Leslar, M., Andelin, E., and Perry, G. (2009). “Using Mobile lidar to survey railway infrastructure.” *Proceedings of the Innovative Lidar Solutions Conference 2009*.

Lillian, B. (2016). “Connecticut DOT Keeps Its Eyes on UAVs for Bridge Inspections - Unmanned Aerial.” <https://unmanned-aerial.com/connecticut-dot-keeps-its-eyes-on-uavs-for-bridge-inspections> (Sep. 6, 2018).

Lillian, B. (2018). “Kansas Partners Test Drones Beyond Line of Sight - Unmanned Aerial.” <https://unmanned-aerial.com/kansas-partners-test-drones-beyond-line-of-sight> (Aug. 28, 2018).

Lin, Y., and Saripalli, S. (2012). “Road detection and tracking from aerial desert imagery.” *Journal of Intelligent & Robotic Systems*, Springer, 65(1–4), 345–359.

Linda, S., and Bill, V. (2017). *Unmanned Aircraft Systems (UAS) UAS Overview IDOT’s UAS Program Bill Viste Project Coordinator Bureau Chief Aviation Safety*.

MaineDOT. (2016). “Airshark and VHB Collaborate | Maine DOT Bridge Inspection - News | AirShark Unmanned Aerial Services - Airshark UAV Services.” <https://www.airshark.io/en/company/news/airshark-and-vhb-collaborate-maine-dot-bridge-inspection/> (Aug. 30, 2018).

Manconi, A., Casu, F., Ardizzone, F., Bonano, M., Cardinali, M., De Luca, C., Gueguen, E., Marchesini, I., Parise, M., and Vennari, C. (2014). “Brief communication: rapid mapping of landslide events: the 3 December 2013 Montescaglioso landslide, Italy.” *Natural Hazards and Earth System Sciences*, Copernicus GmbH, 14(7), 1835–1841.

Mansurov, N. (2018). “What is Distortion? - Photography Life.” <https://photographylife.com/what-is-distortion> (Aug. 11, 2018).

Marinelli, G., Bassani, M., Piras, M., and Lingua, A. M. (2017). “Mobile mapping systems and spatial data collection strategies assessment in the identification of horizontal alignment of highways.” *Transportation Research Part C: Emerging Technologies*, Elsevier, 79, 257–273.

Martin, P. (2012). “Understanding Your Camera: Revisiting Focal Length : Martin Pot - Photography Blog.” <https://martybugs.net/blog/blog.cgi/learning/Revisiting-Focal-Length.html> (Aug. 11, 2018).

Mathworks. (2017). “What Is Camera Calibration? - MATLAB & Simulink.” <https://www.mathworks.com/help/vision/ug/camera-calibration.html> (Aug. 11, 2018).

Mccarthy, N. (2015). “The Commercial Drone Sector Is Set To Contribute Billions To The U.S. Economy [Infographic].” <https://www.forbes.com/sites/niallmccarthy/2015/10/19/the-commercial-drone-sector-is-set-to-contribute-billions-to-the-u-s-economy-infographic/#5d671f1d2bdd> (Sep. 26, 2018).

McCormack, E. D., and Trepanier, T. (2008). *The use of small unmanned aircraft by the Washington State Department of Transportation*. Citeseer.

McGhee, K. H. (2004). *Automated pavement distress collection techniques*.

Transportation Research Board.

McGlone, J. C., Mikhail, E. M., Bethel, J. S., and Mullen, R. (2004). “Manual of photogrammetry.” American society for photogrammetry and remote sensing Bethesda, MD.

McGuire, M., Rys, M. J., and Rys, A. (2016). *A study of how unmanned aircraft systems can support the Kansas Department of Transportation’s efforts to improve efficiency, safety, and cost reduction*. Kansas Department of Transportation.

Metni, N., and Hamel, T. (2007). “A UAV for bridge inspection: Visual servoing control law with orientation limits.” *Automation in construction*, Elsevier, 17(1), 3–10.

Miller, J. S., and Bellinger, W. Y. (2014). *Distress identification manual for the long-term pavement performance program*. United States. Federal Highway Administration. Office of Infrastructure Research and Development.

Miller, R. W., Raman, M., Hossain, M., Cumberledge, G., Reigle, J., Lee, H., and Kang, K. (2003). “Comparison of image-based distress survey results with manual distress surveys for transverse cracking.” *the 82nd Annual TRB Meeting, Washington, DC*.

Mills, J. P., Newton, I., and Graham, R. W. (1996). “Aerial photography for survey purposes with a high resolution, small format, digital camera.” *The Photogrammetric Record*, Wiley Online Library, 15(88), 575–587.

Mohammad, L. N., Puppala, A. J., and Alavilli, P. (1995). “Resilient properties of laboratory compacted subgrade soils.” *Transportation Research Record*, (1504).

MontanaDOT. (2018). “Montana DoT Use Drones to Recce Beartooth Highway before Clearing to See How Much Snow They’ll be up Against - SnowBrains.” <https://snowbrains.com/beartooth-montana-drones-clearing/> (Aug. 30, 2018).

Mora, P., Baldi, P., Casula, G., Fabris, M., Ghirotti, M., Mazzini, E., and Pesci, A. (2003). “Global Positioning Systems and digital photogrammetry for the monitoring of mass movements: application to the Ca’di Malta landslide (northern Apennines, Italy).” *Engineering Geology*, Elsevier, 68(1–2), 103–121.

Murphy, D. W., and Cycon, J. (1999). “Applications for mini VTOL UAV for law enforcement.” *Sensors, C3I, Information, and Training Technologies for Law Enforcement*, International Society for Optics and Photonics, 35–44.

Mustaffara, M., Lingb, T. C., and Puanb, O. C. (2008). “Automated pavement imaging program (APIP) for pavement cracks classification and quantification—A photogrammetric approach.” *The International Archives of the Photogrammetry, Remote Sensing and Spatial Information Sciences*, Citeseer, 37(B4), 367–372.

N.E. Bridge Contractors. (2016). “A-30 UBIU | Bridgeriggers.”

<http://www.bridgeriggers.com/equipment-rentals/a-30-hi-rail> (Sep. 18, 2018).

Negussey, D., and Stuedlein, A. W. (2003). "Geofoam fill performance monitoring." *Utah Dept. of Transportation, Rep. No. UT*, 3.

Newman, M. P., Bartlett, S. F., and Lawton, E. C. (2009). "Numerical modeling of geofoam embankments." *Journal of geotechnical and geoenvironmental engineering*, American Society of Civil Engineers, 136(2), 290–298.

Nex, F., and Remondino, F. (2014). "UAV for 3D mapping applications: a review." *Applied geomatics*, Springer, 6(1), 1–15.

NHDOT. (2018). "Update on Research: Unmanned Aircraft Systems (UAS) for NHDOT." <https://www.nh.gov/dot/org/projectdevelopment/materials/research/documents/2018-1FINAL.pdf> (Sep. 16, 2018).

Ni, D., and Plotnikov, M. (2016). "The State of the Practice of UAS Systems in Transportation." Massachusetts. Dept. of Transportation.

Niethammer, U., James, M. R., Rothmund, S., Travelletti, J., and Joswig, M. (2012). "UAV-based remote sensing of the Super-Sauze landslide: Evaluation and results." *Engineering Geology*, Elsevier, 128, 2–11.

Nikolakopoulos, K. G., Soura, K., Koukouvelas, I. K., and Argyropoulos, N. G. (2017). "UAV vs classical aerial photogrammetry for archaeological studies." *Journal of Archaeological Science: Reports*, Elsevier, 14, 758–773.

Nisser, T., and Westin, C. (2006). “Human factors challenges in unmanned aerial vehicles (uavs): A literature review.” *School of Aviation of the Lund University, Ljungbyhed*, Citeseer.

NOAA. (2018). “What is a hurricane?” <https://oceanservice.noaa.gov/facts/hurricane.html> (Sep. 19, 2018).

Oka, N. (1998). “Application of photogrammetry to the field observation of failed slopes.” *Engineering Geology*, Elsevier, 50(1–2), 85–100.

Pereira, E., Bencatel, R., Correia, J., Félix, L., Gonçalves, G., Morgado, J., and Sousa, J. (2009). “Unmanned air vehicles for coastal and environmental research.” *Journal of Coastal Research*, JSTOR, 1557–1561.

Pereira, F. C., and Pereira, C. E. (2015). “Embedded image processing systems for automatic recognition of cracks using UAVs.” *IFAC-PapersOnLine*.

Perlman, A. (2017). “Inside the FAA’s Pathfinder Program - UAV Coach.” <https://uavcoach.com/what-is-faa-pathfinder-program/> (Sep. 18, 2018).

Pierce, L. M., McGovern, G., and Zimmerman, K. A. (2013). “Practical guide for quality management of pavement condition data collection.”

Puppala, A. J., Congress, S. S. C., Bheemasetti, T. V., and Caballero, S. (2018a). “Geotechnical Data Visualization and Modeling of Civil Infrastructure Projects.” *GeoShanghai International Conference*, Springer, 1–12.

Puppala, A. J., Congress, S. S. C., Bheemasetti, T. V., and Caballero, S. R. (2018b). “Visualization of Civil Infrastructure Emphasizing Geomaterial

Characterization and Performance." *Journal of Materials in Civil Engineering*, American Society of Civil Engineers, 30(10), 4018236.

Puppala, A. J., Hanchanloet, S., Jadeja, M., and Burkart, B. (1999). "Sulfate induced heave distress: a case study." *Proceedings, transportation research board annual meeting, Washington DC, USA*.

Puppala, A. J., Madhyannapu, R. S., Nazarian, S., Yuan, D., and Hoyos, L. R. (2008). *Deep soil mixing technology for mitigation of pavement roughness*.

Puppala, A. J., Manosuthikij, T., and Chittoori, B. C. S. (2013). "Swell and shrinkage characterizations of unsaturated expansive clays from Texas." *Engineering Geology*, Elsevier, 164, 187–194.

Puppala, A. J., Manosuthkij, T., Nazarian, S., and Hoyos, L. R. (2011). "Threshold moisture content and matric suction potentials in expansive clays prior to initiation of cracking in pavements." *Canadian Geotechnical Journal*, NRC Research Press, 48(4), 519–531.

Puppala, A. J., Saride, S., Archeewa, E., Hoyos, L. R., and Nazarian, S. (2009). "Recommendations for design, construction, and maintenance of bridge approach slabs: Synthesis report." *Rep. No. FHWA/TX-09/0-6022-1, Dept. Civil Engineering, Univ. of Texas–Arlington, Arlington, TX*.

Puppala, A. J., Talluri, N., Congress, S. S. C., and Gaily, A. (2018c). "Ettringite induced heaving in stabilized high sulfate soils." *Innovative Infrastructure Solutions*, 3(1), 72.

Puppala, A., Wattanasanticharoen, E., and Hoyos, L. (2003). “Ranking of four chemical and mechanical stabilization methods to treat low-volume road subgrades in Texas.” *Transportation Research Record: Journal of the Transportation Research Board*, Transportation Research Board of the National Academies, (1819), 63–71.

RAIU. (2010). *Investigation Report 2010-R006*.

Rater’s Manual. (2016). *TxDOT PMIS Rater’s Manual*.

Rathinam, S., Kim, Z. W., and Sengupta, R. (2008). “Vision-based monitoring of locally linear structures using an unmanned aerial vehicle.” *Journal of Infrastructure Systems*, American Society of Civil Engineers, 14(1), 52–63.

Rathje, E. M., Woo, K., and Crawford, M. (2006). “Spaceborne and airborne remote sensing for geotechnical applications.” *GeoCongress 2006: Geotechnical Engineering in the Information Technology Age*, 1–19.

Room, M. H. M., and Ahmad, A. (2014). “Mapping of a river using close range photogrammetry technique and unmanned aerial vehicle system.” *IOP Conference Series: Earth and Environmental Science*, IOP Publishing, 12061.

Rubino, J. (2018). “Colorado construction sites abuzz with drones, as industry embraces unmanned aircraft.” <https://www.denverpost.com/2018/02/01/drones-colorado-construction-sites/> (Aug. 29, 2018).

Salvo, G., Caruso, L., and Scordo, A. (2014a). “Urban traffic analysis through an

UAV.” *Procedia - Social and Behavioral Sciences*, Elsevier B.V., 111, 1083–1091.

Salvo, G., Caruso, L., and Scordo, A. (2014b). “Gap acceptance analysis in an urban intersection through a video acquired by an UAV.” *5th European Conference of Civil Engineering (ECCIE’14)*.

Sayers, M. W., and Karamihas, S. M. (1998). “The Little Book of.” (September).

Scratchapixel 2.0. (2018). “3D Viewing: the Pinhole Camera Model (How a pinhole camera works (part 2)).” <https://www.scratchapixel.com/lessons/3d-basic-rendering/3d-viewing-pinhole-camera/how-pinhole-camera-works-part-2> (Aug. 11, 2018).

Seo, J. B. (2005). “The bump at the end of the bridge: an investigation.” Texas A&M University.

Shafikhani, A., Bheemasetti, T. V, and Puppala, A. J. (2017). “Effect of Seasonal Changes on a Hybrid Soil–Geofoam Embankment System.” *International Journal of Geosynthetics and Ground Engineering*, Springer, 3(4), 39.

Shamsabadi, S. S., Wang, M., and Birken, R. (2014). “PAVEMON: a GIS-based data management system for pavement monitoring based on large amounts of near-surface geophysical sensor data.” *27th Annual Symposium on the Application of Geophysics to Engineering and Environmental Problems (SAGEEP)*.

Shastry, A., and Schowengerdt, R. (2002). “Airborne video registration for

visualization and parameter estimation of traffic flows." *Proceedings of Pecora*, 391–405.

Shekharan, R., Frith, D., Chowdhury, T., Larson, C., and Morian, D. (2007). "Effects of comprehensive quality assurance/quality control plan on pavement management." *Transportation Research Record*, SAGE Publications Sage CA: Los Angeles, CA, 1990(1), 65–71.

Siebert, S., and Teizer, J. (2014). "Mobile 3D mapping for surveying earthwork projects using an Unmanned Aerial Vehicle (UAV) system." *Automation in Construction*, Elsevier, 41, 1–14.

Simek, K. (2013). "Dissecting the Camera Matrix, Part 3: The Intrinsic Matrix ←." <http://ksimek.github.io/2013/08/13/intrinsic/> (Aug. 11, 2018).

Skeen, J. (2011). "TxDOT Survey Manual." *Texas Department of Transportation, Texas*.

Smith, D. L., Abdullah, Q. A., Maune, D., and Heidemann, K. H. (2014a). "ASPRS slide presentation, final version for Board Submital." <https://www.asprs.org/news-resources/asprs-positional-accuracy-standards-for-digital-geospatial-data> (Aug. 11, 2018).

Smith, D. L., Abdullah, Q. A., Maune, D., and Heidemann, K. H. (2014b). "New ASPRS Positional Accuracy Standards for Digital Geospatial Data."

Stark, T. D., Arellano, D., Horvath, J. S., and Leshchinsky, D. (2004). *Geofoam applications in the design and construction of highway embankments*.

Steffen, R., and Förstner, W. (2008). “On visual real time mapping for unmanned aerial vehicles.” *21st Congress of the International Society for Photogrammetry and Remote Sensing (ISPRS)*, 57–62.

Stevens, K. (2018). “NDOT Imagery Section Launches UAV Program – State Aviation Journal.” <http://stateaviationjournal.com/index.php/state-news/neveda/ndot-imagery-section-launches-uav-program> (Aug. 30, 2018).

Stewart, C., Luebkeman, C., Morrell, M., and Goulding, L. (2014). “Future of Rail 2050.”

Stott, G., and Tadmori, K. (2018). “Drone program takes off in Bureau of Aeronautics - NJDOT Technology Transfer.” <https://www.njdottechtransfer.net/2018/01/24/drone-program-takes-off-bureau-aeronautics/> (Aug. 30, 2018).

Stuart, T. (2015). “Cyberhawk discuss the advantages of UAVs to the rail industry - Cyberhawk.” <http://www.thecyberhawk.com/cyberhawk-discuss-the-advantages-of-uavs-to-the-rail-industry/> (Aug. 11, 2018).

Sturzenegger, M., and Stead, D. (2009). “Close-range terrestrial digital photogrammetry and terrestrial laser scanning for discontinuity characterization on rock cuts.” *Engineering Geology*, Elsevier, 106(3–4), 163–182.

Suncar, O. E., Rathje, E. M., and Buckley, S. M. (2013). “Deformations of a rapidly moving landslide from high-resolution optical satellite imagery.” *Geo-*

Congress 2013: Stability and Performance of Slopes and Embankments III, 269–278.

Tadros, M. K., and Benak, J. V. (1989). *BRIDGE ABUTMENT AND APPROACH SLAB SETTLEMENT. PHASE 1. FINAL REPORT*.

Tahar, K. N., and Ahmad, A. (2012). "A simulation study on the capabilities of rotor wing unmanned aerial vehicle in aerial terrain mapping." *International Journal of Physical Sciences*, Academic Journals, 7(8), 1300–1306.

Tamouridou, A. A., Alexandridis, T. K., Pantazi, X. E., Lagopodi, A. L., Kashefi, J., and Moshou, D. (2017). "Evaluation of UAV imagery for mapping Silybum marianum weed patches." *International Journal of Remote Sensing*, Taylor & Francis, 38(8–10), 2246–2259.

Tatum, M. C., and Liu, J. (2017). "Unmanned aerial vehicles in the construction industry." *Proc., 53rd ASC Annual Int. Conf., Associated Schools of Construction, Fort Collins, CO*.

Tempcon. (2018). "WHAT IS CALIBRATION AND WHY IS IT SO IMPORTANT | Tempcon." <https://www.tempcon.co.uk/2018/02/26/what_is_calibration/> (Aug. 11, 2018).

The Association of American Railroads. (2015). "Aerial Drones Provide Rail Safety from the Sky."

Thiagarajan, G., Gopalaratnam, V., Halmen, C., Ajgaonkar, S., Ma, S., Gudimetla,

B., and Chamarthi, R. (2010). *Bridge Approach Slabs for Missouri DOT: Looking at Alternative and Cost Efficient Approaches*.

Tim, U. S. (1995). "The application of GIS in environmental health sciences: opportunities and limitations." *Environmental Research*, Elsevier, 71(2), 75–88.

Tony, D. (2018). *35 State DOTs are Deploying Drones to Save Lives, Time and Money Survey Results Featured in Special Report Video: Building Highways in the Sky: State DOTs Leading the Evolution of Drones*.

Tripolitsiotis, A., Steiakakis, C., Papadaki, E., Agioutantis, Z., Mertikas, S., and Partsinevelos, P. (2014). "Complementing geotechnical slope stability and land movement analysis using satellite DInSAR." *Open Geosciences*, Versita, 6(1), 56–66.

Tronin, A. A. (2009). "Satellite remote sensing in seismology. A review." *Remote Sensing*, Molecular Diversity Preservation International, 2(1), 124–150.

TxDOT. (2011). "Texas Highway-Rail Grade Crossing Safety Action Plan."

TxDOT. (2018). *Pavement Manual Notice 2018-2*.

TxDOT Bridge Division. (2016). *Report on Texas Bridges*.

Tziavou, O., Pytharouli, S., and Souter, J. (2018). "Unmanned Aerial Vehicle (UAV) based mapping in engineering geological surveys: Considerations for optimum results." *Engineering Geology*, Elsevier, 232, 12–21.

Udin, W. S., and Ahmad, A. (2014). "Assessment of photogrammetric mapping

accuracy based on variation flying altitude using unmanned aerial vehicle." *IOP Conference Series: Earth and Environmental Science*, IOP Publishing, 12027.

University of Cologne. (2017). "Radial Distortion Correction." <http://www.uni-koeln.de/~al001/radcor_files/hs100.htm> (Aug. 11, 2018).

Wahls, H. (1990). *Design and construction of bridge approaches*.

Wei, D., and Zhou, G. (2008). "Real-Time UAV Ortho Video Generation." *Geoscience and Remote Sensing Symposium, 2008. IGARSS 2008. IEEE International*, IEEE, V-510.

Wells, J., Lovelace, B., and Engineers, C. (2017). *Unmanned aircraft system bridge inspection demonstration project phase II final report*. Minnesota. Dept. of Transportation. Research Services & Library.

Wen, M.-C., and Kang, S.-C. (2014). "Augmented reality and unmanned aerial vehicle assist in construction management." *Computing in Civil and Building Engineering (2014)*, 1570–1577.

White, D. J., Mekkawy, M. M., Sritharan, S., and Suleiman, M. T. (2007). "'Underlying' Causes for Settlement of Bridge Approach Pavement Systems." *Journal of Performance of Constructed Facilities*, 21(4), 273–282.

White, G., Velozo, S., Peshkin, D., and Ram, P. (2016). *Framework for a Pavement-Maintenance Database System*. Transportation Research Board, Washington, D.C.

Wojtowicz, K., Dirckx, M. P., and Baker, W. (2017). *UNMANNED AIRCRAFT SYSTEMS IN PENNSYLVANIA JOINT STATE GOVERNMENT COMMISSION General Assembly of the Commonwealth of Pennsylvania*.

Wu, D., Arkhipov, D. I., Kim, M., Talcott, C. L., Regan, A. C., McCann, J. A., and Venkatasubramanian, N. (2017). "ADDSEN: Adaptive data processing and dissemination for drone swarms in urban sensing." *IEEE transactions on computers*, IEEE, 66(2), 183–198.

Wu, J., Dong, Z., and Zhou, G. (2007). "Geo-registration and mosaic of UAV video for quick-response to forest fire disaster." *MIPPR 2007: Pattern Recognition and Computer Vision*, International Society for Optics and Photonics, 678810.

Wu, J., and Zhou, G. (2006). "Real-time UAV video processing for quick-response to natural disaster." *Geoscience and Remote Sensing Symposium, 2006. IGARSS 2006. IEEE International Conference on*, IEEE, 976–979.

Wurman, J., and Kosiba, K. (2018). "The Role of Small-Scale Vortices in Enhancing Surface Winds and Damage in Hurricane Harvey (2017)." *Monthly Weather Review*, 146(3), 713–722.

Yu, X. (2011). "Pavement surface distress detection and evaluation using image processing technology." University of Toledo.

Yurek, E. E., and Ozmutlu, H. C. (2018). "A decomposition-based iterative optimization algorithm for traveling salesman problem with drone." *Transportation Research Part C: Emerging Technologies*, Elsevier, 91, 249–

262.

Zainuddin, K., Jaffri, M. H., Zainal, M. Z., Ghazali, N., and Samad, A. M. (2016). "Verification test on ability to use low-cost UAV for quantifying tree height." *Signal Processing & Its Applications (CSPA), 2016 IEEE 12th International Colloquium on*, IEEE, 317–321.

Zeng, W., Chen, P., Yu, G., and Wang, Y. (2017). "Specification and calibration of a microscopic model for pedestrian dynamic simulation at signalized intersections: A hybrid approach." *Transportation Research Part C: Emerging Technologies*, Elsevier, 80, 37–70.

Zhang, C. (2008). "An UAV-based photogrammetric mapping system for road condition assessment." *Int. Arch. Photogramm. Remote Sens. Spatial Inf. Sci*, 37, 627–632.

Zhang, C., and Elaksher, A. (2012). "An Unmanned Aerial Vehicle-Based Imaging System for 3D Measurement of Unpaved Road Surface Distresses 1." *Computer-Aided Civil and Infrastructure Engineering*, Wiley Online Library, 27(2), 118–129.

Zhang, L., Peng, Z., Li, L., and Wang, H. (2014). "Road boundary estimation to improve vehicle detection and tracking in UAV video." *Journal of Central South University*, Springer, 21(12), 4732–4741.

Zhang, Z., and Murphy, M. R. (2013). *A web-based pavement performance and maintenance management and GIS mapping system for easy access to*

pavement condition information.

Zheng, C., Breton, A., Iqbal, W., Sadiq, I., Elsayed, E., and Li, K. (2015). "Driving-Behavior Monitoring Using an Unmanned Aircraft System (UAS)." *International Conference on Digital Human Modeling and Applications in Health, Safety, Ergonomics and Risk Management*, Springer, 305–312.

Zhou, G. (2010). "Geo-referencing of video flow from small low-cost civilian UAV." *IEEE Transactions on automation science and engineering*, 7(1), 156.

Zongjian, L. (2008). "UAV for mapping—low altitude photogrammetric survey." *International Archives of Photogrammetry and Remote Sensing, Beijing, China*, 37, 1183–1186.

APPENDIX-A

Survey Questionnaire for Commercial Companies

Based upon the UT Arlington team's UAV research experience, the below questionnaire was prepared and used to contact various UAV-related companies through email:

Parameters of Equipment

- Does your company use multi-rotor, fixed wing, or other UAVs?
- Does your company conduct each survey with one UAV, or more?
- Does your company use any advanced types of GPS units (RTK, PPK, GNSS, etc.)?
- Does your company use ground control points?

Parameters of Survey

- Does your company conduct roadway surveys (e.g. 500 ft pavement)?
- Does your company conduct above-bridge surveys?
- Does your company conduct under-bridge surveys?
- Does your company conduct volumetric measurements (e.g. 5000 cu yard stockpiles, detention ponds, etc.)?
- Does your company conduct surveys down railway lines?
- How much rail track area can your company cover in a business day?

Parameters of Deliverables

- Does your company create 3D model reconstructions? If so, what is the cost?
- Does your company create orthophotos? If so, what is the cost?
- Does your company create any other layers (e.g. vegetation index, thermal, etc.)? If so, what is the cost?
- Are these layers overlaid or independent? What is the cost associated with it?
- What is your company's advertised accuracy of these layers? Does the accuracy vary with cost?
- Does your company conduct any tests for detection of faults, distresses, cracks, rutting, potholes, vegetation, etc.? If so, what is the cost?
- Can your company identify volumetric changes over a period of days or months? If so, what is the cost?
- Are there any additional costs for travelling to remote areas? If so, what is the cost?